Year : 2011

The role of Fungi in the precipitation of calcite - Relationships between fungal filaments, nanofibres, and needle fibre calcite -

Bindschedler Saskia

UNIL | Université de Lausanne

Institut de géologie et de paléontologie
Faculté des géosciences et de l'environnement

The role of Fungi in the precipitation of calcite

- Relationships between fungal filaments, nanofibres, and needle fibre calcite -

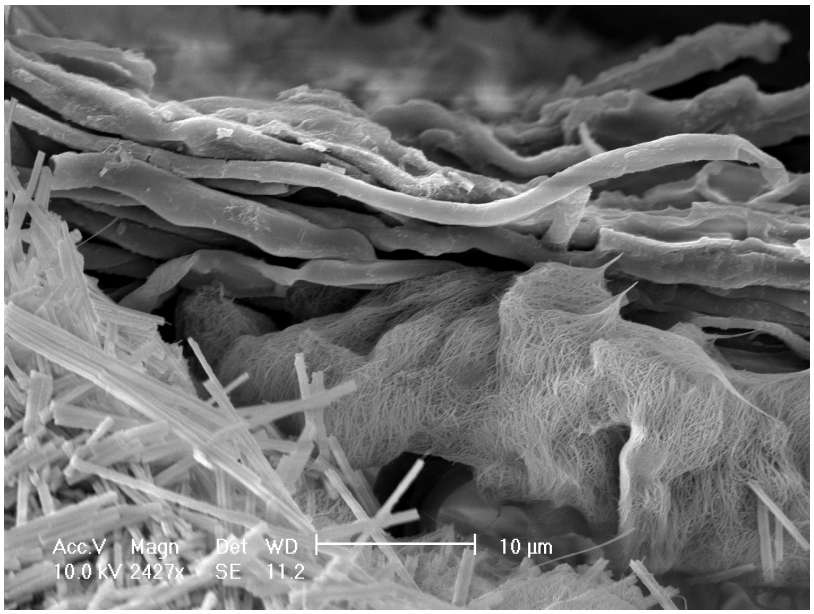

Thèse de doctorat

Présentée à la Faculté des géosciences et de l'environnement
de l'Université de Lausanne par

Saskia Bindschedler

titulaire d'un master en Biogéosciences de l'Université de Neuchâtel

Jury:

Prof. Torsten Vennemann, Université de Lausanne (Suisse); Président
Prof. Eric P. Verrecchia, Université de Lausanne (Suisse); Directeur de thèse
Prof. Peter O. Baumgartner, Université de Lausanne (Suisse); expert interne
DR Dr. Daniel Job, Université de Neuchâtel (Suisse); expert externe
Dr. Karim Benzerara, Université Pierre et Marie Curie, Paris (France); expert externe
Prof. Geoffrey M. Gadd, University of Dundee (Scotland, UK); expert externe

Lausanne, 2011

UNIL | Université de Lausanne
Faculté des géosciences et de l'environnement
bâtiment Amphipôle
CH-1015 Lausanne

IMPRIMATUR

Vu le rapport présenté par le jury d'examen, composé de

Président de la séance publique :	M. le Professeur Torsten Vennemann
Président du colloque :	M. le Professeur Torsten Vennemann
Directeur de thèse :	M. le Professeur Eric Verrecchia
Expert interne :	M. le Professeur Peter Baumgartner
Expert externe:	M. le Docteur Karim Benzerara
Expert externe :	M. le Professeur Geoffrey Gadd
Expert externe :	M. le Docteur Daniel Job

Le Doyen de la Faculté des géosciences et de l'environnement autorise l'impression de la thèse de

Madame Saskia BINDSCHEDLER

Master en Biogéosciences, Neuchâtel

intitulée

The role of Fungi in the precipitation of calcite
- Relationships between fungal filaments, nanofibres, and needle fibre calcite -

Lausanne, le 20 mai 2011

Faculté des géosciences et de l'environnement

Professeur Jean Rüegg, Doyen

Ils ne savaient pas que c'était impossible, alors ils l'ont fait.
Mark Twain

Remerciements

Je tiens à remercier chaleureusement toutes les personnes qui ont contribué à la réussite de cette thèse de doctorat. Il y en a eu tellement qui m'ont aidée ou soutenue ponctuellement… Certaines personnes en particulier ont beaucoup comptés dans l'aboutissement de ce travail :

Laure Millière, mon binôme de thèse, avec qui j'ai eu la chance de collaborer et un immense plaisir à partager ces quatre dernières années.

Le Prof. Eric Verrecchia, mon directeur de thèse, qui m'a fait confiance en m'offrant cette place de thèse dans son groupe. Je le remercie également pour m'avoir transmis, tout au long de mon cursus universitaire, sa passion pour les biogéosciences. Et finalement, dans ce travail de thèse, son esprit de synthèse m'a permis de prendre le recul nécessaire sur mes données… chose parfois difficile quand on a le nez dedans!

Le Dr Daniel Job, le mycologue de ce projet, qui m'a encadrée tout au long de ma thèse. Je tiens à le remercier pour sa disponibilité, ainsi que ses conseils critiques et avisés prodigués au cours de ces quatre années et qui m'ont permis de remettre en question et de structurer mon travail de manière positive et constructive. Ça n'a pas toujours été facile à entendre, mais ô combien fructueux.

Le Dr Guillaume Cailleau, qui a été le « superviseur au quotidien » et qui a été présent tous les jours pour toutes mes crises existentielles, mes doutes, mes questions, et qui bien qu'étant « géologue » comme il le dit, a essayé de m'aider du mieux qu'il le pouvait (et il l'a très bien fait!).

Le Dr Olivier Braissant, pour sa disponibilité et toutes les discussions scientifico-méthodologiques. En particulier, je tiens à le remercier pour ses conseils « enzymatiques », ainsi que pour son aide dans l'étape finale de rédaction du manuscrit de thèse.

Tous les collaborateurs du laboratoire de Microbiologie de l'université de Neuchâtel. Et en particulier, la Prof. Pilar Junier pour son enthousiasme constant, pour m'avoir hébergée dans son groupe quand elle a reprit le laboratoire de Microbiologie et pour son soutien humain dans la dernière année de ma thèse. Nicole Jeanneret, pour sa patiente, sa gentillesse et son efficacité à tenir ce laboratoire et qui fait que c'est un vrai plaisir d'y travailler. Tina Wunderlin qui a re-lu certaines parties de ce manuscrit afin d'en améliorer l'anglais.

Olivier Hasinger qui a fait son travail de master dans le cadre de ce projet, qui y a mis un grand enthousiasme et a ainsi permis d'y apporter dynamisme et données essentielles.

Michèle Vlimant, André Villard, le Dr Massoud Dadras, le Dr Mireille Leboeuf, le Dr Vladislav Spassov et le Dr Pierre Vonlanthen pour toute leur aide et conseils en microscopie électronique. Sans eux, ce travail ne serait pas ce qu'il est…

Le Dr Paul Majcherczyk, le Dr Armelle Vallat, le Dr Mohammad Hassouna et Brice Prudat pour leur aide précieuse dans la partie analyses de matière organique.

Mes amis et collègues, du temps de la géodynamique à l'Unine au groupe biogéosciences à l'Unil : Laurent, Christina, Alex, Olivier, Loraine, Gladys, qui n'ont pas forcément contribué au côté scientifique de ce travail mais pour leur bonne humeur qui permet de créer une bonne ambiance de travail en général.

Tous les autres collègues géologues de l'IGH du temps de Neuchâtel et les nouveaux collègues de l'IGP et de l'IMG à Lausanne. Merci pour les pauses cafés et les dîners animés qui permettent de penser à autre chose.

Mère nature pour produire des structures aussi délicates, extraordinaires et énigmatique que les nanofibres et la calcite en aiguilles.

Tous mes amis (de peur d'en oublier je ne citerai pas de noms…ceux qui comptent savent) qui tout au long de ce travail, m'ont permis de penser à autre chose en partageant de bonnes discussions et des bons moments autour d'un café, d'une bière, d'un repas, etc…

Ma famille, en particulier mes parents qui m'ont permis de réaliser mes études dans les meilleures conditions qui soient et qui ont toujours eu confiance en moi et mes capacités.

Et finalement, Guillaume pour sa patience et surtout pour tout l'amour qu'il me donne. Sans lui, ce travail n'aurait probablement jamais abouti…

Ce travail a été soutenu financièrement par le Fonds National Suisse de la recherche (bourses n° 205320-109497/1 et 205320-122171).

Résumé

Les champignons sont impliqués dans les cycles biogéochimiques de différentes manières. En particulier, ils sont reconnus en tant qu'acteurs clés dans la dégradation de la matière organique, comme fournisseurs d'éléments nutritifs via l'altération des minéraux mais aussi comme grands producteurs d'acide oxalique et de complexes oxalo-métalliques. Toutefois, peu de choses sont connues quant à leur contribution à la genèse d'autres types de minéraux, tel que le carbonate de calcium ($CaCO_3$). Le $CaCO_3$ est un minéral ubiquiste dans de nombreux écosystèmes et il joue un rôle essentiel dans les cycles biogéochimiques du carbone (C) et du calcium (Ca). Le $CaCO_3$ peut être d'origine physico-chimique ou biogénique et de nombreux organismes sont connus pour contrôler ou induire sa biominéralisation. Les champignons ont souvent été soupçonnés d'être impliqué dans ce processus, cependant il existe très peu d'informations pour étayer cette hypothèse.

Cette thèse a eu pour but l'étude de cet aspect négligé de l'impact des champignons dans les cycles biogéochimiques, par l'exploration de leur implication potentielle dans la formation d'un type particulier de $CaCO_3$ secondaires observés dans les sols et dans les grottes des environnements calcaires. Dans les grottes, ces dépôts sont appelés *moonmilk*, alors que dans les sols on les appelle *calcite en aiguilles*. Cependant ces deux descriptions correspondent en fait au même assemblage microscopique de deux habitus particulier de la calcite: la calcite en aiguilles (au sens strict du terme cette fois-ci) et les nanofibres. Ces deux éléments sont des habitus aciculaires de la calcite, mais présentent des dimensions différentes. Leur origine, physico-chimique ou biologique, est l'objet de débats intenses depuis plusieurs années déjà.

L'observation d'échantillons environnementaux avec des techniques de microscopie (microscopie électronique et micromorphologie), ainsi que de la microanalyse EDX, ont démontré plusieurs relations intéressantes entre la calcite en aiguilles, les nanofibres et des éléments organiques. Premièrement, il est montré que les nanofibres peuvent être organiques ou minérales. Deuxièmement, la calcite en aiguilles et les nanofibres présentent de fortes analogies avec des structures hyphales, ce qui permet de confirmer l'hypothèse de leur origine fongique. En outre, des expériences en laboratoire ont confirmé l'origine fongique des nanofibres, par des digestions enzymatiques d'hyphes fongiques. En effet, des structures à base de nanofibres, similaires à celles observées dans des échantillons naturels, ont pu être produites par cette approche. Finalement, des enrichissements en calcium ont été mesurés dans les parois des hyphes et dans des inclusions intrahyphales provenant d'échantillons naturels de rhizomorphes. Ces résultats suggèrent une implication de la séquestration de calcium dans la formation de la calcite en aiguilles et/ou des nanofibres.

Plusieurs aspects restent à élucider, en particulier la compréhension des processus physiologiques impliqués dans la nucléation de calcite dans les hyphes fongiques. Cependant, les résultats obtenus dans cette thèse ont permis de confirmer l'implication des champignons dans la formation de la calcite en aiguilles et des nanofibres. Ces découvertes sont d'une grande importance dans les cycles biogéochimiques puisqu'ils apportent de nouveaux éléments dans le cycle couplé C-Ca. Classiquement, les champignons sont considérés comme étant impliqués principalement dans la minéralisation de la matière organique et dans l'altération minérale. Cette étude démontre que les champignons doivent aussi être pris en compte en tant qu'agents majeurs de la genèse de minéraux, en particulier de $CaCO_3$. Ceci représente une toute nouvelle perspective en géomycologie quant à la participation des champignons au cycle biologique du C. En effet, la présence de ces précipitations de $CaCO_3$ secondaires représente un court-circuit dans le cycle biologique du C puisque du C inorganique du sol se retrouve piégé dans de la calcite plutôt que d'être retourné dans l'atmosphère.

Abstract

Fungi are known to be involved in biogeochemical cycles in numerous ways. In particular, they are recognized as key players in organic matter recycling, as nutrient suppliers via mineral weathering, as well as large producers of oxalic acid and metal-oxalate. However, little is known about their contribution to the genesis of other types of minerals such as calcium carbonate ($CaCO_3$). Yet, $CaCO_3$ are ubiquitous minerals in many ecosystems and play an essential role in the biogeochemical cycles of both carbon (C) and calcium (Ca). $CaCO_3$ may be physicochemical or biogenic in origin and numerous organisms have been recognized to control or induce calcite biomineralization. While fungi have often been suspected to be involved in this process, only scarce information support this hypothesis.

This Ph.D. thesis aims at investigating this disregarded aspect of fungal impact on biogeochemical cycles by exploring their possible implication in the formation of a particular type of secondary $CaCO_3$ deposit ubiquitously observed in soils and caves from calcareous environments. In caves, these deposits are known as *moonmilk*, whereas in soils, they are known as *Needle Fibre Calcite* (NFC – *sensu lato*). However, they both correspond to the same microscopic assemblage of two distinct and unusual habits of calcite: NFC (*sensu stricto)* and nanofibres. Both features are acicular habits of calcite displaying different dimensions. Whether these habits are physicochemical or biogenic in origin has been under discussion for a long time.

Observations of natural samples using microscopic techniques (electron microscopy and micromorphology) and EDX microanalyses have demonstrated several interesting relationships between NFC, nanofibres, and organic features. First, it has shown that nanofibres can be either organic or mineral in nature. Second, both nanofibres and NFC display strong structural analogies with fungal hyphal features, supporting their fungal origin. Furthermore, laboratory experiments have confirmed the fungal origin of nanofibres through an enzymatic digestion of fungal hyphae. Indeed, structures made of nanofibres with similar features as those observed in natural samples have been produced. Finally, calcium enrichments have been measured in both cell walls and intrahyphal inclusions of hyphae from rhizomorphs sampled in the natural environment. These results point out an involvement of calcium sequestration in nanofibres and/or NFC genesis.

Several aspects need further investigation, in particular the understanding of the physiological processes involved in hyphal calcite nucleation. However, the results obtained during this study have allowed the confirmation of the implication of fungi in the formation of both NFC and nanofibres. These findings are of great importance regarding global biogeochemical cycles as they bring new insights into the coupled C and Ca cycles. Conventionally, fungi are considered to be involved in organic matter mineralization and mineral weathering. In this study, we demonstrate that they must also be considered as major agents in mineral genesis, in particular $CaCO_3$. This is a completely new perspective in geomycology regarding the role of fungi in the short-term (or biological) C cycle. Indeed, the presence of these secondary $CaCO_3$ precipitations represents a bypass in the short-term carbon cycle, as soil inorganic C is not readily returned to the atmosphere.

List of original publications

Scientific papers

Bindschedler S, Braissant O, Cailleau G, Millière L, Job D, and Verrecchia EP. *Submitted*. Following the fungal trail: how enzymatic digestion of fungal cell wall may produce soil and cave nanofibres. Naturwissenschaften. **Chapter 5, § 5.3.**

Bindschedler S, Millière L, Cailleau G, Job D, and Verrecchia EP. *In Press*. An ultrastructural approach to analogies between fungal structures and needle fibre calcite. Geomicrobiology Journal. **Chapter 4, § 4.2.**

Braissant O, **Bindschedler S**, Daniels AU, Verrecchia EP, and Cailleau G. *Accepted*. Microbiological activities in moonmilk monitored using isothermal microcalorimetry (Cave of « Vers Chez le Brandt », Neuchâtel, Switzerland). Journal of Cave and Karst Studies. **Annex 3.**

Millière L, Hasinger O, **Bindschedler S**, Cailleau G, Spangenberg JE, Verrecchia EP. 2011. Stable carbon and oxygen isotopic signatures of pedogenic needle fibre calcite. Geoderma 161: 74-87. **Annex 3.**

Bindschedler S, Millière L, Cailleau G, Job D, and Verrecchia EP. 2010. Calcitic nanofibers in soils and caves: a putative fungal contribution to carbonatogenesis. Tufas and Speleothems: Unravelling the Microbial and Physical Controls. Geological Society, London, Special Publications 336, 225-238. **Chapter 4, § 4.1 & Annex 3.**

Posters

Bindschedler S, Millière L, Cailleau C, Job D and Verrecchia EP. Analogy between secondary calcium carbonate crystals and fungal structures: clues for a biogenic origin of Needle Fibre Calcite. International Mycological Congress 9, 1-6 August 2010, Edinburgh. **Annex 3.**

Bindschedler S, Millière L, Cailleau G, Job D and Verrecchia E. Fungal implication in secondary calcium carbonate accumulation in soils and caves. 3rd Swiss Microbial Ecology Meeting, 28-30 January 2009, Einsiedeln, Switzerland. **Annex 3.**

Bindschedler S, Millière L, Cailleau G, Job D and Verrecchia E. The complex and diverse fungal processes involved in soil carbonatogenesis. 2007 Annual Scientific Meeting of the British Mycological Society, 9-12 September 2007, University of Manchester, UK AND SwissSed, 16th meeting of swiss sedimentologists, 22 February 2008, University of Fribourg, Switzerland. **Annex 3.**

Abbreviations

A horizon - Organo-mineral surface horizon of soils, occurring beneath O horizons

AMF - Arbuscular mycorrhizal fungi

ECM - Ectomycorrhizal fungi

B horizon - Structural and/or deeply weathered horizon of soils, mostly mineral

C horizon - Fragmented and weathered deep mineral horizons of soils

$CaCO_3$ - Calcium carbonate

$[CH_2O]_n$ - Carbohydrates empirical formula

CO_2 - Carbon dioxide

CO_3^{2-} - Carbonate ion

CryoSEM - Scanning electron microscopy in cryo (low temperature) mode

DIC - Dissolved inorganic carbon

EDX - Energy dispersive x-ray analysis (also abbreviated EDAX, EDS)

HCO_3^- - Hydrogenocarbonate ion

IC - Ion chromatography

ICP-MS - Inductively coupled plasma mass spectroscopy

K horizon - Soil horizon with secondary $CaCO_3$ accumulations

nanoSIMS - Secondary Ion Mass Spectrometry nano analysis

MA type NFC - Smooth needles composed of multiples rods

MAB type NFC - Intermediate form between MA and MB type

MB type NFC - Serrated-edged needles

NFC - Needle fibre calcite

NFC *sensu lato* - Defines the macroscopic accumulation of NFC in soil secondary $CaCO_3$

NFC *sensu stricto* - Defines the microscopic acicular habit of needle fibre calcite

nm - Nanometer(s)

O horizons - Organic (holorganic) surface horizon of a soil

OM - Organic matter

pCO_2 - Carbon dioxide partial pressure

PPL - Plane polarized light

SEM - Scanning electron microscopy

$SI_{calcite}$ - Calcite saturation index

STXM - Scanning Transmission X-ray Microscopy

TEM - Transmission electron microscopy

XPL - Crossed-polarized light

XRD - X-ray diffraction

µm – Micrometer(s)

Table of contents

Foreword

The role of fungi in calcium carbonate precipitation in terrestrial environments

The understanding of the global carbon (C) cycle has become a major concern for the scientific community. Researches dedicated to the C cycle are two-fold. First, it is crucial to understand how the global C cycle works in order to assess how the Earth is impacted by the current climate change. Second, the clear recognition of all the pools as well as their status as sink, source or transient pool is of great importance in the fluxes regulating the C cycle. Within the carbon cycle, calcium carbonates polymorphs ($CaCO_3$) play a crucial role as they may be alternatively considered either as a carbon source or as a carbon sink, depending on the calcium (Ca) source. C and Ca cycles are therefore closely linked to each other.

Secondary $CaCO_3$ accumulations are ubiquitous in vadose environments. However, the processes leading to their formation are still not completely understood. In particular, the role of fungi is often debated. Indeed, fungi are known to be involved in biogeochemical cycling at different levels. In particular, they are recognized as key players in organic matter recycling, as nutrients suppliers via mineral weathering, and as large producers of metal-oxalate. However, little is known about their contribution to the genesis of other types of minerals such as $CaCO_3$, although they are regularly mentioned as being involved in its precipitation. $CaCO_3$ may be physicochemical or biogenic in origin and several organisms have been recognized to control, induce, or influence calcite mineralization. The involvement of fungi in such a process has regularly been evoked in the formation of a particular type of pedogenic $CaCO_3$ deposit, the Needle Fibre Calcite (NFC *sensu lato*). NFC is an ubiquitous facies of secondary carbonates observed in soils and surficial formations as well as in caves from calcareous environments. Microscopically, it actually corresponds to two distinct and unusual habits of calcite: NFC *sensu stricto* and nanofibres. Whether these habits are physicochemical or biogenic in origin remains under debate.

The unravelling of their origin has several major aspects. First, NFC is often used as a paleoclimatic proxy because it is regularly observed in calcretes. Calcretes are authigenic calcium carbonate accumulations which forms in near-surface terrestrial environments in semiarid to arid areas (Zhou and Chafetz 2009). Therefore, the occurrence of NFC in paleosols is often interpreted as prevailing aridic to semiaridic climatic conditions. However, this assumption is challenged by the observation of NFC in more humid environments such as caves, as well as temperate and intertropical soils. Hence, the definition of the conditions leading to NFC formation will hopefully bring new insights in order to use it as an accurate paleoclimatic proxy. Second, the precipitation of $CaCO_3$ related to fungi has important implications in both C and Ca cycles, as NFC may represent a bypass in the carbon cycle where C is not readily returned to the atmosphere. In a more global perspective, it emphasizes the role of microorganisms in biogeochemical cycling, either through their activity or their sole presence.

The understanding of NFC and nanofibres genesis requires a pluridisciplinary approach; as a result, this project has been conducted using two perspectives, the *geologist*'s one which is presented in Laure Millière's Ph.D. thesis, and the *biologist*'s one, presented in this Ph.D. manuscript.

The main objective of this Ph.D. thesis is to bring insights into the implication of fungi in the formation of NFC and nanofibres by focusing on the biological side of the problematic. The first chapter of the manuscript, the general introduction, aims at defining the different actors involved in the study, i.e. calcium carbonate(s) and fungi, as well as emphasizing their importance in the natural environment and in biogeochemical cycles.

The second chapter intends to define NFC and nanofibres, the main objects of this study. It consists of a review on NFC and nanofibres characteristics as well as current hypotheses regarding their respective origins. This chapter is constructed of both, existing knowledge gathered in the literature and observations realized in the frame of this Ph.D.

Then, the core research itself has been conducted in three steps, presented in three distinct chapters. The first step has consisted of the identification in the field of the different forms of secondary $CaCO_3$ accumulations in relationship with climate and environmental factors. Three climatic zones showing different characteristics, in the Swiss Jura mountains, southwestern France and eastern Pyreneans in Spain, have been investigated. Sites in Switzerland are characterized by a constant humidity, sites in France by a lower humidity and milder temperatures, whereas sites in Spain are under a Mediterranean climatic influence. The field approach allows both the description of the different facies in relationship with the climate, and the identification of the main pedogenetic processes and related biological activities. The field description, as well as the conclusions that can be drawn from these observations, are presented in the chapter 3.

The second step has consisted of the observation of natural samples with microscopic techniques using different approaches. Scanning electron microscopy (SEM) and micromorphology have been used in order to identify the different features of these secondary calcite deposits as well as their mutual relationships. An emphasis has been given on organic structures by using Osmium labelling with SEM as well as CryoSEM observations. Transmission electron microscopy (TEM) has been used as a mean to identify internal ultrastructures, as well as to get a different perspective in comparison to SEM. The “observation” approach allows several microfeatures and recurrent relationships between features to be identified. These observations allow hypotheses on the origin of both NFC and nanofibres to be drawn, in relationship with fungi. The results are presented in chapter 4, which is organized in three parts. The two first parts are accepted publications. The third part consists of micromorphological observations emphasizing the importance of organic matter.

The third step has consisted of an attempt to confirm the hypotheses from chapter 4 by using an experimental approach. Three main questions are going to be addressed:

- How fungi may be a potential source of nanofibres?
- Is calcium sequestrated in fungal structures? Is this step a pre-requisite to NFC genesis?
- If NFC is generated in fungal hyphae, organic matter of fungal origin should be trapped within the crystal lattice?

The results are presented in the chapter 5, which is organized in three parts corresponding to the questions addressed above.

Finally, all the results and observations will be synthesized in the chapter 6 as a general discussion and conclusions.

Chapter 1

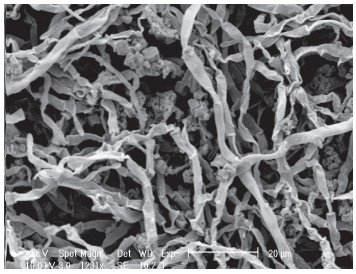

General Introduction

Chapter 1 - General introduction

This general introduction aims at providing the reader key-concepts that are going to be addressed in this manuscript. First, the relationship between the carbon cycle and calcium carbonate will be clarified in order to get an overview of this work in relation with global Earth processes. Then, calcium carbonate, pedogenic carbonates, and fungi will be introduced, to identify the basic properties of the actors involved in this study.

1.1 Importance of calcium carbonate in the carbon cycle

$CaCO_3$ is an ubiquitous mineral on Earth and plays an essential role in the C cycle. $CaCO_3$ is intimately linked to atmospheric carbon dioxide (CO_2) through dissolved inorganic carbon species (DIC; CO_2*, HCO_3- and CO_3^{2-} also called alkalinity). CO_2 is indeed highly soluble in water, and rapidly transformed into anionic carbonate forms (Houghton 2003). Biotic processes influence to a great extent the equilibrium of each species. Similarly, $CaCO_3$ may be physicochemical or biogenic in origin and several organisms have been recognized to control or to induce calcite biomineralization. Biogenicity in secondary $CaCO_3$ formation is indeed among the issues that are currently debated in geomicrobiological studies (Barton et al. 2001).

1.1.1 Carbon and the carbon cycle

C is the central element of life, being the basic component of every life form on Earth. C is a highly versatile element within ecosystems and is present in several pools or reservoirs of different respective importance (Fig. 1.1). C cycling is regulated by the fluxes between these pools. Importantly,

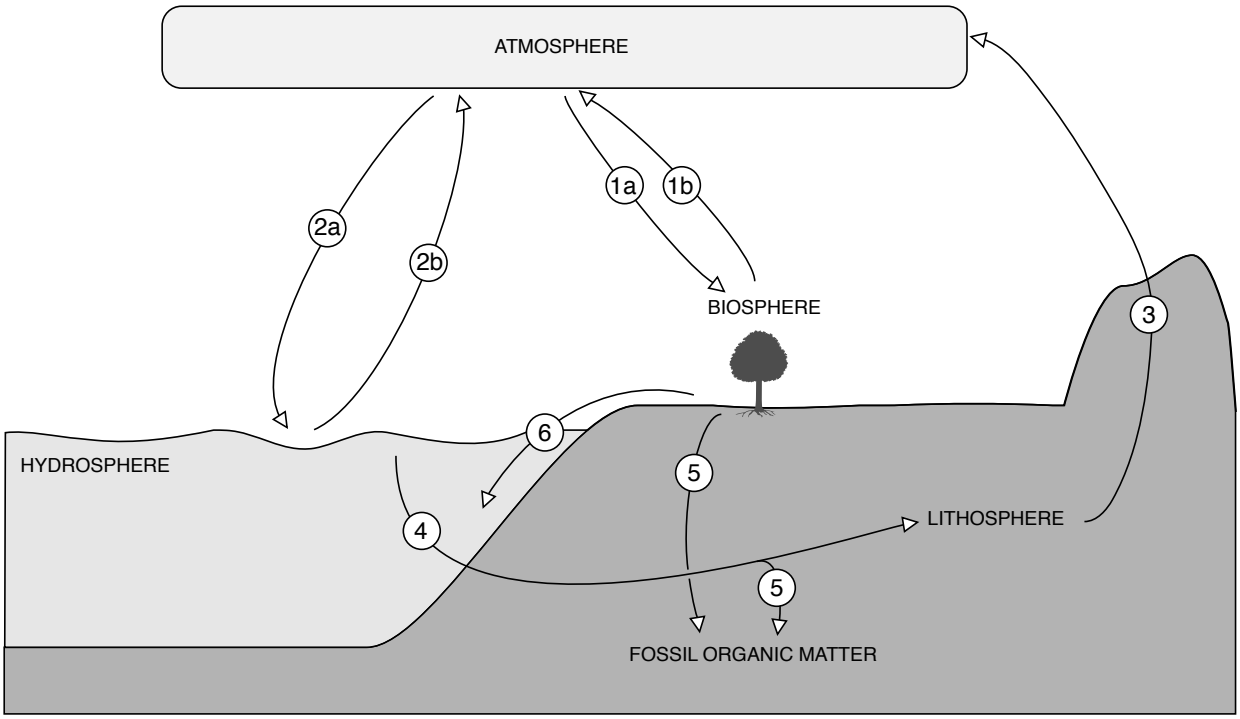

1a: photosynthesis
1b: heterotrophic respiration
2a: CO_2 dissolution
2b: CO_2 degazing
3: metamorphism and volcanism
4: sedimentation and diagenesis
5 : organic matter fossilisation
6: continental weathering

Figure 1.1 - Synthetic and simplified sketch of the geological (long-term) carbon cycle.

the status of the C cycle depends on the time-scale that is considered. Indeed, a geological (long-term) and a biological (short-term) C cycle may be considered. Processes concerning the Earth on a global scale rule the long-term C cycle. Those main processes involved in the long-term C cycle are volcanism, metamorphism, tectonics, orogenesis, sedimentation, diagenesis and erosion (Fig. 1.1). They are affecting ecosystems at a wide time and space scale. On the other hand, the short-term carbon cycle is ruled by biological processes affecting the ecosystems, which act at limited time and space scales. It is mainly formation of organic matter versus mineralization that controls the C turnover. In addition, the equilibrium of DIC species is often controlled or induced by biotic processes (Fig. 1.2). Nevertheless, whatever the time scale being considered, constant features can be recognized. The C cycle principally relies on carbon dioxide *sensu lato* (CO_2 and DIC), carbonate minerals (carbonates) and organic matter ($[CH_2O]_n$) turnovers (Equations 1-3).

(1) $CO_2 + H_2O \rightleftharpoons H_2CO_3 \rightleftharpoons HCO_3^- + H^+ \rightleftharpoons CO_3^{2-} + 2H^+$ *CO_2 dissolution/degazing*

(2) $CO_3^{2-} + Ca^{2+} \rightleftharpoons CaCO_3$ *Calcium carbonate precpitation/dissolution*

(3) $<CH_2O> + O_2 \rightleftharpoons CO_2 + H_2O$ *Respiration/photosynthesis*

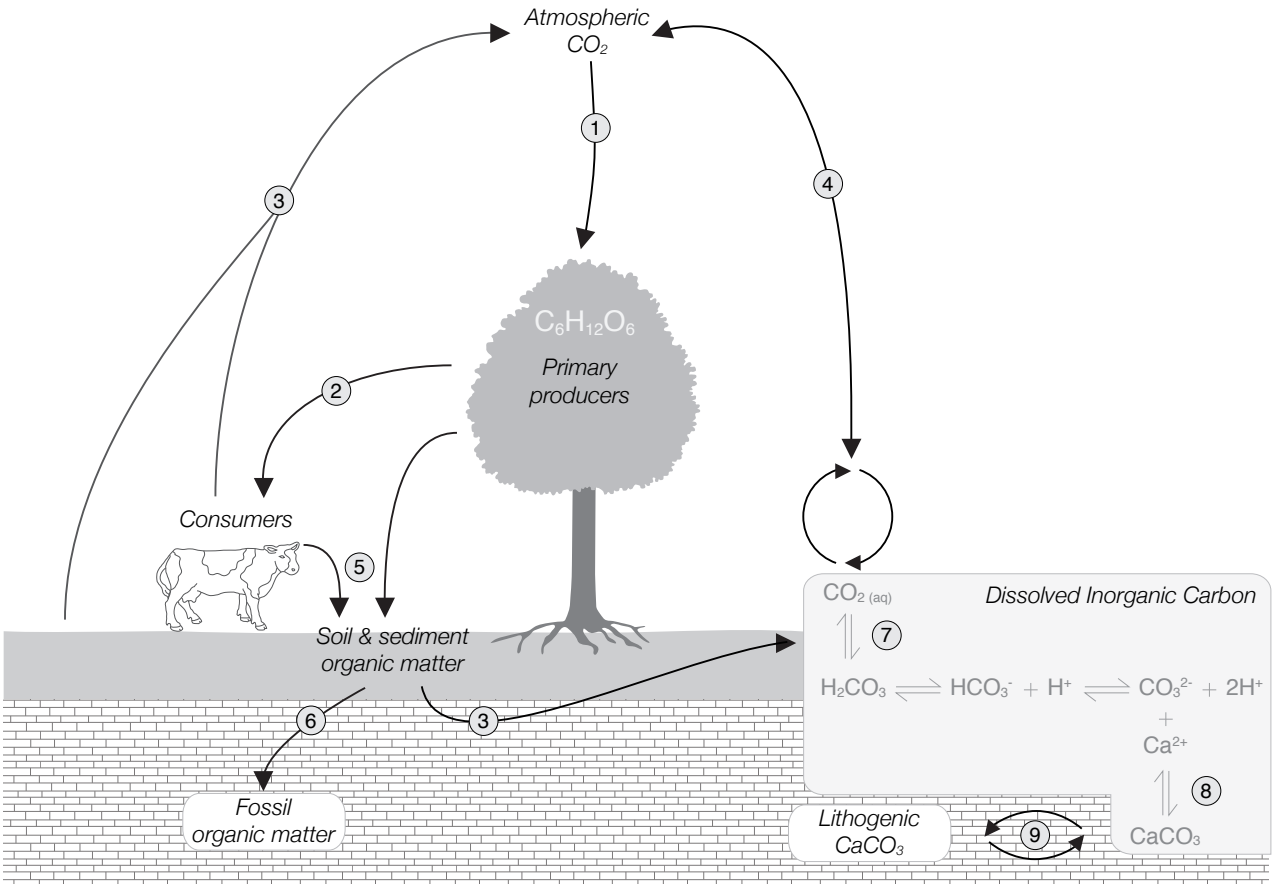

1- CO_2 uptake by photosynthesis
2- transfer of organic matter in trophic chains
3- Production of CO_2 by heterotrophic respiration
4- CO_2 exchanges with aqueous solutions (soil solution, streams)
5- Soil organic matter formation and stabilization
6- Fossilisation of organic C
7- Dissolution of CO_2 in aqueous solutions and carbonate equilibrium
8- Precipitation of $CaCO_3$
9- Transfers between lithogenic $CaCO_3$ and surficial formations

Figure 1.2 - Synthetic sketch representing the biological (short-term) carbon cycle in terrestrial environments.

1.1.2 Dissolved inorganic carbon species and carbonate minerals

Carbonates represent the solid end-member of the dynamic equilibrium between CO_2 and DIC species (Equation 1). Together, carbonates and DIC species represent by far the largest pool of C on Earth, whereas the atmospheric CO_2 pool accounts only for a limited fraction (Ehrlich 2002). DIC species are highly reactive in the conditions of pressure and temperature at the Earth surface, their dynamic equilibrium resulting in the well-known carbonate buffer system (Cojan and Renard 1999). This equilibrium is mostly driven by the pH, pCO_2, and temperature (Fig. 1.3; Stumm and Morgan 1996). These particularities provide the DIC species with a central role in biogeochemical processes related to the C cycle. Carbonate compounds are relatively insoluble and are therefore easily precipitated. Their stability depends further on DIC equilibrium and the factors affecting it.

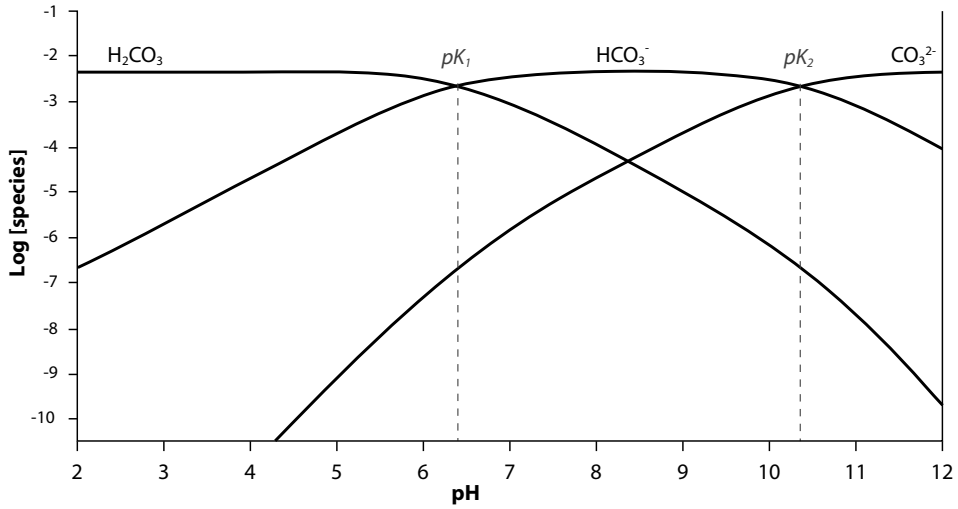

Figure 1.3 - Bjerrum plot representing the DIC speciation at 25°C, pCO_2 of 1 atm, and CT = $5x10^{-3}$ M. Modified from Andersen (2002).

Carbonates solubility increases with decreasing temperatures, increasing pH and pCO_2.

Carbonate minerals are ubiquitous on Earth and they are fundamental regarding the C cycle as they incorporate C. They are strongly related to the biosphere as a large fraction of the Earth carbonates have been precipitated, first under a biological influence (either directly or indirectly) all along geological times, and seconds as a result of metamorphic and magmatic processes. Finally, the carbonate pool represents the second largest reservoir of C regarding the C cycle, the largest one being the fossil organic matter (Ehrlich 2002).

1.1.3 Formation of calcium carbonates

Carbonates may precipitate as several different salts in combination with monovalent or divalent cations (e.g. Ca^{2+}, Mg^{2+}, Sr^{2+}, Mn^{2+}, Fe^{2+}, Cu^{2+}, Na^{+}). However, the most ubiquitous carbonate minerals are of calcium or calcium plus magnesium, observed in both phreatic and vadose environments.

Calcium carbonate ($CaCO_3$) has the particularity to exhibit several polymorphs. Calcite, aragonite, and vaterite are non-hydrated polymorphs of $CaCO_3$. Calcite is the most common polymorph of $CaCO_3$ and it is thermodynamically more stable than the two other polymorphs (Morse and Mackenzie 1990). Aragonite is typically formed in marine conditions or under strict biological control and vaterite has been observed mostly in laboratory conditions or, in a lesser extent, as a biomineral (Mann 2001). Both polymorphs are thermodynamically less stable than calcite (1.5 and 3.7 times respectively; Morse and Mackenzie 1990), leading to their rapid recrystallization into calcite under

average environmental conditions as found in terrestrial ecosystems (Cojan and Renard 1999). Three hydrated polymorphs also exist, monohydrocalcite ($CaCO_3.H_2O$), ikaïte ($CaCO_3.6H_2O$) and amorphous calcium carbonate ($CaCO_3.nH_2O$). Monohydrocalcite and ikaïte are occasionally observed in natural environments but only under particular conditions. Their formation seems to be favoured by low temperatures and high hydrostatic pressure, linked supposedly to biological activity (Morse and Mackenzie 1990). Finally, amorphous calcium carbonate has been observed mainly in plants and in Crustacean (Addadi et al. 2003). It is completely unstable in inorganic systems and readily recrystallizes into calcite if not stabilized by organic matter (Mann 2001; Addadi et al. 2003; Braissant et al. 2003).

Calcite is often found containing variable amounts of foreign ions within its crystal lattice. Indeed, ions analogous to Ca^{2+} may be selectively included in the crystal lattice during crystal growth with no major influence on crystal growth as well as crystal habit. Typically, calcite may occur as magnesian calcite, containing Mg as traces or in amounts up to 30 mole % $MgCO_3$ in some biogenic calcite (Morse and Mackenzie 1990). Dolomite, which is a calcium and magnesium carbonate ($CaMg(CO_3)_2$), is a particular case. It is very abundant in the sedimentary record and the processes leading to its formation remains controversial (Morse and Mackenzie 1990). Other ions may be found in the crystal lattice of calcite, such as Sr^{2+}, Na^{+}, Mn^{2+}, Zn^{2+}, and other analogous cations. In geochemical studies, the presence of foreign ions, their ratio and isotopic signatures, are typically used as proxies to trace environmental patterns related to the formation of calcite.

1.1.4 Terrestrial pools of $CaCO_3$

Most of the $CaCO_3$ pool on Earth is contained as diagenetic $CaCO_3$ in limestones and other sedimentary rocks as sedimentary $CaCO_3$ (Morse and Mackenzie 1990; Ehrlich 2002). Nevertheless, secondary precipitation of $CaCO_3$ in terrestrial environments, such as soils and caves, is a significant process, yet often neglected in pools of terrestrial inorganic carbon (Ehrlich 2002; Paul 2007).

1.1.4.1 Pedogenic carbonates

The soil C pool is often considered as being mostly organic, composed of plant and soil organic matter, whereas the contribution of inorganic C ($CaCO_3$ and DIC) is often considered of minor importance (Schlesinger et al. 2000; Paul 2007). Nevertheless, $CaCO_3$ formed in soils, i.e. secondary carbonates, are quite common and referred to as pedogenic carbonates. They are mostly mentioned in aridic to semi-aridic environments as calcretes or caliches (Phillips and Self 1987; Verrecchia et al. 1993; Dubroeucq et al. 1996; Arnand et al. 1997; Lal et al. 2000; Khormali et al. 2006; Alonso-Zarza and Jones 2007; Shankar and Achyuthan 2007), although their occurrence seems to be ubiquitous. This is probably due to the fact that in aridic to semi-aridic environments, they are easier to observe and more abundant, which makes them easy to study. However, pedogenic carbonates from intertropical, as well as temperate environments, have been regularly observed (Wright 1984 & 1986; Strong et al. 1992; Ould Mohamed and Bruand 1994; Becze-Deák et al. 1997; Loisy et al. 1999; Cailleau et al. 2005; Bajnóczi and Kovács-Kis 2006; Zhou and Chafetz 2009). Yet, in soils of humid climates, the soil C pool is usually dominated by organic C, whereas the opposite is observed in aridic and semi-aridic climates (Fig. 1.4).

Pedogenic carbonates usually occur as calcic or petrocalcic horizons. The calcic horizon as defined in the World Reference Base for soil resource (IUSS Working Group WRB 2006) is a horizon in which secondary $CaCO_3$ has accumulated in a diffuse form or as discontinuous concentrations. The petrocalcic horizon is defined as an indurated calcic horizon that is cemented by $CaCO_3$

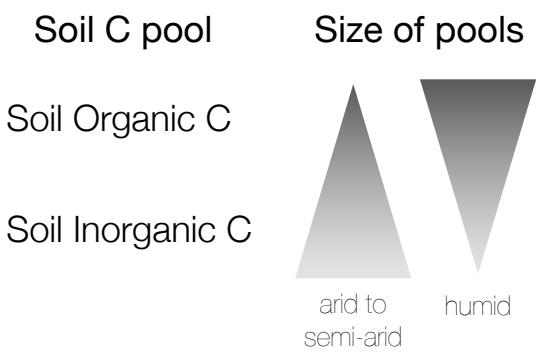

Figure 1.4 - Sizes and types of C pools in function of climatic zones.

and, in places, by calcium and some magnesium carbonate. It is either massive or platy in nature, and extremely hard. Other types of accumulations have been observed occurring as scattered nodules and concretions, which may not be classified in one of the two types mentioned above. Finally, the distinction of geogenic and pedogenic carbonates is sometimes difficult in soils where the parent material is made of gravely to stony calcareous material or where pedogenic carbonates are scarce (Lal and Kimble 2000).

The formation of pedogenic carbonates is the result of complex processes such as dissolution, translocation, and precipitation (Khormali et al. 2006). First, the variation of several factors may influence physicochemical parameters of the soil solution, leading to the further formation of secondary $CaCO_3$. Decrease in the pCO_2 and/or water content or an increase of the temperature, pH and/or calcium concentration are the factors that may directly influence $CaCO_3$ saturation. Carbonates from the parent substrate, are dissolved in the upper parts of the soil due to high humidity and high pCO_2 resulting from soil respiration; free Ca^{2+} and Mg^{2+} ions are leached to the lower parts of the soil. Furthermore, if pH and/or alkalinity as well as free Ca^{2+} allow it, secondary calcite may precipitate in these lower parts (Fig. 1.5).

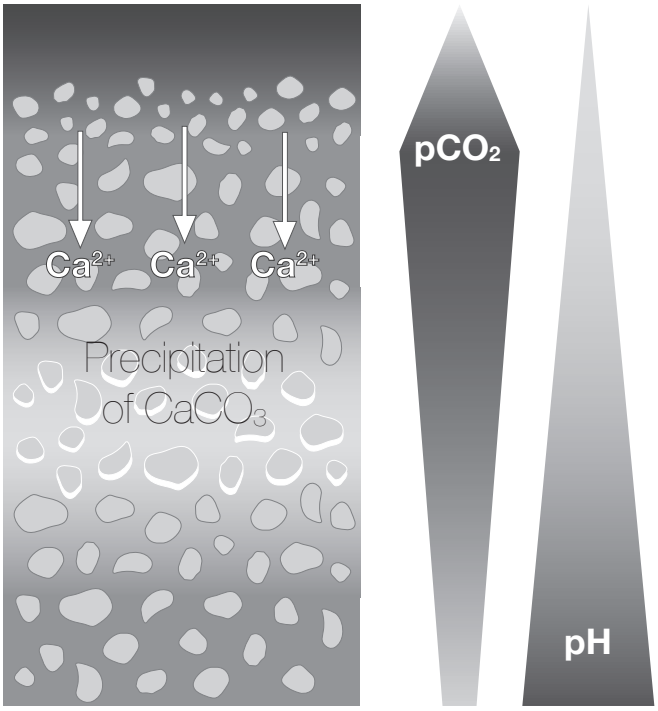

Figure 1.5 - Variation of the main physicochemical parameters, which may lead to the formation of secondary $CaCO_3$ in soils and surficial formations.

Pedogenic $CaCO_3$ is characterized by various micromorphological features, which are influenced by climate, vegetation, and parent material (Khormali et al. 2006; Zhou and Chafetz 2009). The most observed micromorphological feature is micritic clusters present as coatings or tiny grains. Other types are rhizoliths, i.e. calcified root cells, calcified filaments, spherulites and needle fibre calcite (Becze-Deák et al. 1997; Khormali et al. 2006; Shankar and Achyuthan 2007; Zhou and Chafetz 2009).

The distinction between geogenic and secondary carbonates is of importance considering the interpretation that can be drawn in relation to the C cycle. Indeed, the origin of the calcium source is critical in this issue. The importance of pedogenic carbonates lies on the fact that soil inorganic C (SIC) is considered as being more stable than soil organic C (SOC) regarding its mineralization into CO_2. The mean residence time of pedogenic carbonates in soils is in average 100 times higher than the one of organic matter (Schlesinger et al. 2000). The entire C sequestrated in this pool may therefore be withdrawn from the C cycle for a significant period of time. Hence, the size, as well as the turnover rates, of this pool are hence of importance when considering the global C cycle. Most importantly, the source of the calcium contained into pedogenic carbonates is also critical when considering the C cycle. Most of the time, secondary carbonates represent a redistribution of pre-existing calcium carbonate through the dissolution/re-precipitation of calcareous parent material. Nevertheless, in some cases, calcium (at least part of it) trapped into secondary $CaCO_3$ may derive from a carbonate-free source. In such a case, pedogenic $CaCO_3$ may represent a C sink rather than a transient C pool.

1.1.4.2 Secondary carbonates in caves

Secondary $CaCO_3$ deposits also occur in karstic caves, where they are called speleothems. By definition, speleothems are secondary mineral deposits formed by a physicochemical reaction from a primary mineral in a cave (Moore 1952). $CaCO_3$ predominates in most caves and a large number of studies have been done on stalagtites, stalagmites, helictites, moonmilk, pool fingers and cave pearls (see review in Northup and Lavoie 2001). Secondary carbonates in karstic cave actually result from pedogenic-related processes. As water percolates through the soil, its pH decreases due to soil organic acids present in the soil and because of high pCO_2. DIC of the percolating water then increases, enhancing the dissolution of the calcareous host-rock. Eventually, when this water reaches the cave environment, it becomes often supersaturated in $CaCO_3$ due to re-equilibration processes with the cave pCO_2 (Blyth and Frisia 2008; Curry et al. 2009). This property allows secondary $CaCO_3$ to precipitate, mostly by the physicochemical process of CO_2 degassing, but also under the influence of microorganisms (Barton et al. 2001). The biological influence on speleothems formation is actually a hotly debated subject in the field of cave geomicrobiology (Barton et al. 2001).

1.2 Importance of $CaCO_3$, an ubiquitous mineral in the biosphere

1.2.1 Reminder on crystal formation

To introduce $CaCO_3$ biominerals, a summary on the mechanisms of crystal nucleation and growth is necessary. Although biominerals are constrained to the same basic rules of formation than physicochemical minerals, they usually show complete different properties and morphologies than their physicochemical counterparts (Mann 2000).

1.2.1.1 Mechanisms of precipitation and nucleation

Precipitation of a mineral involves a change in physical state, which is termed nucleation. In conditions of supersaturation, ions tend to form metastable clusters and for these clusters to become real nuclei, an input of energy is needed, which is called the activation energy for nucleation (Simkiss and Wilbur 1989). The free energy required to form a nucleus (ΔG_N) corresponds to the difference between the free energy needed to form a new solid interface at the solid-liquid interface (ΔG_I) and

the free energy released by the bond formation in the solid phase (- ΔG_B ; Equation 4).

$$(4)\quad \Delta G_N = \Delta G_I - \Delta G_B$$

ΔG_N Free energy to form a nucleus

ΔG_I Free energy at the solid-liquid interface
Function of the surface area and always > 0

ΔG_B Energy released by the transition to the solid state
Function of the volume and always < 0

When ΔG_N is positive, a stable nucleus may be formed and precipitation can occur (Mann 2001). In addition, a critical cluster size is needed in order to form a stable nucleus. When the specific surface area is too large, no stable nucleus may be formed; only when the specific surface reaches a certain value, the growth of an existing nucleus is favoured in comparison to formation of new nuclei (Simkiss and Wilbur 1989).

Two types of nucleation are known, the homogeneous and a heterogeneous nucleation. Homogeneous nucleation occurs after spontaneous formation of nuclei in a supersaturated solution (Mann 2001), where the number of nuclei formed is a function of the level of supersaturation. This type of nucleation is actually rarely observed in natural environments, as there are always other ions or molecules present, which influence nucleation. Heterogeneous nucleation occurs when pre-existing surfaces are present in the solution. Any ions, molecules or surface may in this case act as nucleus. This type of nucleation requires less free energy of activation, as clusters form in contact with pre-existing nuclei (Simkiss and Wilbur 1989).

1.2.1.2 Crystal growth

A nucleus becomes a crystal when it increases in size by addition of ions on its surface. By definition, a crystal consists of atoms arranged in a repetitive pattern in three dimensions. This pattern is called the unit cell and its iteration is the crystal lattice. The unit cell is considered as a template for the whole crystal and is defined by three axis (a(x), b(y) and c(z)), which represent its dimensions in space (Fig. 1.6; Sands 1993). The addition of ions to the crystal faces happens in agreement with the crystal lattice but not as a uniform process as it occurs more likely in steps. This results in the formation of edges that are called active sites. They represent sites of higher binding energy, which drive the incorporation of further ions to the crystal face. Furthermore, each crystal face exhibits different surface energies, which depend on the position of the ions within the unit cell. As a result, each face of a crystal is characterized by a different growth rate. The fastest rate of growth occurs in the direction that is perpendicular to the face with the highest surface energy. As a result, the slow growing faces dominate the final crystal habit (Mann 2001; Yu 2006).

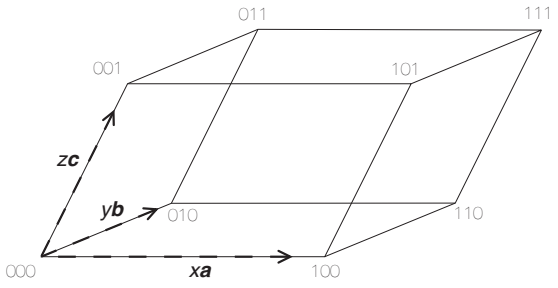

Figure 1.6 - Three-dimensional lattice system describing crystal growth.

1.2.1.3 Crystal habit

The habit of a crystal is characterized by the expression of its faces to the external environment (Mann 2001). In theory, the crystal habit is expected to correspond to the unit cell replication and amplification. However, it is well known that the same compound may exhibit many different habits.

Biominerals, in particular, exhibit a myriad of shapes that challenge the crystallographic rules (Mann 2000). Two aspects related to crystal growth are likely to exert a great influence on crystal shapes: first the variations in surface energy of the different crystal faces and second, the factors related to the external growth environment (Yu 2006).

Anything that alters the availability of active sites will have an effect on crystal growth rate, and hence, on the crystal shape. For instance, needle-shaped crystals exhibit a fast growth along one axis, plate-like crystals along two axes whereas isotropic crystals have grown at equal rates along their three axes (Mann 2001). A change in properties and morphology of crystals may be due to i) the presence of numerous defects on the crystal surface, ii) the overgrowth of another mineral phase, which is less stable, or iii) the presence of adsorbed foreign constituents, such as ions, organic molecules or macromolecules (Mann 2001). For instance, macromolecules or organic polymers adsorbed to specific faces may selectively inhibit the growth in certain directions, modifying the final crystal habit. Crystal habit can also be altered if growth occurs in a confined environment (Yu 2006). Finally, it has been shown that the habit of a crystal reflects more the nature of the environment in which it grows, than the unit cell geometry (Weiner and Dove 2003).

1.2.2 Occurrence of $CaCO_3$ in the biosphere

As already mentioned in a previous section, $CaCO_3$ is strongly related to the biosphere (Ehrlich 2002), although it can be physicochemical or biogenic in origin.

1.2.2.1 Abiotic $CaCO_3$

Physicochemical precipitation of $CaCO_3$ is the result of supersaturated conditions induced by processes, which are not related to any biotic process. Nucleation and growth of calcite are kinetically controlled processes (Lebron and Suarez 1998). Precipitation of $CaCO_3$ is a function of alkalinity and free Ca^{2+} available in the solution. When the product of the concentration of Ca^{2+} and CO_3^{2-} exceeds the solubility product constant of calcite (Equation 5; Simkiss and Wilbur 1989),

$$(5)\quad CaCO_3 \rightleftharpoons CO_3^{2-} + Ca^{2+}$$

$$K_{sp} = \left[CO_3^{2-}\right] \times \left[Ca^{2+}\right]$$

$$SI_{CaCO_3} = \log (IAP/K_{sp})$$

$CaCO_3$ saturation is reached. For instance, at atmospheric pCO_2 and 25°C, an aqueous solution is in equilibrium regarding calcite saturation if the pH is 8.4. Variations in temperature, pH, pCO_2, and/or alkalinity are the main factors influencing the saturation. For instance, a sharp decrease of the pCO_2 in an aqueous solution leads to $CaCO_3$ precipitation, as this is the case in karstic resurgences. Water that circulates within the karstic network has a very high pCO_2 and its re-equilibration with the atmospheric pCO_2 results in an intense CO_2 degassing from the aqueous solution, which causes the immediate precipitation of $CaCO_3$. Besides, high evaporitic conditions can also lead to the physicochemical precipitation of $CaCO_3$. This process is found in evaporatic deposits that occur in closed aqueous systems when evaporation exceeds the water input in form of precipitation (Cojan and Renard 1999).

However, the presence of extraneous substances, such as ions or organic molecules, can also change the solubility product constant of calcite, as well as modify both growth rate and habit of the crystal (Mann 2001). Consequently, calcite and other $CaCO_3$ polymorphs can be found in a

multitude of habits. Calcite, which has been precipitated due to purely physicochemical processes, should, for instance, displays a typical rhombohedral habit. However, in nature, calcite is more often observed in a variety of habits such as acicular and tabular forms or prismatic shapes (Mann 2000). These differences are the result of many different factors such as the presence of foreign ions or organic polymers, which act as crystal growth modifiers during physicochemical precipitation. Then, biological control on crystal growth is known to lead to extraordinary numerous and diverse $CaCO_3$ habits (Mann 2000).

1.2.2.2 Biogenic $CaCO_3$

On the other hand, biogenic precipitation of $CaCO_3$ is the result of processes that have been influenced, induced or controlled by biological activity.

$CaCO_3$ precipitated under, or related to, the influence of biological processes is widespread and represents a greater contribution to the $CaCO_3$ pool on Earth than physicochemical $CaCO_3$ (Ehrlich 2002; Skinner 2005). Moreover, $CaCO_3$ biominerals are the most common biominerals (Lowenstamm and Weiner 1989). Mineral formation under the influence of biological processes is called biomineralization. Different levels of biological influence on precipitation have been defined: i) tight biological control, ii) induction by biological activities and iii) passive biological influence (Dupraz et al. 2009). Biominerals are found in a myriad of different habits, and their recognition as biominerals is often difficult. For instance, biominerals from biologically induced or influenced mineralization often exhibit poorly defined shapes in contrast to biominerals formed under controlled conditions. However, biominerals represent critical indicators of past environmental conditions when observed in fossil records, as they are the witnesses of a biological activity (Weiner and Dove 2003). Therefore, their clear recognition as biominerals, and the processes to which they might be related, is of great importance (Weiner and Dove 2003; Dupraz et al. 2009).

1.2.2.2.1 Biologically controlled mineralization

Biominerals formed under biological control are the direct result of strict cellular processes, which control nucleation, growth, as well as morphology of the final mineral. This control involves specific genes (Mann 2000; Weiner and Dove 2003). Mineral formation may occur either inside cells, on their surface or on an external organic macromolecular matrix secreted by the organism. Biominerals produced under biological control typically display uniform particle size, well-defined composition and structure, complex morphologies as well as preferential crystallographic orientation. Biologically controlled mineralization is regularly encountered in unicellular organisms such as algae and protozoa, and extremely widespread in pluricellular organisms (skeletons, shells, etc.; Mann 2001).

1.2.2.2.2 Biologically-induced and biologically-influenced mineralization

In contrast to biologically controlled mineralization, mineral phases may be formed as a result of the interaction between biological parameters and their environment. Furthermore, there is a difference in the level of implication of the biological activity, either as an active or a passive process, in the conditions leading to mineral precipitation. While induced mineralization results from direct interactions between metabolic processes and their environment, influenced mineralization is the result of passive nucleation on organic matter (Dupraz et al. 2009). Some authors termed this process “organomineralization” to define such a process (Trichet and Défarge 1995; Dupraz et al. 2009; Défarge 2011).

Several metabolic processes have been recognized to induce changes of the physicochemical parameters of solutions, leading to its alkalinization and subsequent supersaturation in $CaCO_3$ (Mann 2001). For instance, oxygenic photosynthesis in aquatic environments, through the uptake of carbon dioxide, leads to the precipitation of $CaCO_3$. In aquatic environments, most of the CO_2 is present as HCO_3^-. Photosynthetic organisms possess therefore an enzyme called carbonic anhydrase, which releases an OH^- in order to provide CO_2 to the autotrophic metabolism (Badger and Price 1994). Other processes may cause alkalinization of aqueous solutions (Equations 6-9), such as oxalotrophy (Braissant et al. 2004), sulfatoreduction (Visscher and Stolz 2005), and ammonification (Castanier et al. 2000).

(6) Oxygenic photosynthesis

$$HCO_3^- \longrightarrow CO_2 + OH^-$$

$$CO_2 + H_2O \longrightarrow O_2 + <CH_2O>$$

(7) Oxalotrophy

$$2CaC_2O_4 + O_2 \longrightarrow 2Ca^{2+} + 2CO_3^{2-} + 2CO_2$$

(8) Sulfatoreduction

$$<CH_2O> + SO_4^{2-} \longrightarrow 2HCO_3^- + H_2S$$

(9) Ammonification

$$R\text{-}NH_2 + H_2O \longrightarrow CO_2 + NH_3$$

$$NH_3 + H_2O \longrightarrow NH_4^+ + OH^-$$

Biologically influenced mineralization relies on processes related to the environment to create the condition leading to $CaCO_3$ supersaturation. Living organisms are not directly required, only their organic by-products are of importance as template for nucleation. Trichet and Défarge (1995) defined organomineralization as a “precipitation mediated by non-living organic substrates in soils and sediments”. Typically, production of CO_2 in soils through heterotrophic root respiration and soil organic matter decay may also lead to modification of the physicochemical parameters of soil solution. While CO_2 is initially dissolved in the soil solution, resulting in a decline of the pH, a decrease of either soil humidity or soil atmosphere pCO_2 may lead to $CaCO_3$ supersaturation (Amrhein and Suarez 1987). In these conditions, organomineralization is likely to occur by nucleation of $CaCO_3$ on soil organic polymers that exhibit the ability to act as nuclei. Hence, some pedogenic carbonates and calcitic speleothems are likely to be the result of organomineralization processes.

1.2.2.2.3 Role of organic matrix in biomineralization

One central point to biomineralization theories is the preponderant role of organic matrices as templates for nucleation. For instance, nucleation occurring directly on cell walls is a well-known process (Mann 2001; Weiner and Dove 2003). On a molecular level, organic molecules containing acidic carboxylic groups are key players in calcite biomineralization due to the similarity of the carboxylic group to a carbonate ion (Mann 2001; Dupraz et al. 2009). Furthermore, any acidic molecule, which is able to bind Ca^{2+} might act in a similar way. In biologically controlled mineralization, an organized matrix, which has been secreted by the organisms under strict genetic control, constrains the crystal growth leading to highly defined and complex morphologies (Mann 2001). Minerals derived from biologically induced or influenced processes, on the other hand, have poorly defined shapes (Mann 2000). The organic matrix acts as a nucleation enhancer and directs

crystal growth, and influences, in a lesser extent, the crystal habit. Several organic polymers have been recognized as enhancers for calcite nucleation, such as cellulose (Dalas et al. 2000; Cailleau et al. 2009a), chitin (Manoli et al. 1997; Ehrlich 2010) and collagen (Ehrlich 2010). Interestingly, these polymers are the three most common polymers in the biosphere, emphasizing once again the intimate relationships that exist between $CaCO_3$ and the biosphere.

1.3 Importance of fungi as essential actors in natural environments

1.3.1 General description of structural features of fungi

Fungi are chimio-organo-heterotrophic organisms, therefore depending on organic matter in order to sustain their metabolism. They are ubiquitous at the surface of the Earth wherever oxygen is present. Some anaerobic fungi also exist, but they remain a peculiarity. Fungi obtain their carbon source either from dead organic matter (as saprotrophs) or from associations with living partners (either as mutualistic or parasitic symbionts). Mutualistic symbiosis may occur with plants (mycorrhizas), cyanobacteria and algae (lichen), and even with animals (Webster 1980; Gadd 2007). Fungi seem to be able to exploit virtually any source of organic C and consequently belong to many ecological categories. Fungi acquire their nutrients by absorption, meaning that they must first pre-digest their substrate using hydrolytic or oxidative exo-enzymes. Solubilized nutrients are then transported inside their cells.

The fungus kingdom is a monophyletic group, containing five phyla: Chytridiomycota, Zygomycota, Glomeromycota, Ascomycota and Basidiomycota (Paul 2007). Chytridiomycetes is a peculiar group of mostly parasitic fungi. Zygomycetes comprise many opportunistic fungi, either parasitic or saprotrophic. Glomeromycetes form characteristic associations with plants called endomycorrhizas. Ascomycetes and Basidiomycetes differ from these three groups, mainly in regard of mycelial characteristics (see below), but also because of their broader ecological distribution (Paul 2007). For these reasons, Ascomycetes and Basidiomycetes will be preferentially considered in the following descriptions.

1.3.1.1 Hyphae and mycelium

Most fungi have a branched filamentous growth habit. They exhibit an apical growth pattern and new apices arise by the creation of lateral branches. This particularity allows them to explore and exploit their environment while maintaining an exponential growth by branching. The vegetative structure of filamentous fungi consists of rigid tubular hyphae, which are composed of elongated cells arranged one after the other (Paul 2007). Hyphae of Basidomycetes and Ascomyctes are mainly 2-6 µm in diameter, but diameters down to 1 µm and up to 10 µm are not uncommon. Hyphae of Zygomycetes and Glomeromycetes are usually wider, between 10-20 µm in diameter (Dix and Webster 1995; Carlile et al. 2001; Paul 2007). The rigidity of hyphae is due to the presence of the fungal cell wall, a highly rigid structure, and because of the turgor pressure exerted by the protoplast on the inner side of the cell wall (Webster 1980; Klein and Paschke 2004). A mesh of hypha is called the mycelium (Fig. 1.7) and may be represented as a three-dimensional network of hyphae that has fractal properties. This pattern is of great advantage for fungi as they usually live in environments displaying both nutritional and structural spatio-temporal heterogeneities (Boswell et al. 2007). Moreover, the fungal mycelium is a dynamic and variable structure that may be represented by two components: the rigid and tubular hyphae and the cytoplasm that can move within the hyphal network (Klein and Paschke 2004). The active cytoplasm moves forward together with the expanding hyphal tips, leaving the older parts of the mycelium as empty tubes, as a result

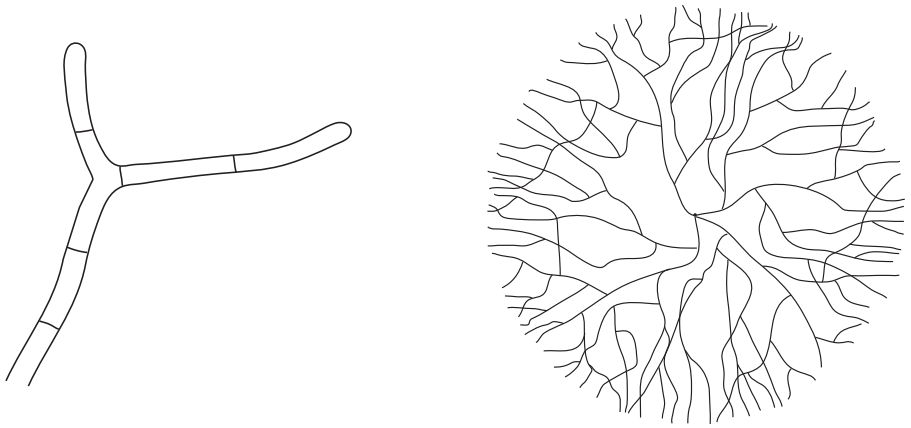

Figure 1.7 - Hyphal filamentous structure and the branched growth pattern of the mycelium.

of high vacuolization (Carlile et al. 2001; Paul 2007). This representation means that the cytoplasm is discontinuous in a given mycelium and is mostly present in actively growing and metabolizing hyphal tips, i.e. where nutrients are available. For instance, in soils, it has been shown that most of the hyphal network is actually made of empty hyphae (Jones and Mollison 1948). Eventually the cell wall of abandoned hyphae may serve as a nutrient source through autolysis and translocation of the nutrients to hyphal tips (Paul 2007).

1.3.1.2 The fungal ultrastructure

Fungi are eukaryotic organisms and possess most of the typical organelles of heterotrophic eukaryotes (Webster 1980). Their plasmalemma contains ergosterol, which is a typical fungal trait and thus often used in ecological studies as a biochemical proxy (Klein and Paschke 2004). Vacuoles are found in large quantities in fungal cells and tend to occupy most of the cell volume in sub-apical regions (Carlile et al. 2001). Behind the apices, which are the youngest and most active parts of a mycelium, hyphae become differentiated. As the number of septa increases, vacuoles are getting larger and the cell wall becomes thicker (Paul 2007). Eventually, the protoplasm entirely regresses leading to hyphae, which are virtually dead in terms of metabolism. Despite this fact, hyphae still perform their role of translocation, delivering nutrients to active parts of the mycelium.

Ascomycetes and Basidiomycetes usually have cross-walls or septa between individual cells. Septa of Ascomycetes are usually perforated (single pore or multiple perforations). Cytoplasmic continuity may be possible depending on the type and size of perforation. More complex septa called dolipores are present in some Basidiomycetes. They display a central pore covered with a membranous structure. It must be pointed out that septa have a role in the branching event, as new branches usually occur behind a septum regarding the direction of the cytoplasmic flow. Zygomycetes and Glomeromycetes, on the other hand, have coenocytic hyphae meaning that no septa are present and cytoplasm is thus continuous.

1.3.1.2.1 The fungal cell wall

Fungi possess a rigid, but labile, cell wall. Overall the fungal cell wall is composed of 80-90% of polysaccharides associated with proteins and some lipids. Basically, two main layers can be distinguished, an outer amorphous one and an inner skeletal or fibrillar one (Ruiz-Herrera 1992). On a finer scale, the outer amorphous layer is constituted of an outermost layer of hydrophobins (α-1,3-glucan) covering a layer of amorphous β-glucans (β-1,3-glucan and β-1,6-glucan) and mannoproteins. This amorphous layer turns gradually into a layer dominated by fibrillar polysaccharides, chitin

(polymerized N-acetylglucosamine) and unbranched β-1,3-glucan (Fig. 1.8). Finally, this innermost fibrillar layer is embedded in an amorphous glycoproteic matrix (Fig. 1.9). Moreover, fibrillar components of the skeletal layer are cross-linked with each other, resulting in a firm structure and enhancing even more the rigidity of the fungal cell wall (Fontaine et al. 1997; Bowman and Free 2006). This description is a generic one, valid mainly for Ascomycetes, Basidiomycetes, and Deuteromycetes, as the cell wall composition varies somewhat with the fungal taxonomy (Webster 1980). Finally, it should be pointed out that the fungal cell wall is a highly dynamic structure. Despite its enhanced rigidity, the presence of enzymes into the cell wall layers allows adaptation when needed.

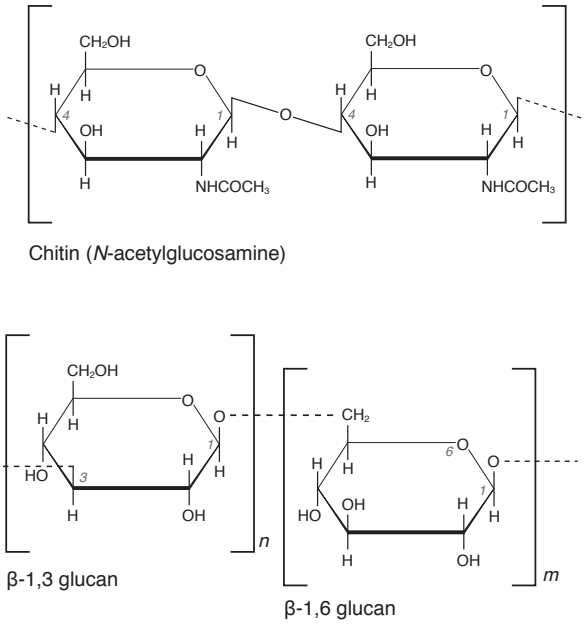

Figure 1.8 - Fibrous polymers from the fungal cell wall: chitin and β-glucan.

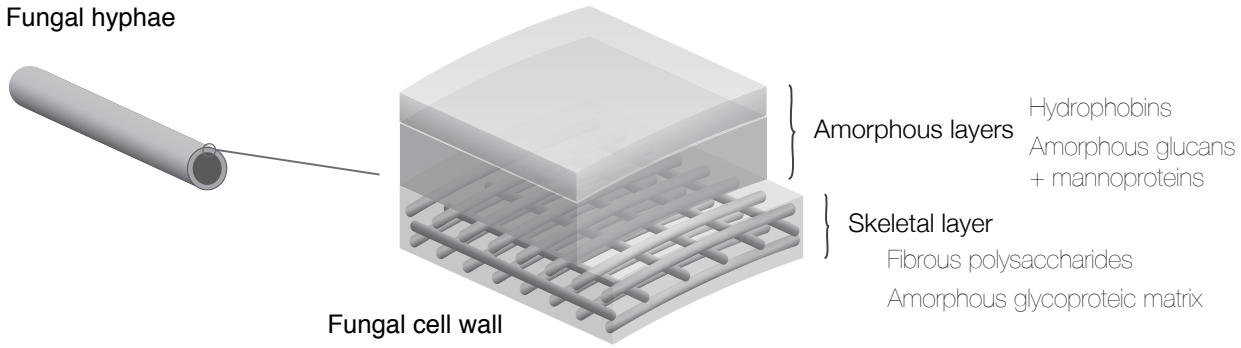

Figure 1.9 - The three main layers constituting the fungal cell wall. From the outer to the inner part: a layer of hydrophobins, an amorphous layer of glucans and mannoproteins, and a skeletal layer of fibrous polymers embedded into an amorphous glycoproteic matrix.

1.3.1.3 Aggregation of hyphae

Basidiomycetes and Ascomycetes have the ability to build specialized structures that are called mycelial strands (or cords) and rhizomorphs. These structures are made of tangentially aligned hyphae, which are able to translocate fluids bi-directionally. They allow fungi to explore their environment and to translocate nutrient to a distant part of the mycelium (Cairney 1991a). This feature is extremely important when foraging into heterogeneous environments. Rhizomorphs and mycelial strands have diameters up to 4 mm, but average dimensions are between 100 µm and 2 mm of diameter (Cairney 1991a). A 1 mm wide rhizomorph or mycelial strand may contain up to 1000 hyphae (Webster 1980).

A difference in structure exists between mycelial strands and rhizomorphs, the latter being defined as a much more differentiated structure (Watkinson 1979; Webster 1980; Carlile et al. 2001). Nevertheless, confusion exists between both terms, the term rhizomorph often being used for describing a mycelial strand (Cairney 1991b). The distinction between both types of structures is indeed rather ambiguous, as a continuum is observed, from undifferentiated bundles of hyphae to more complex structures leading to the highly differentiated pattern that may be observed in some

Armillaria sp. rhizomorphs (Fig. 1.10). Cairney (1991b) suggests that the term rhizomorph should be favoured for differentiated structures and that strand or cord should be used for less differentiated structures. However, the roles of mycelial strands and rhizomorphs remain the same that is, exploring the environment seeking for a nutrient source to further translocate nutrients to other parts of the mycelium.

The least organized pattern of a mycelial strand is represented by hyphae that have merged together in order to propagate through nutrient-poor areas. Furthermore, more organized forms show the presence of thinner hyphae at the outer part of the structure. These outer hyphae have thicker cell walls and are highly branched and anastomosed, in order to toughen the structure. This may lead to mycelial strands showing clearly differentiated inner and outer parts. The outer layer is made of very thin hyphae (down to 1 μm) with very thick cell walls (leading sometimes to the absence of the lumen). These external hyphae are dead and thus non-metabolizing units. In addition, they are melanized in order to enhance their resistance. Due to its composition, this outer layer shows a low permeability. The inner layer is made of wide hyphae with thin cell walls. These hyphae are alive and serve as vessels for the translocation of fluids from one place to another. The inner hyphae are weakly resistant to osmotic stress as they have very thin cell walls. Consequently, it is not unusual to observe mycelial strands or rhizomorphs with a missing inner part in natural samples (Cairney 1992). Nevertheless, studies suggest that translocation carries on, even in the absence of the inner living hyphae (Watkinson 1979). Finally, highly differentiated rhizomorphs of *Armillaria sp.*, by definition, display a basic structure with a cortex, a medulla and a lacuna (Watkinson 1979; Webster 1980; Carlile et al. 2001; Fig. 1.10).

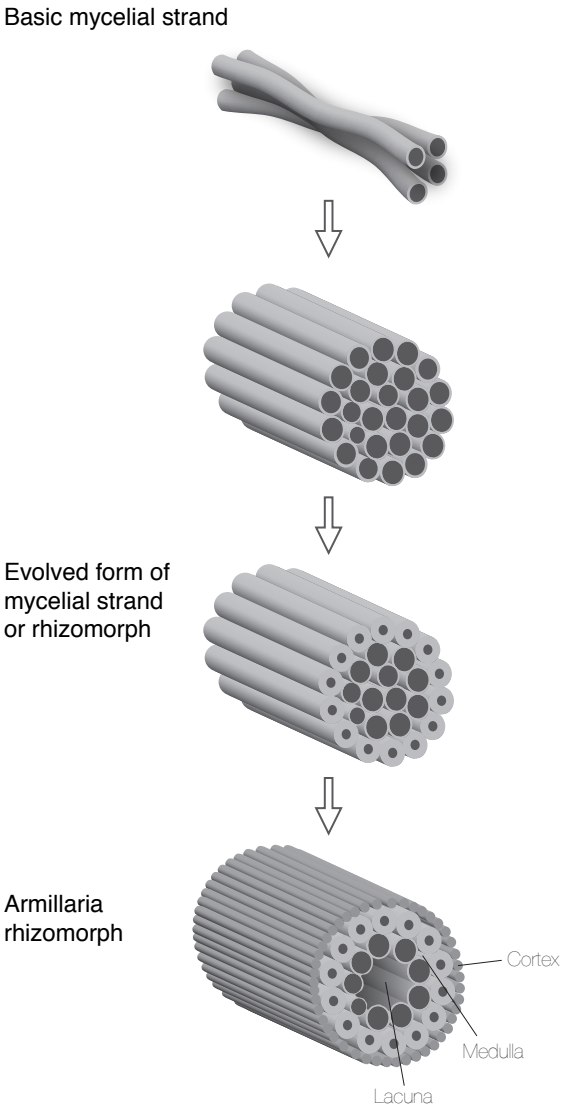

Figure 1.10 - The different types of mycelial strands/ rhizomorphs showing the evolution from the aggregation of a few hyphae to the complex organization of an *Armillaria* rhizomorph.

1.3.2 Fungi in natural environments

Fungi are widely distributed in terrestrial environments and are present virtually everywhere, as long as organic matter is accessible and oxygen is present. For instance, they may be encountered on plant surface as epibionts or as parasites, on rocks surfaces as symbiotic partners of lichens. They may also be associated to animals, mainly as commensal or parasitic partners (Carregaro et al. 2010). They are also present in water, where they are involved in particulate organic matter decay (Dix and Webster 1995). However, soil is believed to be their most characteristic habitat (Gadd 2007).

1.3.2.1 Fungi in soils

The branched filamentous growth habit of fungi, the formation of mycelial strands and rhizomorphs, as well as their resting structures such as spores and sclerotes, provide them with a great advantage in heterogeneous environments. Furthermore, their ability for mutualistic symbiosis, such as mycorrhizal symbiosis, and to produce extremely efficient oxidative exo-enzymes, are key-factors for explaining why fungi are ubiquitous in soils. In fact, they often represent the largest part of the soil microbial biomass (Gadd 2007). For instance, in a temperate soil, at a depth of 20 cm, the total fungal biomass has been estimated to 3'500 kg/ha, whereas the total bacterial biomass is 1'500 kg/ha (Gobat et al. 2003). Active fungi in soils are present either as saprotrophs or mycorrhizas. They play an important role in soils because of their ability to bind soil particles in their hyphal mesh. In addition, they produce exopolymeric substances, which enhance this binding effect even more. Furthermore, they are intensely involved in biogeochemical cycles at different levels, for instance through organic matter decay or mineral weathering.

1.3.2.1.1 Saprophytic fungi

A large part of soil fungi are saprophytic and thus feed on above- and belowground dead organic matter. Saprotrophy is of course prevalent in soils, and competition with other microorganisms is high accordingly. Nevertheless, only fungi can produce efficient lignolytic enzymes, which gives them access to cellulose trapped in lignocellulosic tissue of plants. In soils, where lignocellulosic compounds are widespread, this feature provides them with great advantages in comparison to bacteria (Paul 2007).

1.3.2.1.2 Mycorrhizas

Mycorrhizas are plant symbionts. In exchange of carbon from the plant, the fungal mutualistic symbiont provides the plant with water and nutrient. Moreover, through their hyphal mesh, fungi enhance water absorption and translocation of nutrients to plants. Fossil records from the late Ordovician suggest that fungal associates have mediated land colonization by plants (Coleman et al. 2004). Thereafter, it seems that this association has remained successful throughout geological times, as it has evolved into the five types of mycorrhizal symbioses that are known today (de Boer et al. 2005). Two main types of mycorrhizal symbiosis are oberseved, Endomycorrhizae (or AMF for Arbuscular Mycorrhiza Fungi) and Ectomycorrhizae (ECM). AMF belong to the Glomeromycetes, whereas ECM belong to Basidiomycetes.

AMF fungi are obligate plant symbionts. They are able to hydrolyse organic matter to liberate N and P, but they are not able to utilize C sources from soil organic matter (Paul 2007). AMF extend their hyphal network several centimetres (6-10 cm) away into the surrounding soil matrix (Coleman et al. 2004). They are mainly associated to herbaceous plants as well as tropical trees, and about 80% of land plants are plant species colonized by AMF (Smith and Read 1997).

ECM fungi are completely different regarding their physiology and ecology. They are not obligatory plant symbionts. Some ECM exhibit saprophytic capabilities and thus are able to obtain reduced C by other means. ECM hyphal network extends several meters away in the surrounding soil (Coleman et al. 2004). Mycelial strands are common ECM features, enhancing their exploring capabilities (Smith and Read 1997). In order to enhance weathering of minerals, ECM produce large amounts of organic acids. Nutrients liberated from the mineral substrate are further translocated to the plant. ECM are mainly associated to trees in temperate climates, and overall, 3% of phanerogam species are colonized by ECM (Pinaceae, Fagaceae, Myrtaceae; Smith and Read 1997). To note that those

3% may appear as a low number, however these are widespread tree species and thus represent an enormous biomass.

In soils, saprotrophic and mycorrhizal fungi are distributed along a vertical gradient, linked to the organic matter content (van Schöll et al. 2008). Saprotrophic fungi mostly colonize overlaying organic layers. Similarly, AMF are present in overlying horizons, in the vicinity of their associated plant roots. On the contrary, ECM colonize mineral layers below, where they actively participate to mineral weathering.

1.3.2.2 Fungi in caves

Regarding some environmental factors, cave environments can be compared to mineral soil layers. First, both mineral soil layers and caves are considered as oligotrophic environments. And second, light is present only in restricted areas such as cave entrances, but most of the cave environment is deprived of light. This fact prevents primary production through photosynthesis. For these reasons, caves are considered as extreme environments for life. However, physicochemical parameters, such as temperature and humidity, are buffered and constant throughout the year (Northup and Lavoie 2001). This fact probably allows, despite the extreme conditions, the presence of well-developed underground ecosystems in caves. Microbial communities are often well developed. They may feed either on exogenous organic matter or through chemotrophic-based ecosystems (Cunningham et al. 1995; Sarbu et al. 1996). Fungi, as heterotrophic organisms, are common cave inhabitants (Cunningham et al. 1995; Kirk et al. 2008; Jurado et al. 2010). Their ability to produce resting structures such as spores is an advantage in oligotrophic environments. Moreover, cave ecosystems may be connected to aboveground systems through rock fissures. Water, roots, and even mycelial strands may reach cave environments by these means (Jackson et al. 1999). Connections between caves and soils environments should be taken into account considering that tree roots can extend deep in soils, up to 7 meters in average (Canadell et al. 1996) and that ECM may greatly enhance this distance (Timonen and Marschner 2006).

1.3.1 Fungi in biogeochemical cycles

Fungi are well known as key players in several aspects of biogeochemical cycles. Within the last decades, numerous studies have been dedicated to this topic (Cromack et al. 1977; Gadd 1993; Jongmans et al. 1997; Gadd 1999; Burford et al. 2003; Hoffland et al. 2004; Fomina et al. 2005b; Schilling and Jellison 2005; Gadd 2006; Kolo et al. 2007; van Schöll et al. 2008) and have recognized fungi for their ability to resist to concentrations of toxic metals as well as for their implication in organic matter mineralization, mineral weathering, and metal-oxalate production. Yet, their implication in the genesis of other types of minerals remains poorly documented to this day, although fungi are suspected to be involved in much more biogeochemical processes than what is currently known (Sterflinger 2000; Verrecchia 2000; Burford et al. 2003; Gadd 2007). Geomycology is the field that investigates the interactions between fungi and mineral matter *lato sensu* (Gadd 2007).

1.3.1.1 Involvement of fungi in mineral weathering

The involvement of fungi in the efficient weathering of minerals results from their ability to exploit heterogeneous environments. The filamentous morphology and hyphal structure, as well as the production of molecules with acidolytic and complexing properties, are particularly relevant fungal features in mineral weathering. As a result, fungi may degrade mineral substrates through mechanical

and/or biochemical processes, leading to mineral dissolution and possible further authigenesis (Burford et al. 2003; Gadd 2007). Hyphae are rigid tubes, due to their highly resistant cell wall and the exerted turgor pressure inside hyphae, which allows easy penetration into mineral substrate at the micrometric scale (Jongmans et al. 1997; Fomina et al. 2007 & 2010; van Schöll et al. 2008). However, such mechanical processes are always associated to biochemical processes. These latter happen on the account of several mechanisms. First, production of CO_2 through organic matter respiration may contribute to mineral dissolution by decreasing the soil pH. Then, fungi orientate their growth through thigmotropism (contact with the substrate), using excretion of H^+ as a navigation system and hence enhancing mineral weathering solely by exploring their environment. Furthermore, fungi may excrete acidic molecules, either mucilaginous polysaccharides or organic acids, which are involved in the weakening of various minerals, such as carbonates for instance (Burford et al. 2003). The excretion of organic acids is a widespread fungal process of mineral weathering, resulting in the dissolution and complexation of metallic ions. The excretion of organic acids has been shown to be strongly correlated to the presence of toxic metals. It has been suggested that fungi use this property as a detoxifying pathway (Gadd 1993; Fomina et al. 2005a). ECM fungi are also known to excrete large amounts of organic acids in order to enhance mineral weathering. In these cases, it has been demonstrated that organic acid excretion is a function of nutrients availability (Leake et al. 2008).

Epi- and endo-lithic fungi (black meristematic fungi), lichens, and ECM fungi are the most commonly fungal categories cited as being involved in mineral weathering (Smith and Read 1997; Sterflinger 2000; Burford et al. 2003).

1.3.1.2 Fungi and calcium

Calcium is a crucial element for eukaryotic cells, as it is involved in many cell regulation processes (Pitt and Uglade 1984). However, Ca^{2+} is also strongly cytotoxic when present in high concentrations and is therefore under strict cellular control (Gadd 1993). Ca^{2+} in fungi is closely involved in apical growth mechanisms. Ca^{2+} should be present in high amounts at the apex for the hyphal tip to extend properly. Consequently, Ca^{2+} concentration within the fungal cell must be strictly controlled in order to allow proper growth, concentrating calcium at the apex and instantly decreasing it in subapical regions (Jackson and Heath 1993). Average concentrations of free cytoplasmic Ca^{2+} range from 100 to 350 nM, whereas at the tip, concentrations up to 2'600 nM have been observed. In order to keep this steep gradient, fungi have to efficiently regulate Ca^{2+}. Ca^{2+} enters the cytoplasm both actively and passively, so Ca^{2+} concentration in the cytoplasm is maintained at low levels by actively pumping it either out of the cell, or by sequestration in organelles (mitochondria, endoplasmic reticulum and vacuols), or by binding it onto cytoplasmic proteins (Calmodulins) and within the cell wall (Fig. 1.11; Pitt and Uglade 1984; Gadd 1993; Jackson and Heath 1993).

Fungi growing in Ca-rich environments, such as calcareous surficial formations, are exposed to high concentrations of Ca^{2+} in their growth environment. This likely represents a source of stress due to subsequent osmotic stress and Ca^{2+} cytotoxicity. The formation of Ca-oxalates has been suggested as a mean to immobilize excessive Ca^{2+} (Cromack et al. 1977; Whitney 1989; Gadd 1999). Precipitation of $CaCO_3$ by fungi may represent a similar passive mechanism leading to a decrease of their internal Ca^{2+} content. This process is documented for bacteria (Simkiss 1986; Schultze-Lam et al. 1996; Barton and Northup 2007), but remains a hypothesis regarding fungi. Furthermore, the fungal cell wall is considered as efficient in adsorbing metals. In environments with high metal concentrations, it represents a first rampart of passive metal immobilization (Gadd 1993). Among fungal cell wall polymers, chitin is known for its ability to bind Ca^{2+}, leading to possible

calcium bearing mineral nucleation (Manoli et al. 1997). Cell wall glycoproteins with available acidic groups may display a similar binding capacity (Gadd 1993).

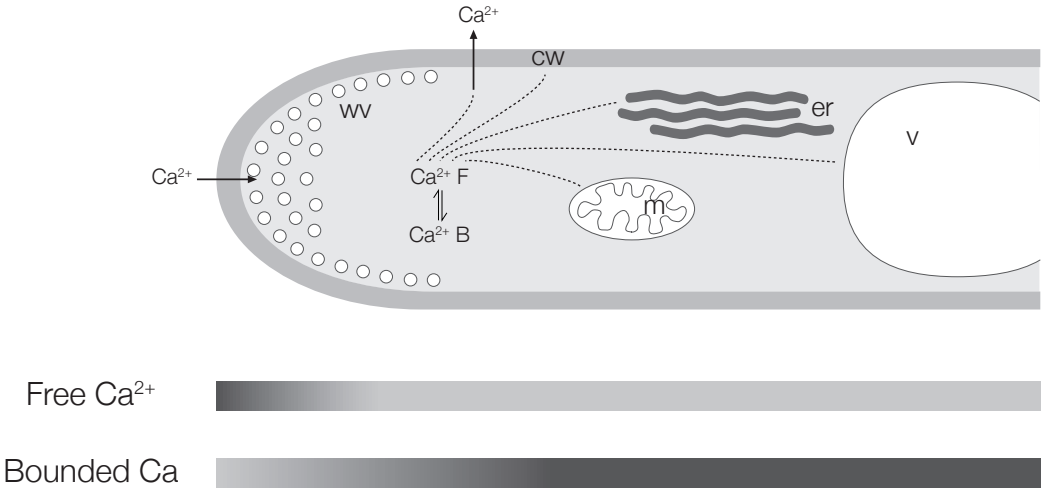

Figure 1.11 - Calcium homeostasis in the fungal hypha. **cw**: cell wall; **Ca^{2+} F** : free cytoplasmic Ca^{2+}; **Ca^{2+} B** : Ca^{2+} bound to cytoplasmic proteins; **er**: endoplasmic reticulum; **m**: mitochondria; **v**: vacuole. Ca^{2+} enters passively, mostly at the hyphal tip in order to create the high Ca^{2+} gradient. Ca^{2+} concentration in subapical compartments needs to be either actively pumped out, bound to the cell wall, or sequestrated into organelles by active transportation. Modified from Jackson and Heath (1993).

1.3.1.3 Metal-mineral precipitation mediated by fungi

Mycogenic minerals are common, either as a direct result of fungal metabolism or as a product of passive nucleation on fungal surfaces (Gadd 2007). Metal-oxalates have been extensively investigated, since fungi are known as common producers of organic acids (mainly citric and oxalic acids; Magnuson and Lasure 2004). Calcium oxalate is probably the most common mycogenic mineral, but several other metals may bind to oxalate. Other types of minerals have been observed associated with fungi and are assumed to be the result of fungal activity (see references in Gadd 2007).

1.3.1.4 Roles of fungi in calcium carbonate precipitation in terrestrial environments

Because calcite is an ubiquitous mineral in natural environments, recent studies have investigated the role of fungi in its precipitation. Ahmad et al. (2004), Burford et al. (2006), and Masaphy et al. (2009) have demonstrated the *in vitro* formation of calcite in the presence of fungi, indicating their possible involvement in the neoformation of this mineral in natural environments. Klappa (1979), Callot et al. (1985a), Phillips et al. (1987), and Verrecchia et al. (1993) discussed the origin of calcified filaments often observed in calcretes, assigning them a fungal origin. Callot et al. (1985b), Phillips and Self (1987), Verrecchia (1990), Verrecchia et al. (1990), and Verrecchia and Dumont (1996) discussed the possible implication of fungi in the formation of pedogenic calcite, including needle fibre calcite. As a consequence, the little information that may be found in the literature emphasizes the potential role of fungi in the precipitation of calcium carbonate. While bacteria have been recognized long ago as enhancing calcite precipitation (Simkiss and Wilbur 1989), it seems that fungi may play a significant role as well. Further investigations should therefore consider fungi as important actors in both weathering and precipitation of calcite.

This Ph.D. intends to develop this aspect by investigating the implication of fungi in the precipitation of needle fibre calcite and nanofibres, two ubiquitous habits of calcite from pedogenic and karstic environments.

Chapter 2

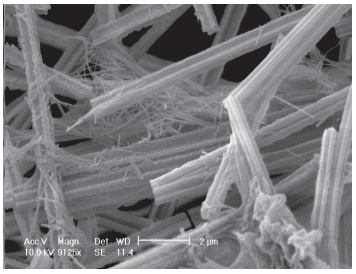

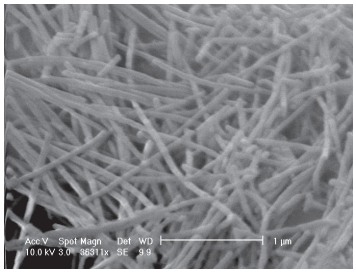

Needle Fibre Calcite & nanofibres

Chapter 2 - Needle Fibre Calcite and nanofibres, existing knowledge and new contributions

This chapter is intended as an update of the knowledge regarding Needle Fibre Calcite (NFC) and nanofibres. Consequently, it summarizes information from both, literature sources and observations realized in the frame of this study. First, morphological characteristics of NFC and nanofibres will be addressed (§ 2.1). Then, the main theories proposed to explain their respective origins will be synthesized under a critical perspective (§ 2.2). Next, their macroscopic appearance will be exposed, based mainly on the observations realized in the field during this study (§ 2.3). Finally, environments of deposition (§ 2.4) and climatic/environmental significance (§ 2.5) of NFC and nanofibres will be presented, again with the aim to compare literature sources and observations of this study.

NFC and calcitic nanofibres are ubiquitous calcitic habits from secondary calcium carbonate ($CaCO_3$) accumulations of vadose environments. Numerous authors have either mentioned their occurrence and/or attempted to explain their origin (Verrecchia and Verrecchia 1994 and references therein and a non-exhaustive but representative list of references: Ould Mohamed and Bruand 1994; Dubroeucq et al. 1996; Newman et al. 1996; Arnand et al. 1997; Becze-Deák et al. 1997; Gradziński et al. 1997; Cañaveras et al. 1999, 2001 & 2006; Loisy et al. 1999; Borsato et al. 2000; Cailleau et al. 2005, 2009a&b; Bajnóczi and Kovács-Kis 2006, Khormali et al. 2006; Alonso-Zarza and Jones 2007; Shankar and Achyuthan 2007; Blyth and Frisia 2008; Richter et al. 2008; Curry et al. 2009; Zhou and Chafetz 2009). Although they commonly occur in the environment, their origin remains enigmatic and hence highly debated. An extensive literature compilation demonstrates that its origin can be attributed to either physicochemical or biological processes (Annex 1). Moreover, NFC, and in a lesser extent nanofibres, are often used as paleoenvironmental and/or paleoclimatic proxies (Wright 1984 & 1986; Jones and Ng 1988; Strong et al. 1992; Becze-Deák et al. 1997; Borsato et al. 2000; Turner and Makhlouf 2005; Shankar and Achyuthan 2007). Thus, the clarification of their origin is essential in order to retrieve accurate information regarding the conditions that lead to the formation of both habits. Finally, it is important to recognize both features as distinct habits of calcite, with different characteristics and properties. Indeed, the study of NFC is not dissociable from the one of nanofibres, as many studies have shown their recurrent association (Vergès et al. 1982; Phillips and Self 1987; Jones and Ng 1988; Ould Mohamed and Bruand 1994; Verrecchia and Verrecchia 1994; Loisy et al. 1999; Cañaveras et al. 1999 & 2006; Curry et al. 2009).

2.1 Morphological characteristics of NFC and nanofibres

Verrecchia and Verrecchia (1994), as well as Cailleau et al. (2009b), have both made extensive review dedicated to NFC, which have led to the definition of a terminology based on basic morphologies of NFC and nanofibres. In this manuscript, their terminology will be used for addressing NFC, with the exception of the M-type (micro-rods) described in Verrecchia and Verrecchia (1994), which correspond to nanofibres (as defined by Borsato et al. 2000). In this manuscript, the term “nanofibres” will be preferred to M-type NFC, as they most likely have no genetic link with NFC (Phillips and Self 1987; Loisy et al. 1999; Bajnóczi and Kovács-Kis 2006) and thus are not considered to be NFC *stricto sensu,* as proposed by Cailleau et al. (2009b).

2.1.1 Needle Fibre Calcite

NFC is a needle-like, or acicular, habit of usually low-Mg Calcite (Phillips and Self 1987; Verrecchia

and Verrecchia 1994; Bajnóczi and Kovács-Kis 2006; Cañaveras et al. 2006; Richter et al. 2008). It exhibits an average width of 1-2 µm and a length from 4 to 10^2 times their width, depending on the authors and the environments from where they are described (see Table 1 in Verrecchia and Verrecchia 1994; Table 1 in Jones and Khale 1993 as well as Annex 1). Due to its high length to width ratio, NFC is a delicate habit, and hence lengths are extremely variable as needles may easily be broken in the natural environment. It is a monocrystalline habit of calcite (Vergès et al. 1982; Phillips and Self 1987; Borsato et al. 2000; Richter et al. 2008; Cailleau et al. 2009b) and several authors have demonstrated that the needle growth axis exhibits a deviation from the calcite *c*-axis. Using optical method (extinction of calcite under plane polarized light), Iwanoff (1906) showed a constant deviation of 40-50° and Mügge (1914) a deviation of 30-40°. Vergès et al. (1982) and Phillips and Self (1987), using electron microdiffraction pattern obtained with a Transmission Electron Microscope (TEM), showed respectively divergences of 45° and 44.6°. Finally, Richter et al. (2008) used Electron backscatter diffraction (EBSD) allowing crystallographic orientation of single needles to be measured in three dimensions. They have shown that the orientations of the crystallographic *c*-axis are independent of the morphological fibre orientation, with a needle growth axis coinciding to the *c*-axis up to a 90° divergence.

Lacroix (1901) has been the first to describe this peculiar habit as a mineral occurring in limestones cavities and having a *fibreuse* or *cotonneuse* texture. Then, in 1906 Iwanoff described a similar habit, which he thought was a distinct mineral species, and called it “lublinite”. Later on, numerous authors have mentioned this habit using different names such as “pseudomycelia” (Kubiëna 1938), “whisker crystals” (Supko 1971; Longman 1980) or “rhomb chains” (Jones and Ng 1988). Finally, Stoops (1976) proposed to use the term “needle fibre calcite”, and to keep the terms of lublinite, whisker crystals, and rhomb chains, to refer to needle-like calcite crystals made of flattened rhomb

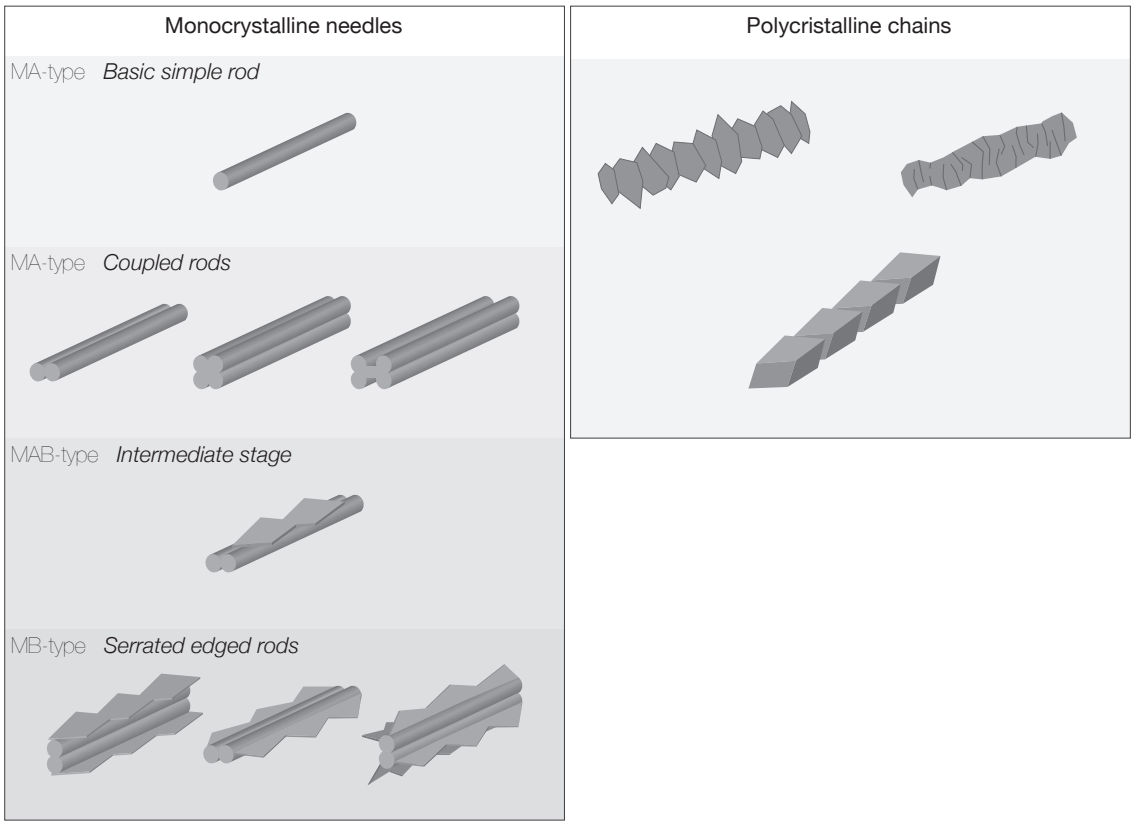

Figure 2.1 - Morphological classification of NFC after Verrecchia and Verrecchia (1994). Monocrystalline needles are represented by: MA-type needles, which are smooth needles composed of multiples rods; MB-type needles, which are serrated-edged all along the needle; and MAB-type needles, which are an intermediate form between MA- and MB-type. Polycrystalline chains are either polycrystalline forms of calcite or MB-type needles with large syntactic growths (rhomb chains; Cailleau et al. 2009b). Modified from Verrecchia and Verrecchia 1994.

crystals arranged in *en echelon* manner.

Two main morphologies of NFC are observed, monocrystalline rods and polycrystalline chains after Verrecchia and Verrecchia (1994) terminology (Fig. 2.1). Monocrystalline rods may exhibit several morphologies, either a smooth (and called the MA-type) or a serrated-edged (called the MB-type). Intermediate forms are observed and thus referred to as MAB types. Polycrystalline chains are the whisker crystals or rhomb chains as described above. As already mentioned, the M-type morphology actually corresponds to nanofibres (Borsato et al. 2000; Cailleau et al. 2009a) and will consequently be treated as a separate habit. Furthermore, at the scale of a single needle, a myriad of different shapes (either longitudinally or transversally) may be recognized, as reviewed in Cailleau et al. (2009b) and synthesized in their Figure 3. This is the result of slight variations at the surface of needles and, as a result, an exhaustive classification of all morphologies is not possible (Cailleau et al. 2009b). At a larger scale, needles may be organized in mesostructures, arranged either as random meshes (Fig. 2.2 a-b) or as bundles that may be ramified or not (Fig. 2.2 c-d).

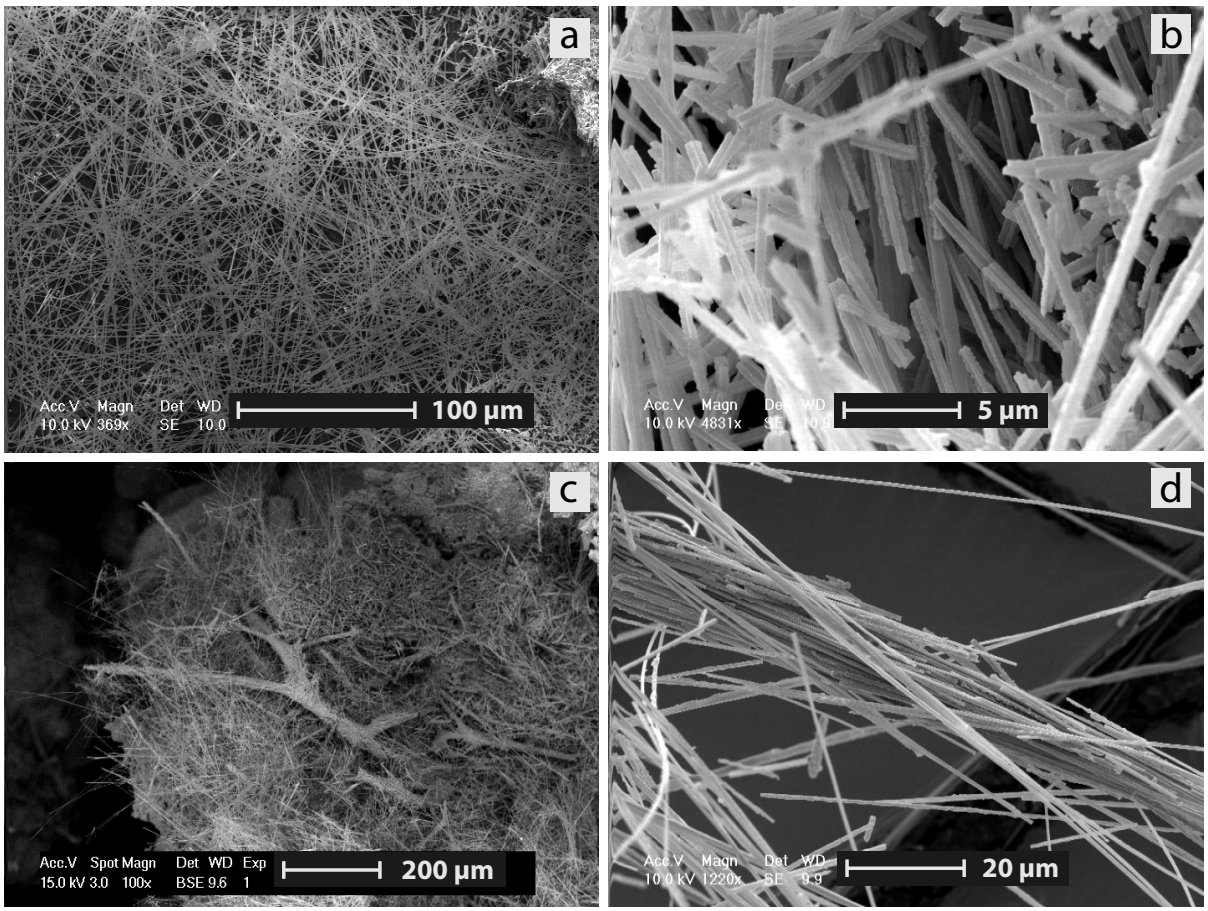

Figure 2.2 - SEM images showing the different organization of NFC into mesostructures. **(a)** Random mesh of NFC; "cotton ball-like" sample from the C horizon, Val de Benasque (SP07) site. **(b)** Close-up on random meshes showing MA-type needles and slightly serrated-edged needles of the MAB-type; "cotton ball-like" sample from the C horizon, Villiers (CH01) site. **(c)** CryoSEM image of ramified NFC bundles lying on a mesh of randomly organized NFC; "cotton ball-like" sample from the C horizon, Savagnier (CH04) site. **(d)** Close-up on a NFC bundle, showing needles arranged side-by-side; "cotton ball-like" sample from the C horizon, Val de Benasque (SP07) site.

2.1.2 Calcitic nanofibres

Calcitic nanofibres, referred to as nanofibres later on in this manuscript, are also elongated needle-like, or acicular, habit of low-Mg Calcite (Loisy et al. 1999; Borsato et al. 2000). They are very frequently observed in association with NFC as already mentioned, and this fact, together with their

morphological similarity, has sometimes led to a confusion between both habits. Nevertheless, their dimensions, as well as their shape, are different. Nanofibres exhibit an average width of 50 to 150 nm and length from 10 up to 10^4 times their width (see Annex 1). Several authors have demonstrated their monocrystalline nature using TEM microdiffraction analyses (Loisy et al. 1999; Borsato et al. 2000, Cailleau et al. 2009a). However, due to their tiny dimensions they are highly versatile under an electron beam and it has not been possible to accurately determine if the calcite *c*-axis corresponds or not to the morphological nanofibre orientation (Cailleau et al. 2009a). Vergès et al (1982) and Phillips and Self (1987) suggested a similar crystallographic orientation for both nanofibres and NFC as a result of their equivalent morphology. TEM measurements performed by Loisy et al. (1999) show a similar result, with the nanofibre length being parallel to the (104) direction. However, Borsato et al. (2000) show that the nanofibre morphologic orientation is parallel to the calcite *c*-axis. They have been able to measure nanofibres crystallographic orientation, probably because of the presence of strongly mineralized nanofibres. Indeed their TEM images suggest the presence of indentation on their surface (Borsato et al. 2000, their Figure 7d), which had probably allowed them to perform a microdiffraction analysis long enough to be able to deduce an accurate diffraction pattern. Richter et al. (2008) were not able to measure crystallographic orientations of nanofibres with EBSD due to their small sizes. As a result, no clear answer regarding the crystallographic orientations of nanofibres is available at present-day, due to the technical limitations put forth by Cailleau et al. (2009a) and Richter et al. (2008), as well as the contradictory results obtained by Loisy et al. (1999) and Borsato et al. (2000).

Nanofibres correspond to the M-type micro-rods described by Verrecchia and Verrecchia (1994) as proposed by Borsato et al. (2000) and later resumed by Cailleau et al. (2009a). They have been known in the scientific community for a long time, but, in many studies, have been either set aside in favour of NFC or wrongly interpreted as microbial filaments (Dubroeucq et al. 1996; Gradziński et al. 1997; Cañaveras et al. 1999). Due to this, many names have been given to these features: “hyphantic threads” by Klappa (1979); “calcite en bâtonnets” by Bruand (1980) and Pouget and Rambaud (1982); “petits cristaux de calcite en aiguilles” by Vergès et al. (1982); “micro-rods” by Phillips and Self (1987), Verrecchia and Verrecchia (1994), Loisy et al. (1999) and Bajnóczi and Kovács-Kis (2006); “needles” by Jones and Ng (1988); “rod-shaped nanobacteria like objects” by Benzerara et al. (2003); “nanofibres” by Borsato et al. (2000), Blyth and Frisia (2008), Cailleau et al. (2009a).

Contrary of NFC, nanofibres do not show extensive types of morphologies, their surfaces appear smooth and their cross section is round to pseudohexagonal (Loisy et al. 1999; Borsato et al. 2000). They are usually observed arranged into meshes that can either be randomly organized (nanofibres randomly distributed; Fig. 2.3 a) or show an organized pattern (nanofibres showing preferential orientations or organization; Fig. 2.3 b-c), ultimately they can also be found sparsely distributed (Fig. 2.3 d).

2.1.3 Differences between NFC and nanofibres

As already mentioned, NFC and nanofibres are distinct habit of low-Mg calcite. Several characteristic differences may be highlighted. Nanofibres sometimes show patterns that have been interpreted as the result of a contact deformation. These kinds of features have never been observed on NFC crystals (Cailleau et al. 2009a). Nanofibres are smooth single rods displaying a constant round section and, as emphasized by Phillips and Self (1987), no evidence of alteration of this shape have been observed. To the contrary, NFC exhibits a wide range of morphologies (cross-section and/or surface) varying from double rods to complex serrated forms as emphasized by Phillips and Self

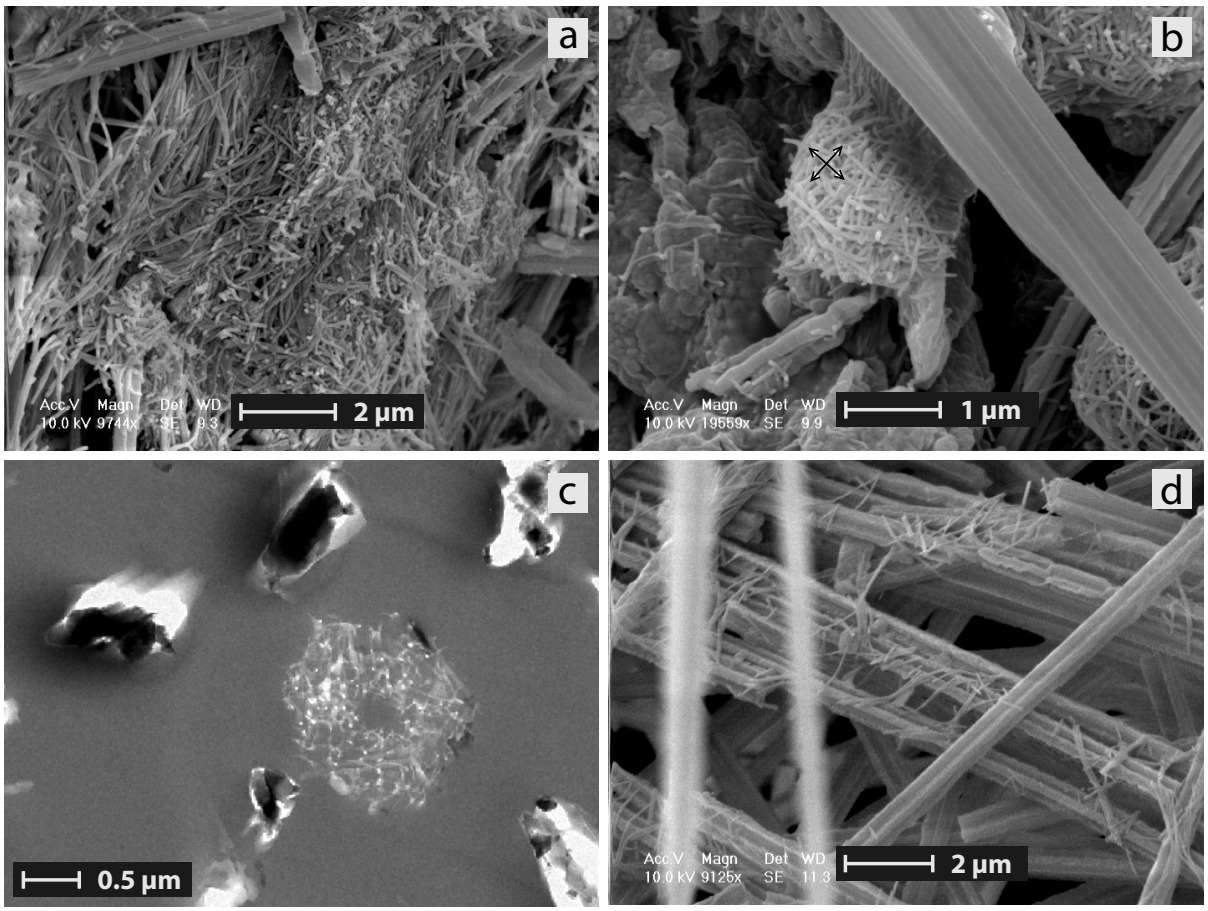

Figure 2.3 - Electron microscope images of different nanofibres organization. **(a-b-d)** SEM images, **(c)** TEM image. **(a)** Randomly organized mesh of nanofibres; "coating" sample from the C horizon, Villiers (CH01) site. **(b)** Organized mesh of nanofibres; note the preferential orientation of nanofibres; "cotton ball-like" and OM sample harvested at the interface between the B and C horizon, Villiers (CH01) site. **(c)** Transversal view of an organized mesh of nanofibres; note that nanofibres were removed while sectioning the sample and only their imprint in the resin remains; "coating" samples associated to a rhizomorph, Villiers (CH01) site. **(d)** Sparsely distributed nanofibres, lying on needles surfaces; "cotton ball-like" and "coating" sample from the C horizon, Villiers (CH01) site.

(1987), Verrecchia and Verrecchia (1994) and Cailleau et al. (2009b). Moreover, NFC often displays slight defects at its surface, whereas nanofibres have always a smooth appearance (Fig. 2.4).

Several authors point to the fact that they most likely have no genetic link, based on the points above and on their differences in dimensions (Phillips and Self 1987; Ould Mohamed and Bruand 1994; Loisy et al. 1999; Bajnóczi and Kovács-Kis 2006; Cailleau et al. 2009a). However, the fact that they are frequently observed together, often displaying an intimate relationship (Fig. 2.5), suggests that a related but non-genetic origin may be considered. As a result, a clear distinction between both habits is crucial and will lead to a better understanding of the condition leading to their formation. In addition, calcified filaments, as well as fungal hyphae coated with calcium-oxalate, are regularly observed in association with NFC and nanofibres accumulations (Klappa 1979; Callot et al. 1985a; Phillips et al. 1987; Verrecchia and Dumont 1996), which represent as well indicators of great value regarding the environmental parameters favouring NFC and nanofibres formation.

2.2 Hypotheses for the origin of NFC and nanofibres

Studies mentioning NFC and/or nanofibres are numerous, and so are the hypotheses regarding the origin of both features. Moreover, confusion between NFC and nanofibres as well as misidentification of NFC and nanofibres might have led to wrong interpretations regarding their origin (Jones and Ng 1988; Dubroeucq et al. 1996; Gradziński et al. 1997; Cañaveras et al. 1999).

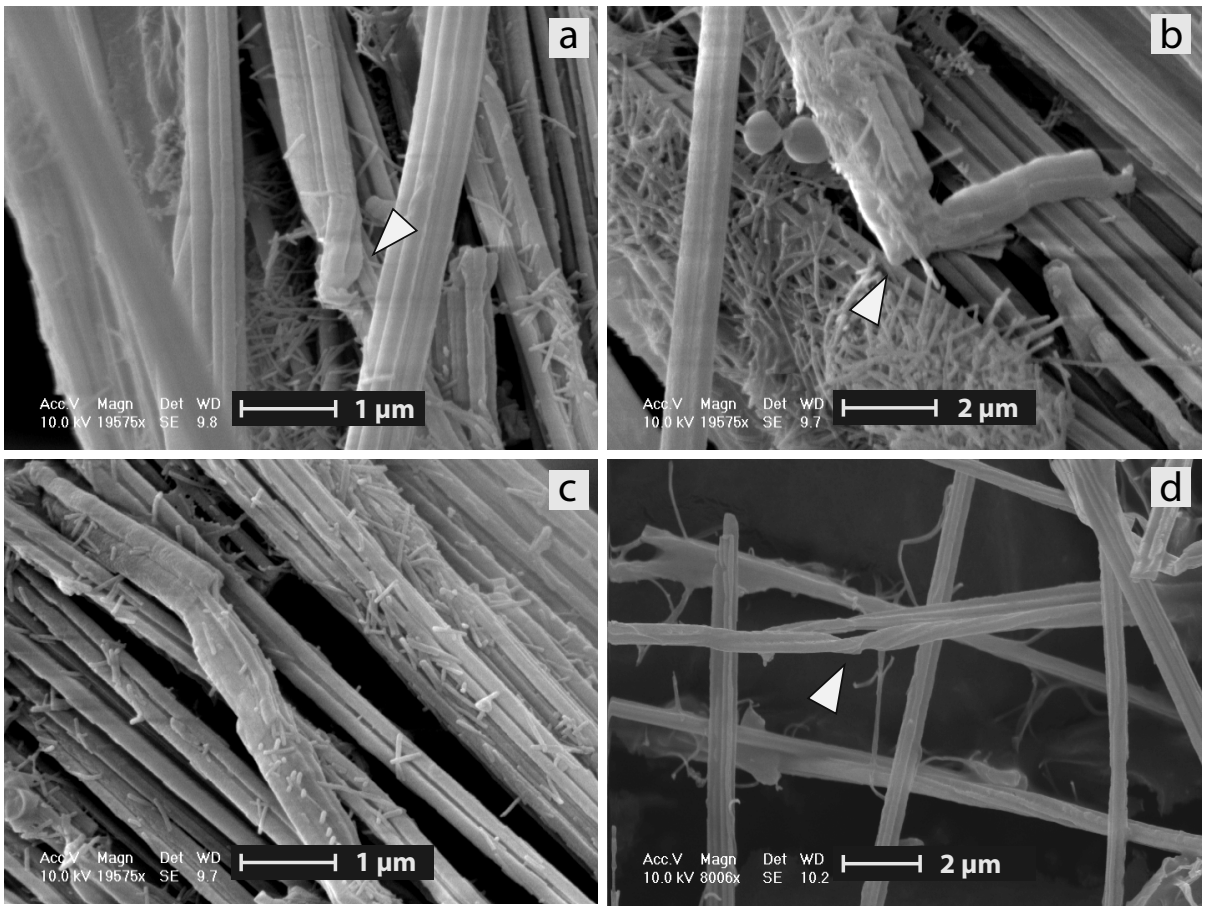

Figure 2.4 - SEM images showing the main differences between NFC and nanofibres : dimensions, contact deformations and surface defects. **(a-c)** "Cotton ball-like" and OM sample harvested at the interface between the B and C horizons, Villiers (CH01) site. **(a)** Needle showing a twisted end (arrow). **(b)** Needle showing a change in growth direction (arrow). **(c)** Needle showing an irregular shape. **(d)** Needle showing a twisted shape (arrow); sample of secondary calcite associated to a fungal strand harvested in a tropical soil from Bolivia (sample provided by M. Mota).

2.2.1 Origin of NFC

Processes ranging from purely physicochemical to biological phenomenon have been suggested to be at the origin of NFC. Numerous hypotheses have been proposed in order to explain the peculiar NFC morphologies and the divergence between the needle lengthening and the calcite *c*-axis. Hereafter, a small review on the main processes that have been mentioned in the literature is proposed in order to emphasize which processes could reasonably be taken into account for discussing the origin of NFC.

2.2.1.1 Hypotheses related to physicochemical processes

Some authors have proposed that NFC might be the result of physicochemical precipitation of highly saturated solutions and subsequent rapid growth under evaporitic conditions (Kubiëna 1938; Vergès et al. 1982; Jones and Ng 1988). An acicular habit is in theory the result of strong evaporitic conditions (Buckley 1951). Besides, the fact that NFC is always observed above the water table level emphasizes the possibility of a precipitation in high evaporitic conditions. These evaporitic conditions could be the result of highly variable climatic conditions prevailing in vadose environments with the alternation of humid and dry periods (James 1972). Likewise, the formation of NFC in cold-temperate climates has been proposed as a result of cryodessication, a process that may cause evaporitic stress (Kubiëna 1938; Cailleux 1965; Ducloux et al. 1984; Adolphe 1972). In addition, some authors

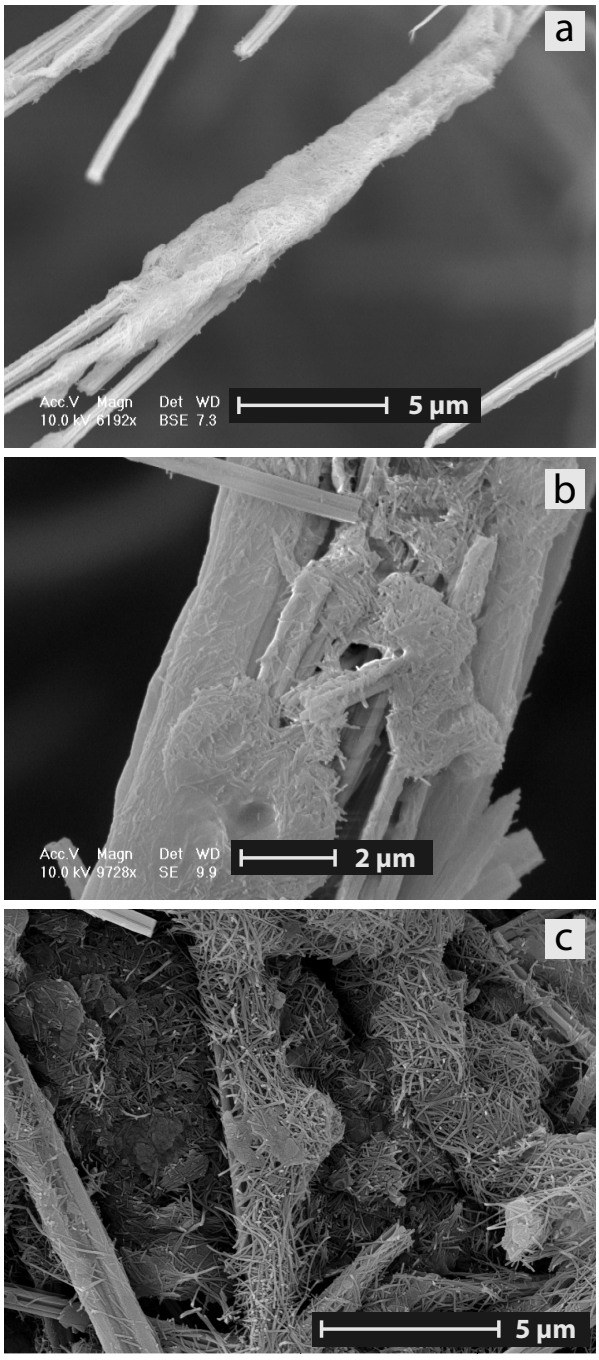

Figure 2.5 - SEM images showing the intimate relationship between NFC and nanofibres. **(a-b)** "Cotton ball-like" and OM sample harvested at the interface between the B and C horizon, Villiers (CH01) site. **(a)** CryoSEM image of a bundle of NFC embedded in a nanofibre mesh. **(b)** NFC bundle showing nanofibre meshes lying on it. **(c)** Nanofibre meshes associated to needles, apparently wrapping some of the needles; decaying OM sample associated with secondary CaCO3, harvested in the B horizon, Villiers (CH01) site.

have suggested that high-supersaturated conditions might be created through root suctions (Steinen 1974; Harisson 1977; Klappa 1980; Longman 1980; Braithwaite 1980; Calvet and Julia 1983; Ducloux et al. 1984). However, as NFC is also observed at some distance of roots, this hypothesis has not been retained. In order to explain the needle habit of NFC, some authors have proposed that the crystalline growth could have been inhibited in one or two directions by adsorbed ions or clays (James 1972; Pouget and Rambaud 1980; Durand 1980; Cañaveras et al. 1999). For instance, the needle habit is a well-known characteristic of aragonite or high-Mg calcite and the presence of Mg in the precursor solution might lead to the needle-like habit of NFC (James 1972). However, as NFC always consist of low-Mg calcite, this hypothesis could not be retained. Furthermore, the physicochemical hypothesis does not explain why the needle growth axis does not correspond to the calcite *c*-axis, as it should be the case if crystal growth occurred as a purely physicochemical process.

2.2.1.2 Hypotheses related to organic matter

Some authors have suggested that the crystalline growth could have been inhibited in one or two directions by adsorbed organic matter (Kubiëna 1938; Pouget and Rambaud 1980; Cañaveras et al. 1999). To the contrary of ions poisoning the crystal growth, this hypothesis seems more realistic as organic matter is well known as inducing divergences between the direction of crystal growth and the calcite *c*-axis (Turner and Jones 2005). Likewise, some authors have proposed the implication of microorganisms as indirect influences (e.g. as nucleation agents) mainly because these organisms were observed associated with NFC. Wright (1984) has proposed that NFC might be the result of an indirect precipitation by fungi involved in the decay of rootlets. Similarly, some authors proposed a heterogeneous nucleation on macromolecules produced by living organisms such as fungi, bacteria or roots (Strong et al. 1992; Cañaveras et al. 2006; Blyth and Frisia 2008). However, while these hypotheses might elegantly explain the divergence between the needle lengthening and the calcite *c*-axis, they still do not explain the complex, although well preserved, morphologies of NFC.

2.2.1.3 The fungal hypothesis

Finally, several authors have proposed that the crystalline growth might be constrained by an organic mould having the shape of a filament. As a matter of fact, four types of filaments may be recognized in soils and cave environments: algae, plant roots, actinomycetes, and fungi. Algae need light for their growth and therefore have not been considered as relevant actors in NFC genesis as NFC is also observed in area deprived of light, such as deep soils and caves. Plant roots should similarly be ruled out, as NFC is also observed at some distance from roots. Actinomycetes have more or less the same ecology as fungi in the sense that they do not need light, forage on dead organic matter and extend in the soil environment through hyphae. However, they have thinner hyphae (between 0.5 and 1 µm in diameter) than fungi. In addition, Actinomycetes hyphae are constituted of bacterial cells arranged one after the other restricting cytoplasmic continuity between them and thus being much shorter than the average NFC length. Therefore, fungal hyphae, with an average diameter between 2-6 µm, have been considered by several authors as the most relevant actor for NFC genesis (Callot et al. 1985b, Phillips and Self 1987, Ould Mohamed and Bruand 1994, Verrecchia and Verrecchia 1994, Cailleau et al. 2009b). NFC is proposed to precipitate directly into fungal hyphae. This hypothesis is based on the strong morphological and dimensional similarities between NFC and fungal hyphae. Furthermore, the implication of fungi is realistic for several other reasons. The environments where NFC is observed are typical fungal environments, with the presence of organic matter (or a link to it through mycelial networks of mycorrhizal fungi) and the lack of light. Then, fungi have an ambiguous relationship with calcium. While the apical region must be over-concentrated in order for the hyphal tip to extend properly, subapical regions have to be able to get rid of this calcium most efficiently due to high cytotoxicity of calcium (Pitt and Ugalde 1984; Gadd 1993; Jackson and Heath 1993). Therefore, the regulation of intracellular calcium is crucial regarding the fungal metabolism and calcium may be immobilized in organelles (e.g. vacuols, cell walls) or on cytoplasmic proteins. While exploring their environment fungi translocate fluids to other parts of the mycelium (Schütte 1956; Cairney 1992; Lindhal and Olsson 2004). In calcareous environments, solutions transiting into the hyphal network are likely to be calcium-rich and saturated in respect to calcite. Hence, nucleation may eventually happen into fungal hyphae. The fungal hypothesis has the advantage to explain both the divergence observed between the needle growth axis with the calcite *c*-axis and the constant morphological traits of NFC. Indeed, nucleation may happen anywhere inside the hyphae with the initial growth happening from randomly orientated nuclei embedded in an organic matrix (Richter et al. 2008). Moreover, the complex but highly reproducible morphologies of NFC are the result of the needle growth inside the constrained hyphal environment.

2.2.1.4 Critical perspective

Most of the studies have used observation methods, such as soil micromorphology and electron microscopy. This allows the relationships between the features to be studied with high precision, some basic analyses such as EDS (bulk chemical composition) and microdiffraction (crystallinity and mineral species) to be performed. However a precise determination of the chemical nature at the scale of one needle is arduous. Other authors have used methods such as isotopic signatures (Bajnóczi and Kovács-Kis 2006), mass spectrometry of fluid inclusion gas (Newman et al. 1996 & 1997), and DNA-based methods (Cañaveras et al. 2006) to decipher the origin of NFC. However, these analyses are based on “bulk” samples and it is not possible to know the exact microscopic assemblage of what is being analysed and thus, the results must be taken cautiously. Newman et al. (1996 & 1997) have analyzed fluid inclusions gas of pedogenic carbonates containing NFC and nanofibres. Surprisingly, methane (CH_4) has been detected as the dominant gas. Therefore, the authors have come to the conclusion that NFC could have been generated in anoxic conditions,

probably linked to the activity of methanogenic bacteria, which may lead to pH increase through CO_2 consumption (Castanier et al. 2000). Using C and O isotopic signatures of NFC Bajnóczi and Kovács-Kis (2006) conclude that NFC may be biogenic in origin, and therefore, support the fungal hypothesis. However, it must be pointed out that a biogenic signature does not allow a fungal- rather than bacterial-related process to be distinguished. Cañaveras et al. (2006) ruled out the implication of fungi as no fungal DNA sequences could be retrieved in their study using amplification of a 18S rRNA gene sequence. In addition, many studies devoted to moonmilk have shown a larger bacterial presence (mostly Actinomycetes) in moonmilk, either through cultivation-based approaches (Cacchio et al. 2004; Curry et al. 2009) or lipidic biomarkers (Blyth and Frisia 2008). However, all these methods have their own bias. In addition, it must be pointed out that the presence of a given organism does not necessarily means that it is actively involved in NFC and/or nanofibres genesis. As mentioned by Richter et al. (2008), the only way to demonstrate with certainty the origin of NFC and nanofibres would be to produce them in laboratory experiments.

2.2.1.5 Relationships between the different NFC morphologies

The different morphologies of NFC are probably genetically related, as emphasized by Cailleau et al. (2009b; Fig. 2.6). MA type needles (or simple needles) are considered as being the original shape, which is formed inside the fungal hypha. The basic unit is of a simple rod, and simple needles are usually composed of two or four rods (Verrecchia and Verrecchia 1994). These rods are supposedly

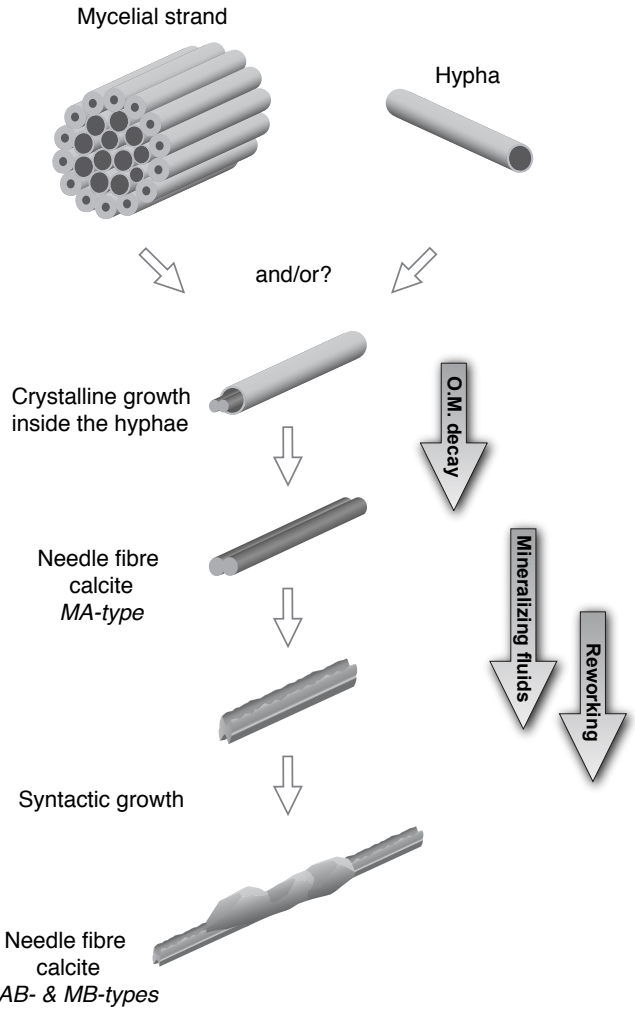

Figure 2.6 - Evolution of NFC after its release from fungal hyphae. The decay of the fungal hyphae leads to the release of MA-type needles. In the soil or cave environments, these latter may serve as template for syntactic growth of calcite leading to MAB- and MB-type needles.

welded in the fungal hyphae as they are always observed welded longitudinally. After their release from the fungal sheaths in the soil or cave microenvironment, simple needles may act as sites for the nucleation of syntaxial calcite through physicochemical precipitation of calcite, leading to MAB type needles (Verrecchia and Verrecchia 1994; Richter and Niggemann 1995; Cailleau et al. 2009b). The further growth of syntactic calcite eventually leads to MB types needles as well as rhomb chains. The transition from the MA to the MB type represents a step of early diagenesis. Indeed, needles with their high specific surface represent a good template for subsequent growth of calcite. Consequently, the great variety of NFC shapes is the result of environmental conditions, with the evolution of more complex forms starting from the basic smooth rods of the MA type.

2.2.2 Origin of nanofibres

Similarly to NFC, the origin of nanofibres is still a subject of controversy and these nanofeatures remain enigmatic at present-day. Moreover, there are more hypotheses for the origin of NFC than for nanofibres. First, this is due to the methodological limitations inherent to the fine study of sub-micrometric size objects. Indeed, until a few years ago, no method was available with a spot size small enough to focus on one nanofibre in detail (Richter et al. 2008; Cailleau et al. 2009a). Second, the fact that nanofibres are very often observed in close association with NFC has probably put nanofibres in the background of NFC features. Moreover, several authors have either wrongly assimilated them to bacterial mats (Cañaveras et al. 1999) and/or thought it was genetically related to NFC (Dubroeucq et al. 1996; Gradziński et al. 1997). However, some authors have attempted to critically discuss their origin either briefly or as a whole study (Klappa 1979; Phillips and Self 1987; Loisy et al. 1999; Borsato et al. 2000; Benzerara et al. 2003; Cailleau et al. 2009a). In addition, numerous hypotheses have been raised based on nanobacteria-like objects, which may be discussed in the frame of nanofibres origin. Current hypotheses propose purely physicochemical processes, mineralization of rod-shaped bacteria or the involvement of an organic template as a nucleation enhancer and/or crystal growth modifier.

2.2.2.1 Physicochemical processes

Several authors have proposed a physicochemical origin for nanofibres (Vergès et al. 1982; Jones and Ng 1988; Jones and Khale 1993; Borsato et al. 2000; Jeong et al. 2006). This hypothesis is mainly explained by the same basic assumptions that led to confer a physicochemical origin to NFC. The elongated shape of these crystals is the result of a precipitation and crystalline growth due to rapid evaporation from a highly supersaturated solution in an aridic environment (Vergès et al. 1982; Jones and Ng 1988; Jones and Khale 1993; Jeong et al. 2006). Borsato et al. (2000), in their study on cave moonmilk, propose that the defect-free pattern of nanofibres is the result of a Vapor Liquid Solid (VLS) mechanism. This process typically allows the growth of a crystal into the shape of a nanofibre from a vapour phase. A liquid phase is created at the tip of the fibre, incorporating constituents of the vapour phase. This leads to a raise in the supersaturation level and thus reduces the surface energy for subsequent crystal growth (Olstza et al. 2004; Zhu et al. 2009). They support their hypothesis by the facts that cave atmosphere is saturated with water vapour and that hydroaerosols as well as dust containing Ca^{2+} and CO_3^{2-}, may be present in the cave environment. Given these observations, unidirectional growth of a calcite crystal may occur through a VLS growth mechanism. However, this mechanism does not explain the existence of highly organized objects composed of nanofibres, such as the one observed in several studies (Klappa 1979 their Figure 3b; Ould Mohamed and Bruand 1994 their Figure 4e; Borsato et al. 2000; their Figure 5; Richter et al. 2008 their Figure 3; Cailleau et al. 2009a their Figure 1).

2.2.2.2 Calcification of rod-shaped bacteria

Several authors proposed the mineralization of rod-shaped bacteria to be at the origin of nanofibres (Phillips and Self 1987; Ould Mohamed and Bruand 1994; Verrecchia and Verrecchia 1994; Dubroeucq et al. 1996; Gradziński et al. 1997; Loisy et al. 1999). This hypothesis is mostly based on morphological similarities. Indeed, nanofibres form densely intertwined meshes that may look alike bacterial mats. As a consequence, some authors have directly identified these nanofibres mats as microbial mats (supposedly Actinomycetes) using electron microscopy (Dubroeucq et al. 1996; Gradziński et al. 1997; Cañaveras et al. 1999; Loisy et al. 1999). Gradzinski (1997), as well as Loisy et al. (1999), proposed a subsequent calcification of these microbial mats. Phillips and Self (1987), as well as Ould Mohamed and Bruand (1994), interpret nanofibres as being calcified rod-shaped bacteria that were actively associated to the decay of fungal hyphae and/or rhizomorphs. They based their hypothesis on the work of Boquet et al. (1973) who demonstrated that soil bacteria where able to induce calcite crystal formation. However, regarding average sizes of nanofibres, the hypothesis of the mineralization of rod-shaped bacteria suggests that these bacteria are rather nanobacteria. Yet, a controversy exits regarding the putative existence of nanobacteria (Folk 1993; Folk and Lynch 2001). Maniloff et al. (1997) have defined that the lowest diameter for a cell to be viable must be 0.005 μm^3. According to this assumption, Kieft (2000) states that nanobacteria defined by Folk (1993) would have no space for a cytoplasm. Even if the lower size limit for a living cell has still to be defined with precision, it is quite unlikely that they would have a diameter lower than 0.2 µm. This theoretical size limitation arises from solution chemistry. Indeed, solute concentration within cells is often at the level of micromoles (µM) and consequently a very small biovolume would be too limited to allow the presence of at least one molecule (Kieft 2000). Accordingly, regarding the above points, natural nanofibres exhibit dimensions under the reasonable limit for a viable cell. With an average diameter of 80 nm and an average length of 500 nm, the total bio-volume is 0.0025 μm^3, which is two-fold smaller than the limit of 0.005 μm^3 defined by Maniloff et al. (1997). As a consequence, the nanofibres with diameters above 200 nm could possibly be nanobacteria. Then again, their presence at such high densities (as represented by the presence of dense meshes of intertwined meshes) in oligotrophic environments such as caves and deep soils remains odd. Therefore, the hypothesis of the mineralization of nanobacteria seems rather unlikely, although it can not be completely occluded based on present-day knowledge.

2.2.2.3 Involvement of an organic template

Alternative origins for nanofibres propose the involvement of organic templates. These latter may act as enhancers of calcite nucleation and/or as crystal growth and shape modifiers (Benzerara et al. 2003; Olstza et al. 2004; Cailleau et al. 2009a; Zhu et al. 2009). This hypothesis lies between physicochemical and biogenic processes, as it involves the presence of organic matter, but the processes of precipitation and crystal growth do not necessarily happen as the direct result of a biological activity. This type of process may be defined as organomineralization (Trichet and Défarge 1995). Several studies related to biomimetics have attempted to reproduce the nanofibre shape using template-assisted synthesis and successfully achieved it (Olstza et al. 2004; Homeijer et al. 2008; Zhu et al. 2009). However, it must be pointed out that experimental protocols usually poorly reproduce conditions from the natural environment. Yet, Olstza et al. (2004) have artificially produced monocrystalline calcitic nanofibres with striking similarities to both NFC and nanofibres using a Solution-Precursor-Solid Mechanism. Briefly, pre-existing calcite substrate crystals were coated with a polymer-based precursor composed of acidic macromolecules, immersed in a Ca-rich solution and exposed to CO_2 vapours at room temperature. This process may explain the nanofibres shape, but not NFC as the fibre morphological orientation corresponds to the calcite

c-axis. However, their synthetic fibres lack the usual smooth appearance of natural nanofibres. Moreover, their hypothesis requires the presence of a pre-existing substrate, which constraints the growth, and thus, does not explain the presence of organized structures of nanofibres such as shown in Figure 2.3 (b-c) and observed by several authors as already mentioned. Closer to environmental conditions, Cailleau et al. (2009a) have proposed the involvement of naturally-occuring nanofibrous polymers, such as cellulose. The nucleation of calcite on organic fibrous polymers has been demonstrated in laboratory experiments by several authors (Manoli et al. 1997; Dalas et al. 2000; Cailleau et al. 2009a; Ehrlich 2010). Nanofibrous organic polymers are widespread features of biological systems as components of the cell walls of plants and fungi (Paul 2007). Moreover, they are arranged in higher order structures, i.e. the cells and the organism made of these cells.

2.3 Description of the different macrofacies: Microscopic fabrics and corresponding macroscopic facies

At a macroscopic scale, secondary $CaCO_3$ accumulations composed of NFC and nanofibres appear as different macroscopic facies. A relationship exists between the large-scale and the fine-scale and each macroscopic facies is expressed by specific microscopic characteristics. It is the amount of each type of NFC or nanofibres, their mutual relationships in terms of structure, and the water content that define the various types of macroscopic facies. Similarly, Zhou and Chafetz (2009), in a study dedicated to biogenic features in caliche from Texas, have emphasized that each type of large-scale feature, such as calcified root structures and laminar crusts, is composed of a specific set of fine-scale mineral components.

In pedogenic environments, three types of macroscopic facies may be described: i) cotton ball-like, ii) coatings on soil grains or soil pores and, iii) alveolar or indurated facies. In caves, two types of macroscopic shapes are observed, cotton-balls and white plastic and porous coating covering cave walls, the latter being the most common facies described in the literature.

The following description is mostly based on the observations performed in this study. Of course, several authors have mentioned the occurrence of these facies using other names. These studies will be mentioned only if some points need to be emphasized or clarified.

2.3.1 The “cotton ball-like” facies

This facies appears as white fluffy aggregates similar to cotton balls (Fig. 2.7 a). Its microscopic assemblage is composed of NFC associated with low amounts of nanofibres and has a low water content (Table 2.1). Needles are mainly present as simple needles of the MA or MAB type. They are mostly arranged as random meshes (Fig. 2.7 b) or as bundles, these latter being branched or not. Most of the nanofibres are present associated with these bundles, lying on their surface together with amorphous material (Fig. 2.7 c-d). Rhizomorphs, and less often roots, have been observed associated with this facies. To note that this facies may be observed in association with organic matter at the interface between the B and C calcic horizon. In caves, a similar facies as been described by Curry et al. (2009) under the name of cotton balls, but has not been observed in this study.

2.3.2 The “coating” facies

This facies is an unconsolidated white and plastic paste, which becomes powdery when dry. In soils, it is present as coatings on surfaces, either soil grains or soil pore surfaces (Fig. 2.8 a). This facies

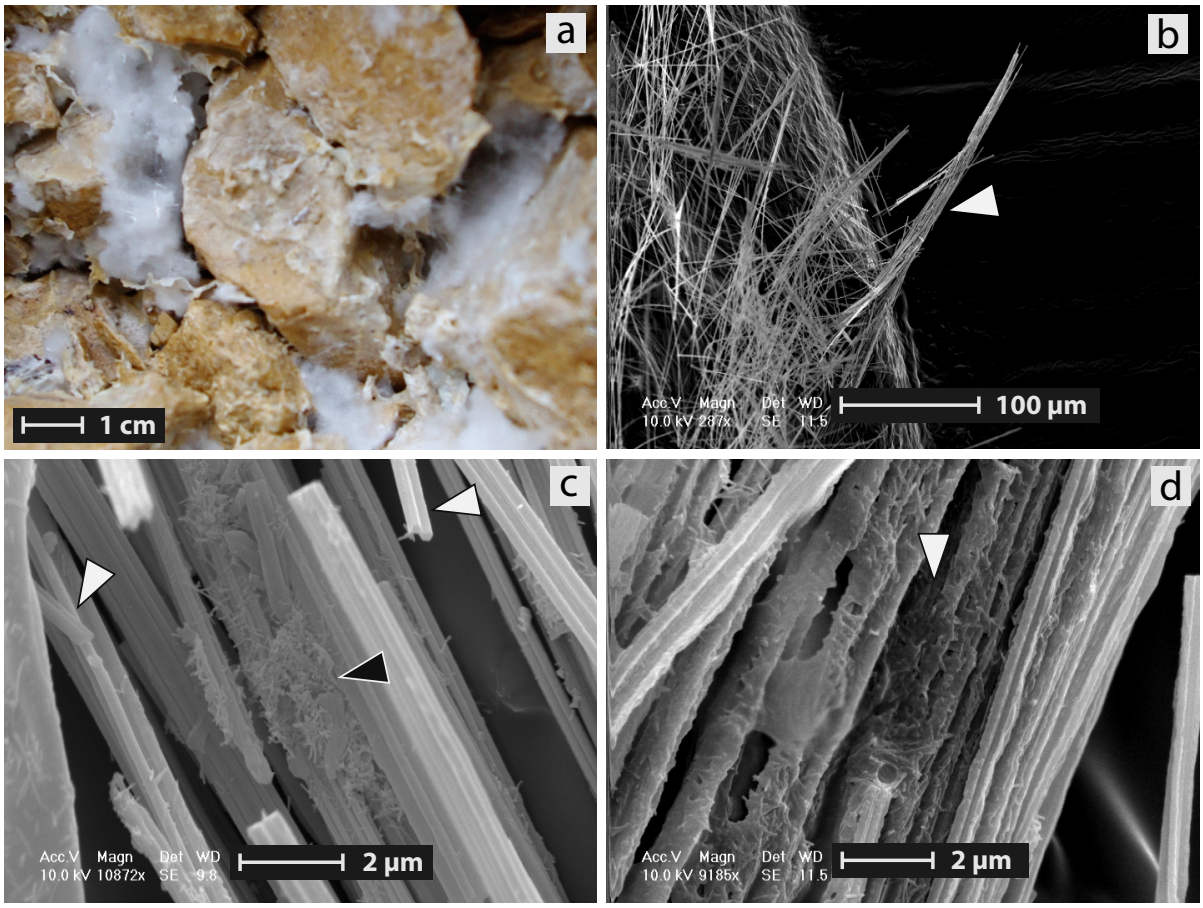

Figure 2.7 - "Cotton ball-like" macroscopic facies and associated microscopic assemblage, Villiers (CH01) site. **(a)** Picture showing its macroscopic appearance as cotton-balls filling inter-grain pores of the C horizon. **(b)** SEM image showing typical random meshes and NFC bundles of the "cotton ball-like" facies; sample harvested in the C horizon. **(c)** SEM images showing MA type needles (white arrows), closely associated to nanofibres (black arrows); sample from the interface between the B and C horizons. **(d)** SEM image showing amorphous material associated to nanofibres (arrow), lying on the surface of a NFC bundle; sample harvested in the C horizon.

Table 2.1 - Mean water content (%) in each of the macroscopic facies, at the exception of the alveolar one. *SD* = standard deviation; n=number of measured samples.

Facies	Water content (% H_2O)		
	Mean	*+/- SD*	n
Cotton-ball-like	8.17	*9.45*	3
Coatings	46.63	*7.47*	7
Moonmilk	67.11	*4.4*	5

corresponds to the typical moonmilk facies, which is described as a white plastic and porous coating covering cave walls (Fig. 2.8 b; Cañaveras et al. 2006). The microscopic assemblage consists of NFC associated to large amounts of nanofibres (Fig. 2.8 c-d). This facies contains a very high water content, up to 45% of its dry weight (Table 2.1). Needles are either simple (MA type) or can have syntactic calcite, leading to MAB as well as MB type needles. Polycrystalline needles may also be observed. This facies may be observed in association with organic matter at the interface between the B and C calcic horizons. In addition, numerous rhizomorphs have regularly been observed either at the surface of or totally embedded in coatings. This point has already been mentioned by Callot et al. (1985b).

2.3.2.1 Moonmilk, an analogous facies from cave environments

At this step, it is necessary to define the term moonmilk, which describes a deposit from cave environments. Also known as “mondmilch”, this facies has 79 synonyms depending from the country according to Hill and Forti (1997), thus demonstrating its ubiquitous distribution worldwide. Moonmilk is defined as a microcrystalline aggregate cave deposit with variable mineralogy, high water content (up to 67 %; Table 2.1), high porosity, and distinguishable macro- and micro-textures

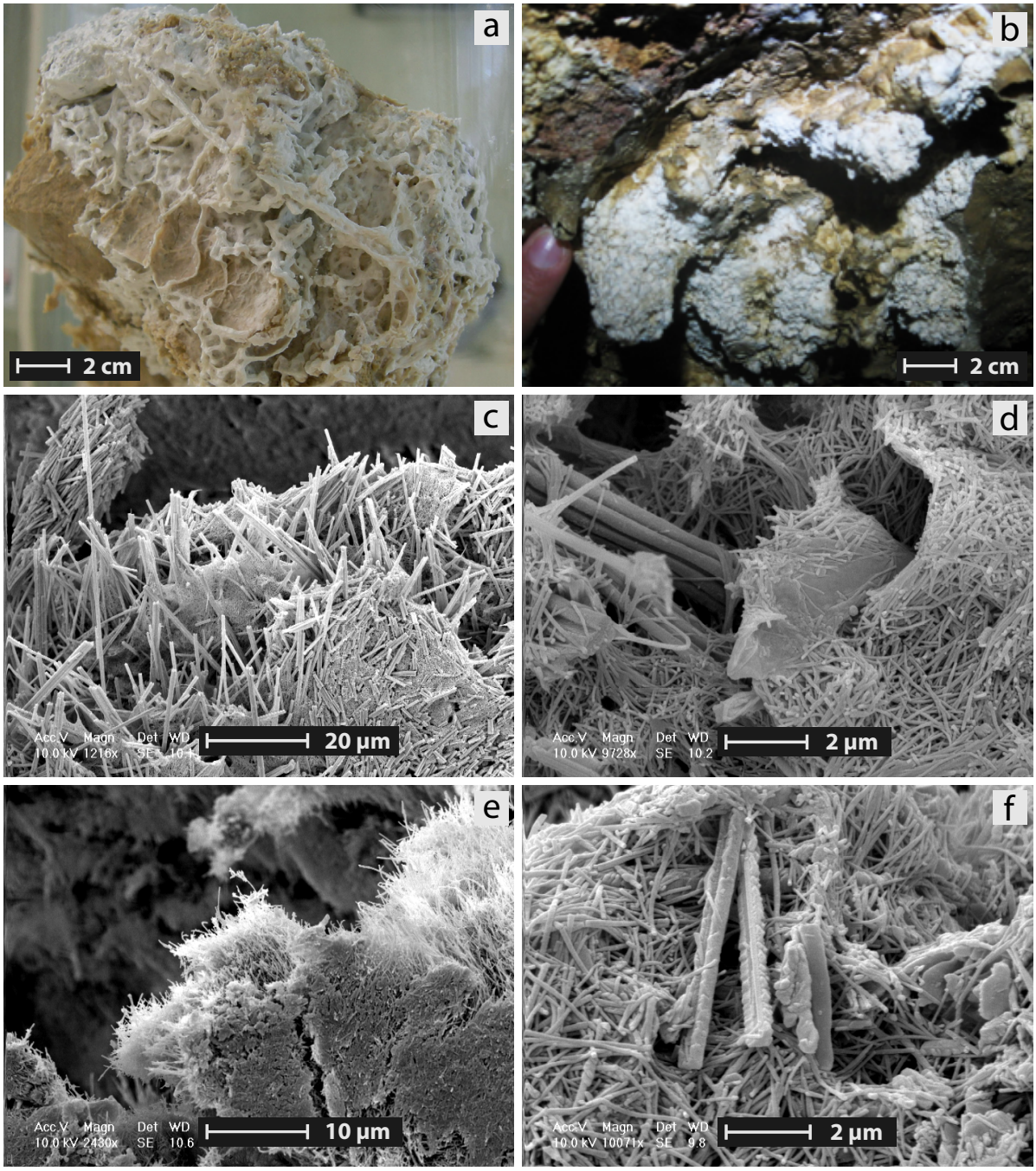

Figure 2.8 – (a) “Coating” macroscopic facies covering scree fragments from the C horizon, Villiers (CH01) site. Note the reticulate-like morphology of the coating, which probably results from water circulation. **(b)** Moonmilk macroscopic appearance covering cave walls, Vers-chez-le-Bandt (CH02) cave. **(c-d)** “Coating” microscopic assemblage; all samples from the C horizon, Villiers (CH01) site; **(e-f)** microscopic assemblage of moonmilk facies from caves, Vers-chez-le-Bandt (CH02) cave. **(c)** Microscopic assemblage from “coating” facies composed of a mesh of NFC and nanofibres. **(d)** Close-up on mesh shows randomly organized nanofibre meshes associated with a few needles. **(e)** Microscopic assemblage from moonmilk wall coatings composed of a mesh of mostly nanofibres. **(f)** Close-up on mesh shows randomly organized nanofibre meshes with a few associated needles.

(Hill and Forti 1997). Moonmilk has a physical appearance ranging from a very soft paste to cottage cheese that may become powdery when dry (Northup and Lavoie 2001; Fig. 2.8 b). Moomilk is mainly a carbonate deposit and the most common minerals encountered are calcite, aragonite and hydromagnesite. However, moonmilk may also be constituted of sulphate, phosphate and silicate (Chirienco 2004). As a result, moonmilk corresponds to a textural rather than a mineralogical definition (Chirienco 2004; Curry et al. 2009). The most distinguishing components of carbonate moonmilk are NFC and nanofibres (Fig. 2.8 e-f), but micrite may also be observed (Gradzinski et al 1997; Cañaveras et al. 1999, 2001 & 2006; Borsato et al. 2000; Blyth and Frisia 2008; Richter et al. 2008; Curry et al. 2009).

2.3.3 The "alveolar" facies

This facies is composed of grains that are cemented in an alveolar-like cement (Fig. 2.9 a). This facies is strongly indurated and this may lead to the complete cementation of gravely layers. Roots may be trapped within such layers. The microscopic assemblage consists of NFC showing numerous large syntactic calcite overgrowths, rhomb chains, and polycrystalline needles (Fig. 2.9 b). Highly cemented NFC bundles, composed of MB type needles, are also common features of this facies (Fig. 2.9 c). Wright (1984), in a study on fossil Carboniferous calcretes, has described this facies under the term of "alveolar textures" and interpreted it as the result of calcification around decaying rootlets as an explanation for the alveolar texture. Finally, calcified filaments have regularly been observed in this facies (Fig. 2.9 d).

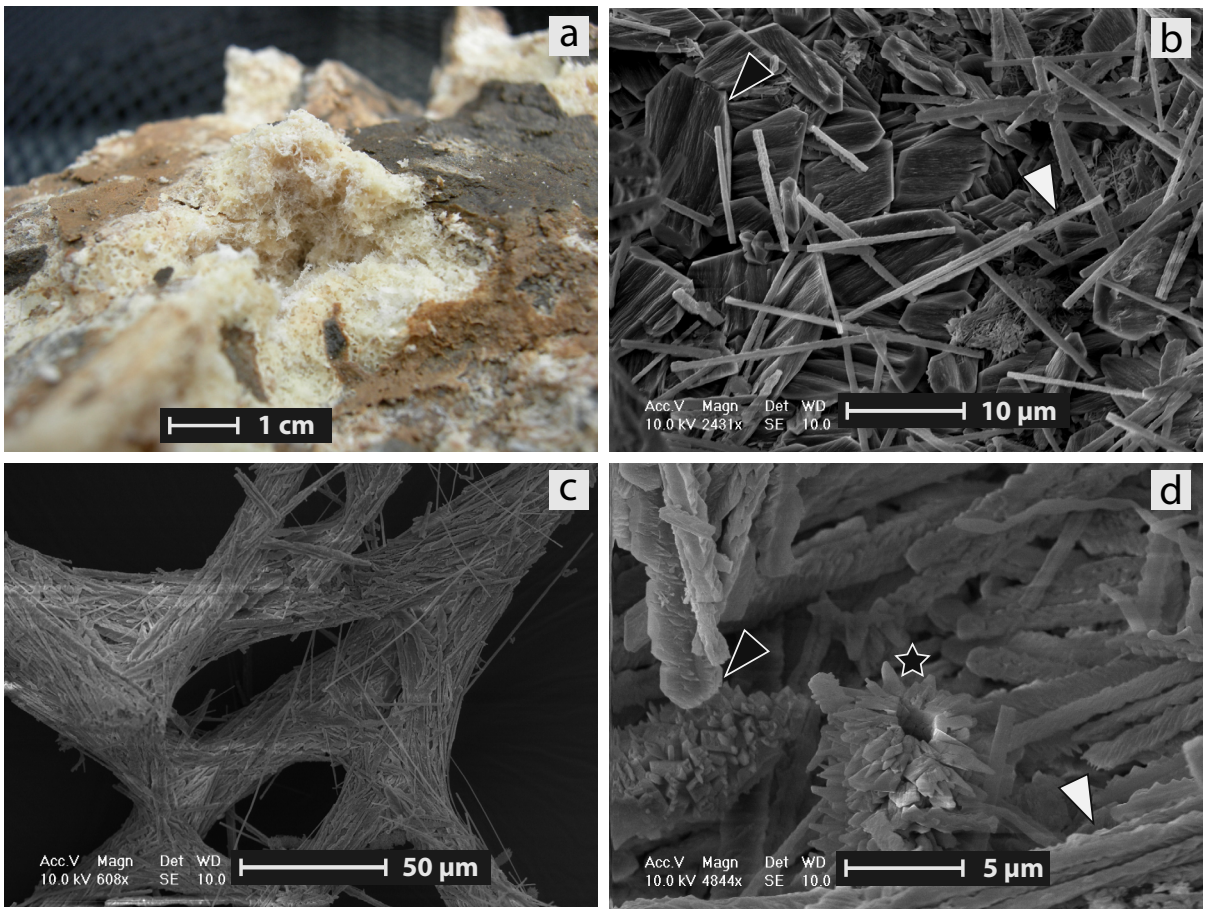

Figure 2.9 - "Alveolar" macroscopic facies from C horizons and associated microscopic assemblage. **(a)** Macroscopic appearance of this facies; note the alveolar appearance, which totally cements some areas of the C horizon, sample from the Campo (SP06) site. **(b)** Microscopic assemblage showing MA-type needles (white arrow) and polycrystals (black arrow), Val de Benasque (SP07) site. **(c)** highly cemented NFC bundles organized in reticulate networks, Boussagou (FR03) site. **(d)** Microscopic assemblage showing MB-type needles (white arrow), polycrystalline chains (black arrows), and calcified filaments (star), Condat (FR04) site.

2.3.4 Genetic relationships between the different facies

These three facies are usually observed together, distributed in distinct areas, or in close association. Vergès et al. (1982) describe the occurrence of "pseudomycéliums" (after Kubiëna's description; 1938) for the "cotton ball-like" facies in Bca horizon and "calcins" as grain coatings in C horizon. Strong et al. (1992) describe the presence of "grains coatings" in association with tubular structure 100 µm in diameter, which they call "rhizocretions". In addition, they also describe the occurrence of "alveolar septal structures" similar to the one described previously by Wright (1984 & 1986). Phillips and Self (1987) describe the "cotton ball-like" facies as a "self-supporting random open mesh, infilling the centres of voids and root channels in the weak to moderately indurated calcretes". Moreover, they emphasize the fact that needles are mostly of the MA type. In addition to the "cotton ball-like" facies, they describe an "alveolar or convoluted texture". However they do not give the description of a facies similar to the "coating" one. From observations in this study, as well as in other studies (Vergès et al. 1982; Wright 1984; Phillips and Self 1987; Strong et al. 1992), a genetic link between these three facies can be drawn. The cotton ball-like facies constituted of mainly simple needles of the MA type is considered as the original facies. This facies further evolves either as a coating facies or as an alveolar facies, depending on prevailing physicochemical factors. Water circulation in the soil pores may rearrange needles and nanofibres and lead to the coating facies. Alternatively, dryer conditions may lead to the precipitation of physicochemical cements on needles networks, resulting on the alveolar indurated texture (Fig. 2.10).

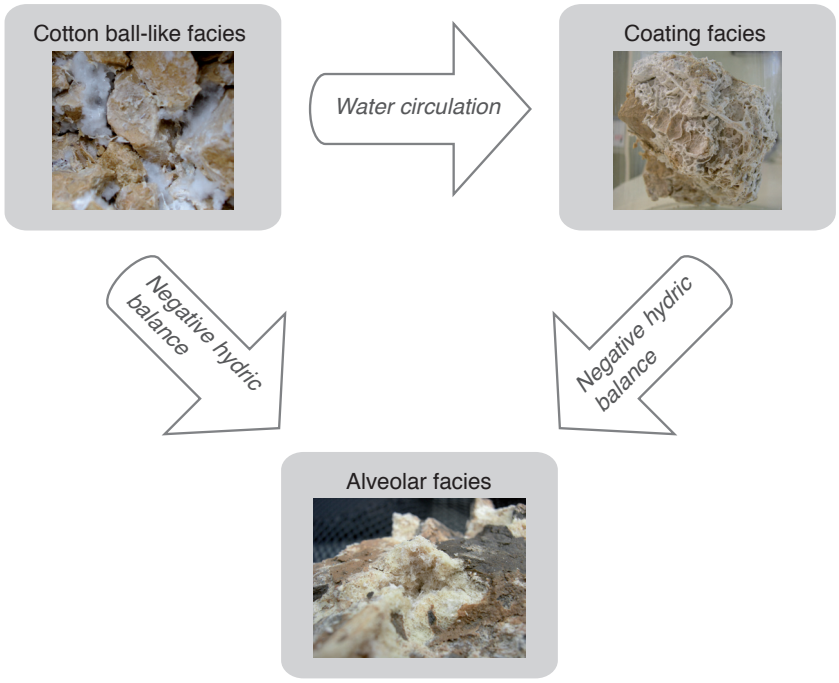

Figure 2.10 - Genetic relationship between the different macroscopic facies. The "cotton ball-like" facies is considered as the initial one, containing mostly MA-type needles released from the fungal sheath and nanofibres. Water circulation leads to the reworking of these features into "coating" facies, which shows accumulations of MA-type needles together with meshes of nanofibres. A deficit in moisture results in a negative hydric balance and subsequent enhancement of physicochemical precipitation of calcite on NFC and nanofibres from both, "cotton ball-like" and "coating" facies, leading to the indurated "alveolar" facies.

2.4 Environments of deposition

NFC and associated nanofibres have been described from environments affected by pedogenic processes such as calcareous soils (chernozems, rendzinas), calcrete/caliche, aeolianites, weathered limestones and limestone caves (Wright 1984; Phillips and Self 1987; Verrecchia and Verrecchia 1994

as well as Table 2.2). These features are restricted to the vadose zone, at the exception of "whisker crystals" mentioned by Supko (1971), which he believed were formed in a phreatic environment. An absolute prerequisite for the occurrence of NFC and associated nanofibres seems to be the presence of pre-existing pores or cavities, such as inter-particle pores, desiccation cracks, scree accumulation resulting from frost shattering, rock fractures, inner pores of substrates (e.g. tufa deposits, vughs), root pores and/or channels resulting from bioturbation (Phillips and Self 1987; Verrecchia and Verrecchia 1994 and references therein; Newman et al. 1996). The only exception to the "pore rule" lies in the presence of NFC in moonmilk deposits on cave walls. However, caves may be considered as giant pores. Yet, the fact that NFC and nanofibres occur in environments with different characteristics, such as caves and soils, is of great interest and is a potential indication regarding the processes leading to their genesis.

Table 2.2 - Environments in which NFC and nanofibres have been mentioned in the literature. Note that it is a representative, but not exhaustive list.

Environments	Authors mentioning the occurence of NFC and nanofibres
Recent calcretes/caliches	Klappa 1979; Phillips and Self 1987; Strong et al. 1992; Verrecchia and Verrechia 1994; Dubroeucq et al. 1996; Arnand et al. 1997; Khormali et al. 2006; Shankar & Achyuthan 2007; Zhou and Chafetz 2009
Acient calcretes/caliches	Wright 1984 & 1986; Jones and Ng 1988; Becze-Deák et al. 1997; Turner and Makhlouf 2005; Bajnóczi and Kovács-Kis 2006; Alonso-Zarza and Jones 2007; Shankar and Achyuthan 2007
Phreatic environments	Supko 1971
calcic horizon of temperate soils	Kubiëna 1938; Vergès et al. 1982; Callot et al. 1985b; Ould Mohamed and Bruand 1994; Loisy et al. 1999; Cailleau et al. 2009b
calcic horizon of intertropical soils	Cailleau et al. 2005
moonmilk deposits in caves	Gradzinski et al 1997; Hill and Forti 1997; Cañaveras et al. 1999, 2001 & 2006; Borsato et al. 2000; Jones 2001; Cacchio 2004; Chirienco 2004; Blyth and Frisia 2008; Richter et al. 2008; Curry et al. 2009; Jones 2010

2.5 Climatic significance of NFC and nanofibres occurrence

NFC and nanofibres have long been thought as occurring mostly in arid to semiarid climates. This is probably the result of the fact that they have been described in great amount from calcretes, which are mainly distributed in semiarid to arid areas (Zhou and Chafetz 2009). In these areas, the moisture deficit and subsequent lack of leaching most likely allows the conservation of these calcitic features (Strong et al. 1992). However, some studies have demonstrated their occurrence in more humid climates than what was previously thought (this study; Strong et al. 1992; Khormali et al. 2006; Cailleau et al. 2009b; Zhou and Chafetz 2009). Khormali et al. (2006), as well as Zhou and Chafetz (2009) in their studies on the occurrence of NFC along a climatic gradient, have both shown that NFC and nanofibres occurrence corresponds to areas with sufficient humidity, which may not be the case in aridic places. In addition, NFC and nanofibres are extensively described from humid cave walls, where physicochemical conditions are known to be mild and buffered, in particular regarding humidity and temperature (Northup and Lavoie 2001). The relationship of NFC with climate is thus not completely clear. Despite this fact, NFC occurrence in ancient calcretes has been widely used to reconstruct paleoclimatic conditions (Zhou and Chafetz 2009). As suggested by Wright (1984) and Zhou and Chafetz (2009), the association of different microfeatures (NFC,

nanofibres, and other biogenic fabrics as defined by Wright 1990), as well as macroscopic facies, is more relevant to propose a diagnostic of particular environmental conditions than the occurrence of a single microfeature. Consequently, an accurate definition of both NFC and nanofibres, as well as the unravelling of their respective origins, is crucial in order to retrieve accurate data on paleoenvironments displaying NFC and/or nanofibres.

2.6 Summary of chapter 2

NFC and nanofibres are characteristic features of secondary $CaCO_3$ deposits from pedogenic environments, such as soils and caves. Both features are acicular habits of low-Mg calcite. However their dimensions, as well as morphologies, clearly show that they are distinct habits. The origin of both features is subject to controversy. Although they are recurrently observed together, a non-genetic link is proposed. Following the critical review of all the literature referring to NFC, it is more likely the result of fungal biomineralization, whereas nanofibres are more likely the result of organomineralization. NFC is extensively used as a paleoenvironmental or paleoclimatic proxy, supposedly indicating aridic to semiaridic conditions. Yet, its observation in soils from temperate and intertropical climates, as well as in humid caves, challenges this view. As a consequence, the unravelling of NFC and nanofibres origins is necessary in order to use them as accurate environmental and/or climatic proxies.

Chapter 3

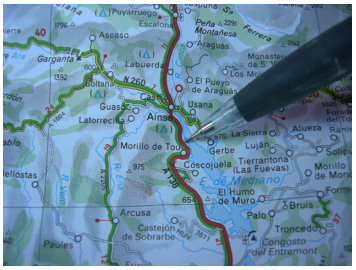

Field approach

Chapter 3 – Field approach: description of sites, macroscopic facies of NFC and nanofibres in relation to the climate, and pedo-chemical settings

During this project several sampling sites with different climatic characteristics, in northwestern Switzerland (Swiss Jura mountains), southwestern France and northeastern Spain (Pyreneans foothills), were visited. For each of these three visited regions, one site has been extensively described including vegetation and soil. These reference stations are Villiers (CH01) in Switzerland, Bonaguil (FR02) in France, and Arcusa (SP02) in Spain.

In the first part of the chapter, field settings for each sampling sites are presented (§ 3.1.1 to 3.1.3) and a synthesis of these descriptions is proposed (§ 3.1.4). In the second part (§ 3.2), pedo-chemical settings for each reference sites have been evaluated, based on pH and soil solution measurements (the latter performed only at Villiers site). This approach allows drawing conclusions on pedogenic processes of the investigated sites (§ 3.2.3 & 3.2.4).

3.1 Field settings

In the field, soil and humus descriptions have been performed using the “guide pour la description des sols” (Baize and Jabiol 1995) and the «Référentiel pédologique» (Association française pour l’étude des sols AFES 2008). However, the soil classes have been identified using the international World Reference Base for soil resources (IUSS Working Group WRB 2006). Soil pH has been estimated using a pH Hellige, and $CaCO_3$ presence, using 10% HCl. Reference colours have been evaluated on fresh soil using the Munsell chart colours.

3.1.1 Sampling sites in Switzerland

Four sites located in the Swiss Jura Mountains have been sampled (Fig. 3.1). Three of them correspond to calcareous scree slope deposits containing large quantities of secondary $CaCO_3$ accumulations: Villiers (CH01), Savagnier (CH04), and Tavannes (CH05). These accumulations occur in the pores created by scree fragment accumulations. Well-developed soil layers and beech and fir forests cover the slope. The fourth site corresponds to a karstic cave, the Vers-chez-le-Brandt cave (CH02), where large moonmilk deposits are covering cave walls.

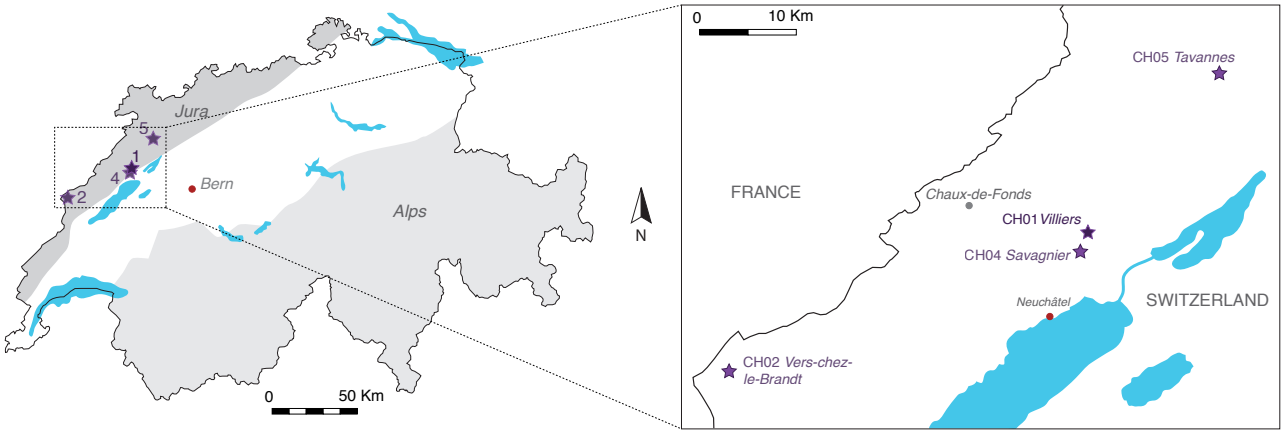

Figure 3.1 - Localization of sampling sites (★) in Switzerland, Swiss Jura mountains.

Climate in the Swiss Jura Mountains corresponds to a degraded oceanic climate with mountainous trends due to the elevation factor. Winter can be rather cold with commonly December through February showing most of their daily temperature under 0°C. Summer is mild, with maximal temperatures in July and August. Precipitations are maximal at the end of both spring and fall, whereas minimal values correspond to early spring and fall and during the month of July. The lowest precipitation values do not correspond to the maximal temperature values (Fig. 3.2 A). Nevertheless, hydric balance values show a clear water deficit during June, July, and August. On the other hand, winter and fall mostly show values over 0, indicating that the water balance is in favour of an accumulation. Spring shows intermediate values (Fig. 3.2 B).

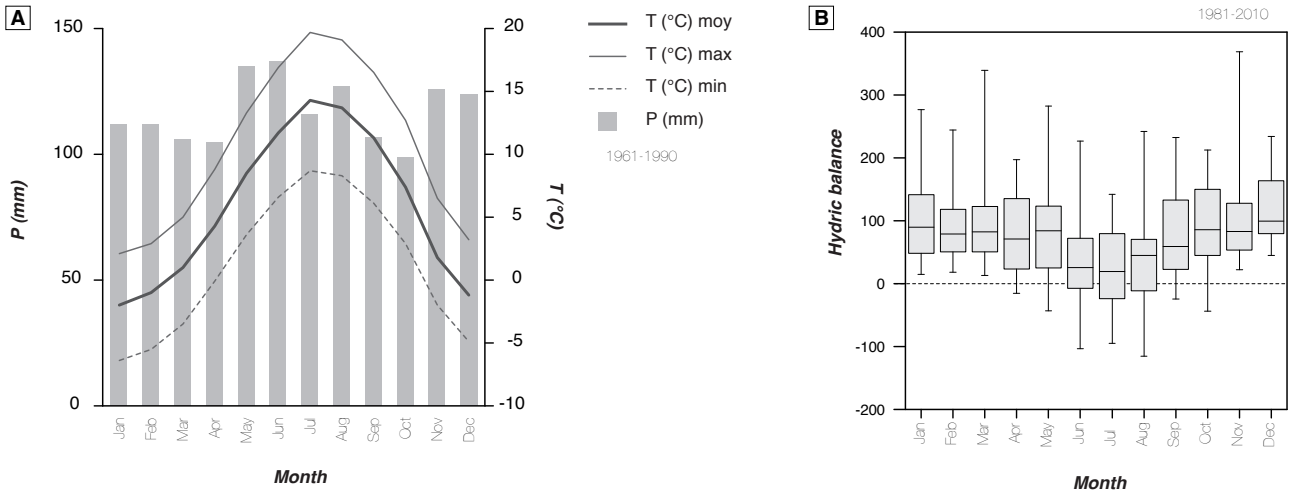

Figure 3.2 - Climatic data for the city of La Chaux-de-Fonds, Neuchâtel area (localization is indicated in Fig. 3.1). **(A)** Ombrothermic diagram showing mean monthly precipitation together with mean, maximal, and minimal values of monthly temperatures recorded between 1961 and 1990. **(B)** Box plot showing the monthly hydric balance recorded between 1981 and October 2010. Data provided by the Federal Office of Meteorology and Climatology MeteoSwiss.

3.1.1.1 Description of the reference site: Villiers (CH01)

The main site of investigation in Switzerland is a scree slope deposit located near the village of Villiers (47°04'N, 6°59'E; altitude 842 m.) in the canton of Neuchâtel (Fig. 3.1). The slope is facing northwest and shows an inclination of approximately 45°. Scree deposits are composed of fragments of Kimmeridgian and Portlandian (Jurassic) limestones (Fig. 3.3). The sampling location corresponds to a quarry, and samples have been harvested both at the outcrop (Fig. 3.4 A-B) and in a soil profile (Fig. 3.4 C).

3.1.1.1.1 Vegetation

The plant community covering the slope is a beech and silver fir forest (Fig. 3.5 A). Beech forests are typically closed forests and total covering reaches 95%. *Fagus sylvatica* is by far the dominant species whereas *Abies alba* is present but sparsely distributed. The shrub layer is composed mainly of young *Fagus sylvatica* individuals. The herbaceous layer is mostly developed in spring before beech leaves appear, and typically comprises species indicating calcareous gravelly soils: *Cardamine heptaphylla* and *Mercurialis perrenis*. In addition, *Fagus sylvatica* seedlings are, once again, the dominant species present.

Biodiversity in Beech dominated and fir forest is often poor. This type of vegetation belongs to the *Abieti-Fagenion* sub-alliance in the phytosociological typology. It typically corresponds to the

climax for the area and indicates mesophilic climatic conditions. These forests are usually exploited for the wood.

3.1.1.1.2 Humus

The holorganic layer is well developed with the presence of an OLn layer, a sporadic OLv layer, a clear OF layer followed by an A layer. The OLn and OLv layers are present throughout the year with leaves currently being in the first stage of decay. The OF layer is composed of leaves strongly fragmented and packed by mycelium. The transition with the organo-mineral layer (A) is sharp (Fig. 3.5 B-C). This latter is clearly granular and displays a deeply brown colour indicating its richness in organic matter (OM). The characteristics, as well as the succession, of these horizons indicate a *dysmull* humus form after Baize and jabiol (1995). This is typically the kind of humus observed under forests of the mountainous stage in the Swiss Jura Mountain. It indicates a good biological activity with, however, a slow-down due to harsher climatic conditions, leading to OM accumulations on the forest ground.

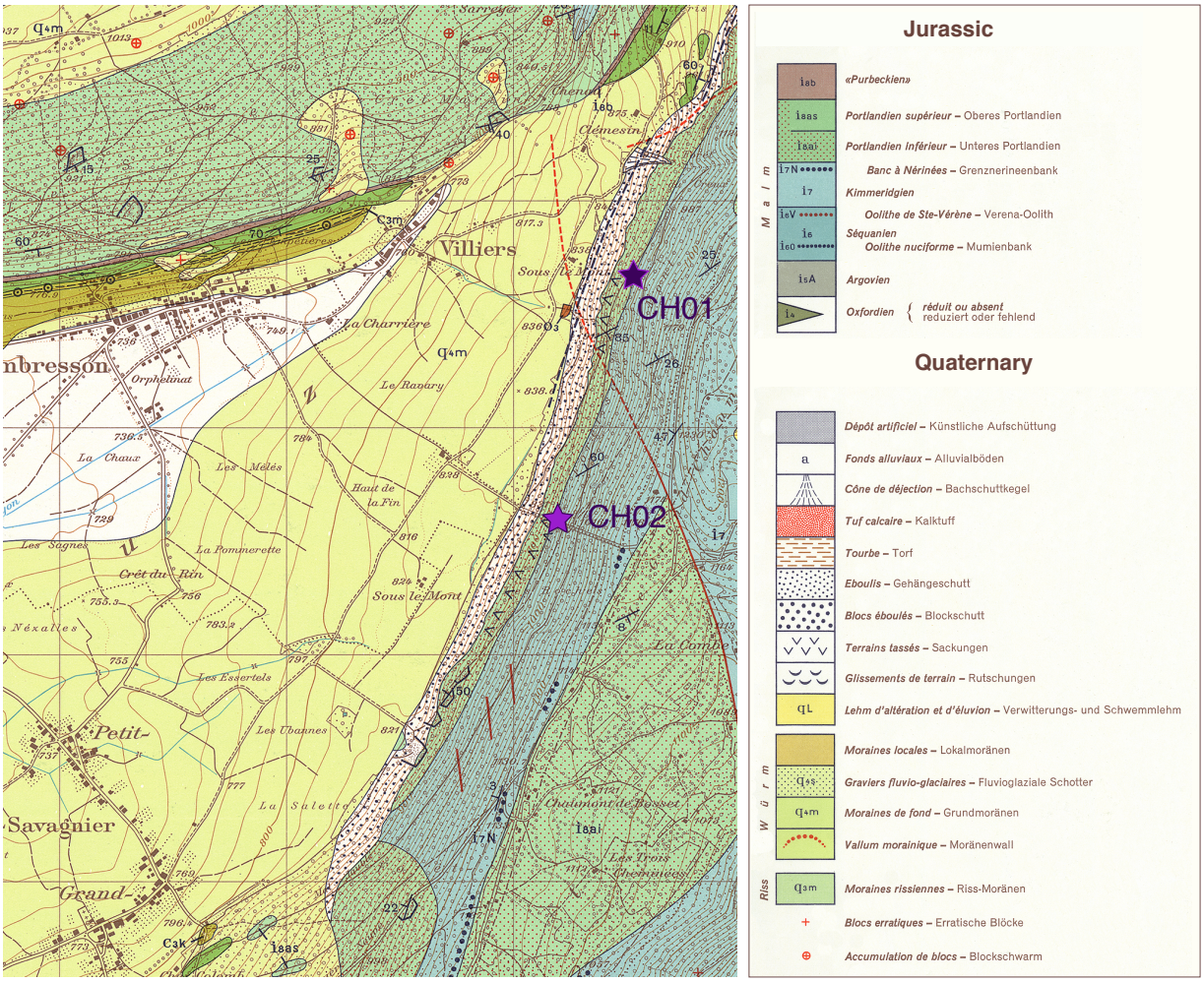

Figure 3.3 - Geological map of the Villiers-Savagnier area (1:25'000 Geological atlas of Switzerland, sheet n° 1144 Val-de-Ruz; Federal Office of Topography Swisstopo). Both sampling sites are indicated (★).

Figure 3.4 - Villiers (CH01) site. **(A-B)** Pictures at the quarry front. **(A)** Massive accumulations of scree slope deposits showing the typical white patches of secondary $CaCO_3$ accumulations under the organic soil layer. **(B)** Lateral distribution of $CaCO_3$ accumulations is not continuous. **(C)** A detailed view in the soil profile shows that the accumulation of secondary $CaCO_3$ occurs already under the A and B soil layers.

Figure 3.5 - Vegetation and humus layer at the Villiers (CH01) site. **(A)** Beech dominated and fir forest showing a high density of individuals leading to a high overall cover, *Abieti-Fagenion* sub-alliance. **(B)** The interface between the organic soil layer and the mineral scree layer is sharp. **(C)** Detail of both, holorganic and organomineral soil layers, showing the accumulation of leaf litter at the surface, high density of roots, as well as dark a colour indicating the high OM content of both, O and A layers. Holorganic layer identified as a *dysmull*.

3.1.1.1.3 Soil and surficial formation description

The soil and associated surficial formations have been described from a soil profile down to a depth of 130 cm. The profile is composed of the following horizons (Fig. 3.6):

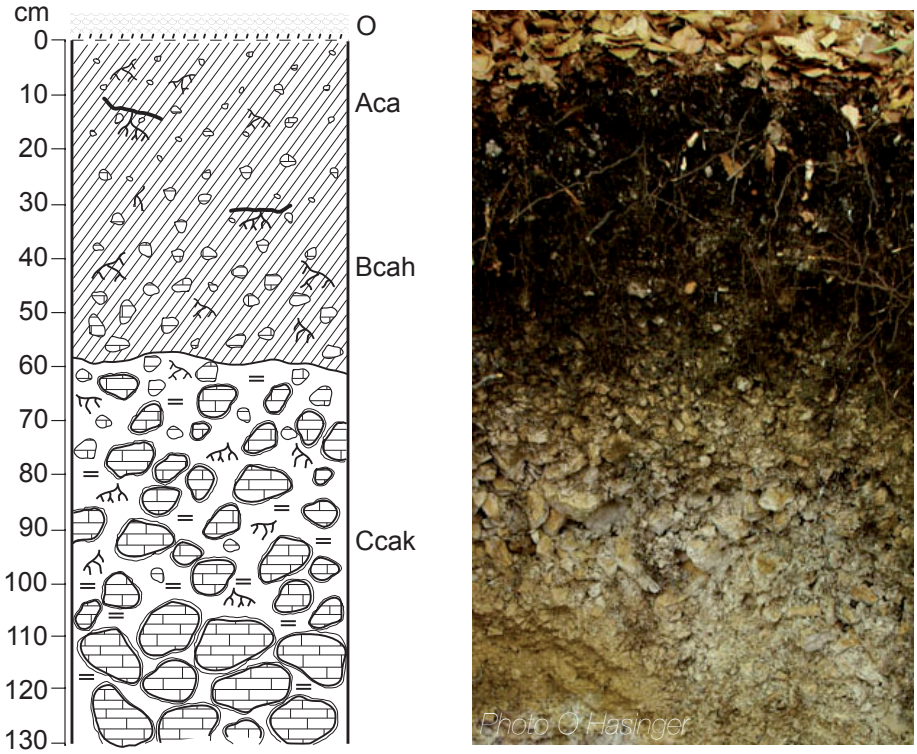

Figure 3.6 - Reference soil profile at the Villiers (CH01) site, a *calcic Cambisol humic calcaric skeletic* (WRB 2006).

Aca (0-20 cm – Munsell colour 10YR 2/1)

The colour of this horizon is dark brown due to very high percentage of organic carbon. Total mineral skeleton represents 76.9 % of soil volume and the dimension of scree fragments mostly ranges between 2-10 mm. HCl reaction is strong and pH is around 7. Texture is loamy and structure is granular. Roots are extremely abundant, virtually binding the soil together. As a consequence, soil pores are well developed. No secondary $CaCO_3$ accumulations have been observed in this horizon.

Bcah (20-60 cm – Munsell colour 2.5Y 3/1)

The colour of this horizon is the same as the overlying A horizon because of a very high OM content. The humic qualifier (h) has thus been added in order to emphasize this character. Total mineral skeleton represents 88.7 % of soil volume and the dimension of scree fragment mostly ranges between 2 and 50 mm. HCl reaction is strong and pH is around 8. Texture is loamy and structure is polyhedrical due to structuration mainly by physicochemical processes. Roots are abundant and porosity is well developed. The transition with the underlying horizon is sharp, and secondary $CaCO_3$, as “cotton bal-like” and “coating” facies, has been observed in the few centimetres above this transition, intimately associated to OM.

Ccak (60-150 cm – Munsell colour 2.5Y 8/2)

This horizon is actually a scree slope deposit and is unsurprisingly mostly mineral. The mineral skeleton is composed of scree fragments being weathered and/or covered/embedded with secondary $CaCO_3$. The total volume occupied by scree fragments is 96.3 % of total soil volume, leading to a highly porous and draining horizon. The dimension of scree fragments mostly ranges between 10 mm and 10 cm. The fine earth fraction is essentially made of secondary calcite and little particulate OM. The pH has been estimated between 8 and 9. Roots are present and observed deep in the scree deposit, often associated to ECM fungi. Fungal rhizomorphs have also been frequently observed at depth in the C horizon (Fig. 3.7 A). This horizon harbours a lot of secondary calcitic deposits in various macroscopic facies, "cotton ball-like", "coating" on grains (Fig. 3.7 C-D) and even an "alveolar" facies, which hardens some scree layers. The type of macroscopic facies most certainly depends on factors that are driving pores development such as texture, dimension, and distribution of scree fragment. Texture and scree dimensions are very heterogeneous along the deposits, making secondary $CaCO_3$ accumulations heterogeneously distributed as well (Fig. 3.4 A-B). However, the cemented layers are present deeper in the scree deposit than the "cotton ball-like" and "coating" facies.

Finally, this soil has been identified as a *calcic Cambisol humic calcaric skeletic* (WRB 2006).

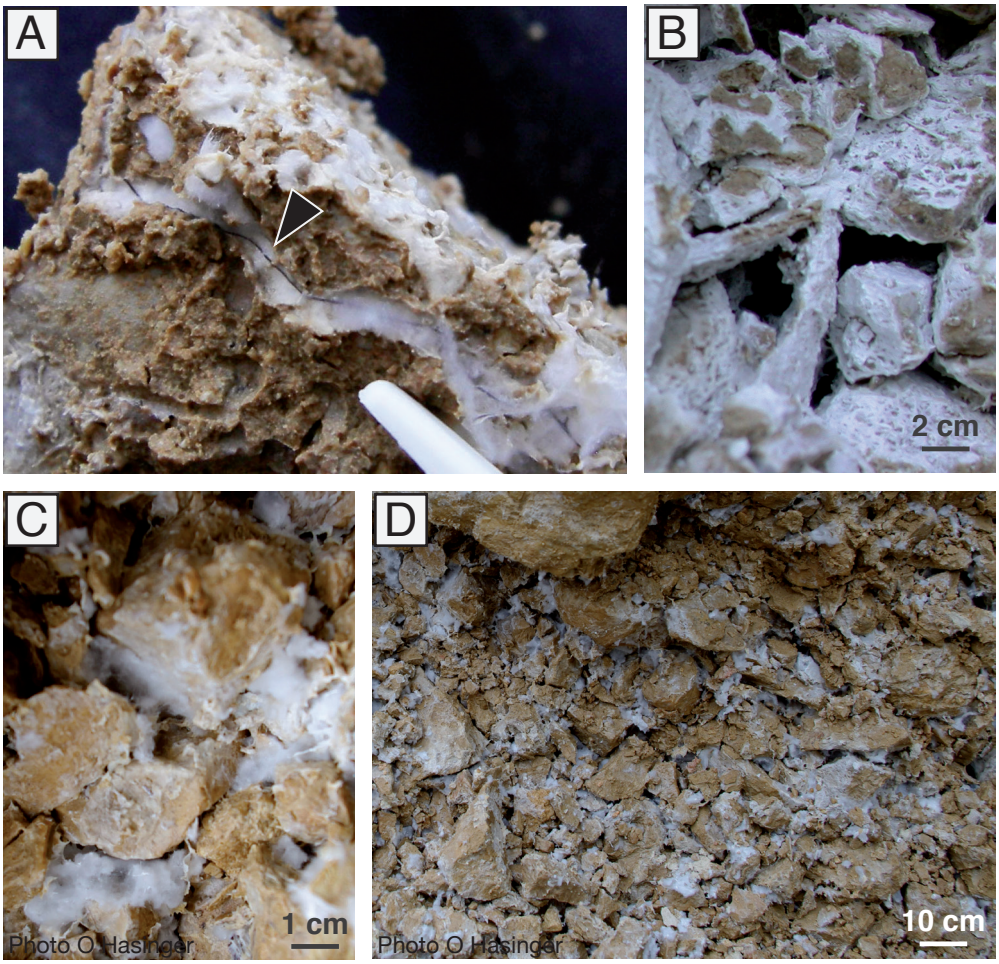

Figure 3.7 - Characteristic aspects of the different macroscopic facies observed in the Swiss sites. **(A)** Close-up on the "cotton ball-like" facies in the C horizon at the Tavannes (CH05) site. Note the presence of a dark filament identified as a rhizomorph associated to this facies (arrow). **(B)** Close-up on the "coating" facies covering soil scree deposits of the C horizon, Savagnier (CH04) site. **(C)** Close-up on scree showing the occurrence of both, "cotton ball-like" and "coating" facies in the same area, Villiers (CH01) site. **(D)** Larger view of C, showing the total volume filled by secondary $CaCO_3$ accumulations in scree deposit pores.

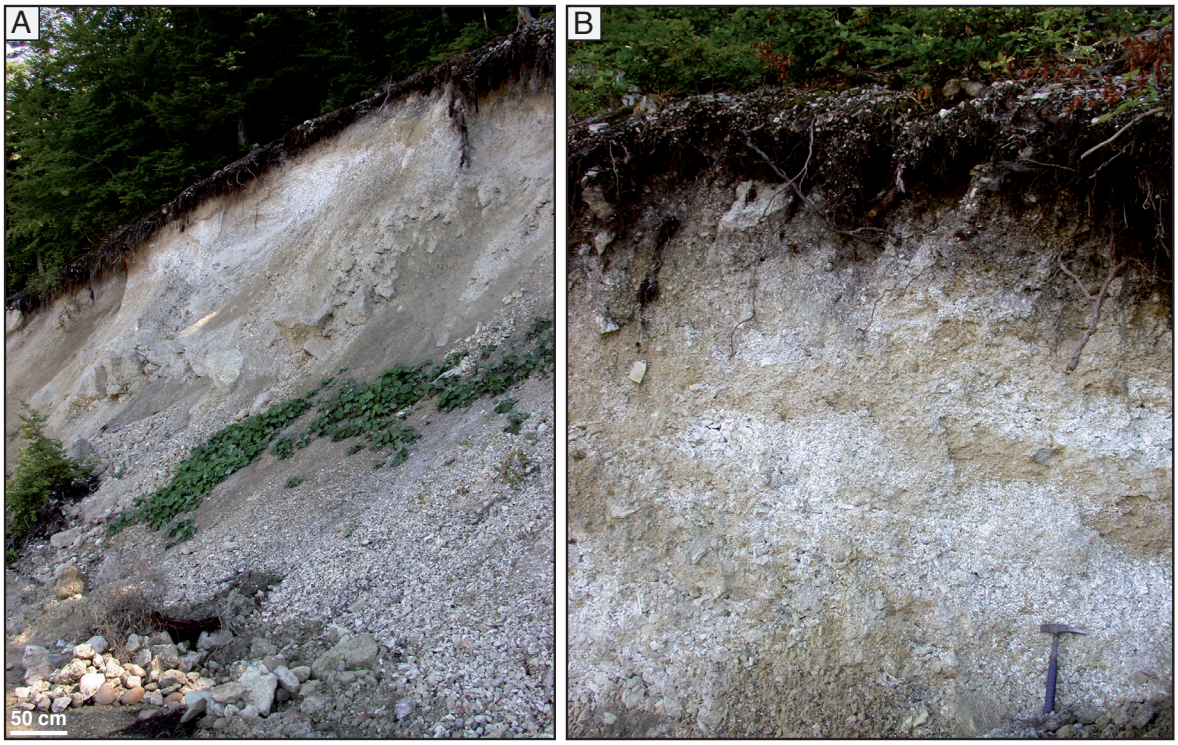

Figure 3.8 - Savagnier (CH04) site. **(A)** Overall characteristics of this site are similar to the Villiers (CH01) site. **(B)** Heterogeneous lateral distribution of secondary $CaCO_3$ accumulation in scree slope deposits.

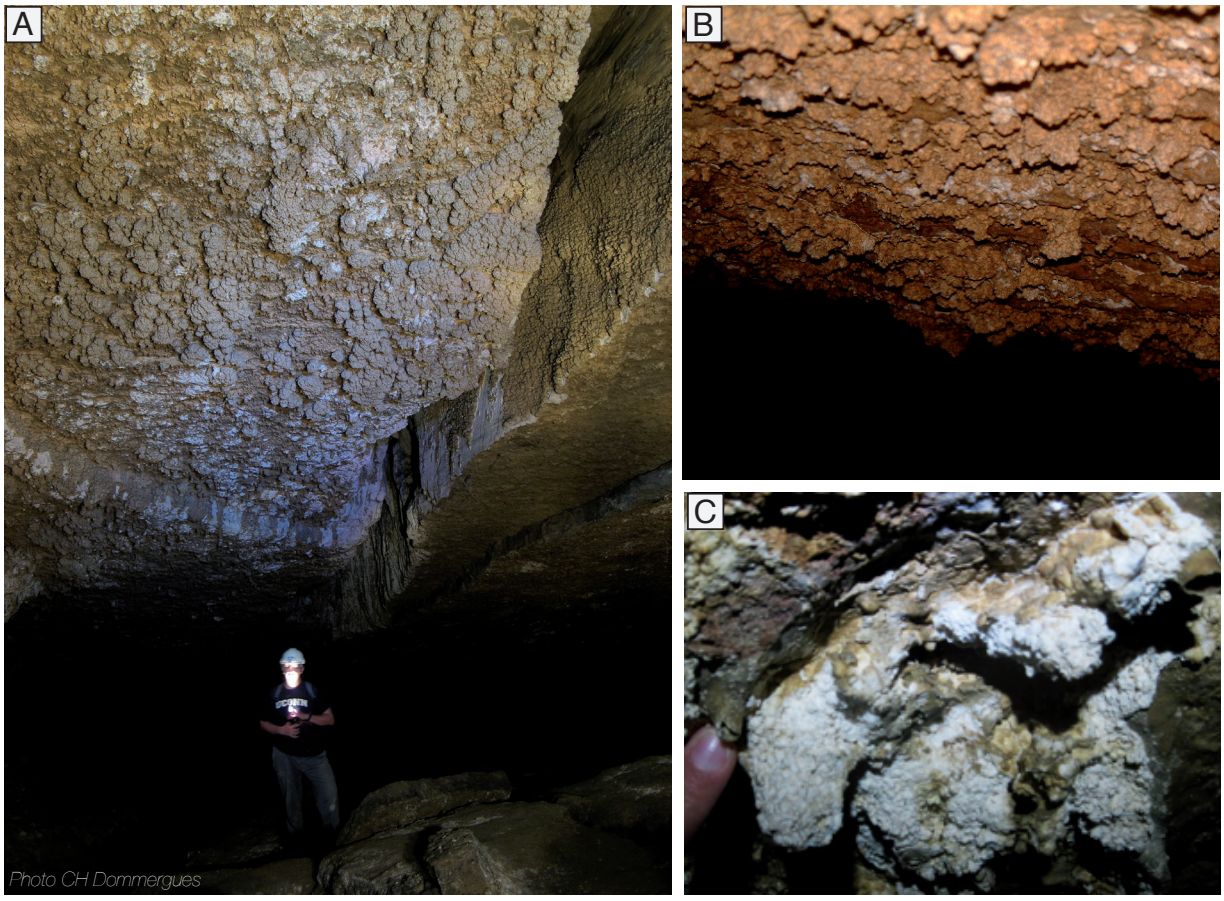

Figure 3.9 - *Vers-chez-le-Brandt cave* (CH02) site. **(A)** moonmilk accumulations are present on the cave walls, as well as along rock fractures. **(B)**. Close-up showing the brownish and nodular appearance of moonmilk. **(C)**. Close-up of nodules showing a thin external brownish layer and inner parts made of a white and plastic porous material.

3.1.1.2 Savagnier (CH04)

Another scree slope deposit from a quarry near the village of Savagnier (47°03'N, 6°58'E; altitude 831 m) has been investigated (Fig. 3.1 & 3.8). This site shows overall the same characteristics as the Villiers (CH01) site (Fig. 3.7 B & 3.8 A). Sites are only 2 km away from each other and are located on exactly the same hillslope with the same exposure, inclination, and lithological quality of scree fragments. Secondary $CaCO_3$ are present in the scree layer and/or at the interface of the soil *sensu stricto* and scree layers. Moreover, secondary $CaCO_3$ deposits are heterogeneously distributed along the outcrop front (Fig. 3.8 A-B) with the presence of mainly the "cotton ball-like" and "coating" facies (Fig. 3.7 B). The "alveolar" facies is present in a lesser extent.

3.1.1.3 Tavannes (CH05)

A quarry near the village of Tavannes (47°13'N, 7°10'E; altitude 910 m.) has also been visited and samples have been collected at the outcrop (Fig. 3.7 A). This site is located 20 km northeast from Villiers (CH01). Climate, geomorphology, and geology are quite similar to Villiers. This site shows the same overall characteristics. Secondary $CaCO_3$ deposits are present in the scree layer and composed of the "cotton ball-like" and "coating" facies. The "alveolar" facies is present in a lesser extent.

3.1.1.4 Cave of «Vers-chez-le-Brandt» (CH02)

Moonmilk deposits from cave walls (Fig. 3.9 A-B) have been sampled in order to compare them with soil deposits. Samples come from the Vers-chez-le-Brandt cave (46°56'N, 6°28'E; altitude 1139 m.) which is a typical karstic cave located in the canton of Neuchâtel, 35 km west of Neuchâtel (Fig. 3.1). Samples of thick wall covering moonmilk have been collected from inside a wide chamber at 100 meters from the cave entrance (Fig. 3.9 C). The cave has been formed in Jurassic (Malm) limestones and is 63 meter deep and 336 meter long. The average temperature in the cave is ca. 10-15°C.

3.1.2 Sampling sites in France

Several sites in the southwestern part of France (Perigord region) around a small city called Fumel, have been investigated (Fig. 3.10). Due to the mainly calcareous geology of this region and the climate from the last glacial maximum, many scree slope deposits are observed in this region. A total of five sites have been sampled and one has been extensively described, Bonaguil (FR02). They all correspond to scree slope deposits with a full soil layer developed on its surface. The scree fragments are made of Mesozoic limestones (Fig. 3.11). The climate of this region is considered as oceanic with continental trends. This is easily visible with the disappearance of the evergreen oak for pine-trees. Winters are relatively cold, with the minimal temperatures observed between November and February. Summers are fairly hot, July and August showing the maximal values, this period corresponding to minimal values in precipitations as well (July to September). Maximum humidity is observed at the end of spring (Fig. 3.12).

3.1.2.1 Description of the reference site: Bonaguil (FR02)

The main site of investigation in France is a scree slope deposit located near Bonaguil castle in the region of Fumel (44°31'N, 1°00'E; altitude 115 m; Fig. 3.10 & 3.13 A). The slope is facing west and

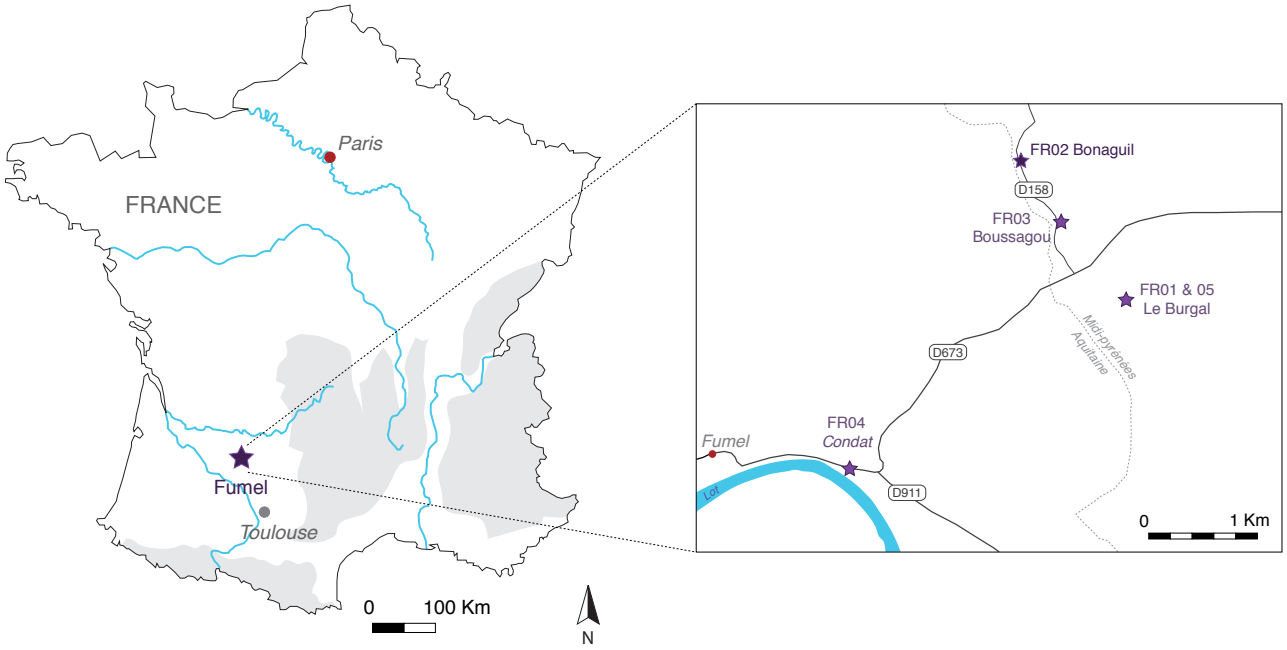

Figure 3.10 - Localization of the sampling sites (★) in France, Lot-et-Garonne county.

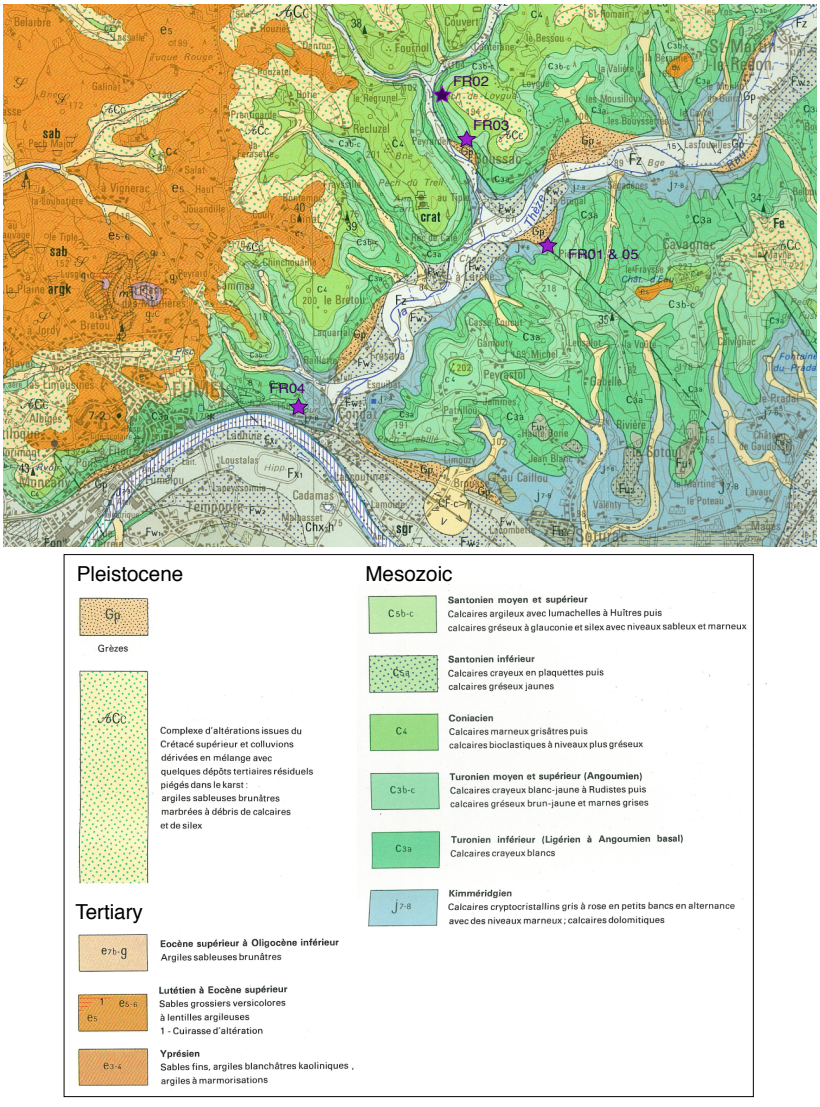

Figure 3.11 - Geological map of the Fumel area (1:50'000 Geological map of France, sheet n° 855 Fumel; BRGM). Sampling sites are indicated (★).

shows an inclination of approximately 45°. Scree fragments are composed of Kimmeridgian and Turonian limestones clasts. Samples have been collected only at the outcrops (Fig. 3.13 B).

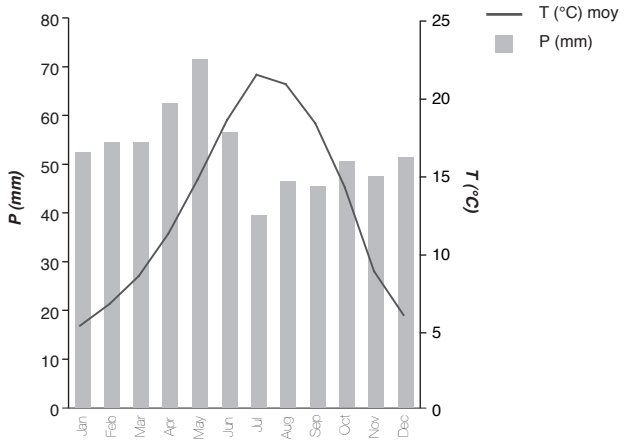

Figure 3.12 - Climatic data for the city of Toulouse, Midi-pyrénées region (localization is indicated in Fig. 3.10). Ombrothermic diagram showing the mean monthly precipitations and temperatures. Data from Météo-France.

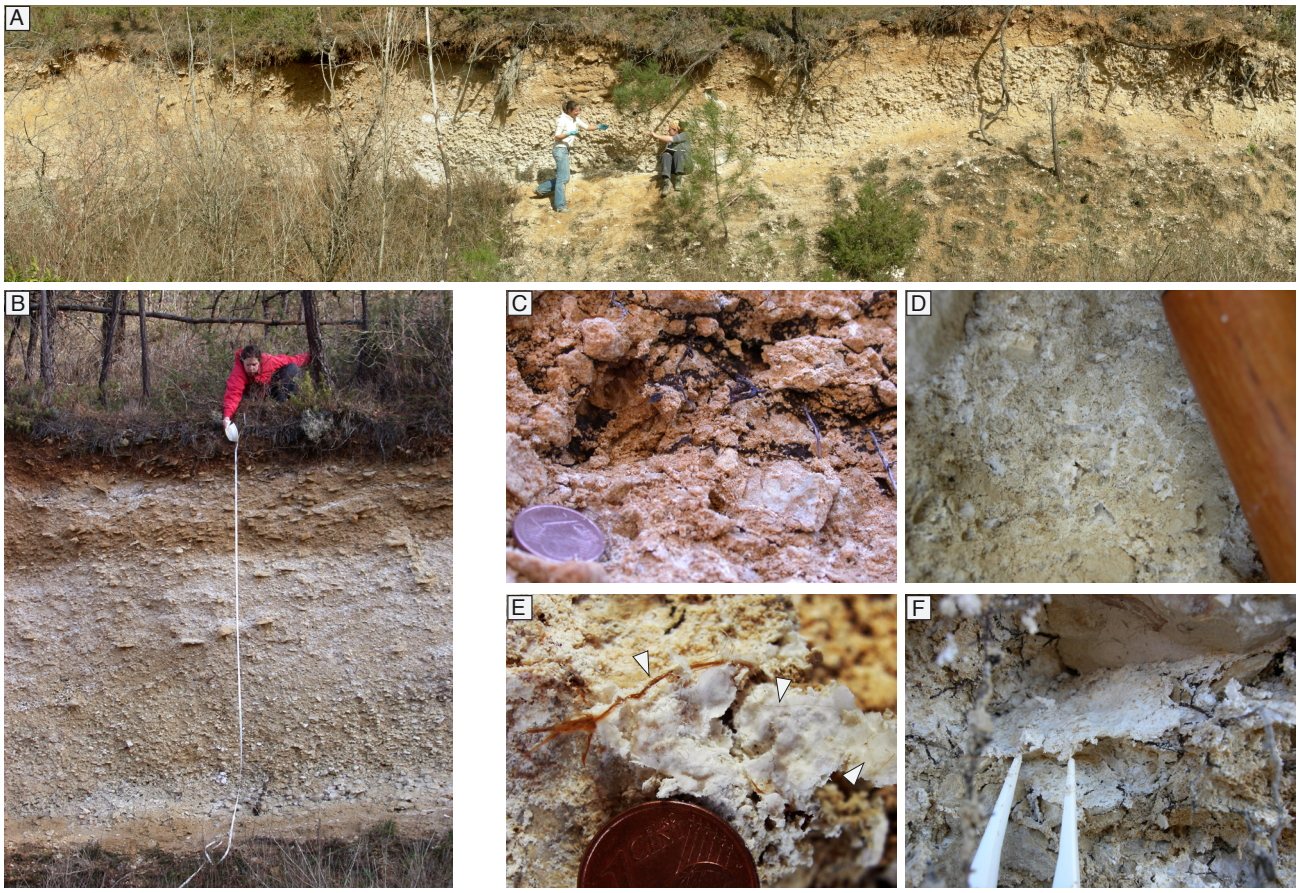

Figure 3.13 - Bonaguil (FR02) site. **(A)** Panoramic view of the site. **(B)** Outcrop front. **(C-D)** Close-up on particular features of the outcrop. **(C)** Black patches of highly humified OM associated to roots at the bottom of the B horizon. **(D-F)** Secondary $CaCO_3$ in intra-grain pores. **(D)** "Alveolar" macroscopic facies in the Kc horizon, few "cotton balls" are also present. **(E)** "Cotton ball-like" facies in the Ccak2 horizon, associated to numerous filaments. **(F)** "Coating" facies from the Ccak2 horizon associated with roots.

3.1.2.1.1 Vegetation

Vegetation cover varies in respect to its position along the slope. Uphill, *Quercus pubescens* is the dominant tree (estimated total tree cover = 5%) and the soil is irregularly covered with colluviums and a sparse herbaceous layer. At the time of the investigation (February), this latter was composed mainly of *Potentilla sp.* and *Helleborus foetidus*. Downslope, *Pinus pinaster* and *Quercus pubescens* are the dominant trees with some interspersed individuals of *Acer monspessulanum* (estimated total tree cover = 10%; Fig. 3.14 A). The bush layer is mostly composed of *Juniperus communis*, a few *Berberis vulgaris*, and juvenile of *Acer monspessulanum* and *Quercus pubescens*. A thick holorganic layer covers here the soil surface. Due to low tree covering, the herbaceous layers is relatively well developed but shows a patchy organization. Some areas are more open and gravelly. In these places, a high herbaceous layer is present with chamaephytous plants such as *Thymus sp.* and another shrub, which could not be identified. The low herbaceous layer is made of non-identified lamiaceae. In closed areas, the herbaceous layer is made of *Teucrium chamaedrys*, *Sesleria caerulea* and another non-identified Poaceae that seems to cover large areas. The herbaceous layer has been described in February and therefore represents its vernal status. A moss layer is also well developed in some places. The type of vegetation belongs to the *Quercion pubescenti-petraeae* alliance in the phytosociological typology, indicating somewhat subxerophilic conditions in the area, influenced by both Mediterranean and temperate conditions.

3.1.2.1.2 Humus

The holorganic soil layer has been described under the pine and oak downslope forest (Fig. 3.14 B). The holorganic layer is composed of an OLn horizon (1-2 cm thick), made of oak and maple fresh leaves and pine needles. A sporadic OLv layer is observed with whitened pine needles mixed

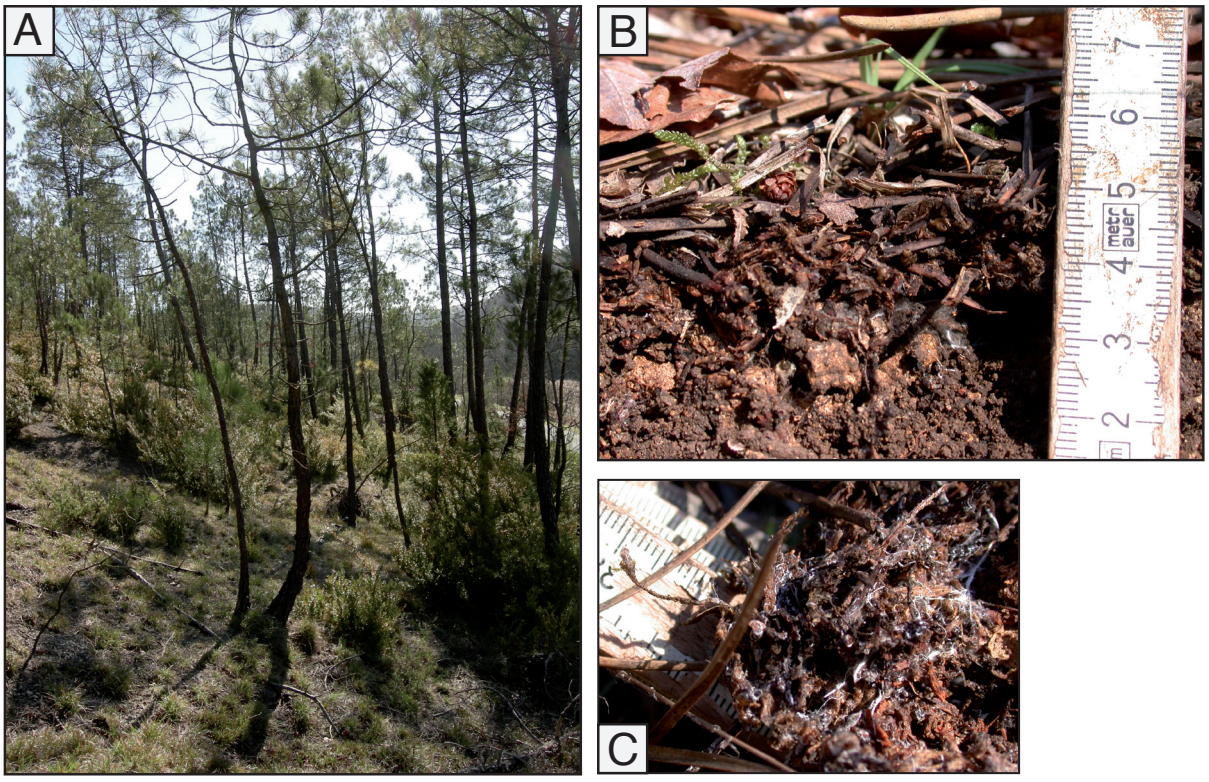

Figure 3.14 - Vegetation and humus layer at the Bonaguil (FR02) site. **(A)** Pine trees and oak forest showing a low density of individuals leading to a small overall cover, *Quercion pubescenti-petraeae* alliance. **(B)** Detail of the holorganic horizon showing a litter made of the accumulation of leaves and needles at the surface and fragmented needles underneath. Holorganic layer identified as a *hemimoder/mycogenic Oligomull*. **(C)** Detail on fragmented needles showing high mycelial development.

with fragments of skeletized leaves. A 1 cm thick OFm layer is present, showing a high density of mycelium packing fine fragments of leaves and needles, leading to a dense and compact layer (Fig. 3.14 C). No OH horizon is present and the transition to the organo-mineral layer (A) is observed directly under the OFm layer. The A horizon shows a microgranular to particular structure. Nevertheless, some macro-aggregates have been observed in the first centimetres. This A horizon has been identified as a juxtaposed A horizon after Baize and jabiol (1995). Finally, the humus has been defined as a *hemimoder/mycogenic Oligomull* (Baize and jabiol 1995). This typology reflects both the heterogeneity of the holorganic layer and a slowed biological activity due to the presence of a litter of low quality.

3.1.2.1.3 Soil and surficial formation description

The soil and associated surficial formations have been described at the outcrop down to a depth of 215 cm. The main rooting depth reaches 25 cm and the maximal extension is up to 170 cm. Moreover, the 60 first centimetres of the top soil are characterised by many cracks used as preferential paths for roots. These cracks exhibit blackish patches identified on the field as amorphous OM, which is strongly humified (Fig. 3.13 C). Coarse scree fragments are present at the bottom of the outcrop, orientated lying on their longer profile. The profile is composed of the following horizons (Fig. 3.15):

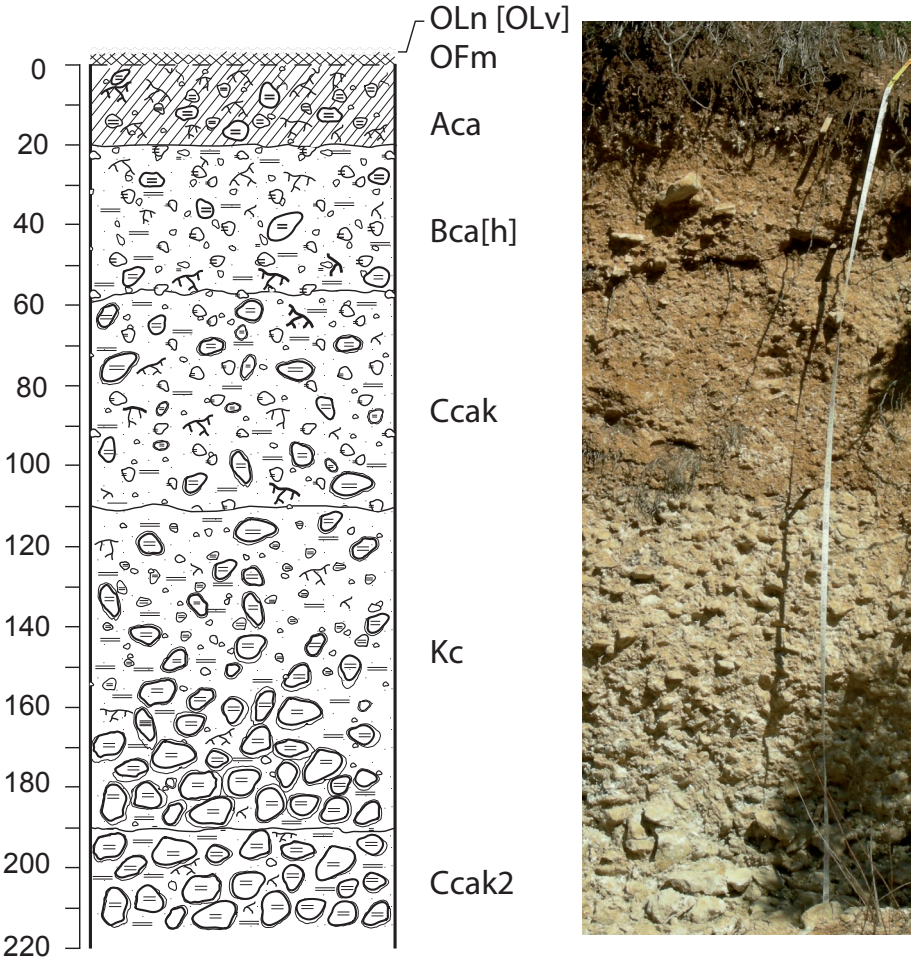

Figure 3.15 - Reference soil profile at the Bonaguil (FR02) site, a *Calcisol calcaric skeletic* (WRB 2006).

Aca (0-20 cm – Munsell colour 10YR 4/3)

The mineral skeleton is composed of a coarse fraction, with 5% of grains between 2-10 mm, 15% between 10-50 mm and 15% with dimensions larger than 5 cm. The 5 centimetres of the top soil are strongly depleted in mineral skeleton. Reaction to HCl is strong and pH has been estimated at 8. Texture is globally sandy-loam and structure microgranular to particular. Structure is mostly granular around roots. This horizon has been considered as a juxtaposed A horizon after Baize and Jabiol (1995). Moreover, the transition with the underlying mineral horizon is abrupt. These observations suggest that the integration between OM and mineral matter is not highly efficient and earthworms are not key-players in these soils. Roots are present in high amounts leading to a quite well developed porosity. In conclusion, it seems that OM decay, reworking, and stabilization is mainly linked to saprophytic fungi, rhizospheric bacteria and plant roots. No secondary $CaCO_3$ accumulations have been observed in this horizon.

Bca[h] (20-55/60 cm – Munsell colour 2.5Y 7/6)

The mineral skeleton is finer than in Aca horizon with 20% of grains between 2-10 mm, 15% between 10-50 mm and 1-5% of grains with dimensions larger than 5 cm. Reaction to HCl is very strong and pH has been estimated between 8 and 9. Texture is sandy-loam and structure particular to massive. Fine roots are present all along the profile creating some porosity, which is otherwise rather low. At the bottom of the horizon, large roots are emerging, creating large pores at the interface between B and C horizons. Black patches are present within the channels created by roots, and they have been identified as highly humified OM. The qualifier humic (h) has been added to this horizon in order to emphasize the presence of these black patches of (supposed) strongly humified OM. Roots channels represent preferential pathways for fluids transfers within this soil as indicated by these black patches. Some small patches of secondary $CaCO_3$ as “alveolar” and “cotton ball-like” facies are already present in this horizon.

Ccak (55/60-110 cm – Munsell colour 10YR 6/6)

The mineral skeleton turns into coarser fragments with 10% of grains between 2-10 mm, 15% between 10-50 mm, and 30% of grains with dimensions larger than 5 cm. Reaction to HCl is very strong and pH has been estimated between 8 and 9. The fine earth fraction has a sandy texture and a particular to massive structure. This is mainly due to the ongoing cementation by secondary $CaCO_3$, which is getting from the “cotton ball-like” to the “alveolar” facies. Roots are present in rather low amounts. However some relatively large roots are sporadically present. Similarly porosity is low because of the ongoing cementation by secondary calcite. The presence of secondary $CaCO_3$ is discontinuous.

Kc (110-190 cm – Munsell colour 2.5Y 7/4)

The mineral skeleton gets even coarser with 5 to 10% of grains between 2-10 mm, 5% between 10-50 mm, and 50% of grains with dimensions larger than 5 cm. The whole horizon is strongly cemented by secondary $CaCO_3$ as “alveolar” facies, arranged in small nodules plugging the inter-scree pores (Fig. 3.13 D). The fine earth fraction is mainly composed of sands derived from the “alveolar” facies of NFC *sensu lato*. HCl reaction is very strong and pH around 9. Some fine roots (diameters of 1-2 mm) are present in this horizon. Porosity is nearly absent due to strong cementation of this horizon.

Ccak2 (190-215 cm – Munsell colour 2.5Y 7/4)

This horizon displays some similar characteristics to the previous one. Mineral skeleton is overall coarser with 1 to 5% of grains between 2-10 mm, 7 to 10% of grains between 10-50 mm, and more than 50% of grains showing dimensions greater than 5 cm. Alteration of mineral grains seems weaker than in the previous horizon and cementation is lower. The fine earth fraction shows a sandy texture and structure is particular to massive due to cementation. Some large tree roots have been observed in this horizon. Free pores remain only in non-cemented zones. This horizon displays the three NFC *sensu lato* macroscopic facies, "cotton ball-like", "coating" and "alveolar" (Fig. 3.13 E-F), whereas in the overlying horizon NFC was mainly observed as "alveolar" facies.

Finally, this soil has been identified as a *Calcisol calcaric skeletic* (WRB 2006).

3.1.2.2 Le Brugal (FR01 & FR05)

A quarry 1.5 km southeast of the Bonaguil (44°30'N, 1°00'E; altitude 124 m; Fig. 3.10 & 3.16 A) has also been visited and sampled in two distinct locations inside the quarry (FR01 & FR05). This quarry corresponds to a massive scree slope deposit, with the quarry front reaching up to 10 meters. The vegetation is composed of *Quercus pubescens*, *Buxus sempervirens*, *Juniperus sp.* and *Thymus sp.* The soil is gravelly and well developed and the transition between the A horizon and the underlying C horizon is sharp. Main rooting depth reaches 30 cm but roots have been observed until 80 cm. Secondary $CaCO_3$ have been observed only in the scree layer as "cotton ball-like" and "alveolar" facies.

3.1.2.3 Boussagou (FR03)

A small outcrop, 500 meters southeast of the Bonaguil station (44°31'N, 1°00'E ; altitude 111 m) has been sampled (Fig. 3.10 & 3.16 B). This outcrop displays large quantity of "cotton ball-like" macroscopic facies of NFC *sensu lato*. Nevertheless, as the pore dimension is rather small, the absolute quantity of secondary $CaCO_3$ is small.

3.1.2.4 Condat (FR04)

Finally, a site near the village

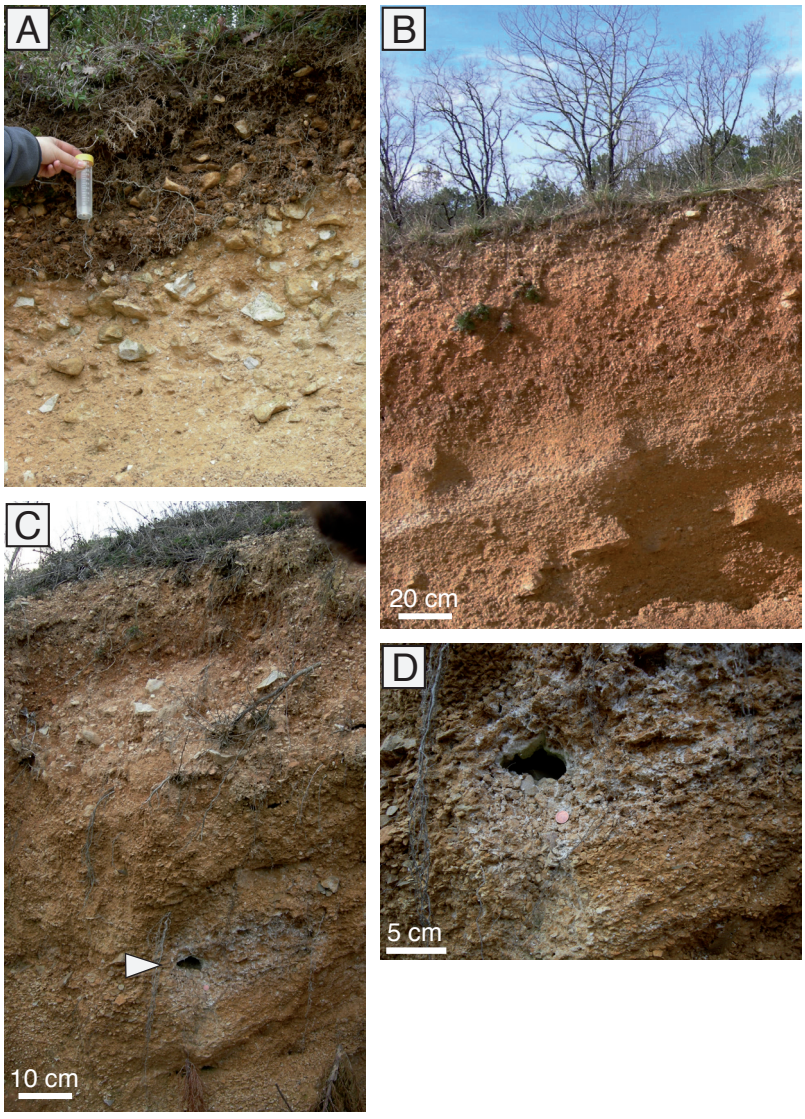

Figure 3.16 - Additional sampling sites in France. **(A)** Le Brugal (FR01) site. **(B)** Boussagou (FR03) site. **(C)** Condat (FR04) site. **(D)** Close-up of C showing a cavity of the lower part of the outcrop associated to highly cemented zones.

of Condat, 1.5 km east of Fumel (44°29'N, 0°59'E ; altitude 89m; Fig 3.10) has been sampled. This site corresponds to several small outcrops in scree slopes deposits. NFC *sensu lato* has been found mainly as "alveolar" facies (Fig. 3.16 C-D).

3.1.3 Sampling sites in Spain

Several sites (Fig. 3.17) in the Spanish Pyrenean foothills have been investigated in the area of Ainsa. One site, near the village of Arcusa, has been extensively described. In addition, two other sites have been visited, briefly described and sampled, one near the village of Campo, 20 km east of Ainsa, and one in the Val de Benasque 40 km northeast of Ainsa (Fig. 3.17). All these

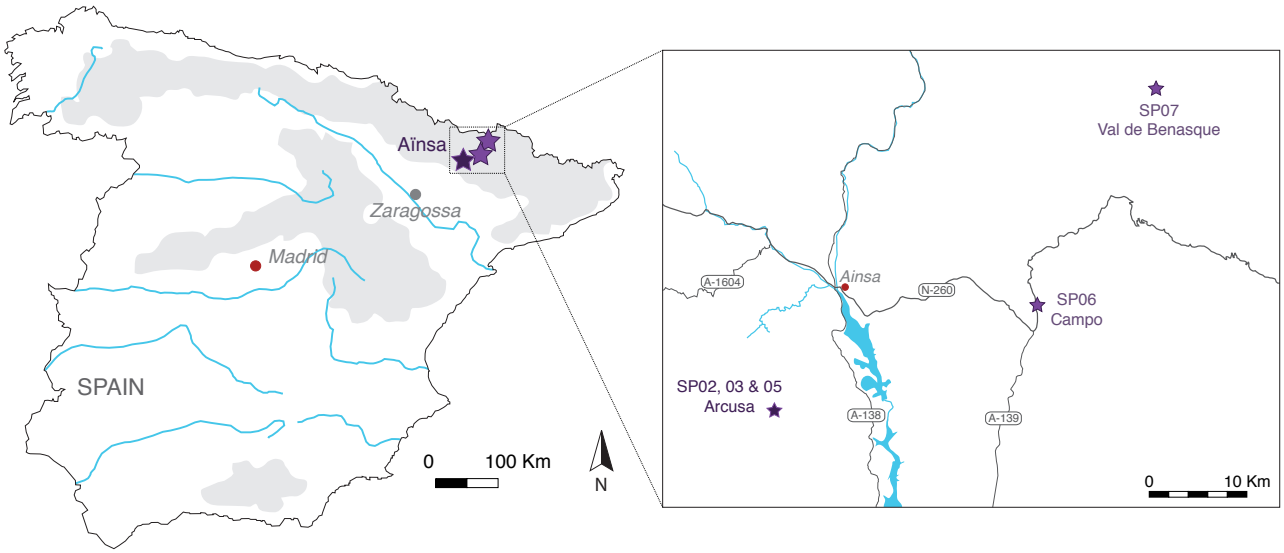

Figure 3.17 - Localization of the sampling sites (★) in Spain, province of Huesca.

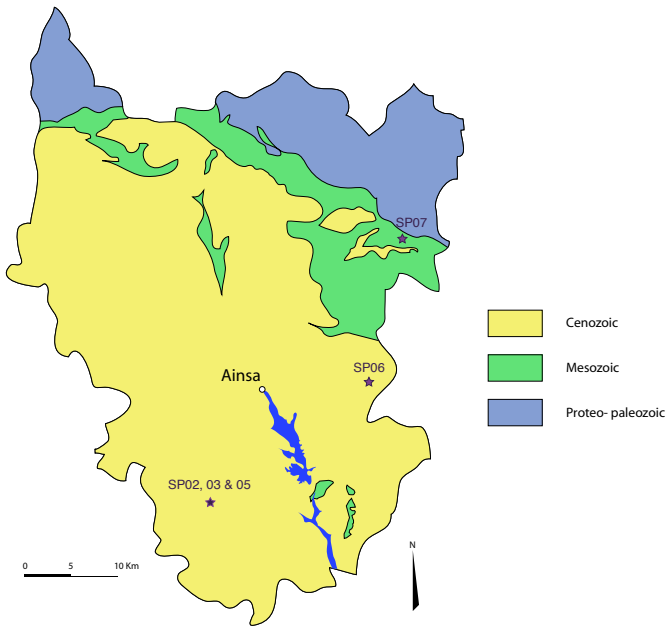

Figure 3.18 - Simplified geological map of the Sobrarbe region (http://www.sobrarbe.com/descargas/mapa_cenozoico.pdf). Sampling sites are indicated (★).

sites correspond to scree slope deposits displaying different levels of secondary $CaCO_3$ cementation and different sizes of scree deposits. Scree deposits are composed of fragments of upper Mesozoic to lower Cenozoic limestones (Fig. 3.18). The climate of the region is mountainous with a moderate continental to Mediterranean influence. Winters exhibit mild to cold temperatures, with the lowest temperature between November and February. Mild winter temperatures are under the influence of the Mediterranean climate, resulting in a mild mountainous climate. Summers on the other hand, are rather hot with the maximal temperature between June and September. Minimal precipitations values correspond to the thermic maximum, whereas maximum precipitations are observed during spring and fall (Fig. 3.19).

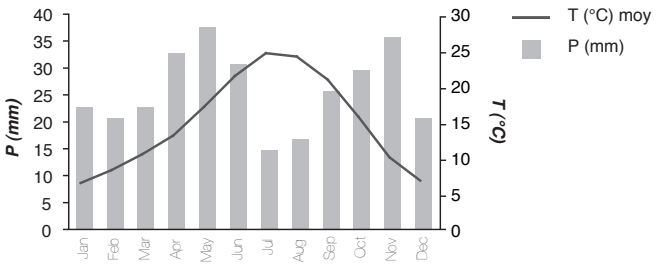

Figure 3.19 - Climatic data for the city of Zaragoza, autonomous community of Aragon (localization is indicated in Fig. 3.17). Ombrothermic diagram showing the mean monthly precipitations and temperatures. Zaragoza is located at an altitude of about 200 m above see level, as a result temperatures in the sites investigated are slightly lower due to the elevation factor (roughly -0.6°C / 100 m). Data from Agencia Estatal de Meteorología – AEMET.

3.1.3.1 Description of the reference site: Arcusa (SP02)

The main study site is located near the village of Arcusa, 15 km southwest of Ainsa at an altitude of 840 m (Fig. 3.17). It is actually composed of several successive outcrops in scree slope deposits (Fig. 3.20). Scree fragments have diameters between 0.5 to 2 centimetres and are made of Eocene limestone cryoclasts. Secondary $CaCO_3$ are found as “cotton ball-like” and “alveolar” facies, but the alveolar facies predominates and as a consequence, several zones are highly cemented (Fig. 3.21). Due to the extension of this site (Fig. 3.20) three outcrops (SP02, 03 & 05) have been investigated and one of them has been extensively described with full vegetation and soil descriptions (SP02).

Figure 3.20 - Panoramic view showing the three successive outcrops at the Arcusa site.

3.1.3.1.1 Vegetation

Three main types of plant communities are covering the slope with an overall cover estimated as follows: tree cover = 5%, shrub cover = 50%, herbaceous layer cover = 20%, and mosses cover = 20% (Fig. 3.22 A)

Plant community from downslope and/or dry and exposed areas:

Moor with chamaephytous shrubs such as *Cytisus scoparius*, *Genista hispanicus*, *Thymus sp.*, and *Rosmarinus officinalis*. The overall cover is low and soil surface is bare and covered essentially by colluviums (Fig. 3.22 B).

Midslope areas – Oak and Pine-tree forests

The tree layer is composed of *Quercus ilex*, *Quercus pubescens*, *Pinus sylvestris*, and a few individuals of *Quercus coccifera*. The shrub layer is made of *Buxus sempervirens* and juveniles

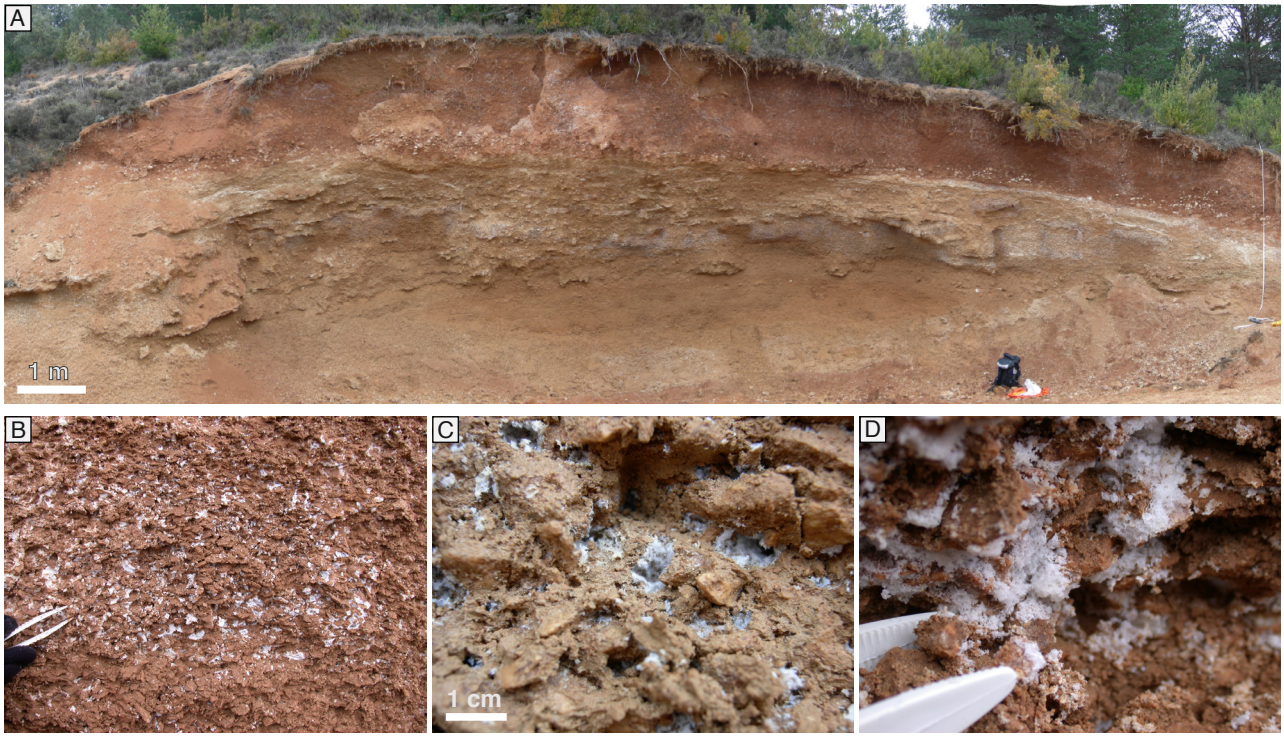

Figure 3.21 - Arcusa (SP02) site. **(A)** Panoramic view of the outcrop front. **(B-D)** Close-up on particular features of the outcrop. **(B)** View showing the total volume filled by secondary $CaCO_3$ accumulations in scree deposit pores in the K horizon. **(C)** Close-up on pores showing a "cotton ball-like" facies in the K horizon. **(D)** Close-up on pores showing an "alveolar" facies in the Km horizon.

Figure 3.22 - Vegetation and humus layer at the Arcusa (SP02, 03 & 05) site. **(A)** Overview of the plant communities cover showing the chamaephytous shrubs from downslope areas, the evergreen oak and pine-trees forest from midslope areas, and the evergreen oak forest of upslope areas with a low density of individuals leading to a small overall cover; *Junipero-Pinion sylvestris* alliance. **(B)** Detail of the chamaephytous shrubs from downslope areas. **(C)** Close-up on the holorganic layer identified as a *mycogenic oligomull*, showing needles accumulation at the surface.

of the different *Quercus sp*. In more open areas, shrubs from the typical open areas are observed together with *Juniperus phoenica*. In this type of area, the soil surface is almost entirely covered by a holorganic layer. In some places, a moss layer is well developed organized in aggregated patches, but with a small lateral distribution.

Upslope areas – Oak forest

Above of the previously described area, pine trees tend to disappear and *Quercus ilex* becomes the dominant species. Overall vegetation cover is lower than in the oak and pine forest, and as a consequence, the soil is covered by colluviums rather than a holorganic layer.

The overall type of vegetation belongs to the alliance of the *Junipero-Pinion sylvestris*, indicating subxerophilic and cold conditions of the area, influenced by both Mediterranean and mountainous conditions.

3.1.3.1.2 Humus

The holorganic soil layer has been described where it was continuous, i.e. under the oak and pine tree forest (Fig. 3.22 C). Litter from chamaephytous shrubs and Quercus ilex is poor both in quantity and quality, and climatic conditions are harsh, between mountainous and Mediterranean trends. Therefore, the holorganic layer is not expected to be either uniform or biologically very active. Mineral grains are present already at the surface suggesting that they are delivered regularly from upslope. The holorganic layer is made of a 1 cm thick OLn layer made of “fresh” litter and a 1 cm thick OLv layer showing the presence of dense meshes of mycelium and fungal strands of saprophytic fungi. Fragmented (OF) and humified layers (OH) are present but sporadic, indicating that OM may be efficiently integrated with the mineral matter in the organo-mineral layer (A horizon), depending on local conditions. The humus has been defined as a *mycogenic oligomull* after Baize and jabiol (1995), indicating that organic material is efficiently decayed but that the presence of fungi is crucial in order to attack recalcitrant material such as pine needles, evergreen oaks litter and hard leaves of chamaephytous shrubs.

3.1.3.1.3 Soil and surficial formation description

The soil at Arcusa sites shows a particular organization, with two groups of horizons already visible on the outcrop (Fig. 3.21 A & Fig. 3.23). Two distinct phases of pedogenesis might be present, however both contain secondary $CaCO_3$. Upper horizons exhibit a reddish colour indicating that dynamic of iron is a dominant process, which is typical in Mediterranean region (fersiallitic soils). Then, a highly cemented horizon draws a boundary with underlying horizons having an ochre colour. This apparent difference between upper and lower horizons does not seem to influence secondary $CaCO_3$ dynamics as it is observed in both groups of horizons. The main rooting depth reaches 20 cm and the maximal extension is up to 160 cm.

The soil profile has been described down to a depth of 310 cm and divided into ten horizons forming two visually distinct groups. The first group of horizon is composed of Aca, Bca, K, and Kc horizons (up to 160 cm.). The lower part of this last horizon represents a visual boundary with the second group of horizons, which is composed of Kc/Km, Km, Cca, Cca/Km, Cca2 and Cca/Kc horizons (Fig. 3.23).

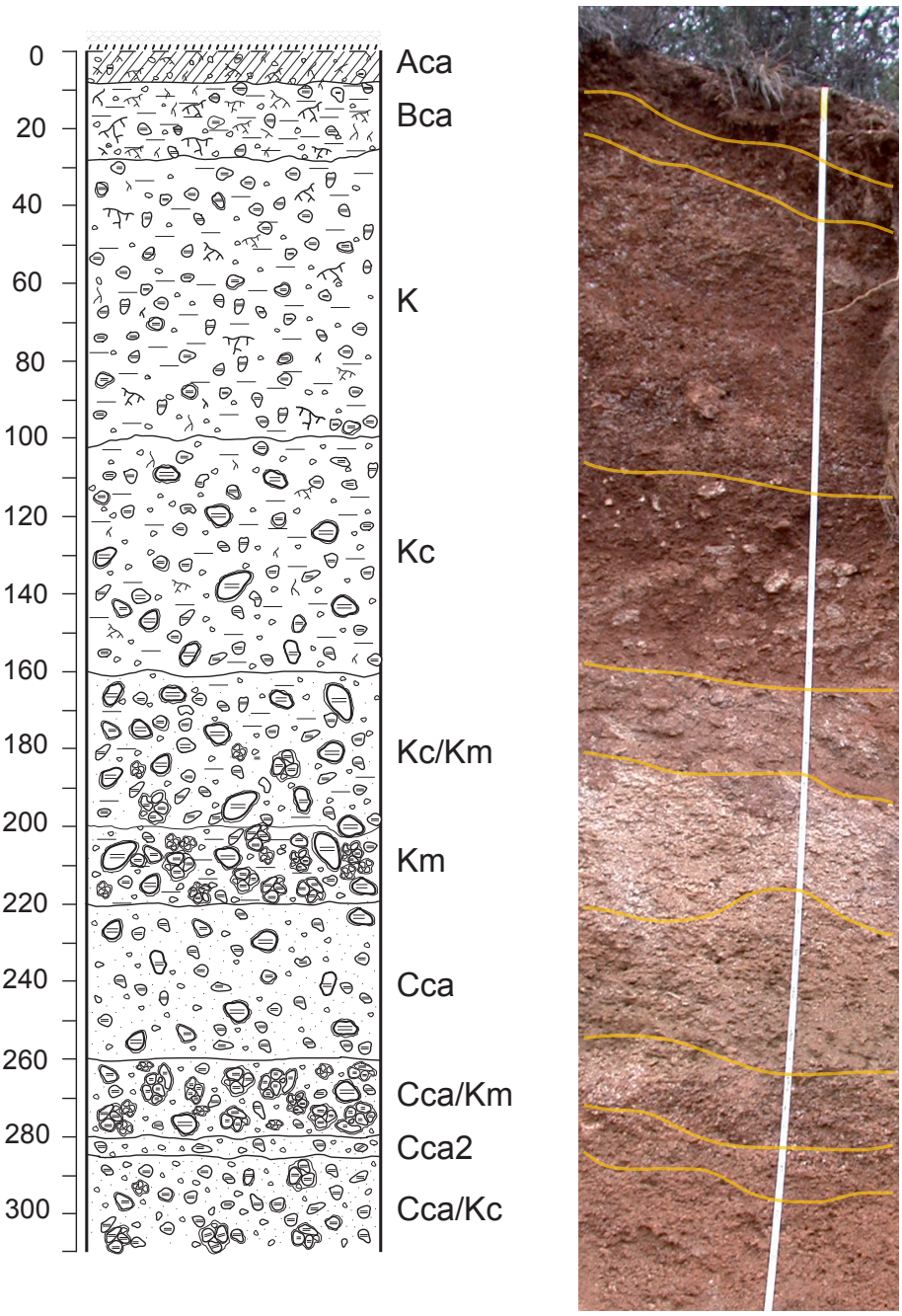

Figure 3.23 - Reference soil profile at the Arcusa (SP02) site, a *Calcisol calcaric chromic skeletic* (WRB 2006).

Aca (0-8 cm – Munsell colour 7.5YR 4/4)

The mineral skeleton is fine, constituted of 30% of grains between 2-10 mm, 20% between 10-50 mm, and no grain showing larger dimensions. HCl reaction is strong and pH has been estimated between 6 and 7. The texture is loamy and the structure microgranular to particular. Roots are extremely abundant and porosity is moderately developed. No secondary $CaCO_3$ accumulations have been observed in this horizon.

Bca (8-28 cm – Munsell colour 7.5YR 4/6)

The mineral skeleton is slightly coarser than in the overlying horizon with 40% of grains between 2-10 mm, 40% of grains between 10-50 mm, and very few grains showing larger dimensions than 5 cm. Strong HCl reaction and pH between 6 and 7. The texture is sandy-loamy and the structure is particular. Roots are abundant and porosity is moderately developed. NFC *sensu lato* accumulations have been observed in this horizon as “cotton balls”, in close association with roots. The transition

with the underlying horizon is sharp.

K (28-100 cm – Munsell colour 7.5YR 5/6)

The mineral skeleton is similar to the one of the overlying horizon. HCl reaction is strong and pH is between 7 and 8. The texture is loamy and the structure is particular. A few roots are present, showing a clear difference with the overlying horizon. Porosity is moderate. Secondary $CaCO_3$ are present as “cotton ball-like” facies and poorly developed “alveolar” facies (Fig. 3.21 A-B). These $CaCO_3$ accumulations are sporadically distributed within the horizon and distributed as diffuse spots, which are organized into patches.

Kc (100-160 cm – Munsell colour 7.5YR 4/6)

Mineral skeleton turns into coarser elements with 30% of grains between 2-10 mm, 40% of grains between 10-50 mm, and 20% of grains showing dimensions larger than 5 cm. The fine earth fraction appears strongly reddish. HCl reaction is strong and pH is between 7 and 8. The texture is loamy with a slight trend towards clays. The structure is still particular and a few fine roots have been observed. Porosity is moderate and NFC *sensu lato* is present as nodules. These nodules have a similar texture as coatings or moonmilk facies, i.e. a white plastic and porous texture. This is a completely different pattern compared to the overlying horizon (K) where it was present as diffuse aggregates. These nodules are most likely brought here by sollifluxion and are the result of secondary $CaCO_3$ reworked from the underlying horizon.

Kc/Km (160-200 cm – Munsell colour 10YR 4/4)

A sudden colour change happens in this horizon with the disappearance of the reddish colour of the overlying horizons to an ochre colour. This is probably the result of both the apparition of a massive quantity of secondary $CaCO_3$ as “alveolar” facies within the pores and a change in clay and/or iron pedogenetic-related processes. The mineral skeleton is composed of 30% of grains between 2-10 mm, 40% of grains between 10-50 mm, and 30% of grains showing dimensions larger than 5 cm. This last category is actually mostly made of smaller grains cemented by “alveolar” NFC *sensu lato* facies. The fine earth fraction exhibits a very strong HCl reaction and pH is between 8 and 9. The texture is loamy with a trend to a sandy one, due the disintegration of the “alveolar“ NFC facies. As a result, the structure is particular. This horizon displays a sparse fine earth fraction as most of the pores are actually cemented by an “alveolar” facies. “Coating” facies on soil grains have also been observed in some places, mostly at the bottom of the horizon.

Km (200-220 cm – Munsell colour 10YR 5/4)

The mineral skeleton is similar to the overlying horizon with the presence of an “alveolar” facies cementing the entire horizon (Fig. 3.21 D). However, a few “cotton ball-like” facies has also been observed. Porosity is accordingly almost absent. HCl reaction is very strong and the pH is between 8 and 9. Disintegrating secondary calcitic cements create a fine earth fraction, which exhibits a sandy-loamy texture. No roots have been observed in this horizon.

Cca (220-260 cm – Munsell colour 2.5YR 5/4)

The mineral skeleton is getting finer with 10% of grains between 2-10 mm, 20% of grains between 10-50 mm and 10% of grains with dimensions larger than 5 cm. Very strong reaction to HCl and pH is between 8 and 9. A large fine earth fraction is present and exhibits a true sandy texture and

a particular structure. This fraction more likely comes from the disintegration of cements coming from the overlying horizon. Surprisingly, no secondary $CaCO_3$ accumulations have been observed in this horizon and the question remains as why this horizon does not contain any accumulations, whereas the above one does? No roots have been observed and porosity is variously developed due to the lack of cementation.

Cca/Km (260-280 cm – Munsell colour 10YR 5/6)

This horizon shows overall similar characteristics to the Km horizon between 200 and 220 cm, with an "alveolar" facies irregularly cementing all the scree deposits. However, mineral skeleton is slightly finer with 30% of grains between 2-10 mm, 50% of grains between 10-50 mm, and larger grains actually made of cemented finer grains. Very strong HCl reaction and pH is around 9. The texture is sandy, likely originating from the disintegration of secondary cements and as a result, the structure is particular. No roots have been observed in this horizon and the macroporosity is almost absent.

Cca2 (280-285 cm – Munsell colour 10YR 5/6)

This horizon is sporadic and shows overall similar characteristic to Cca1. However, the fine earth fraction shows a sandy-loam texture in contrary to the true sandy texture of Cca1. The mineral skeleton is composed of 30% of grains between 2-10 mm, 30% of grains between 10-50 mm, and a few grains with dimensions larger than 5 cm. Strong HCl reaction and pH is between 8 and 9. The structure is particular and no roots have been observed. Porosity is low to moderate.

Cca/Kc (285-310 cm – Munsell colour 10YR 4/6)

This horizon shows similar characteristics to the Kc/Km horizon observed between 160 and 200 cm. However, the mineral skeleton is finer, with 30% of grains between 2-10 mm, 50% of grains between 10-50 mm, and no grains with dimensions larger than 5 cm. Very strong HCl reaction and pH is around 8. The texture is loamy with a slight trend toward sands and the structure is particular. No roots have been observed and porosity is low to moderate.

This soil has been identified as a *Calcisol calcaric chromic skeletic* (WRB 2006).

3.1.3.2 Campo station (SP06)

An outcrop located near the village of Campo, 20 km east of Ainsa (42°24'N, 0°23'E; altitude 647 m; Fig. 3.17 & 3.24 A) has been prospected and some secondary $CaCO_3$ samples have been harvested at the outcrop. The pores of this scree slope deposits are nearly entirely filled with secondary $CaCO_3$, either as "alveolar" or "cotton ball-like" facies. Numerous fine dark filaments are observed in cavities associated to NFC *sensu lato*, they have been identified as fungal rhizomorphs.

3.1.3.3 Val de Benasque (SP07)

Finally, an outcrop located in the Val de Benasque, 40 km north-east of Ainsa (42°36'N, 0°31'E; altitude 1100 m; Fig. 3.17 & 3.24 B) has been sampled. This outcrop corresponds to a huge scree slope deposit, with the quarry front reaching up to 10 meters. Scree deposits are composed of fragments of a Cretaceous limestone. This site has the particularity to display massive quantities of secondary $CaCO_3$, with some areas showing more secondary cements than the parent material in terms of occupied volume. The "alveolar" facies virtually binds the scree fragments together. In

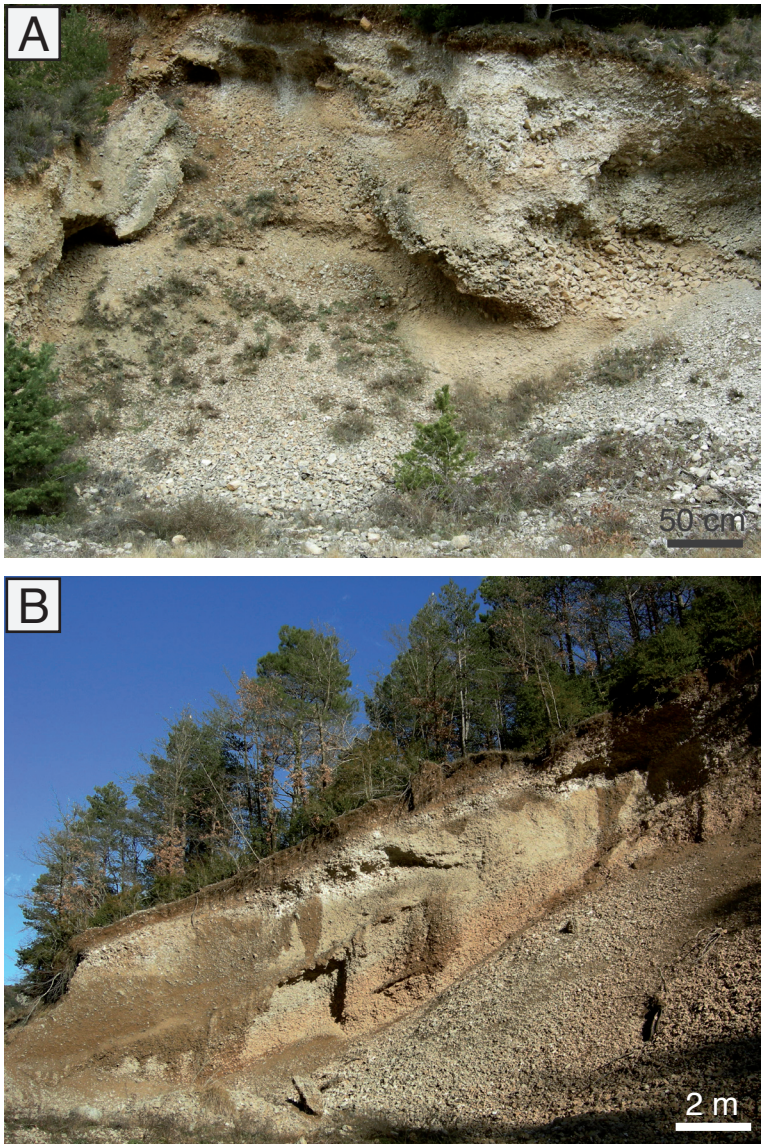

Figure 3.24 - Additional sampling sites in Spain. (A) Campo (SP06) site. (B) Val de Benasque (SP07) site.

free cavities, secondary $CaCO_3$ is also present as "cotton ball-like" facies associated to numerous fine dark filaments identified as fungal rhizomorphs. The vegetation is composed of *Pinus sylvestris*, *Buxus sempervirens* and *Quercus pubescens*. The soil layer is well developed with OM containing horizons (A and B) 20-30 cm thick in average but reaching up to 1 m. The vegetation indicates prevailing subxeric conditions in this site, whereas the accumulation of OM in the topsoil indicates that its decay is somehow slow, due to the mountainous climatic conditions.

3.1.4 Synthesis of field descriptions and observations

The scree slope deposits investigated in this study are the result of periglacial processes that took place during the last glacial period (Würm; between 120'000 – 10'000 BP) or just after it. The alternation of cold and warmer periods during the late Pleistocene and early Holocene has caused the fracturation of the calcareous bedrock, allowing the formation of cryoclasts. These latter may further accumulate as scree deposits at the bottom of a slope forming a typical scree slope. In addition, during glacial periods, or just after when glaciers are retreating, eolian erosion is strong and leads to massive loess deposits in distant areas. As a result, loess deposits may occur on top or within scree slope deposits. Later, during the Holocene, when climatic conditions become

more favourable, soils develop on top of the scree accumulations (Gobat et al. 2003). Therefore, the pedogenesis is the result of the mixing of loess deposits and weathering of carbonate host rocks. Typically, the limit between the organic and mineral horizons is sharp indicating that these soils are still young and pedogenetic processes currently ongoing. Finally, the presence of pores in shallow horizons allows intense drainage of both soil solutions and gases all along the soil profile. The formation of NFC *sensu lato* typically occurs mostly beneath the organic soil horizon, in the well developed pores.

3.1.4.1 Macroscopic facies in relation to the climate

The occurrence of the different macroscopic facies of NFC *sensu lato* shows a different pattern according to the geographical locations (Table 3.1). The Swiss sites (CH01, 04 and 05) mostly display the “cotton ball-like” and the “coating” facies, the “alveolar” facies being far less common. Moreover, no highly cemented layer within 150 centimetres from the soil surface has been observed in any of the sites. To the contrary, French and Spanish sites display extended “alveolar” facies, as well as “cotton ball-like” facies, whereas the “coating” facies is less common. As a result highly cemented layers are more common in the French and Spanish sites, as well as far more developed than in the Swiss site. The French and Spanish sites are both under the influence of a more xeric climate than the Swiss sites, leading to the occurrence of highly cemented layers. A raise in altitude has the same effect as coatings have been more often observed in the Spanish sites of the Pyrenean foothills than in the French sites which are closer to the see level. Finally, the fact that the “cotton ball-like” facies has been observed in all the sites, whatever the climate, supports its

Table 3.1 - Table summarizing the occurrence of each macroscopic facies vs site. Dark dots correspond to the dominant phase and white dots to minor phase. No dots means that the facies has not been observed at the site.

	Cotton ball-like	Coatings	Alveolar
CH01 Villiers	●	●	○
CH04 Savagnier	●	●	○
CH05 Tavannes	●	●	
FR02 Bonaguil	●	○	●
FR01 & 05 Le Brugal	●		●
FR03 Boussagou	●		
FR04 Condat			●
SP02 Arcusa	●	○	●
SP03 & 05 Arcusa II	●	○	●
SP06 Campo	●		●
SP07 Val de Benasque	●	○	●

status of original facies in the evolutionary succession of these secondary $CaCO_3$. In conclusion, as mentioned in the chapter devoted to NFC and nanofibres (chapter 2), the climate has a great influence on the macroscopic facies, resulting in specific syntactic growth of calcite on simple needles and cementation of nanofibre meshes.

3.1.4.2 Dynamic of NFC genesis

Conclusions regarding the dynamic of NFC *sensu lato* genesis may be drawn regarding the age of the surficial formation. These scree slope deposits apparently all took place during late Pleistocene to early Holocene, as a result of periglacial processes. It may be hypothesized that the genesis of secondary $CaCO_3$, at the earliest, started after the scree slopes have established. For instance, at the Villiers site, the presence of a local glacier has been demonstrated and its retreat has occurred at the end of the Würm period (15'500-12'000 BP; Arn 1992). The formation of the scree slope deposits rationally post-dates the glacier retreat. Furthermore, the presence of NFC *sensu lato* is presumably linked to the presence of variously developed soils. Therefore, NFC *sensu lato* genesis may have occurred only after pedogenic process were established, i.e. at least later than 10'000 BP. Importantly, this means that NFC *sensu lato* genesis has occurred under an average temperate climate. Although climate variability in the Holocene is recognized (Mayewski et al. 2004), it is not significant enough as to change completely the soil and the vegetation functioning. As a result, secondary $CaCO_3$ consisting of NFC and nanofibres are formed under xeric conditions, as well as in more humid climates.

3.2 Pedo-chemical settings

Soil pH from the three main sites (SP02, FR02 and CH01) has been measured. In addition, basic physicochemical characterization of the soil solution of the Villiers (CH01) site has been performed in order to determine the calcite saturation index of these solutions. These data aim at defining the basic pedo-chemical parameters of the soils and surficial formations where NFC and nanofibres occur. Eventually, it will allow to briefly discuss the importance of pedogenic processes in their formation.

3.2.1 Methodology

3.2.1.1 pH measurement of the bulk soil

This analysis has been performed based on the manual of soil analysis of the Soil & Vegetation Laboratory, University of Neuchâtel. pHs have been measured from bulk soil samples, previously air-dried, from Arcusa (SP02), Bonaguil (FR02) and Villiers sites (CH01), harvested on a 10 centimetres step pattern.

Two types of pH have been measured: the active acidity (H_2O pH) and the exchange acidity (KCl pH). The H_2O pH represents the H^+ that are liberated after rehumectation of the soil samples. These H^+ are in equilibrium with the clay-humic complexes. The KCl pH represents the exchange acidity, i.e. the total amount of H^+ present in the soil sample. The difference between the KCl pH and the H_2O pH, called Δ pH, represents the potential acidity of the soil sample. This is the quantity of H^+ that are bound by the clay-humic complexes. Values above 1 demonstrate a high potential acidity. Highly calcareous soils usually have no potential acidity, to the contrary of argillaceous soils.

Briefly, 20g of 2mm-sieved soil samples that have been previously air-dried are immersed in either deionised water or a 1M KCl solution in a soil/liquid ratio of 1/2.5. Solutions are homogenised by mild shaking for 2 hours and pH is measured by immersing the electrode directly in the solution.

3.2.1.2 Characterization of the “soil solution”

Basic physicochemical parameters from the soil solution of Villiers soil profile have been characterized: pH, alkalinity, calcium (Ca^{2+}) and magnesium (Mg^{2+}) concentrations as well as calcite saturation index ($SI_{calcite}$).

3.2.1.2.1 Sampling of the soil solution

Sampling of the soil solution has been performed using three different methods. Water percolating within the soil profile has been collected using i) bottles connected to 340cm^2 polypropylene laboratory tray buried at two depths in the soil profile (in the A and C calcic horizons) and ii) conventional lysimeters buried at the interface between the B and C calcic horizons. “Soil solution” from the “coating” facies of the C calcic horizon, as well as from the moonmilk coatings, has been retrieved using an ultracentrifugation method after a modified protocol of Giesler et al. (1996). About 50 g of “coating” facies samples are centrifuged at 15’000 rpm for 150 minutes at 10°C. Supernatants are immediately transferred into 2mL ependorf tubes. pH of the solutions are measured using a pH meter. In addition, samples are then separated into two portions, one for the alkalinity titration and one for the Ca^{2+} and Mg^{2+} quantification, the latter being acidified with 20 µL of ultrapure 65% HNO_3.

Some “coating” and moonmilk samples did not deliver a sufficient volume of water in order to

determine all or part of the physicochemical characteristics, even though the total water content was similar to the other samples. Actually, most of the water present in «coating» and moonmilk samples could not be retrieved with centrifugation. This fact indicates that water is strongly bounded to the microfeatures of this facies.

3.2.1.2.2 Alkalinity titration – Gran titration method

Alkalinity titrations have been realized after the Gran titration method described in Andersen (2002). In this study total alkalinity has been considered as resulting only from carbonate alkalinity (concentration of DIC, H^+ and OH^-), due to the calcareous nature of the sampled site. However, in certain conditions, organic compounds and other anions may contribute to total alkalinity in other systems (Stumm and Morgan 1996; Andersen 2002). The Gran titration method consists in titration of a water sample with known amounts of a low concentrated acid and measurment of the subsequent pH change. These data allow a Gran function $[(V_{sample} + V_{acid}) \times 10^{-pH}]$ to be calculated. A plot is drawn with the volume of acid on the x-axis and the Gran function on the y-axis. Extrapolation of the linear portion of the Gran function to the *x*-axis allows the titration endpoint to be determined with great precision. Alkalinity is subsequently determined using the following equation:

$$\text{Alkalinity (mg/L)} = \frac{V_{acid} \times N_{acid} \times gfw}{V_{sample} \times |z|}$$

V_{acid}: volume of acid used to titrate to the end point
N_{acid}: normality of the acid
gfw: gram formula weight in mg/mol
V_{sample}: inital volume of sample
|z|: absolute value of the charge associated with the carbonate species

and expressed as mg/L of $CaCO_3$. Water retrieved by the centrifugation method typically delivered low water volumes. Therefore, samples were diluted in ultrapure water before titration and the alkalinity value of ultrapure water was subtracted from to the final result.

3.2.1.2.3 Ca^{2+} and Mg^{2+} quantification

Ca^{2+} and Mg^{2+} have been quantified using Inductively Coupled Plasma Mass Spectrometry (ICP-MS) and Ion Chromatography (IC). ICP analyses have been carried out with two instruments, a quadrupole ICP-MS ELAN 6100 from Perkin Elmer at the University of Neuchâtel and a sector-field Element XR ICP-MS at the University of Lausanne. IC analyses have been carried out on a ICS-1100 from Dionex at the University of Lausanne.

3.2.1.2.4 Determination of the calcite saturation index

The calcite saturation indexes ($SI_{calcite}$) have been determined by modelling the solution chemistry using the online version of PHREEQC (WEB-PHREEQ). The data used to calculate the $SI_{calcite}$ were: pH, alkalinity, Ca^{2+} and Mg^{2+} concentrations and temperature. Temperature was set at 10°C after measurements performed in the field.

3.2.1.2.5 Methodological considerations

Sampling methods, as well as time lapse between collecting and titration, are factors that may falsify the alkalinity levels (Giesler et al. 1996; Andersen 2002). Number of samples in this study is

not sufficient enough in order to draw a general conclusion. However, a large difference for the same type of samples is observed for the soil solution retrieved from the A horizon. Alkalinity values for soil solution retrieved using the tray method are two times lower than for the soil solution retrieved using lysimeters. However, alkalinity values for the B horizon and the B-C interface are similar and consistent with theoretical expectations, i.e. values are not in equilibrium with atmospheric pCO_2 (Stumm and Morgan 1996). Similar samples from the C calcic horizon using centrifugation and lysimeters show similar values. These observations may indicate that the most suited methods for collecting the soil solution for alkalinity purpose are centrifugation and lysimeters extraction. Yet, Giesler et al. (1996) have shown that the use of lysimeters may induce changes from natural conditions of the soil solution and thus tend to favour the centrifugation method, in particular for investigations dealing with natural conditions of the soil solution. Finally, the tray method seems to provide unreliable results, probably because of reequilibration processes with atmospheric pCO_2 if the sampling system is not well sealed.

In addition, the use of different methodologies for the measurements of calcium and magnesium has led to differences between similar types of samples. Measurements from similar C calcic samples with the ICP-MS at Neuchâtel University confer Ca^{2+} concentrations two times higher than those obtained with the IC and ICP-MS at Lausanne University. Differences observed regarding Mg^{2+} concentrations show the same pattern. However, comparison of the same samples using ICP-MS from both Neuchâtel and Lausanne has shown that differences are between 6 and 11% with a maximal value of 20%. For details, see Annexes (Annex 2). Therefore, for the samples that have been analyzed using both methods, due to analytical considerations, data from Lausanne ICP-MS will be preferred. For samples analyzed only in Neuchâtel, data will be considered even though an uncertainty can be assigned to the results. Differences between similar samples might be the result of natural heterogeneity, as soil is a patchy environment by definition. Measurements of Ca^{2+} and Mg^{2+} with IC at Lausanne deliver inconsistent results. Values for “coating” samples are about 2 and 10 times less concentrated regarding Ca^{2+} and Mg^{2+} respectively, than samples analyzed with ICP-MS. To the contrary, values for the moonmilk samples are 3 and 16 times more concentrated regarding Ca^{2+} and Mg^{2+} respectively. Consequently, IC data will not be further considered and moonmilk data are too inconsistent to be discussed further (Annex 2).

3.2.2 Pedo-chemical settings – results of measurements

3.2.2.1 Villiers site (Fig. 3.25)

H_2O pH increases with depth. It increases faster from the surface down to 60 cm, which corresponds to the A and B horizons, than in the C calcic horizon. This pattern typically results from the influence of the buffering effect of the secondary $CaCO_3$. KCl pH has not been measured on a 10 cm basis but once per horizon. It shows that the Δ pH is around 0.7 all along the profile (Table 3.2). A slight increase between A and B horizons in observed, probably as a result of a slight clay accumulation in the B layer subsequent to pedogenetic processes.

The soil solution parameters show that the alkalinity, pH and, to a lesser extent Ca^{2+} concentration, increase with depth, leading to the overall increase of the calcite saturation index with depth (Table 3.3). The A horizon is clearly undersaturated in respect to calcite, whereas the solution retrieved from the coatings from the C calcic horizon are saturated. However, $SI_{calcite}$ at the interface between the B and C horizons is either undersaturated or slightly supersaturated. This shows that the interfacial zone display localized microenvironments with different properties.

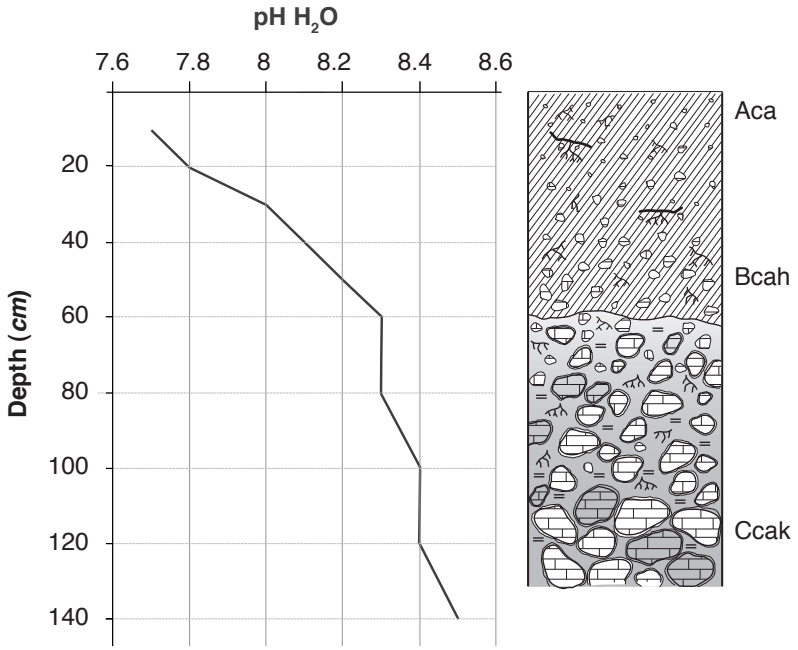

Figure 3.25 - H_2O pH evolution in function of depth for the reference soil profile, Villiers (CH01) site. Data from Hasinger (2009). Shaded areas represent the presence of secondary $CaCO_3$.

Table 3.2 - H_2O and KCl pH of the Villiers soil profile. Measurements have been carried out on one sample per horizon. Data from Hasinger (2009).

	pH H_2O	pH KCl	Δ pH
Aca	7.60	6.93	0.67
Bcah	8.04	7.28	0.76
Cca	8.20	7.49	0.71

Table 3.3 - Physicochemical parameters of soil solutions from Villiers (CH01). The sampling method is specified for each sample. T: tray method; L: lysimeters method; C: centrifugation method. The instrument used for measuring Ca^{2+} and Mg^{2+} concentrations is indicated. ICP LS: ICP-MS measurements performed at Lausanne University; ICP NE: ICP-MS measurements performed at Neuchâtel University.

	Alkalinity [mg $CaCO_3$/L]	pH	Ca^{2+} [mg/L]	Mg^{2+} [mg/L]	$SI_{calcite}$	Sampling method	Ca/Mg method
soil surface - organic layer A	81.32	7.67	36.56	0.57	-0.37	T	ICP LS
soil surface - organic layer A	73.01	7.69	36.10	0.56	-0.40	T	ICP LS
soil surface - organic layer A	177.14	7.98	*n.a.*	*n.a.*	*n.a.*	L	
mid soil - mineral layer B	122.75	8.19	*n.a.*	*n.a.*	*n.a.*	L	
interface organic-mineral layer B-C_{ca}	146.38	6.98	52.73	0.78	-0.67	T	ICP LS
interface organic-mineral layer B-C_{ca}	125.44	8.01	35.88	0.53	0.14	T	ICP LS
in scree clasts pores C_{ca}	156.42	8.32	56.11	0.97	0.70	L	ICP NE
in scree clasts pores C_{ca}	162.81	8.00	60.22	1.29	0.43	C	ICP NE
in scree clasts pores C_{ca}	*n.a.*	*n.a.*	32.45	2.45	*n.a.*	C	ICP LS

3.2.2.2 Bonaguil site (Fig. 3.26)

H_2O and KCl pH clearly show the same behaviour from the surface down to 90 cm. H_2O pH decreases down to the same values as the KCl pH from 120 cm. Therefore, while Δ pH was around 0.8 until 100 cm, it decreases down to 0 at 130 cm. Δ pH shows also a slight difference with lower values between 0 and 40 cm compared to the 40-90 cm interval. This fact may be interpreted as a slightly higher clay or silt content in deeper soil layers, probably originating from periglacial aeolian deposition (loess) that occurred in late Pleistocene to early Holocene (Ehlers and Gibbard 2004). The sharp H_2O pH decrease leading to a zero potential acidity, corresponds to the Kc horizon, indicating that the functioning between the upper and lower soil layers is different. Kc is a highly cemented horizon, which probably restricts the per-descensum transfer of material from overlying horizons to deep mineral soils. This fact is emphasised by the observation in the field of large root channels, which abruptly stop at the bottom of the Cca horizon, associated to supposedly highly humified OM. This indicates that root penetration is limited to deeper soil layers. Yet it is not completely restricted, as roots have been observed in the Ccak2 horizon.

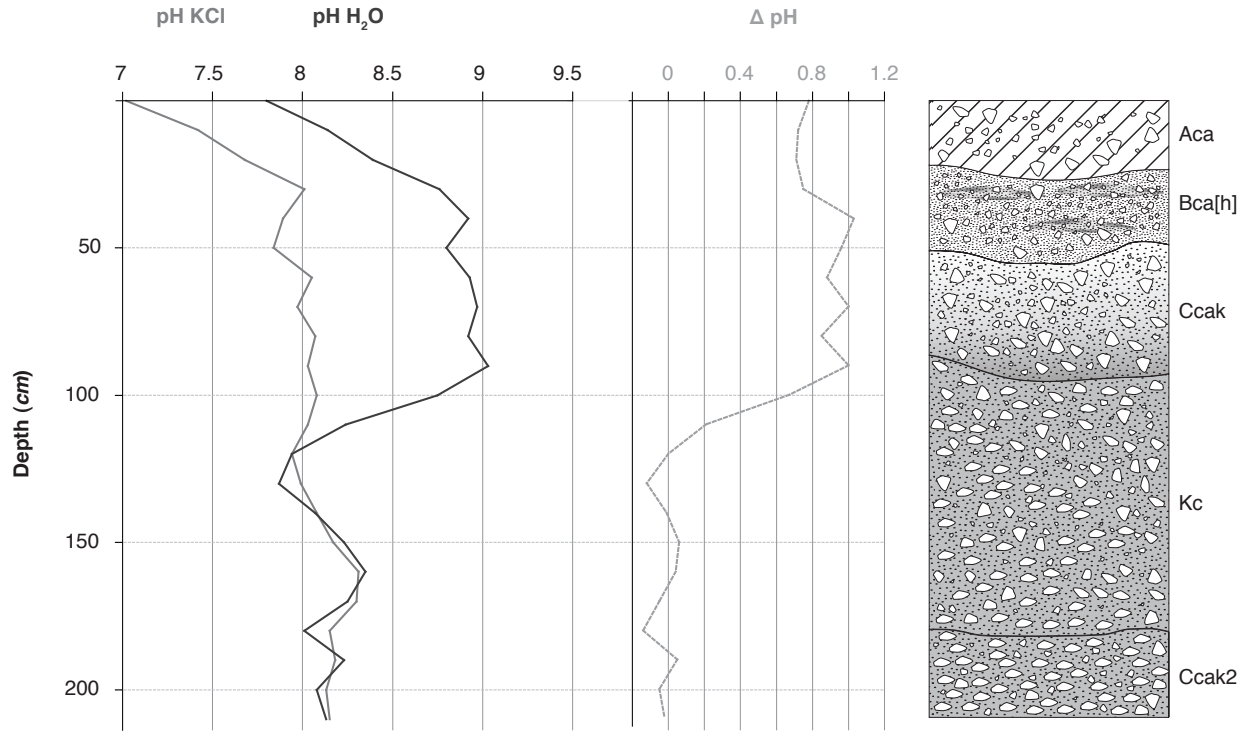

Figure 3.26 - H_2O pH, KCl pH and Δ pH evolution in function of depth for the reference soil profile, Bonaguil (FR02) site. Shaded areas represent the presence of secondary $CaCO_3$.

3.2.2.3 Arcusa site (Fig. 3.27)

The H_2O pH increases in the first thirty centimetres from the surface and remains in a steady state until 160 cm. Then, it gradually increases until 200 cm where it increases in a last step to become fairly stable until the bottom of the profile. The KCl pH shows the same trend as the H_2O pH, at the exception of the surface horizon that has a higher KCl pH than the underlying horizon. The Δ pH is around 1, indicating that the potential acidity is significant. It shows a rapid increase at the surface up to 1.3, remains around 1.3-1.4 until 50 cm, decreases around 1.2 between 50 and 100 cm, remains stable until 160 cm and then decreases gradually down to 1-0.8 until the bottom of the soil profile.

The rapid Δ pH increase observed at the surface is interpreted as being the result of OM decay. The aboveground litter is mostly made of oak-tree leaves, pine needles, which are considered as acidifying litter materials (Gobat et al. 2003). Between 10 and 100 cm, Δ pH is above 1, indicating a high potential acidity. This is probably related to the presence of the reddish fine earth fraction in this part of the soil profile, supposedly containing iron-rich clays and/or iron oxide minerals. The slight Δ pH decrease observed between 50 and 100 cm is probably the result of the carbonate precipitation activity observed in the K horizon, where sparsely distributed zones of secondary calcite occur. The change of patterns for both H_2O and KCl pHs occurring at 160 and 200 cm are reflected in the Δ pH, which shows a net decrease. It corresponds to the occurrence of highly cemented horizons.

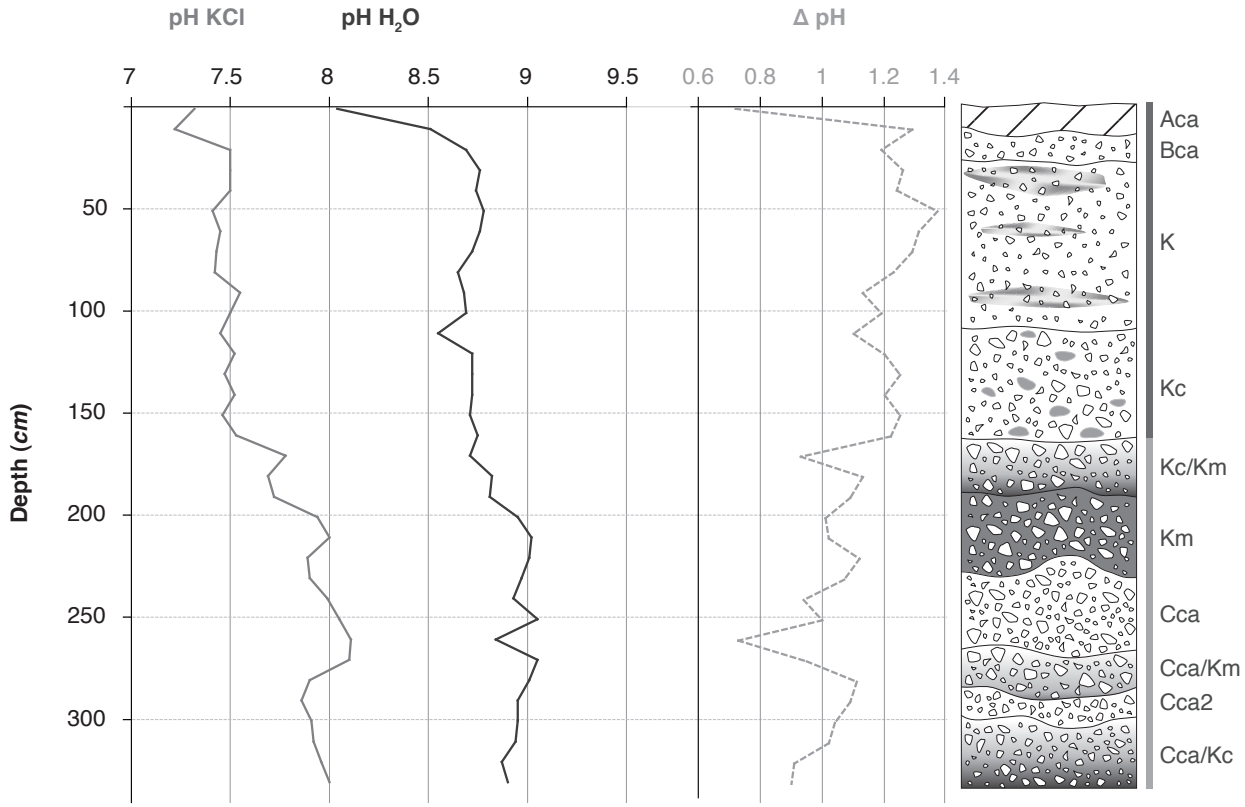

Figure 3.27 - H_2O pH, KCl pH and Δ pH evolution in function of depth for the reference soil profile, Arcusa (SP02) site. Shaded areas represent the presence of secondary $CaCO_3$.

3.2.3 Pedo-chemical parameters and pedogenic processes

pH may be a good physicochemical indicator of pedogenesis evolution (Gobat et al. 2003). The pH pattern along the soil profile allows general conclusions to be drawn. However, as no other soil analyses have been performed regarding soil parameters, the following remarks would definitely need analytical confirmations.

Unsurprisingly, the pH is overall in accordance with field descriptions and the presence of $CaCO_3$ either as host rock or as secondary deposits. Its value is almost always above 8 at the exception of surface horizons containing OM. This is readily visible in the Villiers (CH01) soil profile (Fig. 3.25), where the OM content is high and pH 8 only reached at a depth of 30 cm. To the contrary, in Bonaguil (FR02) and Arcusa (SP02) soil profiles, pH 8 is reached already at 10 cm of depth (Fig. 3.26 & 3.27). OM dynamics is clearly different between CH01 and both FR02 and SP02, as a direct result of climatic conditions. Further, the evolution of the pH with depth overall increases at all the

three sites. This is the direct result of the presence of $CaCO_3$, either from scree weathering or from secondary $CaCO_3$ accumulations. However, at the FR02 site, a sharp decrease of the pH at a depth of 90 cm may be observed, the pH falling down from almost 9 to 8. The potential acidity decreases with depth, probably related to less developed material regarding pedogenic processes. At CH01 and SP02, the potential acidity is always above 0.7 and 0.8 respectively (Fig. 3.25, 3.27 & Table 3.2), even in horizons with high secondary calcitic cements. This suggests that buffering material, either as OM (probably humic compounds) or as clays, are present, and thus, is an indication of ongoing pedogenic processes. To the contrary, at the FR02 site, the potential acidity becomes null at a depth of 120 cm (Fig. 3.26). This probably indicates that these highly cemented layers do not contain particles that may bind H^+ and thus are not currently subject to direct pedogenic processes.

Undersaturated $SI_{calcite}$ of the soil solution suggests that weathering of the mineral material of the A horizon may occur, leading to the release of Ca^{2+}, which may further be transferred to deeper soil layers. Concentrations of Ca^{2+} in the C horizon vary from 60 to 30 mg/L of Ca^{2+}. While a large part of the pedogenic Ca^{2+} is already fixed in secondary $CaCO_3$ accumulations in the form of NFC and nanofibres, physicochemical parameters are still in favour of calcite precipitation as demonstrated by positive $SI_{calcite}$. In addition, scanning electron microscope images never show dissolution traits on NFC and/or nanofibres. As a result, the C horizon is currently undergoing processes of early diagenesis that might be the result of physicochemical processes. However, the $SI_{calcite}$ for the interface of the B and C horizons is, either undersaturated, or slightly supersaturated (Table 3.3). Yet secondary $CaCO_3$ is also observed at this location, despite the fact that $SI_{calcite}$ indicates either dissolution processes or difficult achievement of calcite nucleation. Indeed, even in slightly supersaturated conditions, stable nuclei are difficult to form (Stumm and Morgan 1996). This suggests that an alternative mechanism than physicochemical precipitation must apply for NFC and nanofibres observed at this location. Hence, the presence of organic material, which may act as an enhancer for calcite nucleation is a reasonable explanation (Dupraz et al. 2009).

3.2.4 Conclusions

The three soils that have been extensively described present similar soil characteristics related to $CaCO_3$ cycle. As a result, they all might correspond to the following *WRB* definition (2006) of: “Calcisols accommodate soils in which there is substantial secondary accumulation of lime (…), within 100 cm of the surface”. However, the WRB adds to this definition a climatic pre-requisite and only soils of aridic and semiaridic regions may be termed calcisols. The presence of massive accumulations of NFC and nanofibres in various climatic conditions emphasizes the need of a redefinition of calcisols extension and/or definition.

pH values characterise processes related to $CaCO_3$ cycle and the subsequent carbonate buffering system. Consequently, the main processes that are currently undergoing are likely to be OM stabilization by Ca^{2+}-OM-clay aggregates as well as Ca^{2+} lixiviation and subsequent precipitation of secondary $CaCO_3$ in deeper horizons. Geochemical modelling of the Villiers (CH01) soil solution demonstrates that mostly mineral soil layers are supersaturated regarding calcite. However, processes happening at the B and C horizons interface seem to be critical regarding the understanding of NFC and nanofibres genesis as $SI_{calcite}$ may vary from supersaturated to undersaturated conditions and yet $CaCO_3$ phases remain stable. Additional analyses should be performed in order to confirm processes happening around Ca^{2+} and OM cycles.

3.3 Summary of chapter 3

Field descriptions of vegetation and soils have brought indications regarding environmental conditions of the investigated sites. Sites in France and Spain show typical indications of rather dry climates, with subxerophilic vegetation composed of shrubs, pine and oak trees; however they may not be qualified as semiaridic climates. Sites in Switzerland are completely different regarding climatic conditions, mostly regarding humidity. These differences are shown in the macroscopic facies distribution, the “alveolar” one being more common in France and Spain, whereas the “coating” one is more common in Switzerland. The “cotton ball-like” facies is constantly present in all stations, confirming its status of initial facies in the evolutionary sequence of NFC. Thus this approach has confirmed the importance of considering macroscopic facies in relation to the climate, rather than considering the sole microscopic habitus as an indicator of climatic conditions.

The field approach has also emphasized the importance of pedogenic features in the formation of NFC. Structure of the sites harbouring NFC, as well as pedo-chemical parameters and pedogenic processes, are critical to understand the conditions leading to NFC and nanofibres formation.

Chapter 4

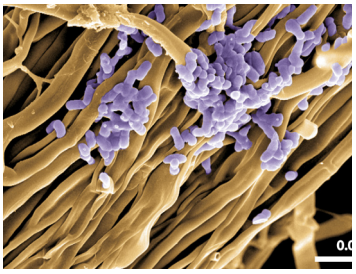

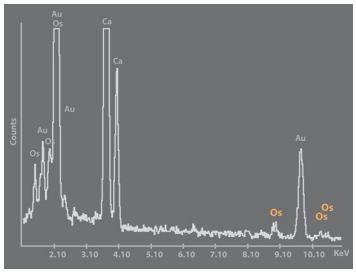

Contribution of observation methods

Chapter 4 - Contribution of observation methods to the understanding of NFC and nanofibres formation

The observation of natural objects, defined as the naturalistic method, is probably the most ancient and empirical type of scientific approach. It requires a thorough description of the investigated object as well as of its associated features. It is probably the most important approach in the first steps of a study. The study of NFC and nanofibres origins is not an exception to this rule.

In this study, as in numerous previous studies, the first aim was to unravel the origin of NFC. However, early, it became obvious that a thorough description of NFC was not dissociable from that one of nanofibres, as both features are recurrently observed together. Furthermore, it seemed clear that the examination of the relationship between NFC, nanofibres and associated filamentous structures were likely to bring some new insights in the enigma of their origin. However, a meticulous description of NFC, nanofibres, and associated microorganisms at the micro- and sub-micrometric scale requires powerful methodological tools. Hence, quite logically, electron microscopy has been chosen as the main tool of investigation. Several modes of electronic microscopy are available at present-day. By using different microscopic techniques, it was possible to emphasize different aspects of the relationship between NFC, nanofibres and associated features. Electron microscopy has been used either in scanning (SEM) or in transmission (TEM) mode. SEM observations have been performed using the high-vacuum conventional mode as well as in cryo or low-temperature mode. In addition, SEM and TEM allow performing elemental analyses on a small area of the sample by using the energy dispersive analysis of x-rays (EDAX), also known as energy dispersive spectroscopy (EDS). SEM allows the surface of samples to be observed, whereas TEM enables to look at the internal structure of samples. Both methods require the pre-treatment of environmental samples before their observation. Water needs to be removed and if organic matter (OM) is present in high amount, it requires to be fixed using chemical or physical (such as cold) methods (Dykstra and Reuss 2003). In addition, TEM requires the embedding of the samples in an epoxy resin in order to cut them as ultrathin sections. These procedures may be time consuming as well as sources of artefacts. Several studies have mentioned this latter fact as an explanation of unidentified features (Cañaveras et al. 1999; Barton et al. 2001). However, an adequate preparation of the sample allows major artefacts to be avoided (Dykstra and Reuss 2003). Moreover, cryotechniques are known to preserve in a good shape the three-dimensional structures of highly hydrated organic frameworks (Dupraz et al. 2004). As a matter of fact, in this study, the observation of similar samples using both, high-vaccum and cryo SEM did not show any significant difference which could alter the conclusions drawn from the images and associated microanalyses.

The observation of numerous environmental samples of different macroscopic characteristics have led to the collection of images of great informative value regarding the possible fungal implication in NFC and nanofibres genesis. These results have been synthesized in two publications. The first one deals mainly with the origin of nanofibres (§ 4.1), while the second deals with numerous analogies between fungal features and NFC specific characteristics (§ 4.2). In addition to this approach, thin sections of soil and NFC aggregates from the Villiers site (CH01) and moonmilk crust from *Vers-chez-le-Brandt* cave (CH02) have been performed. They have been investigated using both photonic microscopy and SEM. The results are presented in the last section of this chapter (§ 4.3).

4.1 Calcitic nanofibres in soils and caves: a putative fungal contribution to carbonatogenesis

Published in Geological Society, London, Special Publications 2010; v. 336; p. 225-238 doi:10.1144/SP336.11

Saskia Bindschedler[1], L. Millière[1], G. Cailleau[1], D. Job[2] and E. P. Verrecchia[1]

[1] Institut de Géologie et de Paléontologie, Université de Lausanne, Anthropole, 1015 Lausanne, Switzerland.
[2] Institut de Biologie, Université de Neuchâtel, Rue Emile Argand 11, 2007 Neuchâtel, Switzerland.

4.1.1 Abstract

The origin of soil mineralized nanofibres remains controversial. It is attributed to either biogenic factors or physicochemical processes. Scanning electron microscope and transmission electron microscope observations show that nanofibres could originate from the breakdown of fungal hyphae, especially its cell wall. It is hypothesized that during the decay of organic matter, cell wall microfibrils are released in the soil where they are exposed to mineralizing pore fluids, leading to their calcitic pseudomorphosis and/or are used as a template for calcite precipitation. When associated with needle fibre calcite bundles, nanofibres could indicate the relict of an organic sheath in which calcite has precipitated. This paper emphasizes the important roles of both organic matter and fungi in carbonatogenesis, and consequently in the soil carbon cycle.

4.1.2 Introduction

Natural nanofibres have been observed in various environments such as subtropical and temperate soils (Verrecchia and Verrecchia 1994; Cailleau et al. 2005) and cave deposits such as moonmilk (Borsato et al. 2000; Cañaveras et al. 2006). They are often associated with Needle Fibre Calcite (NFC; Verrecchia and Verrecchia 1994; Borsato et al. 2000). The aim of this study is to provide new insight into the processes at the origin of nanofibres.

In order to differentiate between organic and mineral nanofibres, the term organic nanofibre will be used for nanofibres whose organic nature has been determined by analytical methods. The term mineral nanofibre will be used i) for nanofibres observed in scanning electron microscopy (SEM), in absence of specific labelling (see Materials and methods), and ii) for nanofibres diffracting the electron beam under transmission electron microscopy (TEM). The term nanofibre alone refers only to a shape or an object and therefore used for morphological descriptions.

4.1.2.1 Previous work on mineral nanofibres

Since 1980, many authors have reported mineral nanofibres from various environments (Table 4.1). The four following authors have specifically observed organized structures related to mineral nanofibres: (i) filamentous, ramified, microscopic structure composed by a dense nanofibre scaffolding (Borsato et al. 2000; Richter et al. 2008); (ii) a straight macro-structural alignment (3 to 5 μm wide and >70 μm long) of unordered nanofibres observed close to an organic filament (possibly actinomycetes, cyanobacteria, or fungi; Benzerara et al. 2003); and (iii) 3 μm wide and >50 μm long filaments interpreted as “calcified filaments with needles in grain-coating needle mat” have also been observed by Jones and Ng (1988).

Table 4.1 - Review of nanofibres in the literature. Review of nanofibres present in soils and caves: nomenclature, occurrence, and interpretation in the literature.

Authors	Nomenclature	Geological Setting	Interpretation/Context
Pouget and Rambaud (1980)	Calcite "en bâtonnets"	Soil with calcareous crust	Mesh of monocrystaline calcite crystals
Vergès *et al.* (1982)	Small needle-shaped crystals	Calcareous soils	Tangled crystals
Ducloux *et al.* (1984)	Calcite "en bâtonnets"	Developed on screeslope	Covering larger needle-fiber calcite crystals
Phillips and Self (1987)	Micro-rods	Pedogenic calcrete	Interpreted as calcified rod-shaped bacteria
Phillips *et al.* (1987)	Submicron size rods	Pedogenic calcrete	Interpreted as calcified rod-shaped bacteria
Jones and Ng (1988)	Needles	Rhizolith from the Pleistocene Ironshore Formation	Calcified filaments coated with needles (i.e. nanofibers)
Verrecchia and Verrecchia (1994)	Micro-rods	Quaternary calcretes, Israel	Disordered mesh
Loisy *et al.* (1999)	Micro-rods	Carbonate paleosol in scree deposits	Mineralized threadlike and bacilliform bacteria
Borsato *et al.* (2000)	Nanofibers	Moonmilk (cave deposits)	Probably abiogenic precipitation
Benzerara *et al.* (2003)	Nanobacteria-like rods	At the surface of the Tataouine meteorite	Straight micro-alignment of nanofibers; possible organic origin
Cailleau *et al.* (2005)	Micro-rods	Orthox soils	Observed on burnt oxalate crystals embedded in tree tissues
Jeong and Chun (2006)	Nanofiber calcite	Aerosols coming from loess plateau and desert	-
Richter *et al.* (2008)	Nanofibres	Moonmilk (cave deposits)	-

4.1.2.2 Filamentous organisms and structures in soils and caves

Filamentous organisms living within the soil or in caves must be heterotrophic organisms. Algae and cyanobacteria are photosynthetic organisms and thus are present only at the soil surface or in rock fractures near a light source. Indeed, in mineral substrates that are faraway from any light, these organisms are absent due to the lack of their energy source. Accordingly, filamentous fabrics present in these environments could be fungi, filamentous bacteria (in soils and caves mostly actinomycetes), and roots (Paul and Clark 1996; Gobat et al. 2003). Taking into account their sizes and morphologies summarized in Table 4.2, fungi are the most suitable organisms associated with nanofibres and NFC.

4.1.2.3 Fungal presence and activity in soil and caves

Fungi are present in large amounts in soils. As an example, one meter square of fertile soil can contain a 10000-km long fungal network (Gobat et al. 2003). About 80% of land plant species are colonized by arbuscular mycorrhizal fungi (endomycorrhiza), and around 3% of phanerogam species are colonized by ectomycorrhizal fungi (EcM), especially plants with a large distribution at a global scale (Pinaceae, Fagaceae). In soils, a vertical distribution can be distinguished regarding fungal type in terms of their ecology. Organic layers are mostly colonized by saprophytic fungi, whereas mineral layers are colonized by EcM fungi (van Schöll et al. 2008). The latter has been demonstrated as being a significant agent of mineral weathering of ecosystem-wide importance (van Schöll et al. 2008).

The mycelial network is able to efficiently translocate nutrients in solution from one place to another (Gobat et al. 2003). Basidiomycetes, and among them EcM fungi, are able to build structures named fungal strands that can extend meters away from the roots (Finlay and Söderström 1992; van Schöll et al. 2008). Thus, the presence of mycorrhized roots, fungal hyphae and strands in deep mineral

Table 4.2 - Characteristics of filamentous organisms in soils and caves. Review of the different filamentous organisms in soils synthesising characteristics such as filament diameter and morphology and their cell wall morphology and biochemistry. References from Jones 1970; Dix & Webster 1995; Paul & Clark 1996; Bouma et al. 2001; Carlile et al. 2001; Pregitzer et al. 2002; Prescott et al. 2003; Coleman et al. 2004; Pessoni et al. 2005; Hishi 2007.

	Diameters	Morphologies / Structures	Cell wall morphology	Cell wall biochemistry
Fungi	3-6 µm on average 1 µm (min) - 30 µm (max) Strands: 0.02->1 mm	Hyphae with or without septum, more or less ramified. Bundles of differentiated hyphae forming linear organs: fungal strands.	Tick-walled (up to 1 µm) and thin-walled (100-200 nm) hyphae	Two layers: a fibrillar component with chitin and β-glucans and an amorphous component with glycoproteins specific to taxonomic groups
Actinomycetes	0.5-1 µm in average, max 2 µm in some genus	Ramified mycelium, sometimes fragmented	Wall 20-80 nm thick	Gram positives bacteria with one homogenous layer of peptidoglycan (murein). Four types of peptidoglycans depending on genus
Fine roots	<2-0.2 mm Single conducting vessel 10-30 µm	Ramified structure composed, at a micromorphological level, of complex arrangements of linear vessels	Highly variable in thickness, from 0.1 µm in young cells to 100 µm in mature cells	Primary wall: network of fibrous cellulose and hemicellulose embedded in a matrix of pectin. Secondary wall: only in mature cells, can contain lignin

layers or in caves is not surprising. Canadell et al. (1996) showed an average rooting depth of 4.6 m +/- 0.5 m, with a maximum depth of 7.0 m +/- 1.2 m for trees. In their review, only the root itself is taken into account. Considering the mycorrhiza, it can considerably extend the root network (Timonen and Marschner 2006). Observations of roots at depths below 2-3 m in caves have also been observed (Canadell et al. 1996). Jasinska et al. (1996) demonstrated that root mats could be the sole source of food for faunal communities in an Australian cave.

4.1.2.4 Cave geomicrobiology

Caves are nutrient-limited environments due to the absence of light that prevents primary production through photosynthesis, contrary to other common environments on Earth. Thus, in terms of presence of life, this kind of environment can be considered as “extreme”. On the other hand, physicochemical parameters tend to be buffered and constant throughout the year (e.g. mild temperature normally equals MAST - Mean Annual Surface Temperature - and fairly high humidity). These extreme but constant conditions allow the presence of underground ecosystems, which may or may not be connected to aboveground energy-sources (Jasinska et al. 1996; Sarbu et al. 1996). Prokaryotes and fungi are the most common organisms that can be encountered in caves, and their link in speleothem formation is often proposed and debated. Moonmilk is a common speleothem mineral, and its biological or physico-chemical origin has long been discussed. To-day most of the theories involve microbial mediation in its formation, but the exact role that microorganisms play, whether it is bacterial or fungal, is still being discussed (Gradzinski et al. 1997; Northup and Lavoie 2001; Cañaveras et al. 2006; Barton and Northup 2007). In caves, moonmilk is more likely to be present in the vicinity of soils (Gradzinski pers. comm.). This increases the probability of cave

access for roots and their fungal associates, and consequently their involvement in the moonmilk's genesis.

4.1.2.5 Fungal strands and hyphae ultrastructure

4.1.2.5.1 Fungal hyphae size

Single fungal hyphae diameter is highly variable, depending on the taxonomic position, environmental conditions, age, and function of hyphae. Nevertheless, for functional hyphae, an average diameter of 3-6 μm is found in the literature (Dix and Webster 1995; Carlile et al. 2001). Non-functional hyphae, such as those from the cortex of fungal strands, can have a diameter of 1 μm, with an inner diameter of <0.5 μm.

4.1.2.5.2 Fungal strands

Basically, a fungal strand is a bundle of juxtaposed linear hyphae. They are organs produced by fungi to explore their environment and to translocate nutrients from one place to another. They have the ability to extend over long distances, i.e. up to 30 m. In addition, macromorphologically, they exhibit a variable diameter, depending mostly on their age and remoteness from nutrient sources. This diameter ranges from a few μm up to 4 mm in some wood decaying species (Thompson 1984). The structure of the fungal strand is composed of: i) an outer layer (the cortex) composed of a thick layer of narrow thick-walled multiseptate dead hyphae (average diameter of 1 μm) and ii) an inner layer (the medulla) composed of a few linear wide thin-walled sparsely septate living hyphae (average diameter of 6-10 μm). The latter seems to be less resistant to hydrostatic pressure (Watkinson 1979) and thus is more rapidly exposed to decay processes than hyphae with a thick melanized wall in the outer layer. The inner part often collapses, leaving fungal strands composed of a thick layer of narrow hyphae with empty wide channels in the middle (Watkinson 1984). The cortex of the fungal strands makes it an impermeable organ where fluids can be bidirectionally translocated (Watkinson 1979; Dix and Webster 1995).

4.1.2.5.3 Composition and structure of the fungal cell wall

The thickness of the cell wall also shows great variability depending on physiological processes and the function of hyphae. Single hyphae have an average thickness of 150 nm (Jones 1970; Beckett et al. 1974; Farkas 1979; Ruiz-Herrera et al. 1996; Pessoni et al. 2005). On the other hand, hyphae from the cortex of a fungal strand can exhibit very thick cell walls, up to 500 nm. The wall thickening can even occlude the hypha lumen (Watkinson 1984). Moreover, the walls of these hyphae often present a high degree of melanization, which is also a factor in impermeabilization (Paul and Clark 1996).

The fungal cell wall can be described by two main types of materials, an outer layer composed of amorphous material (mainly mannoproteins), and an inner layer composed of fibrous material, chitin and β-glucans (Burnett 1979; Ruiz-Herrera 1992; Bowman and Free 2006). Chitin is a polymer of a polysaccharide, N-acetyl-glucosamine. It is present in the form of long microfibrils, sometimes over 1 μm, with a diameter of 10-25 nm. It is located in the innermost part of the wall, arranged as an intertwined mesh embedded in an amorphous matrix (Aronson and Preston 1960; Carlile et al. 2001). β-glucans are homopolysaccharides of glucose. In the fungal wall, it is present either as β–1,3-glucan or in a lesser amount as β–1,6-glucan. They are found in greater amounts than chitin (Carlile et al. 2001; Farkas 2003). Figure 4.1 shows a sketch of the fungal cell wall.

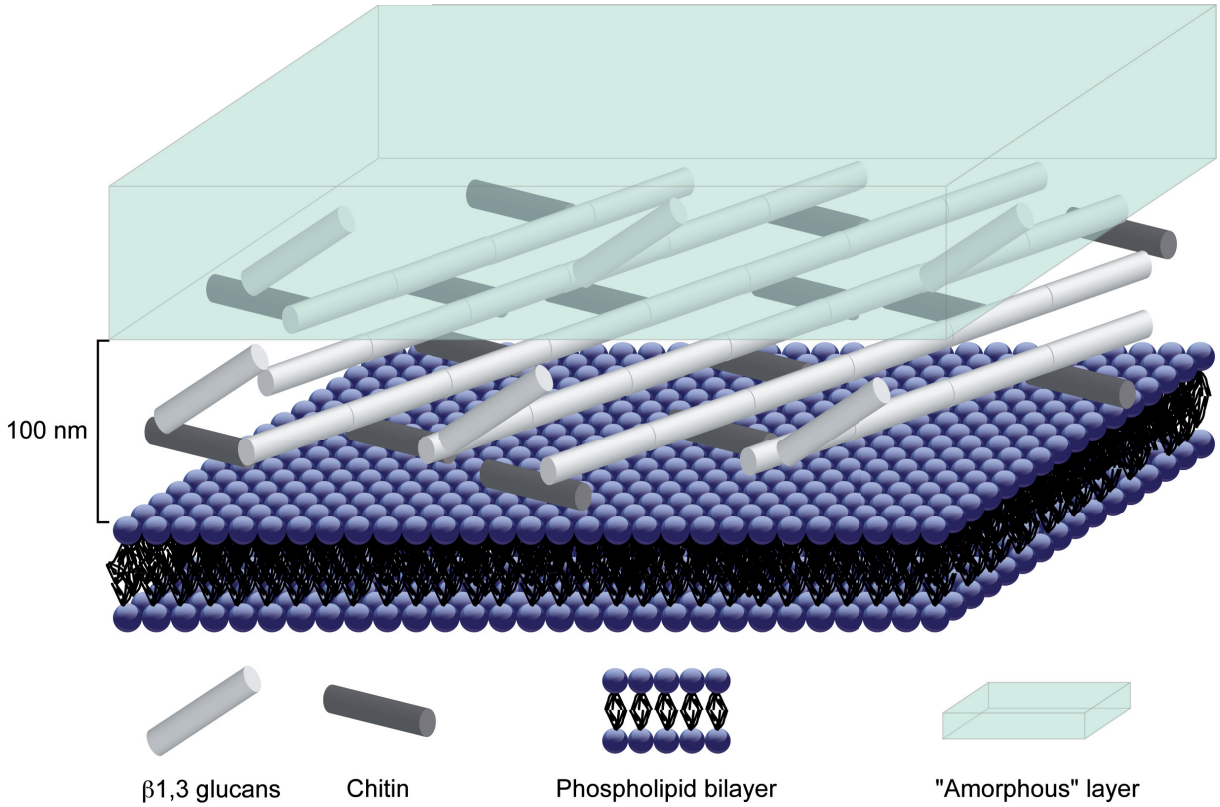

Figure 4.1 - Sketch of the fungal cell wall (modified from Latgé 2003). Note the fibrous layer composed by chitin and β-glucan fibres and the amorphous layer. In order to give an orientation to this sketch, the plasma membrane of the fungal cell has been represented by the phospholipids bilayer.

Cell wall material can be a significant part of the resistant organic matter in soils. Depending on physico-chemical parameters, enzymatic degradation of polymerous substances from the cell wall may or may not be possible (Paul and Clark 1996; Coleman et al. 2004).

4.1.3 Materials and methods

Secondary carbonate accumulations have been sampled at four sites: i) in the mineral layers (calcic horizon of a *calcisol* ; IUSS Working Group WRB 2006) at a quarry near Villiers (Swiss Jura Mountains, 47°04'N, 6°59'E), as well as ii) at an outcrop near Aïnsa (Spain, 42°21'N; 0°04'E), iii) in the narrow entrance of a cave near les Cornettes de Bises (Swiss Alps, 46°19'N, 16°48'E), and iv) in the vers chez le Brandt cave, inside a wide chamber at 100 meters from the entrance (Swiss Jura Mountains, 46°56'N, 6°28'E). At the first two sites (soils developed on scree slopes), samples exhibit two different morphologies directly visible in the outcroup: i) cotton-ball-like NFC that accumulates in the soil pores, ii) coatings on grains and centimetric to decimetric cryoclasts. When wet, these coatings constitute a plastic paste, which becomes pulverulent when dry. At the third and fourth sites (caves), only moonmilk deposits were sampled in the form of a wet plastic wall coating, up to 30 cm thick. In addition to crystals, fungal strands associated with different macroscopic morphologies of NFC have been sampled for electron microscope observations. Strands have been taken from cotton-ball-like NFC, associated with rock fragment coatings, or free in the soil pores. All samples were collected using polypropylene tweezers and stored in sterilized 50 mL tubes at low temperature.

Bulk samples were analysed by X-ray diffraction (XRD) using a Scintag diffractometer in order to determine their mineralogical nature. In each sample, quartz powder was added in order to normalize and compare samples with each other.

In order to detect organic from mineral material, prior to observations, each macromorphological sample was stained using a 4% osmium aqueous solution from a modified Pearson et al. (2004) protocol. However, using this labelling method, the presence of the organic matter can be determined but not its nature. Samples were gold-coated (10 nm) and observed using a Phillips ESEM-FEG XL30 Field Emission Gun Scanning Electron Microscope (FEG-SEM). Osmium staining was detected with an EDAX Energy Dispersive Spectrometer (EDS) coupled to the electron microscope. With natural non-flat samples and absence of a standard, EDS spectra only give qualitative information.

In order to check possible artifacts due to high-vacuum, some representative samples were observed using XL30 SEM in its LTSEM cryo mode (Low-temperature SEM).

Some fungal strands and coatings were embedded in an epoxy resin, and ultrathin sections were performed using a Reichert Ultracut S (Leica) microtome with a diamond knife. Ultrathin sections (200-220 nm thick) were observed using a Phillips CM-200 Transmission Electron Microscope (TEM) with a voltage of 200 kV. Crystal properties were determined using microdiffraction.

4.1.4 Results

XRD analysis of the three types of samples (cotton-ball-like structures, coatings on grains, and moonmilk) shows that their mineralogy is calcitic in nature (Fig. 4.2 a-c). Moreover, the absence of shift (expected in presence of Mg in the crystal lattice) after normalization with quartz powder characterizes the presence of low magnesium calcite (LMC) at these sites.

SEM observations of soil samples show recursive associations between NFC, unidentified nanofibres, and fungal strands. NFC is characterized by a width between 0.5 and 2 μm and a length < 100 μm. Some epitactic growths are present but no important development is observed (no big euhedral crystals due to epitactic cementation). The NFC is present either as random meshes, or as bundles, 3 to 30 μm in diameter (average 10 μm; Fig. 4.3 a). This microscopic feature constitutes the macroscopic cotton-ball-like structures. Bundles contain some nanofibres, occasionally associated with amorphous matter assumed to be an organic veil (Fig. 4.3 b). These nanofibres are rarely observed on NFC when the latter are randomly oriented and/or strongly modified by epitactic growth. At a microscopic scale, coatings from soil grains exhibit various amounts of NFC and nanofibres, in which needles are less represented than in the cotton-ball-like morphology. NFC often shows random orientations, whereas nanofibres are packed in clusters. This morphology shows great similarity with microstructures of moonmilk samples, in which NFC is even less represented.

SEM measurements show that nanofibres are up to 6 μm long (the shortest is 0.2 μm long) with an average width of 78.6 nm (standard deviation of 22.5 nm, based on 106 measurements; Fig. 4.3 c). They are characterized by a high flexibility (as mentioned by Borsato et al., 2000), leading to spectacular curvature (Fig. 4.3 c). They appear smooth under TEM. Two kinds of structures are observed: i) a randomly-oriented framework of nanofibres, in which widespread putative organic veils and calcitic micro-aggregates are present; these meshes are often associated with other components (i.e. NFC, fungal strands, hyphae, etc.) as observed in moonmilk deposits (Fig. 4.3 d), and ii) organized structures of nanofibres (Fig. 4.4), either as small pieces that have apparently undergone a breakdown, or as a tubular/circular microscopic network (Fig. 4.4 a & c). The term organized refers to a non-random distribution of nanofibres, whatever their nature. These networks are composed by intertwined nanofibres oriented in two main directions (Fig. 4.4 b & d).

Another main component is frequently observed associated with soil samples: macroscopic, brown organic filaments, identified as fungal strands. Their average diameter can reach 100 μm and they are composed of the two typical mycelial strand structures, an external part made of several narrow

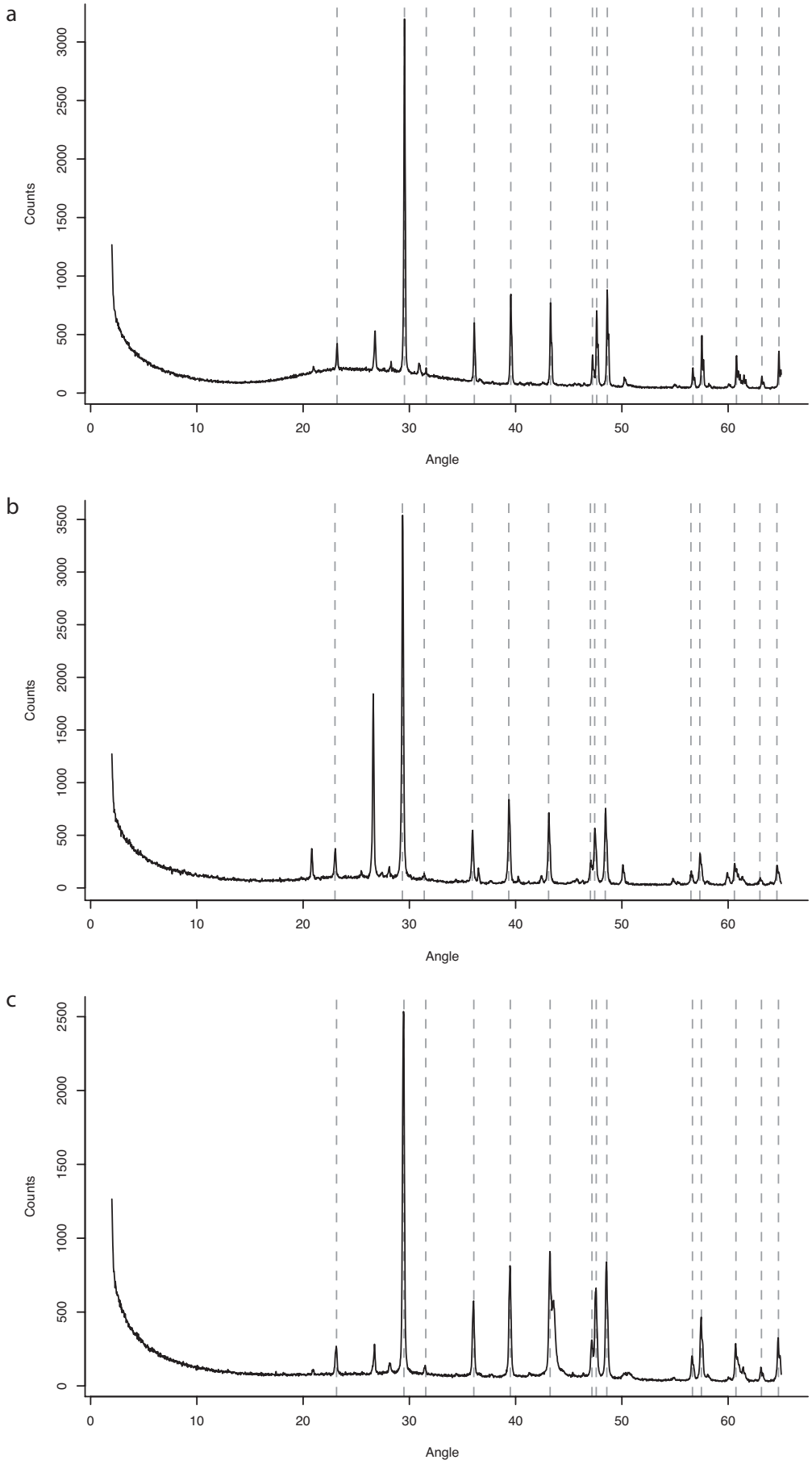

Figure 4.2 - X-ray diffractogramme showing the low-magnesium calcite nature of **(a)** cotton-ball like NFC from the Swiss Jura Mountains, **(b)** coatings on blocks from Swiss Jura Mountains and **(c)** moonmilk from the Vers chez le Brandt cave in the Swiss Jura Mountains samples. Dotted lines correspond to the main peaks of low-magnesium calcite ($CaCO_3$), the other peaks mainly correspond to quartz (quartz added prior to analysis to allow peak correction).

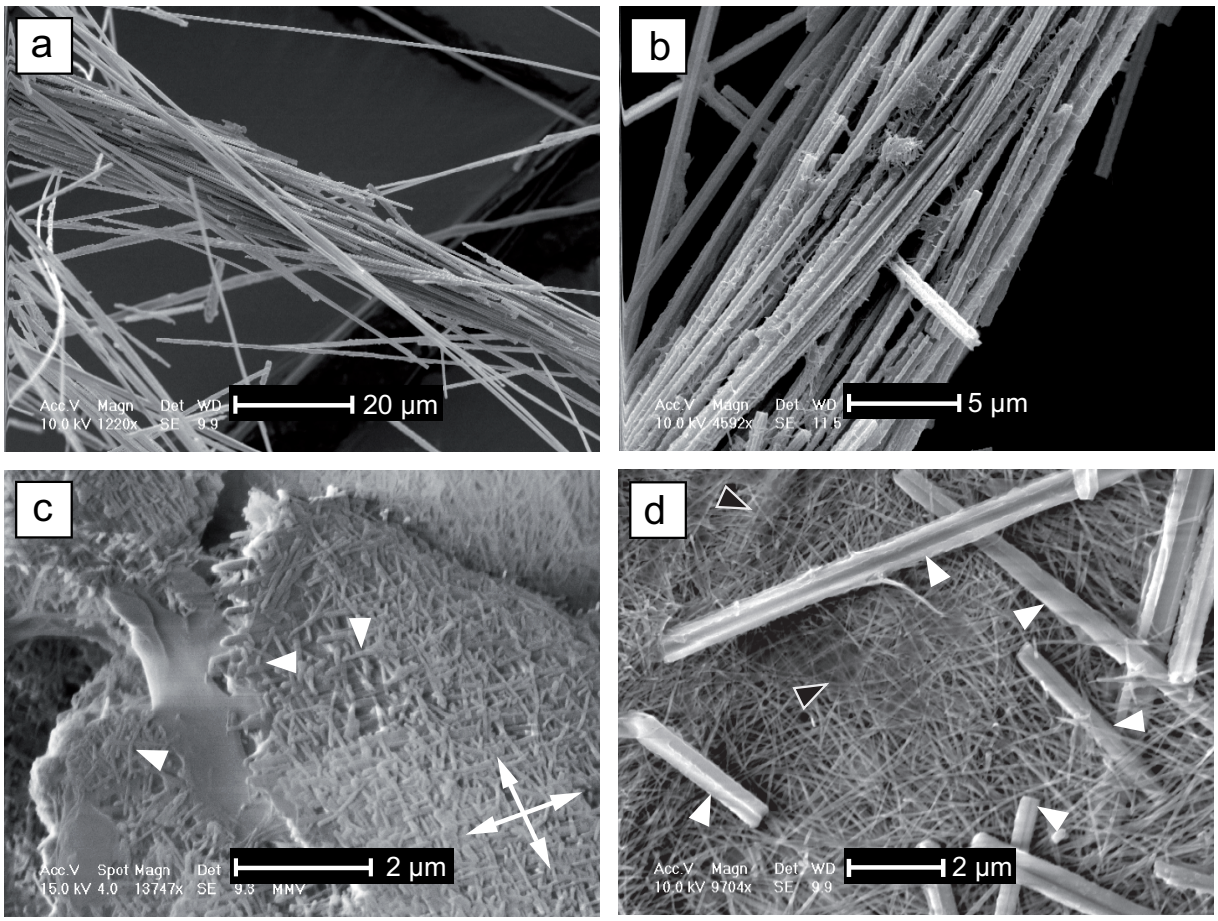

Figure 4.3 - (a-d) SEM photomicrographs. **(a)** bundle of NFC present in a sample from the Spanish site of cotton-ball-like NFC associated with a fungal strand (observed macroscopically). **(b)** bundle of NFC covered by putative organic veils. Some organic nanofibres are also present. Sample from a grain coating associated with a fungal strand and some cotton-ball like NFC. **(c)** Close-up of an organized mesh composed by nanofibres (moonmilk, Swiss Alps). Preferential orientations of nanofibres are shown by the crossed double-headed arrows. Some nanofibres are curved (arrows). This characteristic indicates a contact-deformation. **(d)** Mesh composed by randomly-oriented nanofibres associated with NFC (white arrows) and putative organic veils (black arrows). Swiss Jura Mountains, coatings on block.

fungal hyphae with a thick cell wall and an inner part characterized by a few wide thin-walled hyphae, which often lack in our observations due to their ability to be rapidly decayed (Fig. 4.5 a-b). Nanofibres are abundant all along the macroscopic filament where fungal strands seem to breakdown.

A cross-section of a fungal hypha shows that the fungal wall is composed of two layers, an inner part composed of fibrous material and an external part composed of an amorphous material (Fig. 4.5 c-d). From these observations, it is obvious that there is an intimate relationship between the hyphae and the nanofibres (Fig. 4.5 c-d). Optical observations, hydrochloric acid tests on moonmilk, as well as TEM microdiffractions (Borsato et al. 2000) indicate that the nanofibres are mineral in nature. In order to test this hypothesis, in situ analyses were performed to distinguish organic from mineral matter using osmium labelling with EDS control on samples. The osmium stains only organic matter and not mineral material (Pearson et al. 2004). Osmium peaks indicate that non-organized frameworks composed of only nanofibres do not contain organic material (Fig. 4.6 a-b) and organized meshes do contain organic matter (Fig. 4.6 c-d).

4.1.5 Discussion

The presence of nanofibres in various vadose environments has been widely observed. Their origin is either attributed to a biogenic factor (“probably rod-shaped calcified bacteria” Phillips and Self

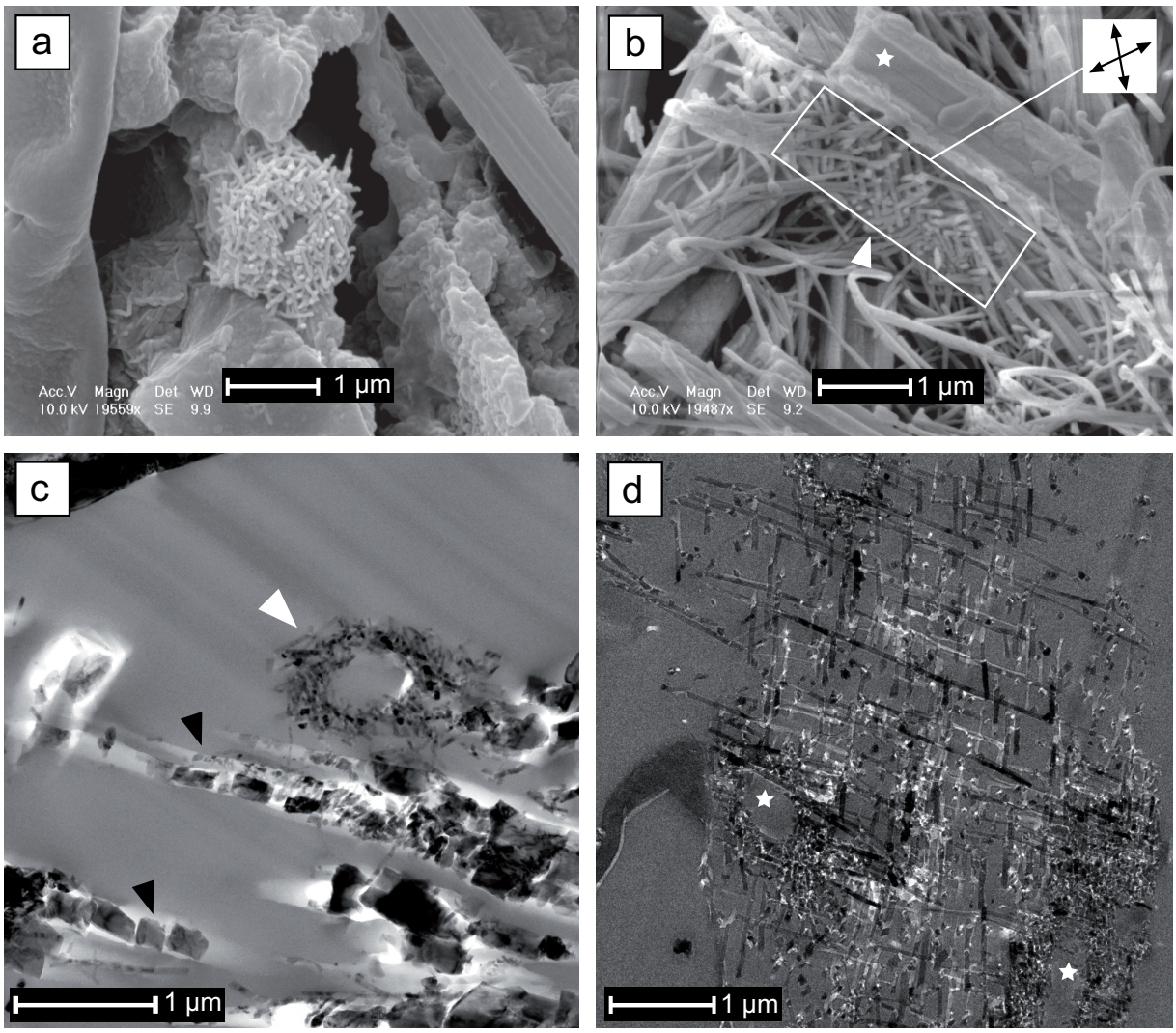

Figure 4.4 - Samples from the Swiss Jura Mountains site. **(a)** SEM photograph showing a tubular-like structure resembling an organic filament (e.g. a fungal hypha) and composed by nanofibres (cotton-ball-like NFC associated with decaying organic matter). **(b-d)** Sample from coatings on a cryoclast associated with decaying fungal strands. **(b)** SEM photograph showing a network of intertwined nanofibres oriented in two main directions (white rectangle). White star indicates a NFC crystal. **(c)** TEM photomicrograph showing a section of a circular structure interpreted as a possible organic filament (e.g. a fungal hypha) and composed by nanofibres. **(d)** TEM photomicrograph showing a network of intertwined nanofibres oriented in two main directions. Also note the presence of a circular section similar to the one shown in Fig. 4.2 c (stars).

1987; Ould Mohamed and Bruand 1994; "microrod attributed to bacteria or nuclei in gel" Verrecchia and Verrecchia 1994; Loisy et al. 1999) or physicochemical processes ("precipitation from pore filling fluids", sometimes assoicated with organic filaments i.e. nanofibres "cannot be fully attributed to direct organic activity", Jones and Ng 1988; "nanofibres show microstructures that are typical of inorganic, crystalline material", Borsato et al. 2000). Therefore, the origin of terrestrial accumulations of nanofibres remains controversial.

The nanofibres discussed in this paper are similar to those described in Phillips and Self (1987), based on their size and flexibility. It is important to note that they identified the organic filaments associated with nanofibres as fungi, and the same conclusion is drawn in this study, based on their size and morphology, as well as presence of macrostructures such as mycelial strands (Fig. 4.5 a-b). Two layers are visible during the breakdown of the hyphal cell wall (Fig. 4.5 d). It is known that the inner wall layer is composed of a hard microfibril framework (theoretically 10-25 nm in diameter, Carlile et al. 2001) made of chitin and β-1,3 + β-1,6-glucan. Based on this fact and the recognition of the organic nature of some nanofibres (Fig. 4.6 c-d), the organized meshes of nanofibres are considered as the result of a slightly destructive decay of the fungal fibrous cell wall

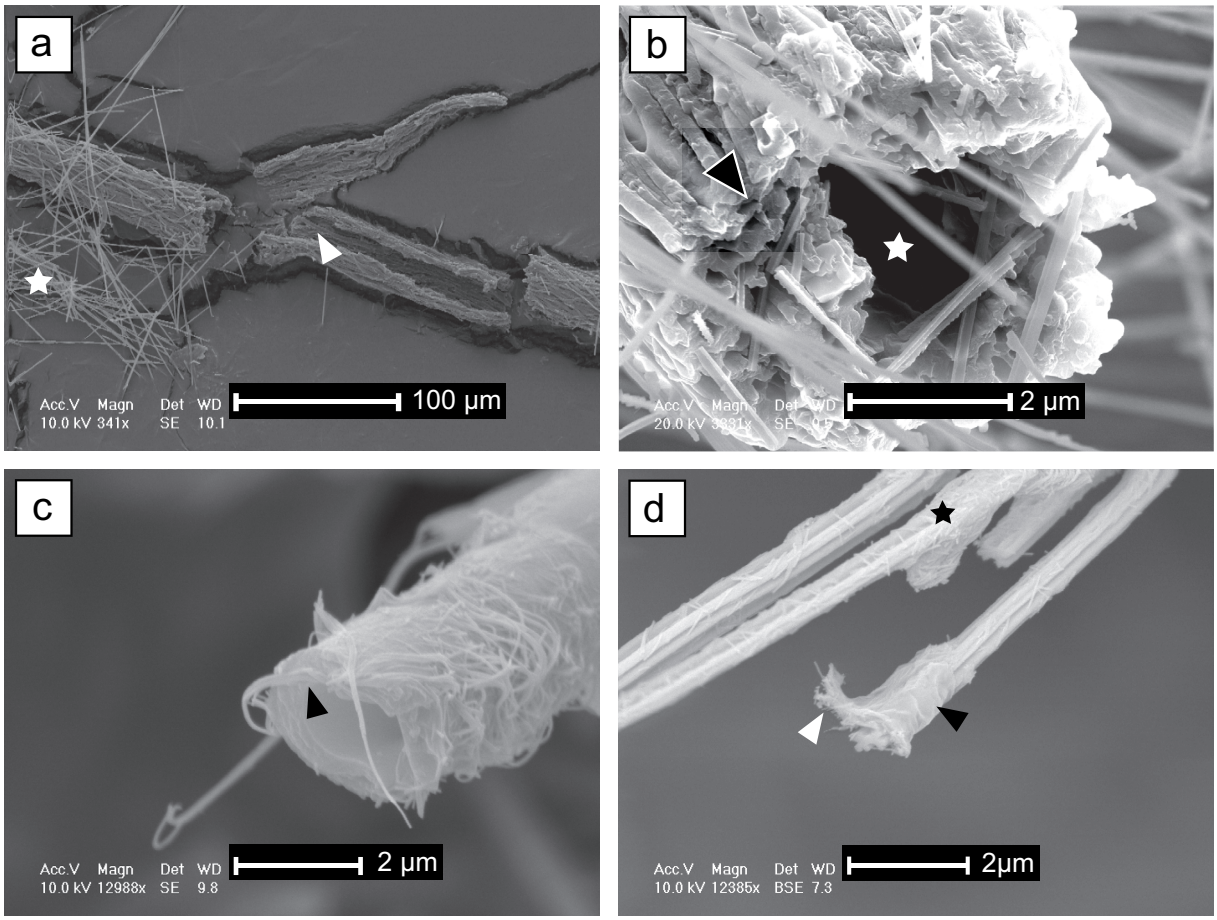

Figure 4.5 - (a-d) SEM photomicrographs. **(a-b)** Samples from Aïnsa (Spain). **(a)** Fungal strand associated with cotton-ball-like NFC (star). Note the absence of the inner hyphae (arrow), which seem to have already undergone breakdown. **(b)** Close-up of another fungal strand showing the narrow and thick-walled hyphae from the outer part (black arrow). Note that the internal wide thin-walled hyphae are absent (white star). **(c-d)** Swiss Jura Mountains samples. **(c)** Close-up of a decaying hypha from a grain coating sample showing the release of cell wall fibrous material (e.g. chitin, β-glucan) from its cell wall (arrow). **(d)** Remains of a putative fungal hyphae on needle fibre calcite. Two textures can be distinguished, an outer one that appears to be smooth (black arrow) and an inner one that appears to be composed of nanofibres (white arrow). Note also the presence of a mesh of nanofibres along the other calcite needles in this picture (star). Sample from cotton-ball like NFC associated with decaying organic matter.

material. At this stage, the organized meshes are interpreted as the first step in the breakdown of the fungal hyphae cell wall, whereas the non-organized mats represent the ultimate state of decay and reworking of this organic matter. In other words, the nanofibres could be interpreted as organic in origin and being the result of an incomplete decaying of fungal matter. During early diagenesis, their calcitic pseudomorphosis (Cailleau, 2005, Cailleau et al. 2005) and/or their role as a template for calcitic precipitation results from the release of the nanofibres in the soil environment, followed by their exposure to mineralizing pore filling fluids. This could explain why non-organized meshes (interpreted as the oldest decay product) are often composed of nanofibres of calcite, due to the longer exposure time to soil fluids. To conclude, the release of nanofibres may represent a partly destructive decay of the fibrous cell wall material.

Moreover, this interpretation has an important implication for NFC origin. The observation of NFC inside organic sleeves and the presence of small mats of nanofibres on bundles of NFC (Fig. 4.5 d star; Cailleau et al. 2009b) suggest a large contribution of organic matter for their genesis. As first noted by Phillips and Self (1987), NFC bundles could be the first step in the distribution of NFC in soil pores. Indeed, with time, the collapse of bundles due to various processes, such as weathering and bioturbation, would lead to a random distribution of NFC (mesh). Nanofibres on bundles would then be a relict of the organic sheath (assumed to be fungal in origin). The presence of mycelial

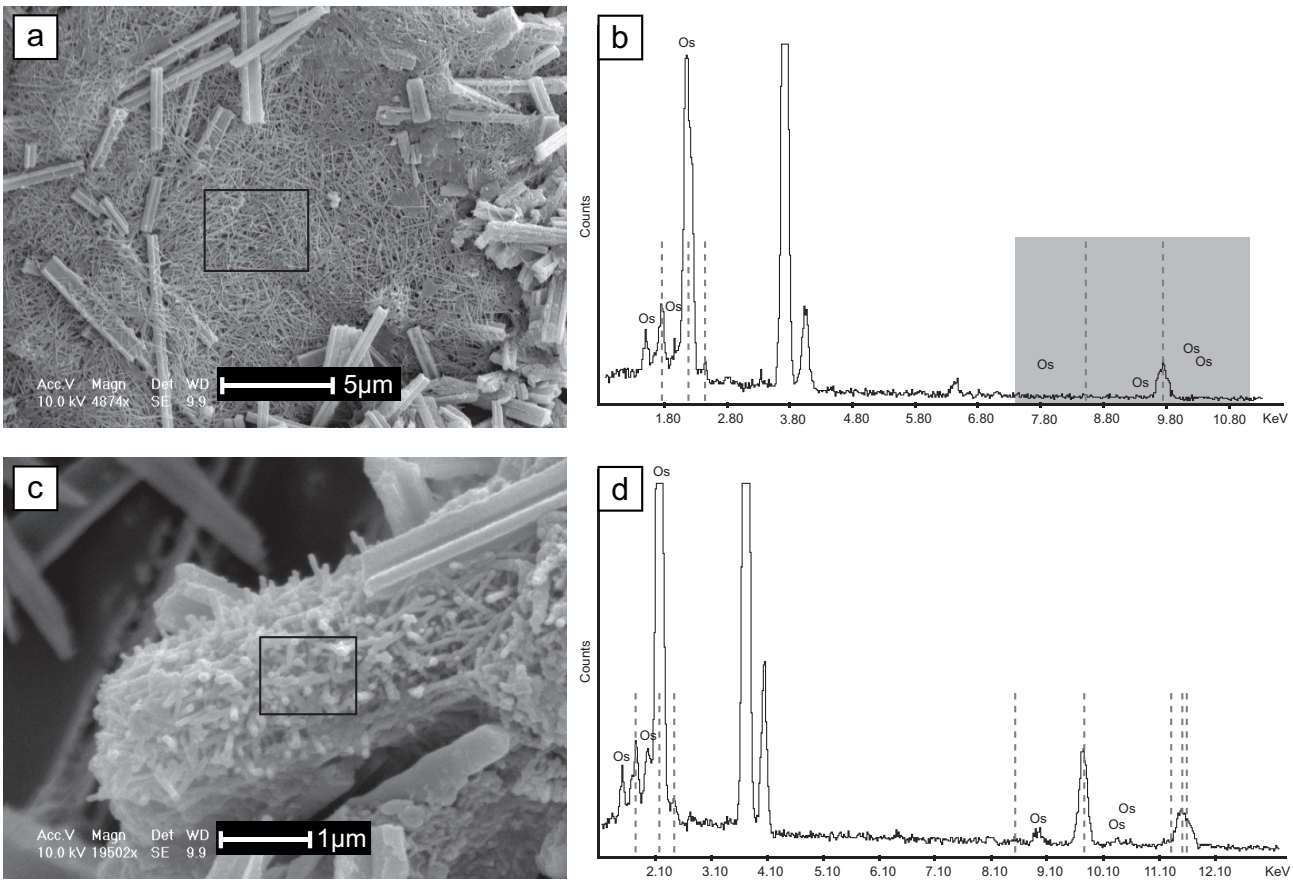

Figure 4.6 - (a) & **(c)** SEM view of samples. The black window shows the area analysed. **(b)** & **(d)**: EDS spectra, dotted lines correspond to Au peaks (samples coated with gold for SEM observations) and Os is the osmium labelling. **(a-b)** Analysis performed on a dense unorganized mesh of nanofibres (sample from coatings on a block). Note the absence of an osmium peak on the spectrum in the grey box due to the purely mineral nature of nanofibres. **(c-d)** Analysis performed on a dense non-random mesh of nanofibres (sample from a coating on a block associated with a decaying fungal strand). Note the presence of osmium peaks on the spectrum due to the organic nature of nanofibres.

strands is critical to understand the origin of the bundles. Strands and bundles are both organized as a tubular structure (Fig. 4.3 a and 4.5 b) composed of sub-parallel components. They have similar diameters: 2-30 µm on average for the bundle and 8-80 µm for the whole fungal strand. But the outer layer of the mycelial strand is usually wide and often represents between a third to a half of the strand section. Thus, only the inner diameter should be considered in this case. The outer layer is composed of hyphae with thick cell walls. Their central hole is probably too small to contain any NFC, whereas the inner part of the strand contains wider hyphae that would have enough room to allow the formation of a crystal such as a needle.

One of the most important elements for fungal growth is calcium. Indeed, it is implicated in the apical growth control. Nevertheless, Ca^{2+} is considered as toxic when present in high concentrations (Gadd 1993). Consequently, its concentration within the fungal cell, and especially in the apex, must be under strict control of the organism in order to allow proper growth (Jackson and Heath 1993). Under hydrous stress conditions, the concentration of calcium could reach a high level, close to saturation. As it has been suggested for metal-oxalate (Whitney 1989; Gadd 1999), fungi could induce the precipitation of carbonate, possibly leading to a decrease of their internal Ca^{2+} content (Gadd 2007). This process is documented for bacteria (Schultze-Lam et al. 1996; Simkiss 1986; Barton and Northup 2007). The inner layer of the fungal cell wall is composed by a large amount of chitin known to be a good template for calcite precipitation (Manoli et al. 1997). Consequently, nucleation of calcite crystals inside the inner functional hyphae from mycelial strands constitutes a serious hypothesis. The role of fungal hyphae as a crystal nucleation enhancer has already been suggested in the past (Went 1969; Northup and Lavoie 2001; Gadd, 2007). Any other cell wall

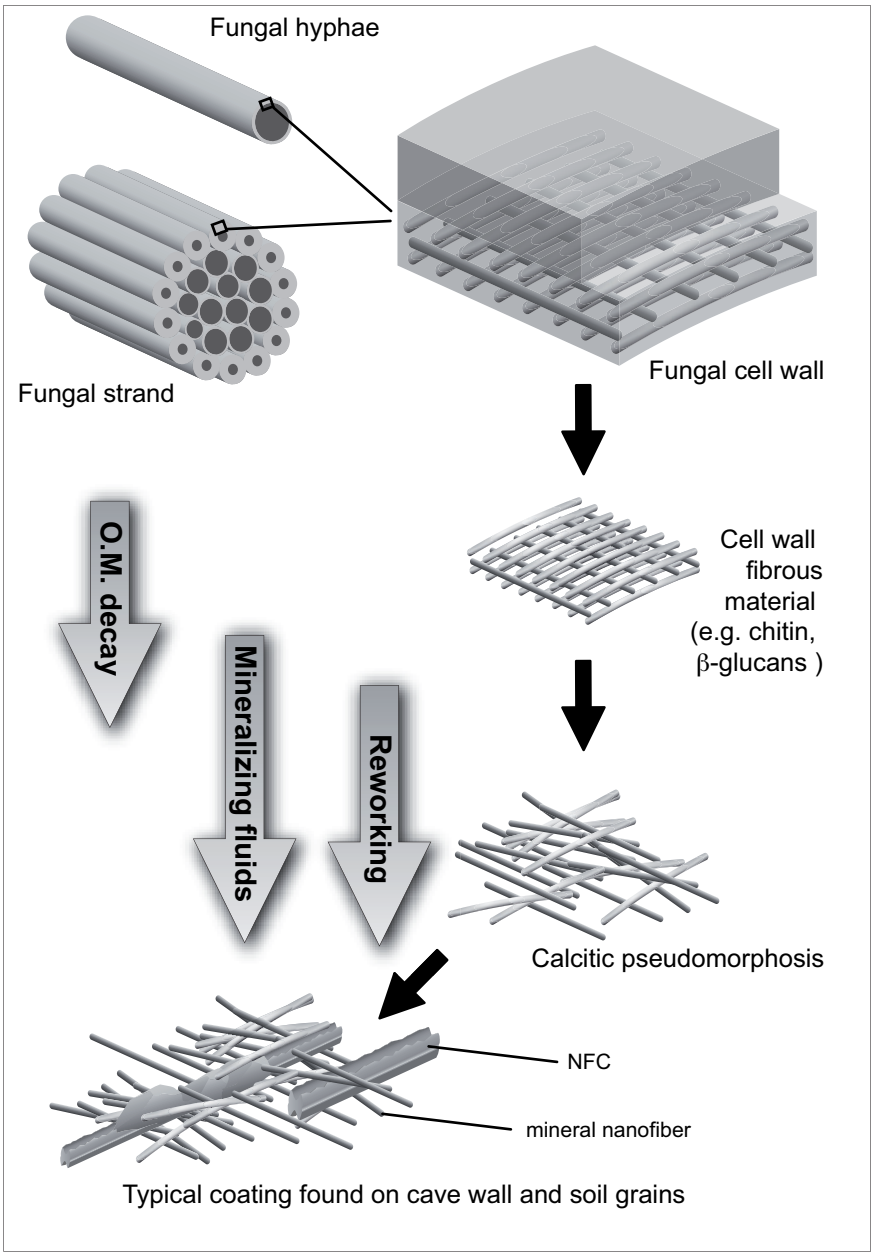

Figure 4.7 - Hypothetical sketch recapitulating the potential processes of fungal organic matter decay and mineralization of cell wall fibrous material. This model is based on observations, analysis, and interpretations given in this paper. The first stage starts with a fungal hyphae or a group of hyphae forming a fungal strand. The cell wall is constituted by two main layers, an amorphous one (on the top) and a fibrous one (at the bottom; for more details see Fig. 4.1). It is assumed that the cell wall fibrous material is not decayed at the same rate than the amorphous material. When released in the soil microenvironment, these nanofibres could act as template for calcite nucleation, eventually leading to calcitic pseudomorphosis. The ultimate step is represented by possible reworking due to various processes (bioturbation, water movements, cryoturbation, etc.). Nanofibres are often associated with other calcitic features, such as NFC, leading to the complex microfabric observed in soil and cave deposits.

fibrous material or polymeric substance, e.g. β-1,3-glucan or a glycoprotein, may have the same effect (Burazerovic et al. 2007; Shen et al. 2007). To conclude, all our observations are recapitulated in a step-by-step hypothetical model (Fig. 4.7), showing the potential relationships between fungal organic matter and calcium carbonate precipitation.

4.1.6 Conclusions

Considering previous hypotheses on the origin of nanofibres (i.e. biogenic or purely physico-chemical), the results presented here indicate that nanofibres could also originate from the breakdown of fungal hyphae, especially their cell walls. During the decay of organic matter, microfibrils such as

chitin or β-1,3-glucan, are released from the inner layer of the fungal cell wall. When these organic nanofibres are exposed to mineralizing pore fluids, they could undergo calcitic pseudomorphosis and/or be used as templates for calcitic precipitation. In the case of NFC bundles, which have an intimate relationship with nanofibres, these nanofeatures could indicate the relict of an organic sheath. As interpreted by Phillips and Self (1987), the implication of fungal strands in the genesis of NFC is now better supported. In other words, bundles could be the ultimate remains of the presence of a fungal strand. This hypothesis emphasizes the important role of organic matter in carbonatogenesis as well as the fundamental role of fungi in the terrestrial carbon cycle.

4.2 An ultrastructural approach to analogies between fungal structures and needle fibre calcite

Accepted in Geomicrobiology Journal

Saskia Bindschedler[1], Laure Millière[1], Guillaume Cailleau[1], Daniel Job[2] and Eric P. Verrecchia[1]

[1] Institute of Geology and Palaeontology, University of Lausanne, Anthropole, CH-1015 Lausanne, Switzerland.
[2] Laboratory of Microbiology, Institute of Biology, University of Neuchâtel, Emile Argand street 11, CH-2009, Switzerland.

4.2.1 Abstract

Needle fibre calcite (NFC) is an ubiquitous terrestrial secondary calcium carbonate mineral often associated with calcitic nanofibres. NFC's origin has been debated for a long time and a fungal origin is often proposed. Fungi are known to be involved in mineral weathering and production of metal oxalate, but little information exists regarding the genesis of other minerals, such as calcite. In this study, a comparison of similar ultrastructural characteristics of fungal hyphae and NFC has been performed in order to highlight analogies between both features. These analogies clearly demonstrate the probable close relationship between fungal filaments (hyphae and rhizomorphs) and NFC and its associated nanofibres.

Key words: geomycology, needle fibre calcite, biomineralization, hyphal cell wall, ultrastructure

4.2.2 Introduction

Secondary calcium carbonate deposits, known as needle fibre calcite or NFC, are frequently observed in soils and caves (Figure 4.8 I-IV). These deposits are characterized by two different habits of calcite: needle fibre calcite (NFC *stricto sensu*; Figure 4.8 a-e white arrows) and nanofibres (Figure 4.8 a-e black arrows). Their occurrence is widely documented in the literature (Vergès et al. 1982; Wright 1984; Callot et al. 1985b; Phillips and Self 1987; Strong et al. 1992; Jones and Khale 1993; Ould Mohamed and Bruand 1994; Verrecchia and Verrecchia 1994; Dubroeucq et al. 1996; Loisy et al. 1999; Borsato et al. 2000; Turner and Makhlouf 2005; Bajnóczi and Kovács-Kis 2006; Khormali et al. 2006; Richter et al. 2008; Cailleau et al. 2009a&b). Although extensively studied in terrestrial environments, the origin of both habits (NFC and nanofibres) remains controversial. In particular, the origin of NFC has long been hotly debated. The discussion about the genesis of NFC was first mainly based on petrographic and/or crystallographic evidences (Vergès et al. 1982; Jones and Khale 1993; Dubroeucq et al. 1996; Loisy et al. 1999; Borsato et al. 2000). Other studies investigated the isotopic signature of these crystals (Bajnóczi and Kovács-Kis 2006; Richter et al. 2008; Cailleau et al. 2009b). Finally, Callot et al. (1985b), Phillips and Self (1987), Ould Mohamed and Bruand (1994) as well as Verrecchia and Verrecchia (1994) emphasized the potential relationships of NFC with recurrent features such as fungal filaments, a hypothesis which seems to be more and more supported by observations and data. Therefore, the aim of this paper is to focus on ultrastructural features associated with NFC using electron imaging of natural and laboratory mycological samples in order to support the strong relationship between fungal filaments and NFC.

4.2.3 State of the art

NFC is one of the most widespread habits of calcite in terrestrial environments. It has the shape of a needle, with an average width of 1 µm and a length from 4 to 10^2 times its width. It is a monocrystalline habit of calcite and the crystal growth axis often exhibits a deviation from the calcite *c*-axis (Vergès et al. 1982; Verrecchia and Verrecchia 1994; Richter et al. 2008; Cailleau et al.

2009b). Different shapes of needles are observed arranged either in randomly organized meshes or bundles which may be ramified or non-ramified (see figure 3 in Cailleau et al. 2009b).

Calcitic nanofibre is also a very common habit of calcite in terrestrial environments and similarly to NFC exhibit a “fibre-like” shape. Nevertheless, regarding dimensions, calcitic nanofibres show a slightly different pattern with an average width of 50 to 100 nanometers and length from 10 up to 10^4 times their width. It is also a monocrystalline habit of calcite, but present-day methods do not allow as to determine if the growth axis of calcitic nanofibres is parallel or not to the calcite *c*-axis. Nanofibres always have a round cross-section and, in addition, their surface appears smooth. They are mainly arranged into meshes that can be organized (nanofibres showing preferential orientations or organization) or non-organized (nanofibres randomly distributed), but they can also be found sparsely distributed.

There are many differences between NFC and calcitic nanofibres. Calcitic nanofibres sometimes show patterns that have been interpreted as the result of a contact deformation. These kinds of features have never been observed on NFC crystals (Cailleau et al. 2009a). Another difference is the variability of the shape of one single crystal: calcitic nanofibres always show the same round cross-section and a smooth-looking surface, whereas NFC exhibits a wide range of morphologies (cross-section and/or surface; Cailleau et al. 2009b).

Both NFC and calcitic nanofibres are observed in natural calcium carbonate-rich environments, such as calcareous soils and surficial formations, as well as karstic caves. In soils and surficial sediments, NFC and calcitic nanofibres are found as calcium carbonate accumulations in the pores resulting from various factors (Figure 4.8 I-1II), such as frost shattering (scree slope accumulations), root channels, effects of bioturbation (e.g. earthworm channels) and/or inner pores of substrates (e.g. tufa deposits, intra-grain voids in rocks, basalt vughs, etc.; James 1972; Harrison 1977; Vergès et al. 1982; Strong et al. 1992; Dubroeucq et al. 1996; Loisy et al. 1999; Khormali et al. 2006). They have even been observed in tropical soils associated with bio-induced calcium carbonate accumulations (Cailleau et al. 2005).

In caves, they are one of the components of speleothem deposits called “moonmilk” (Figure 4.8 III-1IV). Moonmilk has been widely described in the literature (Gradzinski et al. 1997; Borsato et al. 2000; Northup and Lavoie 2001; Cañaveras et al. 2006; Barton and Northup 2007; Richter et al. 2008; Jones 2010). Karstic caves are environments where many secondary minerals occur, and among them, calcite is extremely common. Indeed, as water percolates within the soil and the rock substrate, dissolved inorganic carbon (DIC) concentration increases through high pCO_2 soil atmosphere contact and/or dissolution of calcareous host-rock along its way. Eventually, when percolating water reaches the cave environment, it is often supersaturated in calcium carbonate (Blyth and Frisia 2008; Curry et al. 2009). This property allows the precipitation of secondary calcium carbonate, mostly by the physicochemical process of CO_2 degassing, but also under the influence of microorganisms. Processes at the origin of speleothems have long been a subject of debate and are still under discussion (Cunningham et al. 1995; Barton et al. 2001; Cañaveras et al. 2001; Jones 2001).

At a macroscopic scale, these particular deposits appear different (Figure 4.8 I-IV), these differences being expressed by specific microscopic characteristics (Figure 4.8 a-e). It is the amount of each type of NFC or nanofibres, their mutual relationships in terms of structure, and the water content that define the various types of macroscopic facies. In soils, three types of macroscopic shapes are found: i) a cotton ball-like form (Figure 4.8 II; black arrows), composed mainly of NFC associated with low amounts of nanofibres (Figure 4.8 a; white arrow for NFC and black arrow for nanofibres) with a low water content; ii) coatings on soil grains (Figure 4.8 II; white arrows) composed of NFC

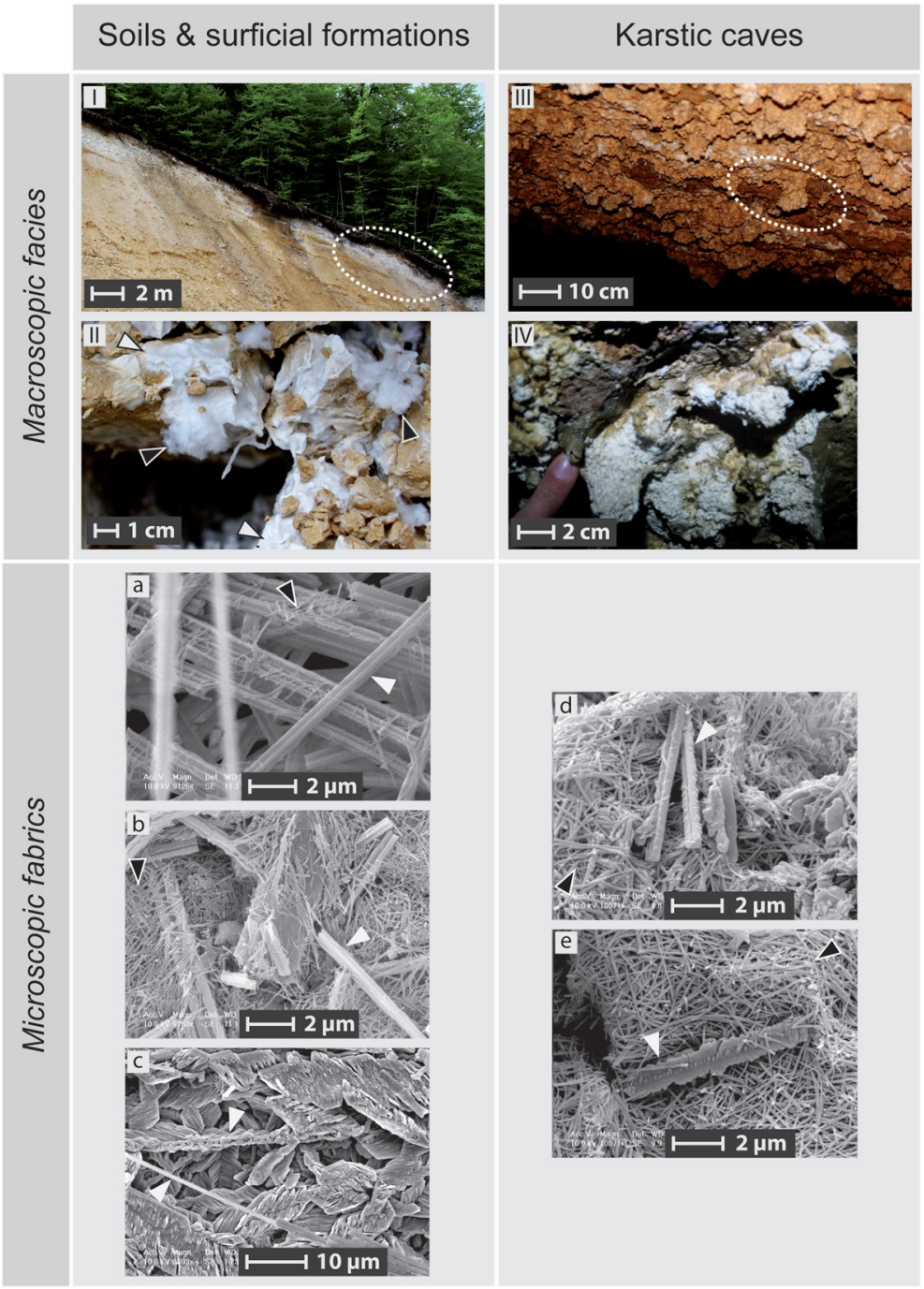

Figure 4.8 - Macroscopic facies and corresponding microscopic fabrics of secondary calcium carbonate deposits. Macroscopic facies description. **(I)** Scree slope deposits with a white layer of secondary carbonates under the organic soil layer (Villiers, Switzerland). **(II)** Close-up of two different macroscopic shapes in pores of the scree accumulation, cotton ball-like (black arrows) and coatings on scree clasts (white arrows). **(III)** Deposits in a cave made of a brownish and nodular layer ("Vers chez le Brandt" cave, Switzerland). **(IV)** Close-up of nodules showing a thin external brownish layer and inner parts made of a white and plastic porous paste. **(a-e)** Scanning electron microscope (SEM) images of microscopic fabrics of corresponding macroscopic facies; black arrows point to nanofibre meshes and white arrows to NFC. **(a-c)** Microscopic fabrics observed in soils and surficial formations. **(a)** Cotton ball-like microscopic fabric. **(b)** Microscopic fabric of coatings on scree clasts. **(c)** Microscopic fabric of a cemented layer of cotton ball-like NFC and coatings. Note the presence of larger crystals due to overgrowth of syntactic calcite on NFC. **(d-e)** Microscopic fabric observed in cave moonmilk deposits. **(d)** Dense mesh of nanofibres with simple needles. **(e)** Dense mesh of nanofibres with needles showing syntactic growth.

associated to a large amounts of nanofibres (Figure 4.8 b; white arrow for NFC and black arrow for nanofibres) and a high water content; and iii) cemented layers of grains showing an alveolar structure composed mainly of NFC, showing numerous syntactic over-growths of calcite (Figure 4.8 c; white arrows for NFC). In caves, two types of macroscopic shapes are observed: i) a white plastic and porous coating covering cave walls with protuberances at regular intervals (Figure 4.8 III-4.8

IV). It is composed mainly of a large amount of nanofibres associated with NFC which can either be simple (Figure 4.8 d; white arrow for NFC & black arrow for nanofibres) or can have syntactic growth of calcite (Figure 4.8 e; white arrow for NFC & black arrow for nanofibres). This type of moonmilk facies has a high water content; ii) the second type of morphology is cotton ball-like but has not been encountered in this study. Nevertheless this facies has been described in Gradzinski et al. (1997, "furry moonmilk") and in Curry et al. (2009, "Cottonballs").

The origins of both NFC and nanofibres – purely physicochemical or biological – are still under discussion (Vergès et al. 1982; Wright 1984 & 1986; Callot et al. 1985b; Phillips and Self 1987; Jones and Khale 1993; Ould Mohamed and Bruand 1994; Verrecchia and Verrecchia 1994; Dubroeucq et al. 1996; Loisy et al. 1999; Borsato et al. 2000; Turner and Makhlouf 2005; Bajnóczi and Kovács-Kis 2006; Khormali et al. 2006; Richter et al. 2008; Cailleau et al. 2009a&b). An intriguing and interesting fact is that calcitic nanofibres and NFC are very often observed together, which has led to some confusion between these two habits in the literature. Indeed, many authors omit to make a difference between these two features (Jones and Ng 1988; Cañaveras et al. 2006; Richter et al. 2008) when discussing their origin. On the other hand, other authors distinguish NFC from nanofibres as being two distinct habits of calcite (Phillips and Self 1987; Borsato et al. 2000; Cailleau et al. 2009a&b). They emphasize that two different processes must be involved in their respective origin and that there is probably no genetic link between these two calcitic habits.

The origin of nanofibres is still subject to controversy. Over the years, many names have been given to these features ("micro-rods" by Phillips and Self 1987, Verrecchia and Verrecchia 1994, and Loisy et al. 1999; "needles" by Jones and Ng 1988; "nanofibres" by Borsato et al. 2000 and Cailleau et al. 2009a&b). Many hypotheses have been proposed regarding their origin. For some authors (Jones and Ng 1988; Jones and Khale 1993; Borsato et al. 2000), they result from purely physicochemical processes. For others (Phillips and Self 1987; Verrecchia and Verrecchia 1994; Loisy et al. 1999), they could originate from the mineralization of rod-shaped bacteria. Yet others, (Benzerara et al. 2003; Olstza et al. 2004; Cailleau et al. 2009a) propose an organic template to act as an enhancer for calcite nucleation. Recently, a new hypothesis for the genesis of calcitic nanofibres has been put forth, emphasizing a possible fungal origin (Bindschedler et al. 2010). The incomplete decay of the fungal cell wall leads to the release of organic nanofibres in the environment. These nanofibres can further act as a template for calcite nucleation or undergo a calcitic pseudomorphosis. In this hypothesis, there is no metabolic implication of the fungi and its cell wall acts only as a template for calcite nucleation.

A similar controversy exists regarding the origin of NFC. NFC has been proposed to be either biogenic (Wright 1984 & 1986; Callot et al. 1985b; Phillips and Self 1987; Cailleau et al. 2009b), or purely physicochemical (Vergès et al. 1982; Jones and Khale 1993) in origin. The physicochemical origin hypothesis is based on the fact that NFC is always observed above the water table level, allowing the precipitation of calcite in high evaporitic conditions. Indeed, intense evaporitic conditions are known to produce crystals with an unusual elongated habit (Buckley 1951). The main problem with this hypothesis is that NFC has never been obtained in laboratory conditions, although the field physicochemical conditions seem fairly easy to reproduce. Theoretically, calcite needles should exhibit a growth axis parallel to the *c*-axis (preferential growth axis of calcite), which is not the case (Iwanoff 1906; Mügge 1914; Stoops 1976; Vergès et al. 1982; Richter et al. 2008). On the other hand, the biogenic hypothesis suggests the involvement of biotic processes, which could be direct or indirect. Some authors (Harrison 1977) have proposed an indirect origin related to the evapotranspiration associated with plants, causing calcite supersaturation next to the root environment, and therefore, allowing the precipitation of NFC due to high evaporitic conditions. This hypothesis has not been retained as NFC is also observed at some distance from roots. Another

biogenic origin hypothesis involves fungal hyphae, which act as moulds during NFC formation (Wright 1984 & 1986; Callot et al. 1985b; Phillips and Self 1987; Ould Mohamed and Bruand 1994; Verrecchia and Verrecchia 1994; Cailleau et al. 2009b). This hypothesis is based on the following arguments: i) there are morphological and dimensional similarities between NFC and fungal hyphae, ii) the environments where NFC is observed are typical fungal environments, iii) translocation of fluids is a known phenomenon in fungal hyphae (Schütte 1956; Cairney 1992; Lindhal and Olsson 2004), and iv) intracellular calcium regulation is crucial for fungal metabolism (Pitt and Ugalde 1984; Gadd 1993; Jackson and Heath 1993). These last two points are particularly important in calcareous environments where solutions are likely to be calcium-rich and possibly saturated in calcite.

Interactions between fungi and mineral matter – a field known as geomycology (Gadd 2007) – have gained interest over the last two decades. While the involvement of fungi in mineral weathering and metal-oxalate production is well documented (Cromack et al. 1977; Jongmans et al. 1997; Gadd 1999; Burford et al. 2003; Hoffland et al. 2004; Schilling and Jellison 2005; Kolo et al. 2007; van Schöll et al. 2008), only a few studies have been carried out on their implication in the genesis of minerals, such as calcite. Ahmad et al. (2004), Burford et al. (2006) and Masaphy et al. (2009) have shown the *in vitro* formation of calcite in the presence of fungi, indicating their possible implication in the neoformation of this mineral in natural environments. Klappa (1979), Callot et al. (1985a), and Phillips et al. (1987) discussed the origin of calcified filaments often observed in calcretes, assigning them a fungal origin. Phillips and Self (1987), Verrecchia (1990), and Verrecchia and Dumont (1996) discussed the possible implication of fungi in the formation of pedogenic calcite, including NFC. In conclusion, even if only little information is found in the literature, the role of fungi in the precipitation of calcium carbonate seems to be as important as weathering, yet remains underestimated.

4.2.4 Materials and Methods

4.2.4.1 Geological setting

Secondary calcium carbonate accumulations have been sampled in two types of natural environments: surficial formations and associated soils, and caves. Soil samples have been taken from calcic horizons of soils (IUSS Working Group WRB 2006) developed on carbonate scree slope deposits. Five sites were sampled: i) a quarry near Villiers (Swiss Jura Mountains, 47°04'N, 6°59'E); samples were taken both at the quarry front and at the interface of the B and C calcic horizons; ii) a quarry near Savagnier (Swiss Jura Mountains, 47°03'N, 6°58'E), iii) a quarry near Tavannes (Swiss Jura Mountains, 47°13'N, 7°10'E); iv) an outcrop near Ainsa (Spain, 42°21'N, 0°04'E), and v) an outcrop near Fumel (France, 44°31'N, 1°00'E). Cave samples have been collected from moonmilk deposits in i) the narrow entrance of a cave near les Cornettes de Bises (Swiss Alps, 46°19'N, 16°48'E) and ii) the Vers chez le Brandt cave, inside a wide chamber at 100 meters from the entrance (Swiss Jura Mountains, 46°56'N, 6°28'E).

Pedogenic carbonates sampled in calcic horizons and developed on scree slope deposits exhibit three different macromophologies: i) cotton ball-like NFC that accumulates in soil pores resulting from scree accumulation and root voids (Figure 4.8 II, black arrows), ii) coatings on centimetric to decimetric cryoclasts (Figure 4.8 II, white arrows), and iii) indurated accumulations in soil pores. The macromorphology of moonmilk samples appears as a wet plastic paste resulting in a wall coating up to 30 cm thick (Figure 4.8 IV). When possible, fungal rhizomorphs associated with the different macroscopic morphologies have been sampled in addition to the sampling of the various calcium carbonate morphologies. All samples were collected using polypropylene tweezers and stored in sterilized 50 mL tubes at 4°C.

4.2.4.2 Electron Microscopy

Samples have been observed using electron microscopy in various modes. High vacuum Scanning Electron Microscopy (SEM) has been performed using a Phillips ESEM-FEG XL30 Field Emission Gun Scanning Electron Microscope (FEG-SEM), as well as a Tescan Mira LMU, both coupled to an EDAX Energy Dispersive Spectrometer (EDS). Environmental samples for SEM observations have been fixed with osmium tetroxide vapours following a modified protocol from Pearson et al. (2004), freeze-dried, and then gold-coated (15 nm thick).

Low-temperature Scanning Electron Microscopy (LTSEM) has been performed using a Gatan cryotransfer system coupled to a Phillips ESEM-FEG XL30. Environmental samples are frozen into liquid nitrogen, transferred into a cryo-preparation chamber in order to remove water by sublimation, and then coated with platinum (10 nm thick). Samples are transferred into the observation chamber of the microscope and all observations are performed at low temperature (-180°) and high vacuum. SEM and LTSEM observations have been performed at 10-15 keV acceleration and at a distance of 10 mm.

Transmission Electron Microscopy (TEM) has been performed using a Phillips CM-200 Transmission Electron Microscope with a voltage of 200 keV acceleration. Environmental samples containing mineral matter as a dominant phase have been freeze-dried, whereas organic dominated samples, such as fungal strands (sometimes associated to some remaining mineral material) have been primary fixed with 2.5% glutaraldehyde in Phosphate Buffer Solution (PBS), secondarily fixed with 1% osmium tetroxide in PBS, and dehydrated in a series of increasing concentrations of ethanol, with a final step in Tetramethysilane (TMS). After these treatments, both mineral and biological samples have been embedded in an epoxy resin and ultrathin sections (200 nm thick) have been cut using a Reichert Ultracut S (Leica) microtome with a diamond knife. When necessary, crystal properties were determined using microdiffraction analysis coupled to the TEM.

In order to build a database of fungal structures, one Ascomycete (*Peziza sp.*) and two Basidiomycetes (*Armillaria mellea* and *Boletus edulis*) have been selected as representatives of fungi that may be encountered in mineral-dominated soil layers. In addition, all three strains are able to generate mycelial strands. Laboratory cultivated mycelial strands (*Peziza sp.*) and mycelial hyphae of the three different strand-forming strains (*Peziza sp.*, *Armillaria mellea* and *Boletus edulis*) have been prepared for SEM and TEM observations following the procedure for biological samples mentioned above.

4.2.5 Results

Ultrastructures of fungal features are compared with NFC and associated nanofibres in order to emphasize their striking analogies. The terminology defined by Verrecchia and Verrecchia (1994) and Cailleau et al. (2009b) will be used when discussing NFC morphology, with the exception of the M-type (micro-rods) described in Verrecchia and Verrecchia, which correspond to nanofibres. In this study, the term “nanofibres” will be preferred to M-type NFC, as they are not considered to be NFC *stricto sensu* as proposed by Cailleau et al. (2009a).

4.2.5.1 Analogies between NFC bundles and rhizomorphs

An analogy of size and structure can be observed between bundles of NFC and rhizomorphs. Both features exhibit: i) the same arrangement of adjacent elongated features (Figure 4.9), ii) diameters within the same range (Bindschedler et al. 2010), and iii) the same branched morphology (Figure 4.10).

Basically, rhizomorphs (sometimes called fungal strands) are bundles of hyphae (Figure 4.9 a-c). NFC bundles show also the same structure of elongated features arranged side by side (Figure 4.9 a - 4.9 d). Furthermore, rhizomorphs are composed of two types of hyphae: the outer part is made of thin hyphae with a very thick cell wall and the inner part is made of thick hyphae with a thin cell wall. In natural samples, this inner part is often missing, creating a hollow tube as shown in Figure 4.9 c. The same feature can be observed on NFC bundles (Figure 4.9 d).

Regarding sizes of both fungal strands and NFC bundles, measurements performed with SEM have shown that they have diameters within the same ranges (Bindschedler et al. 2010). Rhizomorphs exhibit a larger range of diameters on average than NFC bundles: 10-100 µm widths for fungal strands compared to 3-30 µm for NFC bundles. This difference is explained by the fact that NFC most likely crystallizes in the inner wide translocating hyphae rather than in the external thin hyphae. The external hyphae of fungal rhizomorphs are known to be very thin (1 µm in average) and to have very thick cell walls often melanised, leading to the absence of hyphae lumen (Figure 4.9 c).

The third analogy is related to branching structures (Figure 4.10). Both NFC bundles (Figure 4.10 a & b) and rhizomorphs (Figure 4.10 c) exhibit branched morphologies. This analogy is also related to another characteristic of NFC bundles as they can exhibit two main types of morphologies (Figure 4.10 b & d). The first type of morphology is constituted by bundles of needles showing syntaxial

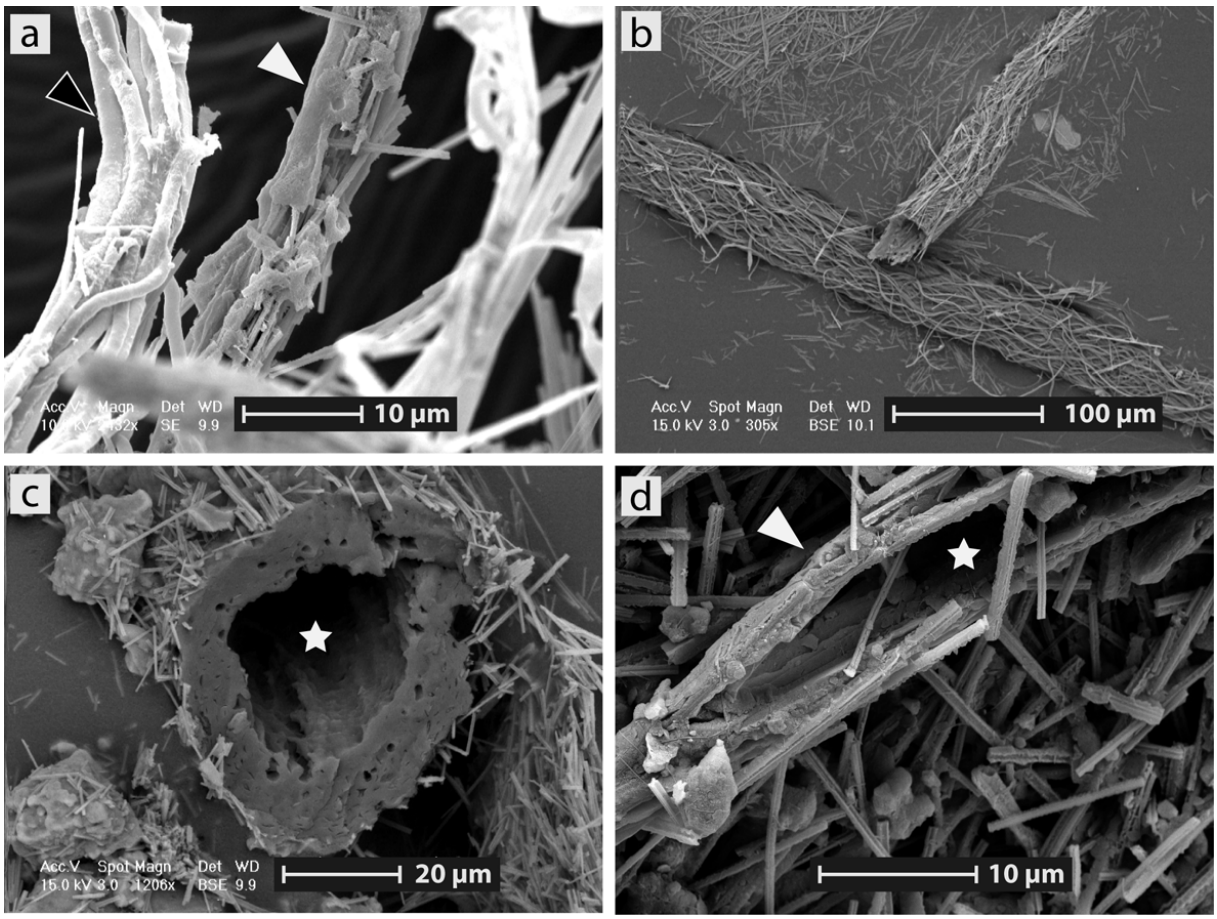

Figure 4.9 - Photographs demonstrating the analogy between fungal rhizomorphs and NFC bundles. **(a)** SEM image of a NFC bundle (white arrow) and a bundle of hyphae (black arrow). The bundle of hyphae is actually made of a group of hyphae that stems from a rhizomorph. Both structures (NFC and hyphae bundles) show a similar organization and diameter. Sample taken at the interface between the organic and mineral layers, containing both OM and secondary $CaCO_3$, Villiers quarry. **(b-c)** Low temperature SEM (LTSEM) images. Samples from pores in a scree slope accumulation containing cotton ball-like NFC, Tavannes quarry. **(b)** Longitudinal view of a rhizomorph showing the side-by-side arrangement of hyphae. **(c)** Transversal view of a rhizomorph; note the typical rhizomorph morphology with narrow hyphae in the outer part and wider hyphae in the inner part. The latter is missing (white star). **(d)** SEM image of a NFC bundle (white arrow) with an inner void (white star). Note the presence of syntactic calcite on the needles. Sample of secondary $CaCO_3$ coatings on scree clasts, Villiers quarry.

growth of calcite (the complex type of Cailleau et al. 2009b; Figure 4.10 b). This morphology shows the presence of lateral branches. The second type of morphology is characterized by bundles of simple needles (the smooth type of Cailleau et al. 2009b) with nanofibres lying all around them in various amounts, sometimes associated with amorphous veils (Figure 4.10 d). This type of morphology usually does not show branches.

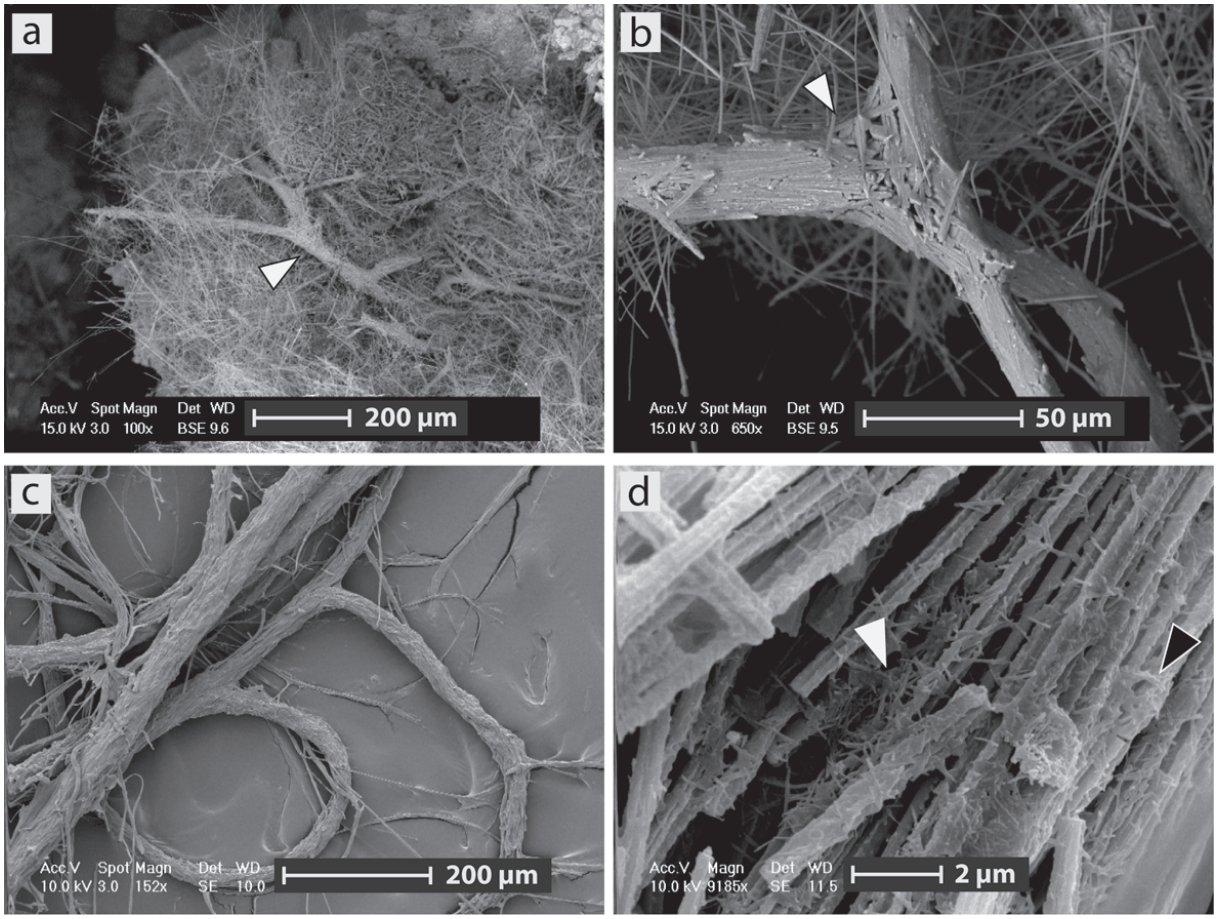

Figure 4.10 - Analogy between fungal rhizomorphs and NFC bundles. **(a-b)** LTSEM images of samples of cotton ball-like macrofacies, Villiers quarry. **(a)** NFC bundle showing a branched morphology. **(b)** Close-up of a branching zone in a NFC bundle from the same sample. Note that the needles show syntactic calcite that seems to cement needles together. **(c-d)** SEM images. **(c)** Rhizomorph from *Peziza sp.* grown in the laboratory. Note the similar branched morphology, as well as the same range of diameter compared with NFC bundles. **(d)** Close-up of a NFC bundle of simple needles showing the absence of syntactic calcite. Note the presence of nanofibres (white arrow) and amorphous matter (black arrow) on the bundle surface. Observed from a rhizomorph sampled in secondary $CaCO_3$ deposits (cotton ball-like mixed with coatings on scree macrofacies), Villiers quarry.

4.2.5.2 Irregular needles as casts of the fungal hypha

Several types of imperfections on needles have been listed and classified into four groups, each related to a specific fungal structure. From the most to the less frequent imperfection, they are: i) needles with acute irregular ends rather than truncated straight ends (Figure 4.11 a-c); ii) needles showing twisted shapes. This particular shape is easy to distinguish by following the grooves along the edges of needles (Figure 4.11 c & d). This is particularly obvious on Figure 4.11 d, where the NFC on the right side (black star) exhibits the same twisted shape as the hypha on the left side (white star). These two types of imperfections are identified as being the result of NFC crystallization within the hyphal hollow centre, considered as an imperfect cylinder. In addition, these two types of defects are the most common ones on NFC, emphasizing their importance as an argument

for the discussion related to NFC's origin. The other types of imperfections are represented by iii) scars on NFC oriented perpendicularly to the needle length (Figure 4.11 e & f). These imprints are identified as representing the scar of a hypha septum; and iv) dichotomization of needles (Figure 4.11 f) identified as being the remains of hyphal branching. The latter two types of defects are far less common than the two first ones. However, they are typical fungal features, which makes them remarkable enough to be noteworthy.

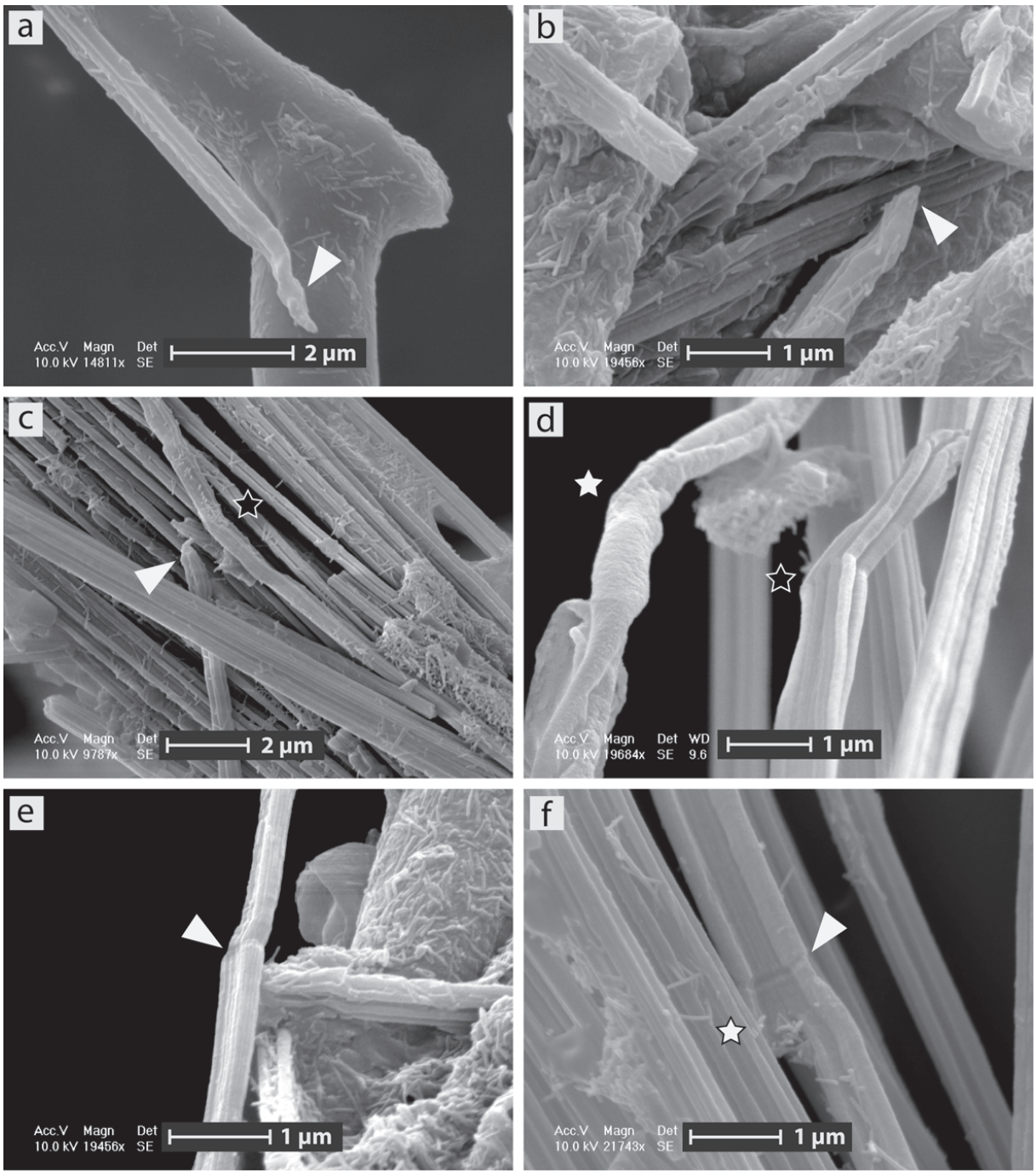

Figure 4.11 - Imperfections on needles. SEM images of soil samples containing both OM and secondary $CaCO_3$ located at the interface between the organic and mineral layers, Villiers quarry. **(a-c)** Needles showing irregular acute ends indicated by a white arrow. **(c-d)** Needles showing twisted shapes indicated by black stars. The twisted shape is easily observable by following the grooves of the needles. Note on **(c)** the NFC bundle containing both imperfections, one needle with an acute irregular end and another one showing a twisted shape. On **(d)**, note the analogy with the hypha showing the same twisted shape as the needle on its right (white star). **(e-f)** Needle with a scar perpendicular to its length (white arrow). **(f)** Under the scar, note the dichotomization of the needle illustrated by the white star.

4.2.5.3 Tube-like structure of nanofibres associated with NFC as a remain of the hyphal sheath

Nanofibres are recurrent features found together with NFC. They appear as meshes with no preferential orientations or organization (Figure 4.8 b – 4.8 d - 4.8 e) or as meshes showing an organized network, often as tubular shapes (Figure 4.12 a-c). Meshes of nanofibres organized into tubes could be fungal in origin as demonstrated by Bindschedler et al. (2010). Briefly, nanofibres are assumed to be the result of an incomplete decay of the fungal cell wall, resulting in the conservation of the fibrous chitin and/or β-glucan from the hyphal walls. Tube-like organized meshes of nanofibres represent an ultimate remain of the former hyphal structure. Further investigations in natural samples support this hypothesis, highlighting the intimate relationship between tube-like meshes of nanofibres, NFC, and fungi (Figure 4.12). First, the nanofibres constituting these tube-like structures often organize with preferential orientations (Figure 4.12 a). This fabric is believed to be biogenic in origin since reworking processes in the environment would more likely yield random structures. Second, the diameter of a section of nanofibres, organized as a tube, is similar to a hyphal section (Figure 4.12 b). It is important to note that NFC's diameter generally fits within these tubes (Figure 4.12 a & c).

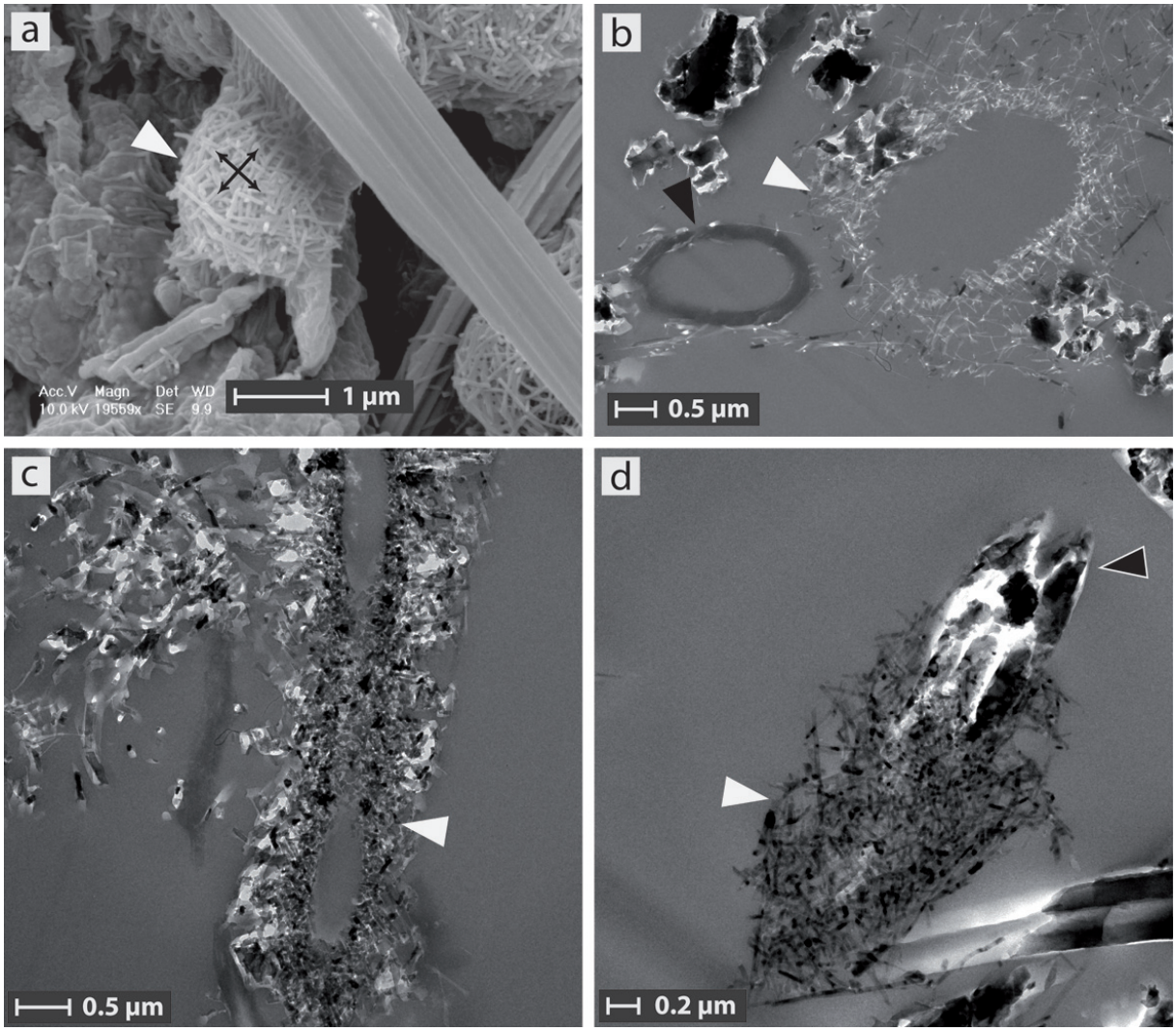

Figure 4.12 - Tube-like structures of nanofibres and NFC. **(a)** SEM image of a mesh of nanofibres (white arrow) showing both a preferential organization in the shape of a tube and a preferential orientation of nanofibres in two directions (illustrated by the black arrows). Samples of both OM and secondary $CaCO_3$ located at the interface between the organic and mineral layers, Villiers quarry. **(b-d)** TEM images of rhizomorphs associated with coatings on scree macrofacies, Villiers quarry. **(b)** Transversal view of both a fungal hypha (black arrow) and a tube-like structure of nanofibres (white arrow); note the similarity between diameters of both structures. **(c)** Longitudinal view of a tube-like structure of nanofibres (white arrow). **(d)** Organized mesh of nanofibres (white arrow) surrounding a needle (black arrow) showing the intimate relationship existing between both features.

Third, NFC is observed intimately associated to tube-like organized nanofibres (Figure 4.12 d). The nanofibres represent the remains of the fungal hypha that generated the NFC. Therefore, tube-like structures of nanofibres, associated with NFC and showing a close relationship between both features, emphasize a concomitant origin for both features.

4.2.5.4 Ring-like and nest-like structures - enigmatic structures identified as hyphal anastamosis remains

Other intriguing features regularly observed with NFC and associated to nanofibres are “ring-like” (Figure 4.13 a - c) and “nest-like” structures (Figure 4.14 a-c). Ring-like structures have been observed on bundles of NFC (Figure 4.13 a), on randomly organized meshes of needles (Figure 4.13 b), as well as on fungal hyphae in natural samples (Figure 4.13 c). Ring-like structures exhibit an obvious analogy with similar structures observed on *in vitro* cultivated hyphae (Figure 4.13 d). In the latter, these ring-like structures are interpreted as being remains either of a hypha anastomosis, hyphal branching, or plasmogammy. These three hypotheses imply the union of two individual hyphae, resulting in a fusion zone. A scar remains when this zone is disturbed for any reason. Surprisingly, this scar seems to be resistant enough to reworking processes, as it is often observed fairly intact.

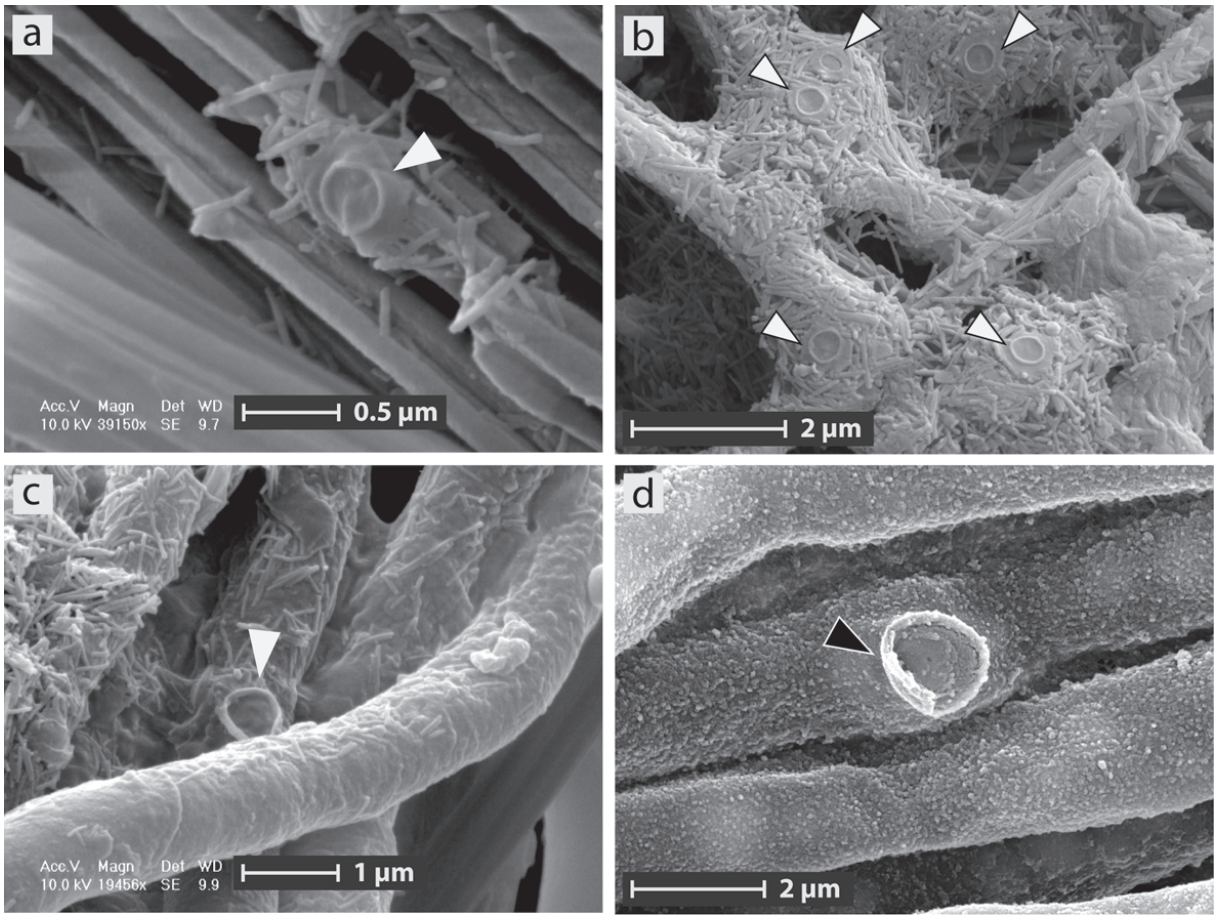

Figure 4.13 - SEM images of ring-like structures. **(a)** Ring-like structure (white arrow) lying on a bundle of NFC. Note the presence of a few nanofibres. Samples of both OM and secondary $CaCO_3$ located at the interface between the organic and mineral layers, Villiers quarry. **(b)** Ring-like structures (a total of five indicated by white arrows) lying on a mesh of randomly distributed NFC. Note that these ring-like structures are associated with non-organized meshes of nanofibres. Sample of secondary $CaCO_3$ (cotton ball-like mixed with coatings on scree clasts), Villiers quarry. **(c)** Ring-like structure (white arrow) lying on a fungal hypha of a rhizomorph. Note the presence of numerous nanofibres associated with the fungal hyphae. Samples of both OM and secondary $CaCO_3$ located at the interface between the organic and mineral layers, Villiers quarry. **(d)** *In vitro* structure observed on a hypha of *Peziza sp.* during its mycelial stage (black arrow). Note the similarity with ring-like structures of natural samples.

Nest-like structures, the other enigmatic feature, are made of nanofibres arranged in a nest shape (Figure 4.14 a - c). They are usually observed lying on the surface of NFC bundles, sometimes associated with amorphous veils (Figure 4.14 a). They can also be observed on smooth surfaces identified as fungal hyphae (Figure 4.14 b). Most of the time, the inside seems to be made of a smooth material rather than being empty. It should be pointed out that similar nest-like structures are also observed as part of non-organized meshes of nanofibres (Figure 4.14 c). This latter type of nest-like structure seems to possess hollow centres. It is believed that this type of nest-like structure might have an alternative origin. While the first type is considered as a true fungal remain, the second type might be considered as being the result of fungal tunnelling. Therefore, in some cases, nest-like structures in non-organized meshes of nanofibres might not be considered as a nest-like structure *stricto sensu*.

Both ring-like and nest-like structures are identified as being remains of a hyphal anastomosis or branching. However, their dissimilar appearance is still curious. Whereas ring-like structures show an obvious analogy with similar structures observed *in vitro* with cultivated hyphae, nest-like structures do not have an identified fungal counterpart at the moment.

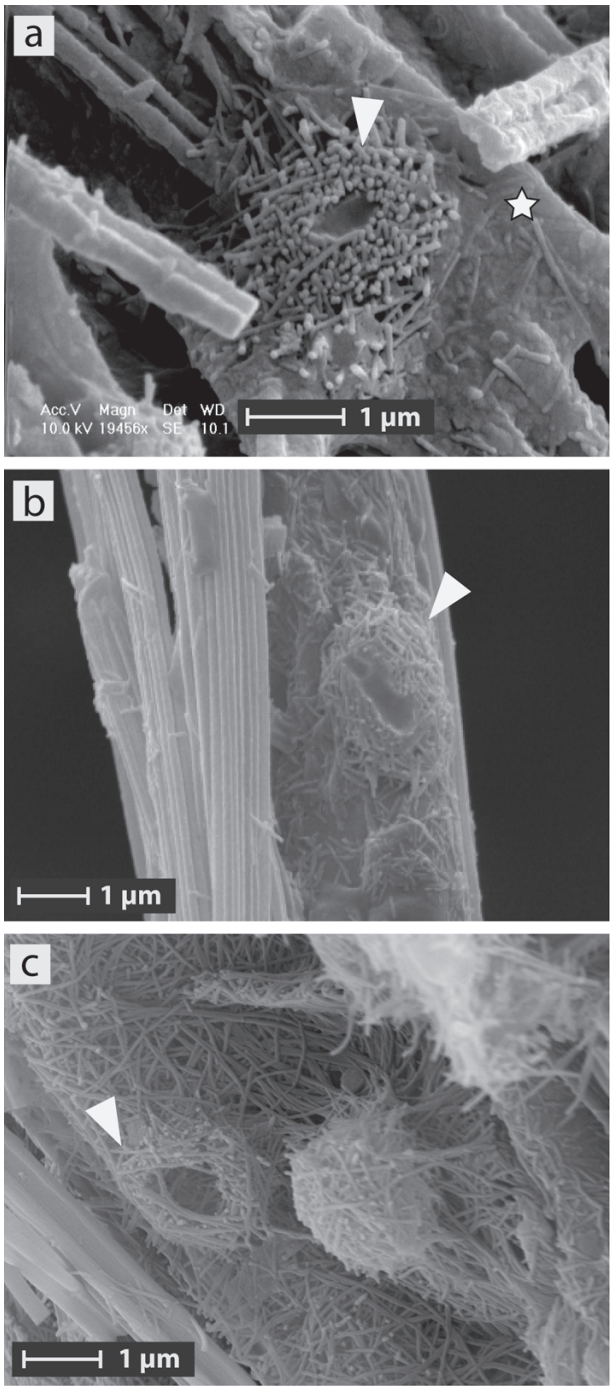

Figure 4.14 - SEM images of nest-like structures. **(a)** Nest-like structure (white arrow) lying on a bundle of NFC and made of a mesh of nanofibres showing preferential orientations in two main directions. Note the presence of amorphous veils (white star) lying on the NFC bundle. Cotton ball-like macrofacies, Villiers quarry. **(b)** Nest-like structure (white arrow) lying on a smooth filament identified as a fungal hypha. Samples of both OM and secondary $CaCO_3$ located at the interface between the organic and mineral layers, Villiers quarry. **(c)** Nest-like structure nestled in a mesh of nanofibres. Soil sample containing decaying OM, rhizomorphs, and secondary CaCO3, Villiers quarry.

4.2.6 Discussion

Four main types of analogies have been highlighted in the previous section: i) analogies of shape and structures between NFC bundles and rhizomorphs; ii) imperfections on needles as imprints or fingerprints of the fungal mould; iii) recurrent association with NFC of nanofibres organized into tube-like structures, which represent remains of the fungal hypha; and iv) observation of enigmatic ring-like and nest-like structures, which can be identified as hyphal anastamosis or branching remains. All these features observed on NFC crystals or associated with nanofibres can be identified as fungal-related structures. This provides strong arguments regarding the biogenic origin of NFC.

4.2.6.1 Analogies between NFC bundles and rhizomorphs

The analogy of size and structures between NFC bundles and rhizomorphs is interpreted as being the result of NFC genesis into the rhizomorph as already suggested by Bindschedler et al. (2010). The three analogies described in this study give strong clues to the genetic link between both features. Moreover, operating rhizomorph supports the assumption that rhizomorphs most likely have a role in NFC genesis. The external hyphae give rhizomorphs their property of impermeability, allowing fluid to translocate without exchange with the external environment (Watkinson 1979; Dix and Webster 1995). In calcareous environments where secondary calcite occurs, solutions translocated through rhizomorphs are likely saturated, or slightly undersaturated, in calcite (Lal and Kimble 2000; Blyth and Frisia 2008; Curry et al. 2009). Therefore, it is easily conceivable that, within these impermeable structures, calcite nucleation can happen, whether through mediated precipitation on organic template (heterogeneous nucleation), or after supersaturation (homogeneous nucleation), or even moderate undersaturation (Wollast 1971).

Secondly, the two main morphologies of NFC bundles, needles with syntaxial calcite and no nanofibres (Figure 4.10 b) and simple needles associated to nanofibres (Figures 4.10 d) can be explained by two different processes. The sequence of events leading from one shape to the other is given in Figure 4.15. First, NFC forms inside rhizomorphs, which further undergo a partial decay leading to the disappearance of most of cell walls, except the fibrillar part of chitin and/or β-glucan (Bindschedler et al. 2010). Then, these bundles, which are assumed to be weakly resistant to reworking, can be easily reworked inside the soil or the cave environment. Therefore, when exposed to reworkings, most of these bundles are disassembled and needles, with their associated nanofibres, are heterogeneously rearranged (Figure 4.15 a). Nevertheless, in some cases, NFC bundles are only partially arranged or not rearranged at all. The first option, a partial rearrangement, is indicated by the remains of bundles made of simple needles and nanofibres lying all around (Figure 4.15 b). In this case, the nanofibre sheath is resistant enough or protected by local conditions from reworking processes to allow the conservation of the bundle structure, but not the branched morphology. The second option explains how branched bundles of NFC with syntactic growth of calcite can be formed. When NFC bundles are released from their fungal mould, they are exposed to supersaturated fluids in the environment. In this case, needles might act as nucleation sites for syntactic calcite, leading to the formation of typical NFC bundles showing needles with syntactic growth features (Figure 4.15 c). This process is a step in early diagenesis as it cements needles together, at the same time allowing the preservation of the branched as well as the bundle morphologies.

4.2.6.2 Irregularities on needles as imprints of the hyphal ultrastructure

Irregularities on needles are thought to be imprints of the hyphal ultrastructure. Indeed, when NFC crystallizes inside the fungal hypha, most certainly some imprints of fungal ultrastructural features should be present at some point. When a crystal is generated, it follows rules related to the crystal habits as well as thermodynamics of the nucleation and crystal growth conditions. For example, calcite usually appears as micrite when solutions are highly supersaturated, and as sparite when solutions are close to equilibrium (Bricker 1971). Furthermore, a relationship exists between lattice symmetry and the shape of a crystal. When no constraint exists, crystals exhibit habits governed by the physicochemical conditions and the crystallographic laws. Nevertheless, very often, the presence of impurities creates large variations from theoretical crystal habits (Buckley 1951; Sands 1993). OM has a strong influence on calcite habits, allowing the existence of many different shapes of calcite crystals (Simkiss and Wilbur 1989; Berman et al. 1993).

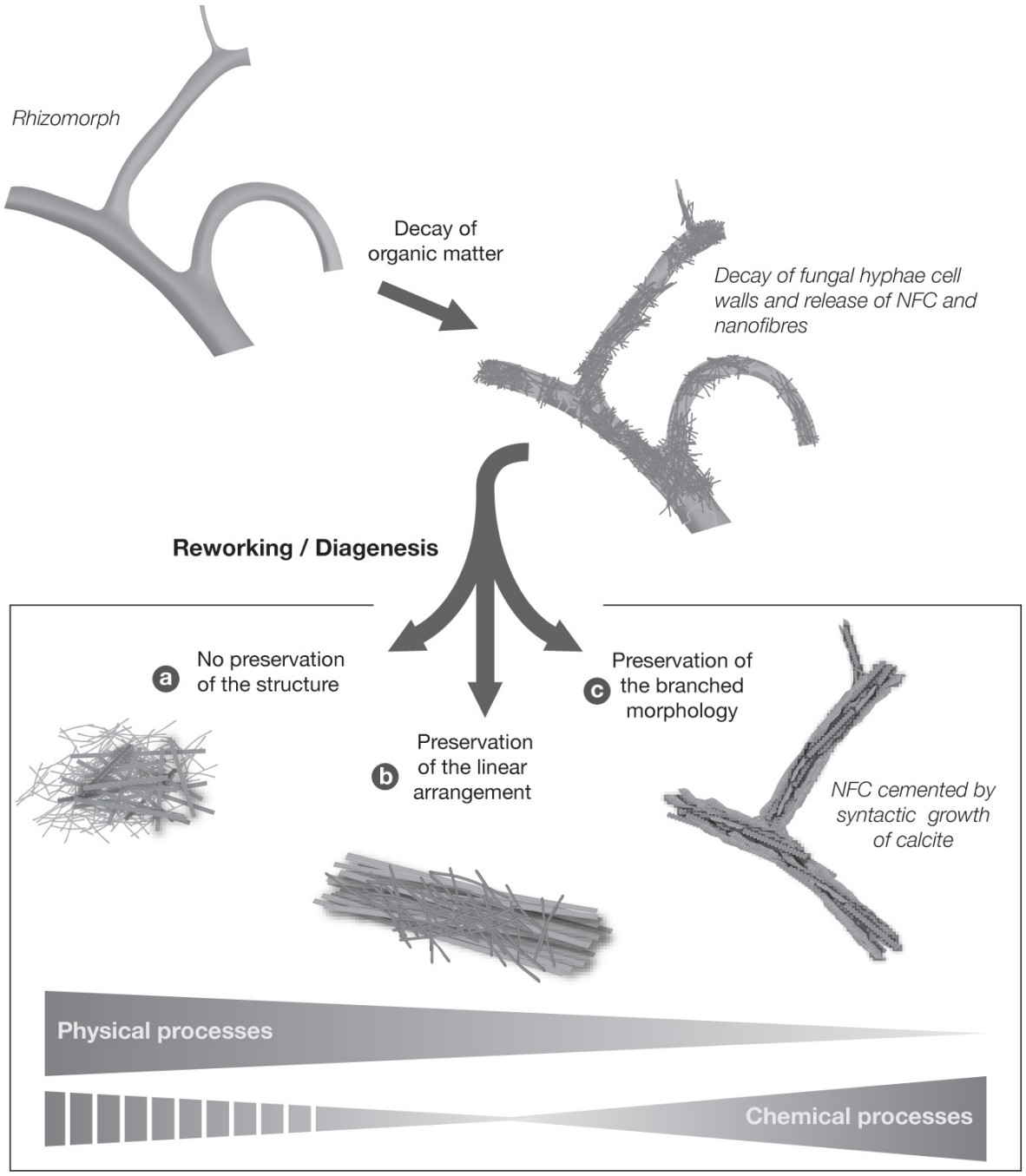

Figure 4.15 - Synthetic sketch summarizing the sequence of events, from the release of NFC bundles into the environment to the various possible arrangements of NFC and nanofibres, and accordingly to the different morphologies of NFC bundles. Reworking processes act differently in heterogeneous environments. Chemical and physical processes do not have the same intensity depending on local conditons. **(a)** Strong physical reworking leading to randomly organized meshes of NFC and nanofibres. **(b)** Weak chemical and moderate physical reworking leading to linear NFC bundle and overlying nanofibres. **(c)** Poor physical and strong chemical reworking leading to branched bundles of syntactic NFC and absence of nanofibres.

First of all, the NFC's growth axis is divergent from calcite *c*-axis as reported in the state of the art section. Moreover, NFC's needle shape demonstrate that the crystal growth has preferentially occurred along one axis, which is not in agreement with the theory of purely physicochemical precipitation. Indeed, the NFC crystal shape, as well as its growth axis, does not correspond to the rhombohedral *c*-axis, typical of calcite when physicochemically precipitated. Secondly, NFC often shows imperfections that are interpreted as imprints related to fungal ultrastructural features (Figure 4.11). If variations in habits can be attributed to organic templates, random imperfections at a sub-micrometric scale may not be attributed to the presence of an organic matrix. Indeed, as organic molecules can create particular shapes of crystals, they produce regular lattices (Simkiss and Wilbur

1989; Berman et al. 1993). Therefore, it is reasonable to assume that defects observed on NFC are neither part of a regular shape, nor the result of dissolution processes. Consequently, a realistic explanation for these random defects is the presence of an “irregular” sheath that constrained the growth of the needle as already discussed by several authors (Phillips and Self 1987; Verrecchia and Verrecchia 1994; Cailleau et al. 2009b).

The fungal hypha is most certainly not considered as a perfect tubular and linear cylindrical mould when NFC is formed inside it. This is why needles with acute irregular ends and twisted shapes are quite common imperfections. Indeed, they represent the simplest expression of the effect that a mould can exert. The two other types of imperfections, septum scars and dichotomisations, are far less frequent.

Septum scars are supposed to be quite rare as not all fungi present a septum. In addition, the septum specificity depends on the taxonomic position of the fungus. Higher fungi usually have perforated septa between cells. The type of perforation, and consequently cytoplasm continuity, is specific to septa. Septa of Ascomycetes, Deuteromycetes, and some Basidiomycetes, commonly have a single central pore, which is large enough in some cases to allow cytoplasm continuity between cells. Other types of septa are (i) dolipores of Basidiomycetes and (ii) multiperforate septa present in some Ascomycetes and Deuteromycetes. These two types of septa have a very small perforation, which does not allow cytoplasmic continuity (Carlile et al. 2001). Therefore, not all fungi present in soils and caves have the ability to produce septum scars on NFC as septa can represent obstacles between cells, and accordingly, to NFC growth. In addition, the length of each cell constituting the hypha varies, and is characteristic depending on the species. Thus, cell length of septate fungi has a minimal value of 30 µm and can reach up to 600 µm, with apical compartments usually showing the greatest values (Trinci 1984; Carlile et al. 2001; Buchalo et al. 2009). NFC lengths are 10-100 µm on average although some can rarely reach 500 µm according to the authors (Strong et al. 1992; Verrecchia and Verrecchia 1994; Loisy et al. 1999; Zhou and Chafetz 2009). In consequence, the probability for a crystal of NFC to reach a septum when growing inside the hypha is expected to be rather low.

Finally, regarding the last type of imperfection, i.e. dichotomous needles, their scarcity is explained by the mechanism of hyphal branching itself. The fungal mycelium extends apically and maintains its exponential growth by branching. Branching can either be apical, with the apex forming two adjacent apices, or lateral, with the formation of a new apex along a hypha, the latter case being more common. In lateral branching, studies suggest that a relationship exists between branching and septation, branching usually occurring before a septum in the direction of the cytoplasmic flow (Prosser and Trinci 1979; Trinci 1979; Carlile et al. 2001). Therefore, there are at least three possibilities to generate a dichotomous needle in a hypha (assuming that NFC crystallization follows cytoplasmic flow). In the first case, a needle is generated at the apex during the branching event and NFC crystallization follows the hyphal extension. In the second case, the needle is formed in a hypha having septa with a large central pore allowing NFC crystallization to carry on after branching. In the two former cases, NFC is expected to go through a septum. Consequently a septum scar should be present on the needle as observed on Figure 4.11 f. In the third case, the needle is formed in a non septate hypha and NFC crystallization can carry on following two branches without being stopped by a septum. Nevertheless, the fact that dichotomous needles are not common imperfections is not really explained. Physiological processes leading to NFC formation are poorly understood but might bring insight into this question.

4.2.6.3 Tube-like structures of nanofibres associated with NFC as remains of a fungal hypha

Tube-like structures of nanofibres are frequently observed in natural samples, whatever the macroscopic shape of deposits (cotton ball-like, coatings on soil grains, moonmilk from caves). In addition, it is important to mention that some authors have observed these structures in moonmilk deposits (Borsato et al. 2000, their figure 5; Richter et al. 2008, their figure 3; Cailleau et al. 2009a, their figure 1B). Nevertheless, they do not propose an interpretation of their origin. On average, diameters of tube-organized nanofibres range between 1 and 5 µm. In natural hyphae, average size ranges from 1 to 6 µm in diameter depending on the type of hyphae and species (Dix and Webster 1995; Carlile et al. 2001; Buchalo et al. 2009). Diameters of tube-like structures of nanofibres and hyphae are therefore in the same order of magnitude and are in the same range as NFC widths (Figure 4.12).

4.2.6.4 Ring-like and nest-like structures - enigmatic structures identified as hyphal anastamosis remains

Ring-like and nest-like structures, two features regularly observed associated to NFC and nanofibres, are identified as being either the remains of a hyphal anastomosis or hyphal branching, or the trace of plasmogammy. Ring-like structures in natural samples (Figure 4.13 a - c), are systematically smaller than the similar structure observed in *in vitro* grown hyphae (Figure 4.13 d). This is probably due to the fact that microorganisms usually have smaller dimensions in natural conditions than those in *in vitro* conditions. This is the result of more oligotrophic conditions in natural environments compared to culture media (Bae et al. 1972; Casida 1977; Kieft 2000). Keeping this fact in mind, the similarity of ring-like structures associated to NFC (Figure 4.13 a & b) with the ones associated to hyphae in natural samples (Figure 4.13 c), as well as with *in vitro* cultivated hyphae (Figure 4.13 d), is another clue to the close relationships that exist between fungi and NFC. Consequently, ring-like structures most likely represent an ultimate remain of a septum and thus of the fungal sheath that generated the NFC, in the same way as meshes of nanofibres that surround NFC.

There are two main types of nest-like structures: the ones that are found in non-organized meshes of nanofibres and the ones that are observed as single structures. When observed in non-organized meshes of nanofibres (Figure 4.14 c) they may also be the result of fungal tunnelling, which is a well-known ability of fungi (Jongmans et al. 1997; van Schöll et al. 2008). In this case, even though it is not a fungal remain *stricto sensu*, it still represents the vestige of a fungal hypha transit. Nevertheless, tunnelling does not explain the nest-like structures illustrated in Figure 4.14 a - b, emphasizing their possible alternative origin. First, these structures are not associated to any mesh of nanofibres; it is therefore very unlikely that they result from tunnelling. Second, when these nest-like structures are isolated, they are associated either to amorphous matter (Figure 4.14 a) or directly to a filament identified as a fungal hypha (Figure 4.14 b).

Ultimately, they can be observed lying on meshes of randomly oriented NFC. Nest-like structures are supposed to represent remains of an incomplete decay of the fungal cell wall, in particular a septum.

4.2.6.5 Dynamics of NFC genesis

It must be pointed out that, whereas all the analogies described above give valuable information about the intimate relationships existing between NFC, nanofibres and fungal filaments, they give very little information regarding the dynamics of the system with time. A maximal time span for NFC genesis can be inferred at the ecosystem scale, by comparing NFC occurrence to the age of the host

formation. For example, in Cailleau et al. (2005), the occurrence of NFC is described together with bio-induced calcium carbonate derived from the presence of trees and associated microorganisms. As these soils did not contain calcium carbonate before the system was established, the associated NFC is at least as old as the tree, which is 170 +/- 30 years (^{14}C datation). However, the time span required for the formation of NFC at the cell scale is not known. It seems clear from the observations made in this study that a necessary link exists between the overlying vegetation and associated microflora, the decay of its dead OM and the subsequent physicochemical conditions allowing calcium carbonate precipitation. NFC genesis is also most certainly driven by kinetics of CO_2 dissolution in the soil solution, and further by the kinetics of $CaCO_3$ nucleation. Finally, it is expected that all the processes described above are under the control of the fungal cell physiology that induces an overall control on carbonate equilibria within the cell compartments.

4.2.7 Conclusions

NFC's origin has been debated for a long time. However, current hypotheses seem to increasingly support the biogenic fungal origin. The implication of fungi is a realistic hypothesis for several reasons. First, it is well accepted that environments where NFC is observed are typical fungal environments. Second, the similarity in dimensions of NFC and fungal filaments (hyphae and rhizomorphs) strongly supports a close relationship between both features. Third, metabolic capabilities of fungi regarding calcium and translocation of solutions are in favour of a fungal implication in calcite authigenesis, in particular in environments where natural fluids are likely close to saturation or saturated in calcite. Nevertheless, this last point needs to be further investigated in order to get more insight into the physiological processes involved in hyphal calcite nucleation. And finally, the present study demonstrates that numerous similarities with fungal structures can be recognized in the NFC morphologies as well as nanofibres. This last point is a strong argument supporting an intimate relationship between fungi and NFC during their genesis. In conclusion, data acquired over the last few decades regarding NFC's origin constitute strong converging arguments for the fungal origin. Moreover, it highlights the implication of fungi as essential players in the coupled calcium-carbon cycle by emphasizing their role in the precipitation of minerals in addition to their already well-known abilities in mineral weathering.

4.3 Soil micromorphology

4.3.1 Introduction

Observations of thin sections have been performed as a mean to observe and identify the relationships between the microfeatures present in the various macroscopic facies. The advantage of using thin sections compared to the observation of bulk samples is the conservation of the structures and relationships in an undisturbed state (Stoops 2003). However, it allows observation in two dimensions as only the polished surface plane may be observed. Nevertheless, it represents valuable additional information to conventional electron microscopy observations, allowing to work on a slightly larger scale. Zones of interest may be selected under the photonic microscope at low resolution and further be observed at high resolution with SEM.

In this study, the focus on the presence of fungi, as well as on particular features, which could possibly be fungal related, has been chosen on purpose as a mean to emphasize the recurrent association of fungi with NFC and nanofibres.

4.3.2 Methodology

Aggregates of soil grains associated with different macroscopic facies (from the Villiers CH01 site), as well as moonmilk crusts (from the Vers-chez-le-Brandt cave CH02 site), have been sampled and brought undisturbed to the laboratory. Then, they have been enclosed in sealed containers, which have been immersed in liquid nitrogen. Samples have been immediately transferred into a lyophilizer and freeze-dried for 3 days. The aggregates have been included in an epoxy resin and cut as thin section down to 25-30 µm. Thin sections have been observed with photonic microscopy, either by transmitted light (plane- and crossed-polarized light) or by ultra-violet epifluorescence using a x100 oil-immersed objective. In addition, observations with scanning electron microscope (SEM) have been performed using the BSE (Backscatter Electron) detector, at a distance of 8 mm and an acceleration voltage of 15kV.

4.3.3 Results

4.3.3.1 Fluorescence, plane-polarized and crossed-polarized light observations

Four types of samples have been observed: i) grain and soil aggregates containing mycorrhized roots and the “cotton ball-like” and “coating” macrofacies, sampled from the interface between the B and C horizons (CH01 site); ii) grain aggregates displaying the “cotton ball-like” facies in the intergrains pores, sampled from the C horizon (CH01 site); iii) grain aggregates encrusted with “coating” facies, sampled from the C horizon (CH01 site); and iv) a moonmilk crust (CH02 site).

Calcitic features from soil samples are all autofluorescent (Fig. 4.16), which is common for calcite formed in pedogenic environments (Altemüller and Van Vliet-Lanoë 1990). Yet, the causes of this fluorescence are still not clearly established (Khormali et al. 2006). Van Beynen et al. (2001) and Khormali et al. (2006) suggested that it might be linked to the presence of adsorbed organic matter (OM) on calcite crystals. On the other hand, moonmilk shows a poor autofluorescence (Fig. 4.17 A-B). Nevertheless, some particular structures display a slight autofluorescence (Fig. 4.17 C-D). Features showing a similar shape appear to be highly unstable under the electron beam (Fig. 4.18), which happens often with non-fixed organic material.This fact emphasizes a possible organic nature and thus the subsequent autofluorescence. In all samples, at the exception of the moonmilk one, fungal structures have been observed. However, small rounded bodies, 2 to 5 µm in diameter, have been observed in moonmilk crust (Fig. 4.19). They seem melanized and could be either fungal or

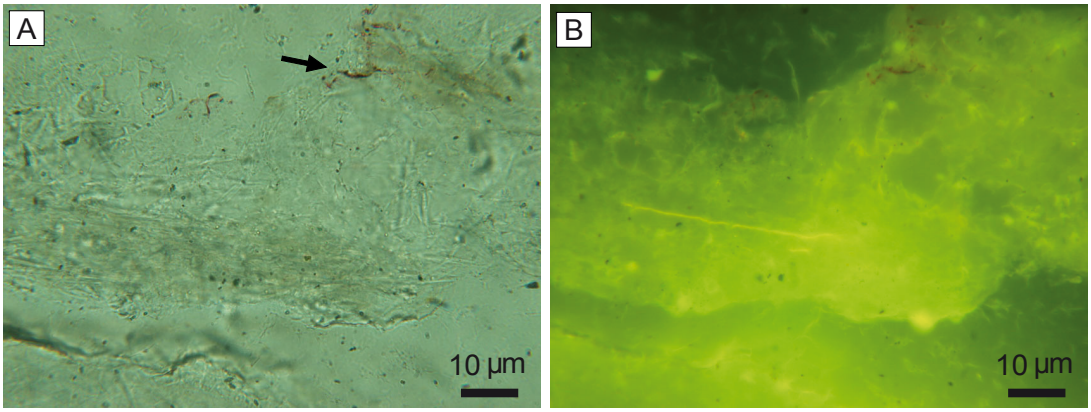

Figure 4.16 – Thin section photographs in "coating" macroscopic facies. **(A)** Plane polarized light (PPL) observation of a layer of "coating" macroscopic facies showing NFC and associated organic remains (probably colloidal humic substances; black arrow). Note that nanofibres are probably present but are too small to be detected at this magnification. **(B)** UV epifluorescence observation of exactly the same area as in B showing the autofluorescence of pedogenic $CaCO_3$; note the heterogeneous pattern of fluorescence.

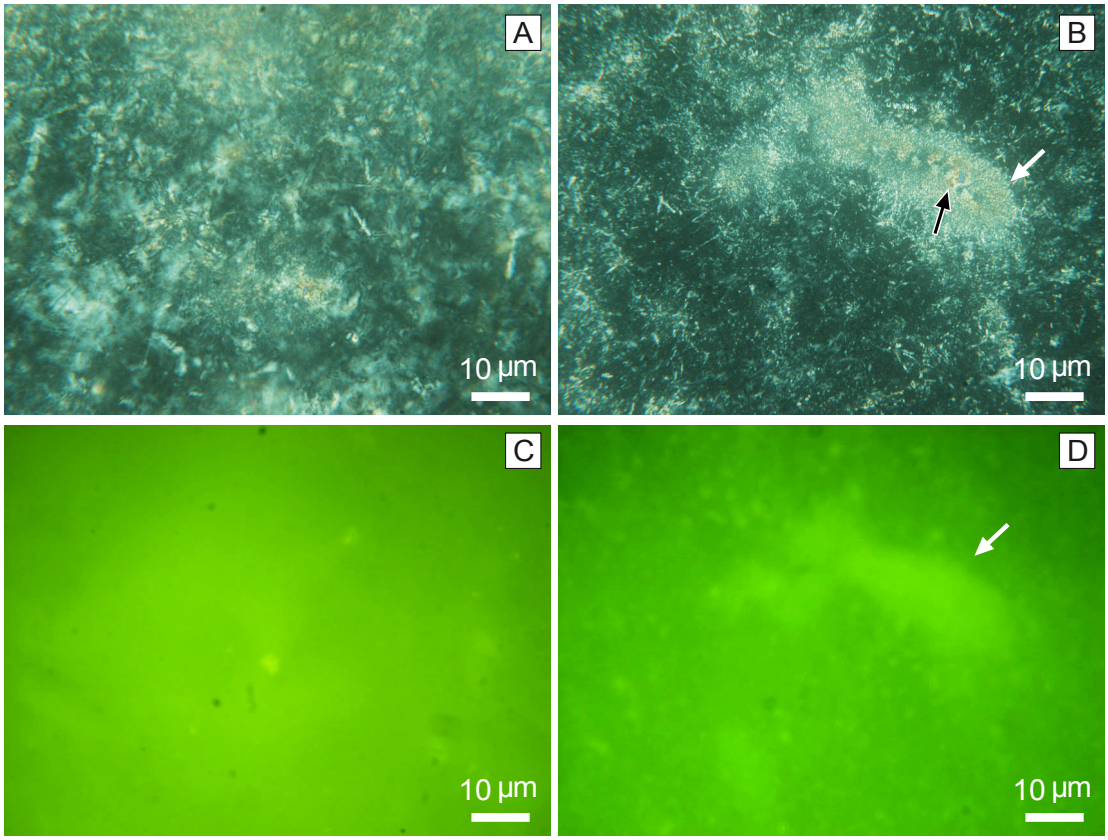

Figure 4.17 - Thin section in a moonmilk crust. **(A)** Crossed-polarized light (XPL) observation showing no particular feature. Moonmilk is composed of mostly nanofibres, which are too small to be detected under light microscope magnification. **(B)** Poor autofluorescence of moonmilk, exactly the same area as in A (UV epifluorescence). **(C)** Particular structures observed in moonmilk appearing as tubular shapes, with an outer layer of acicular crystals (white arrow) and an inner filling of larger crystals (black arrow). **(D)** Slight autofluorescence of the tubular feature from C (arrow); exactly the same area as in C (UV epifluorescence).

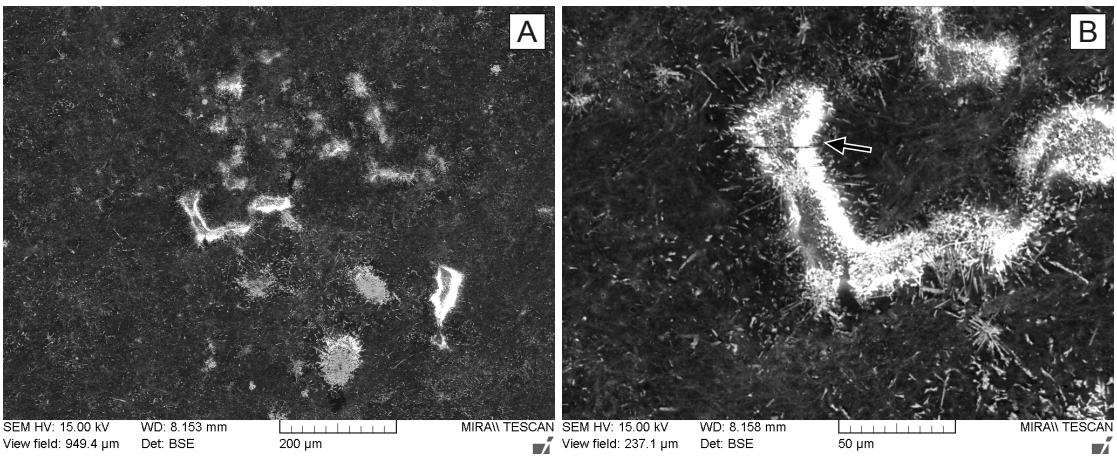

Figure 4.18- SEM images of thin sections in a moonmilk crust. **(A)** Tubular shape similar to the one observed in Fig. 4.2 C, note its bright appearance under the electron beam. **(B)**. Close-up of the structure in A showing two distinct nature of material. The external layer is extremely bright as a result of electron accumulation. These structures are highly unstable under the electron beam (arrow). This kind of feature is often observed with non-fixed organic materials, suggesting that these tubular features might be composed of OM.

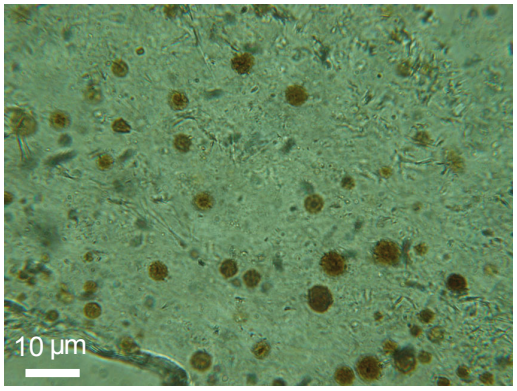

Figure 4.19 - Thin section in a moonmilk crust. PPL obsvervation of small rounded bodies, which seem melanized (2 to 5 µm in diameter). They could be either spores of fungi or actinomycetes.

actinomycetes spores regarding their dimensions. In pedogenic samples, secondary $CaCO_3$ are observed in close association with OM (Fig. 4.20 A). OM is present as living roots, recognizable fragments of decaying OM as well as amorphous OM. A close-up on calcitic aggregates shows that melanized hyphae are closely associated to NFC (Fig. 4.20 B). Furthermore, melanized fungal hyphae have appeared as ubiquitous features in “coating” macrofacies (Fig. 4.21). Samples taken at the B-C interface shows mycorrhized roots (Fig. 4.22 A black arrows) that are associated to several NFC bundles (Fig. 4.22 A white arrows - B), as well as meshes of NFC (Fig. 4.22 C black star & 4.23 A). Hyphae are present within this aggregate as observed on Fig. 4.22 A (black arrows). Moreover, highly autofluorescent areas (Fig. 4.22 D black star & 4.23 B) indicate a high OM content of these areas, which could be either fungal hyphae,

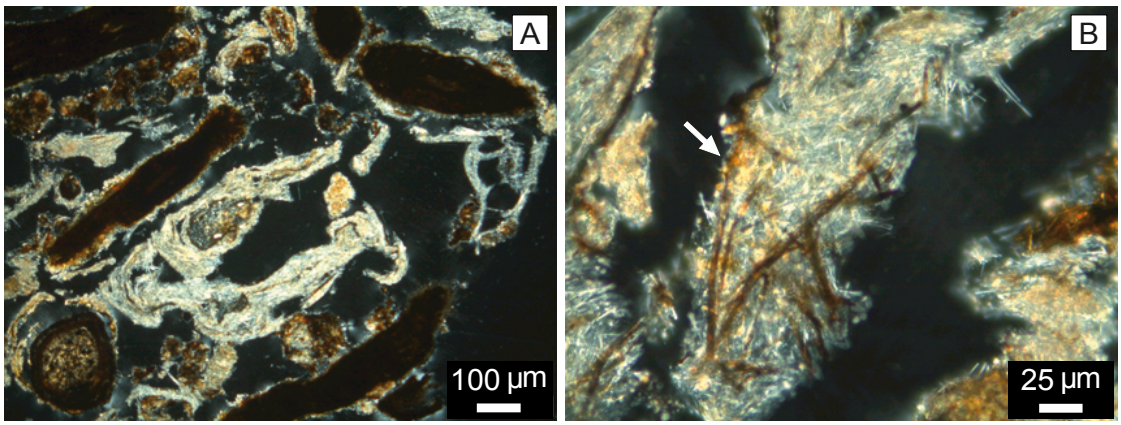

Figure 4.20 - Thin section in grain and soil aggregates containing OM, “cotton ball-like” and “coating” macrofacies from the interface between the B and C horizons. **(A)** XPL overview showing the close relationship between secondary $CaCO_3$ features and OM present either as living roots, recognizable fragments of decaying OM, or amorphous OM. **(B)** XPL close-up on a secondary $CaCO_3$ area showing melanized filaments (arrow) within a mineral accumulation.

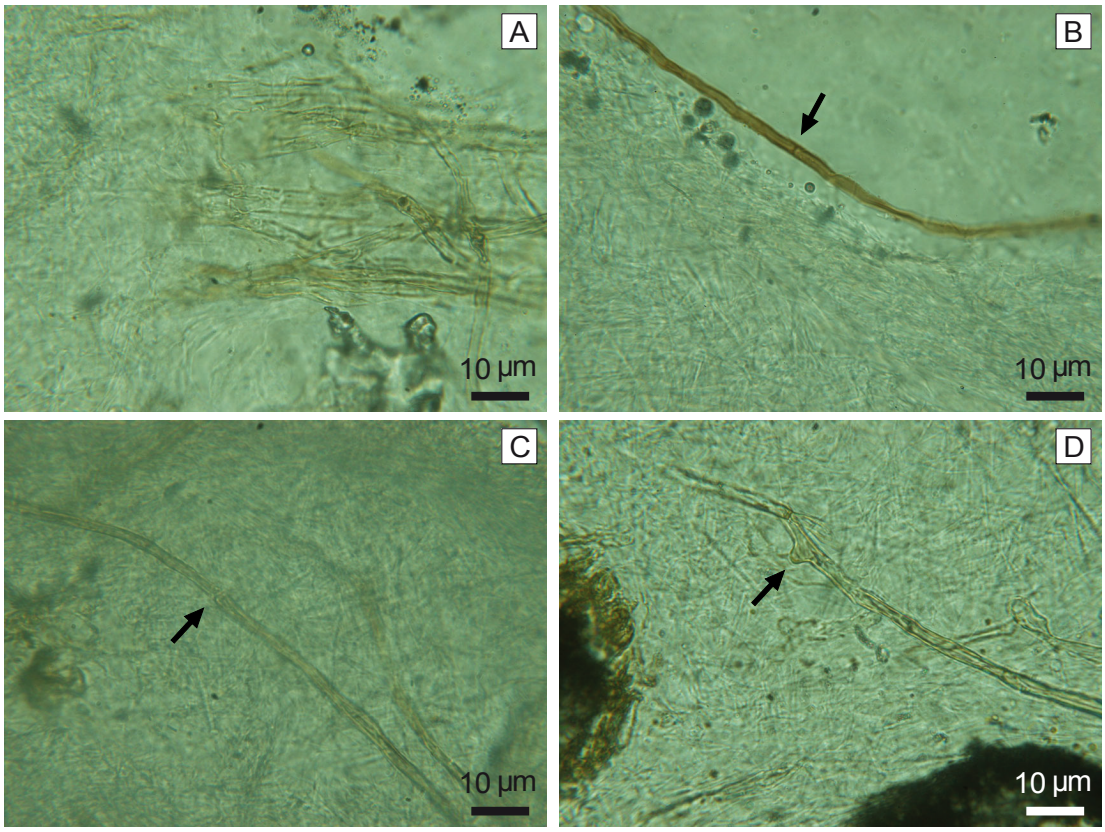

Figure 4.21 – **(A-D)** PPL photographs of a thin section in "coating" macroscopic facies showing recurrent association of melanized fungal hyphae within NFC and nanofibre meshes. Note that nanofibres cannot be distinguished at this magnification. **(B-C)** Septa in hyphae (arrow). **(D)** Clamp connection (arrow)?

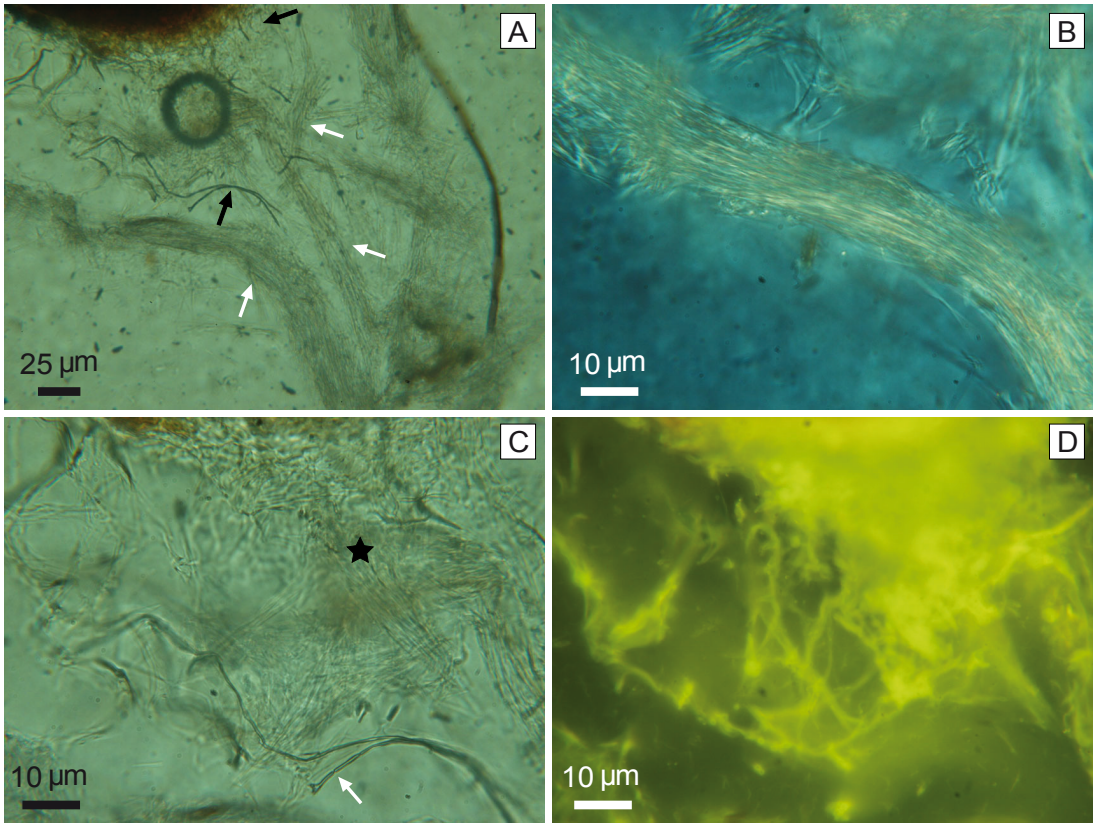

Figure 4.22 - Thin section in grain and soil aggregates containing OM, "cotton ball-like" and "coating" macrofacies from the interface between B and C horizons. **(A)** PPL observation of a mycorrhized root (upper black arrow) and mantle hyphae (lower black arrow) associated to several NFC bundles (white arrows) as well as meshes of NFC. **(B)** XPL close-up on a NFC bundle from the root vicinity. **(C)** PPL close-up on a mesh of randomly organized needles (star) and associated hyphae, note the typical septate structure of hyphae (arrow). **(D)** UV epifluorescence observation of exactly the same area as in C, showing high autofluorescence, probably resulting from the root microenvironment (fungal hyphae, associated rhizospheric bacteria and mucilaginous substances).

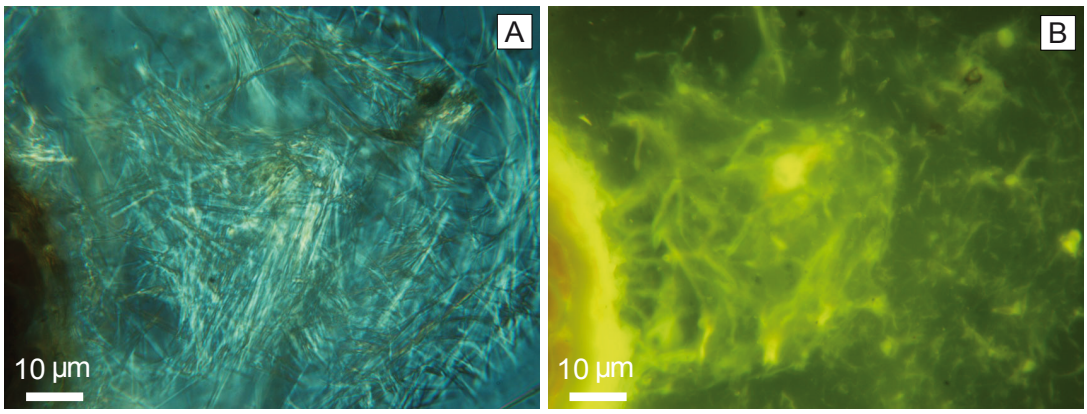

Figure 4.23 - Thin section in grain and soil aggregates containing OM, "cotton ball-like" and "coating" macrofacies from the interface between the B and C horizons. **(A)** XPL close-up on a mesh of randomly organized needles in the vicinity of a root (probably mycrorrhized; however, no hyphae may be distinguished). **(B)** UV epifluorescence of exactly the same area as in A, showing highly autofluorescent spots associated to needles mesh.

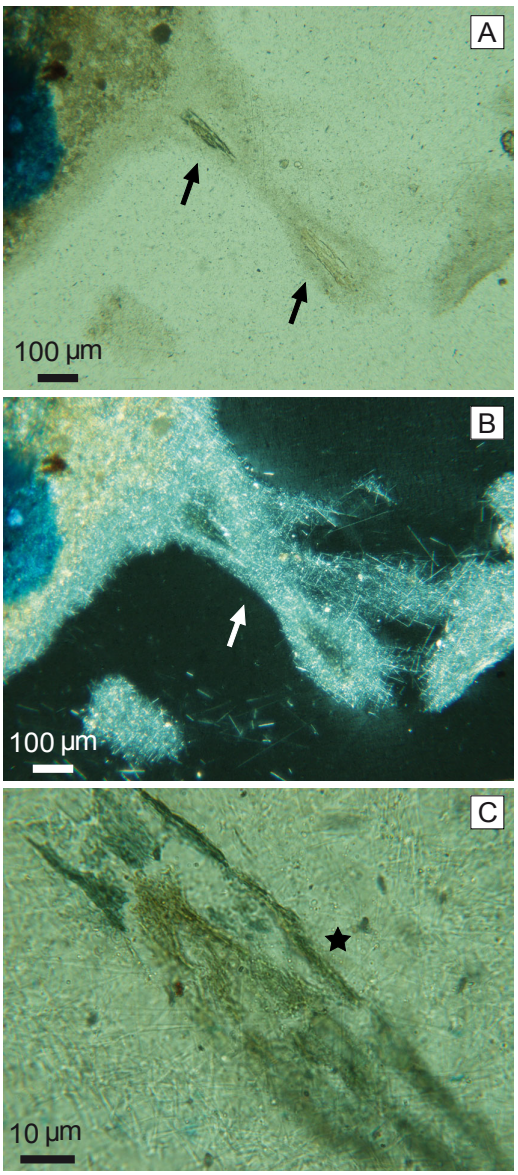

rhizospheric bacteria or mucilaginous substances. In the "cotton ball-like" facies, bundles of NFC have been observed, associated to purported OM (Fig. 4.24 & 4.25). On Figure 4.24, the bundle, easily distinguishable from the background using crossed-polarized light (Fig. 4.24 A-B), seems to be associated with another filamentous structure (Fig. 4.24 A-C), which has been identified as a mycelial strand, based on its dimension, colour, and structure. Figure 4.25 shows another bundle of NFC observed from the same sample. At low magnification, it may appear as a mycelial strand due to a well defined linear shape (Fig. 4.25 A white arrow). A closer observation of the extremity of this filamentous structure shows that it is composed of needles, which seem to burst out of the linear feature (Fig. 4.25 B). This latter is composed of needles arranges side-by-side (Fig. 4.25 C), but seems to be associated with organic filaments (from a mycelial strand?) as suggested by epifluorescence observations (Fig. 4.25 D).

4.3.3.2 SEM observations

Using photonic microscopy, NFC and organic features are easily recognized, but nanofibres are impossible to see. Observations of the thin sections with the SEM allowed nanofibres and their particular features to be clearly seen. Indeed, moonmilk observation with the photonic

Figure 4.24 - Thin section in "cotton ball-like" macroscopic facies. **(A)** PPL observation of a bundle of NFC in which a brownish, probably, organic remain is present (arrows). **(B)** XPL observation of exactly the same area as in A showing the extent of NFC (arrow) and the brown area in the middle of the bundle. Note that NFC is better seen using XPL light. **(C)** PPL close-up on the brown area (star) showing a "filamentous-like" organization of this feature, suggesting that it might be remains of a fungal strand.

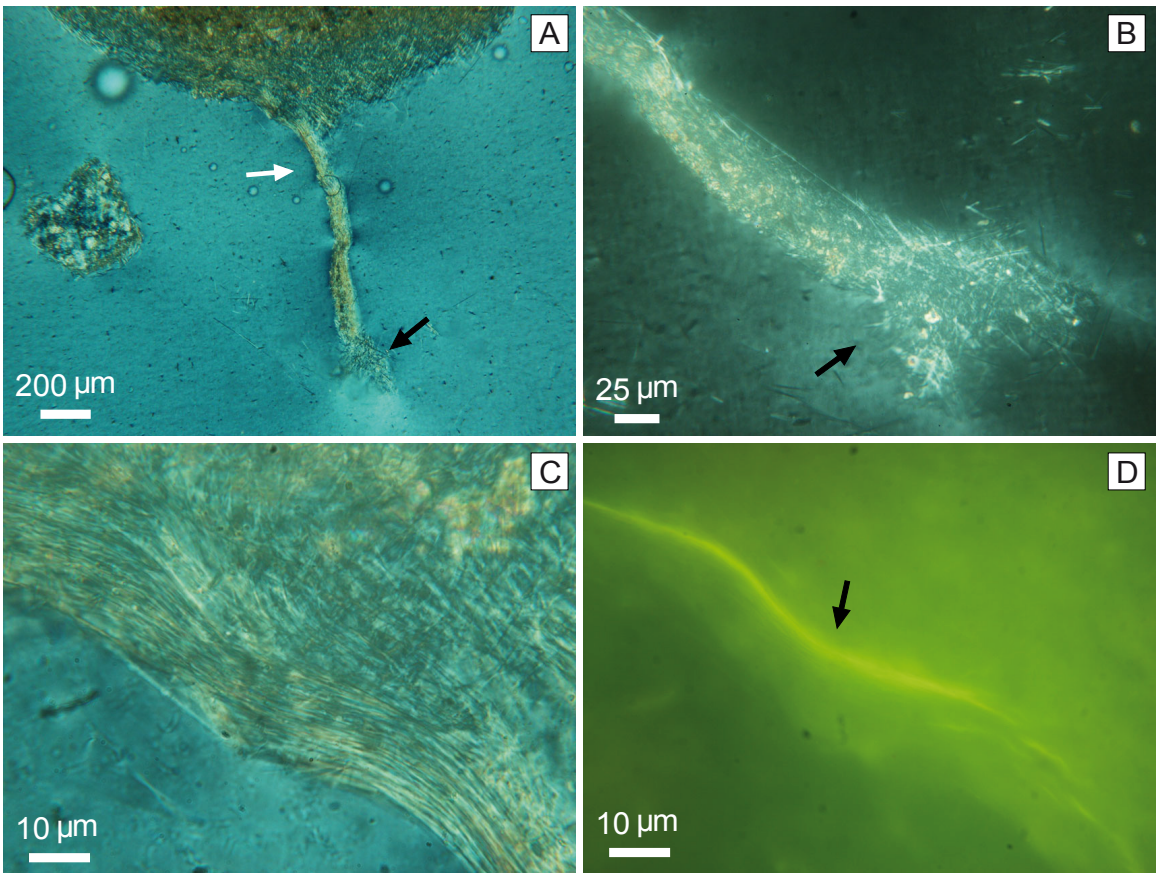

Figure 4.25 - Thin section in "cotton ball-like" macroscopic facies. **(A)** XPL observation of a filamentous shape (white arrow) extending from a limestone grain coated with NFC. Black arrow point at a mesh of randomly organized needles. **(B)** XPL close-up shows randomly organized needles associated to the tip of the filamentous shape (arrow). The mesh of needles seems to be bursting out of the filament. **(C)** XPL close-up on the side of the filamentous shape shows side-by-side arranged needles showing non-linear morphologies, suggesting that the filamentous shape is a fungal strand and associated NFC bundle. **(D)** UV epifluorescence observation of exactly the same area as in C, showing autofluorescing pattern of the structure and the presence of highly fluorescent areas within the bundle (arrow).

microscope was much less informative than those of the soil thin sections. This is mainly due to the fact that moonmilk is largely constituted by dense meshes of nanofibres, which are too small to be seen as individual objects under a conventional microscope. Under the SEM, moonmilk seems built by accumulations of successive layers of nanofibres (Fig. 4.26 A-B). In closer observations, these successive layers resemble "filament-like" structures composed of nanofibres (Fig. 4.26 B-C). Furthermore, "tubular" structures have been observed in moonmilk crusts (Fig. 4.27 A-C). They seem to be the result of microborings inside the nanofibre mesh, however no filamentous organisms, either actinomycete or fungi are observed inside them. Similar structures have been observed in the soil sample coming from the B-C interface (Fig. 4.28 & 4.29). Numerous rounded voids are present within the nanofibre mesh (Fig. 4.28 A-C) as well as filamentous/ tubular shapes (Fig. 4.28 D). Closer observation shows that they are associated to structures having the shape of thick walled hyphae (Fig. 4.29 A-B). In addition, they may be observed arranged together in what seems to be a non-random pattern (Fig. 4.29 C). Finally, it must be pointed out that organic structures such as roots could not be observed under the SEM due to their high instability under the electron beam. To the contrary, thick-walled hyphae have been observed without any problem. This results most likely from differences in material density and chemical quality.

4.3.4 Discussion

The observation of soil and moonmilk thin sections has brought new information on the relationship

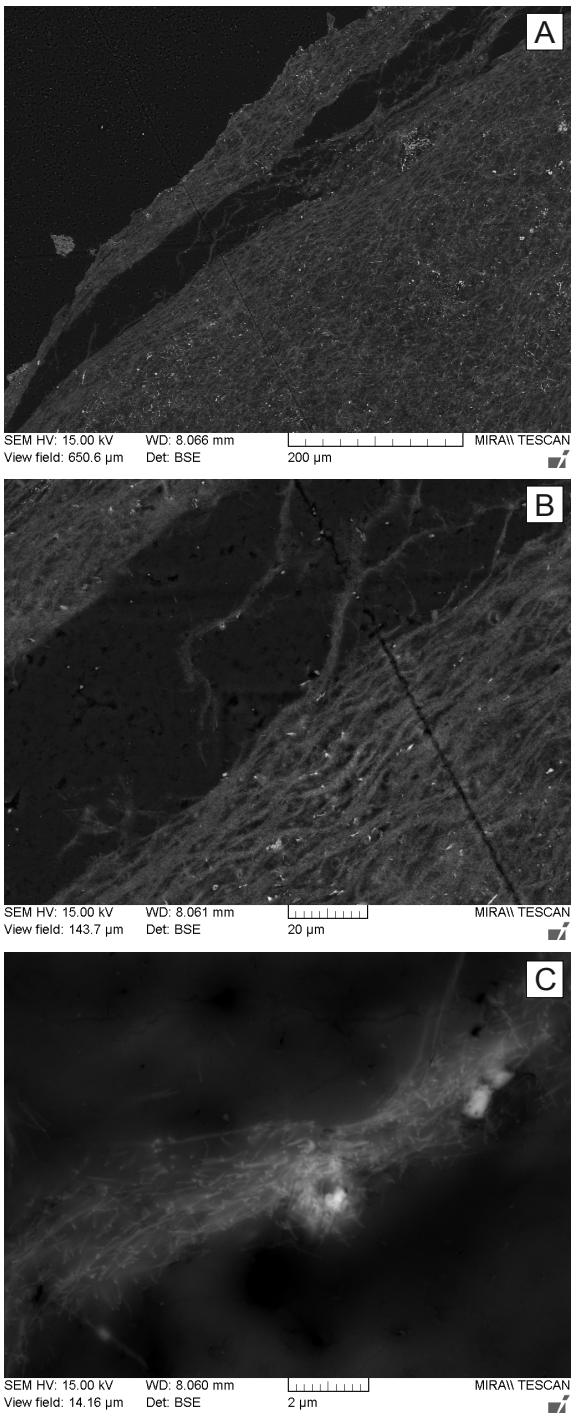

Figure 4.26 - SEM images of thin section in a moonmilk crust. **(A)** Overview of the moonmilk crust, showing that it is composed of a mesh of nanofibres with heterogeneous inclusions dispersed within the mesh. **(B)** A close-up of the meshes shows that the moonmilk crust is made of successive layers constituted by "filament-like" structures. **(C)** A close-up of the "filament-like" structures shows that each of them is composed of nanofibres.

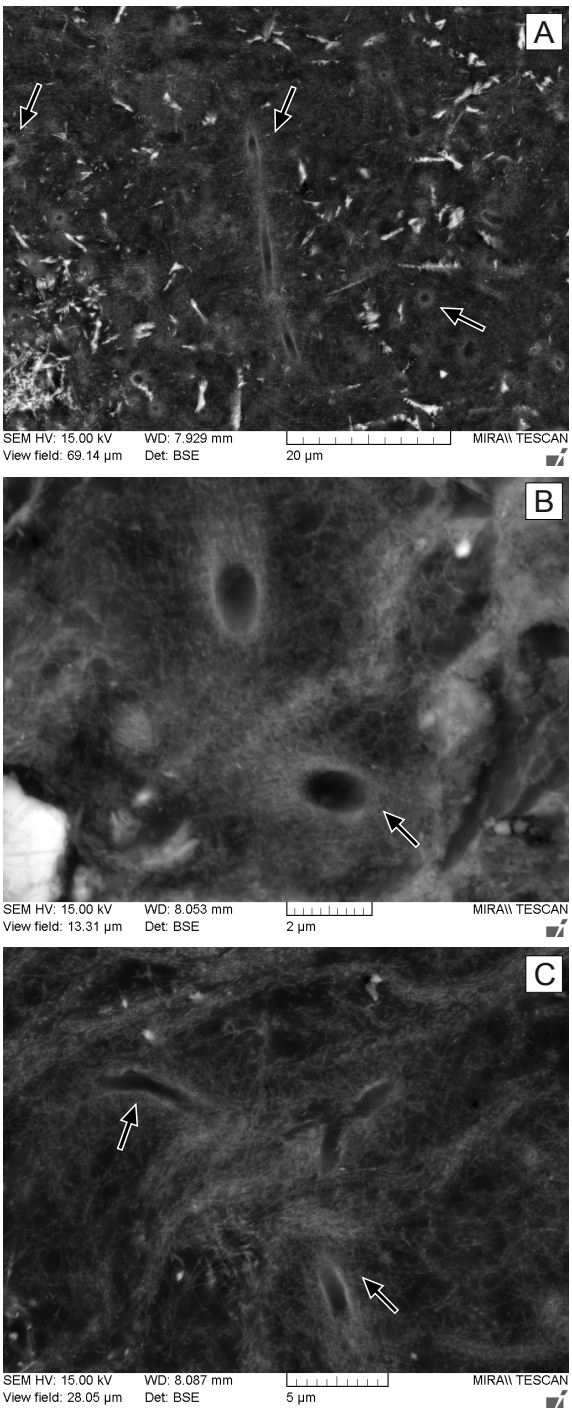

Figure 4.27 - SEM images of thin section in a moonmilk crust. **(A-C)** Tubular and circular structures commonly observed within nanofibre meshes of moonmilk and resembling hyphal structures (either from fungi or actinomycetes).

between NFC, nanofibres, and fungi. In soil thin sections, fungi, either as single hyphae or as mycelial strands/rhizomorphs, are ubiquitously present (Fig. 4.21 - 4.23 & 4.25). It must be pointed out that samples were unstained, and as consequence, only melanized hyphae could be detected. The observation of stained samples might lead to the observation of more hyphae, as hyaline hyphae will also be visible. Moreover, in thin sections the recurrent presence of NFC bundles is again highlighted. The importance of these features in NFC genesis has already been suggested in § 4.1

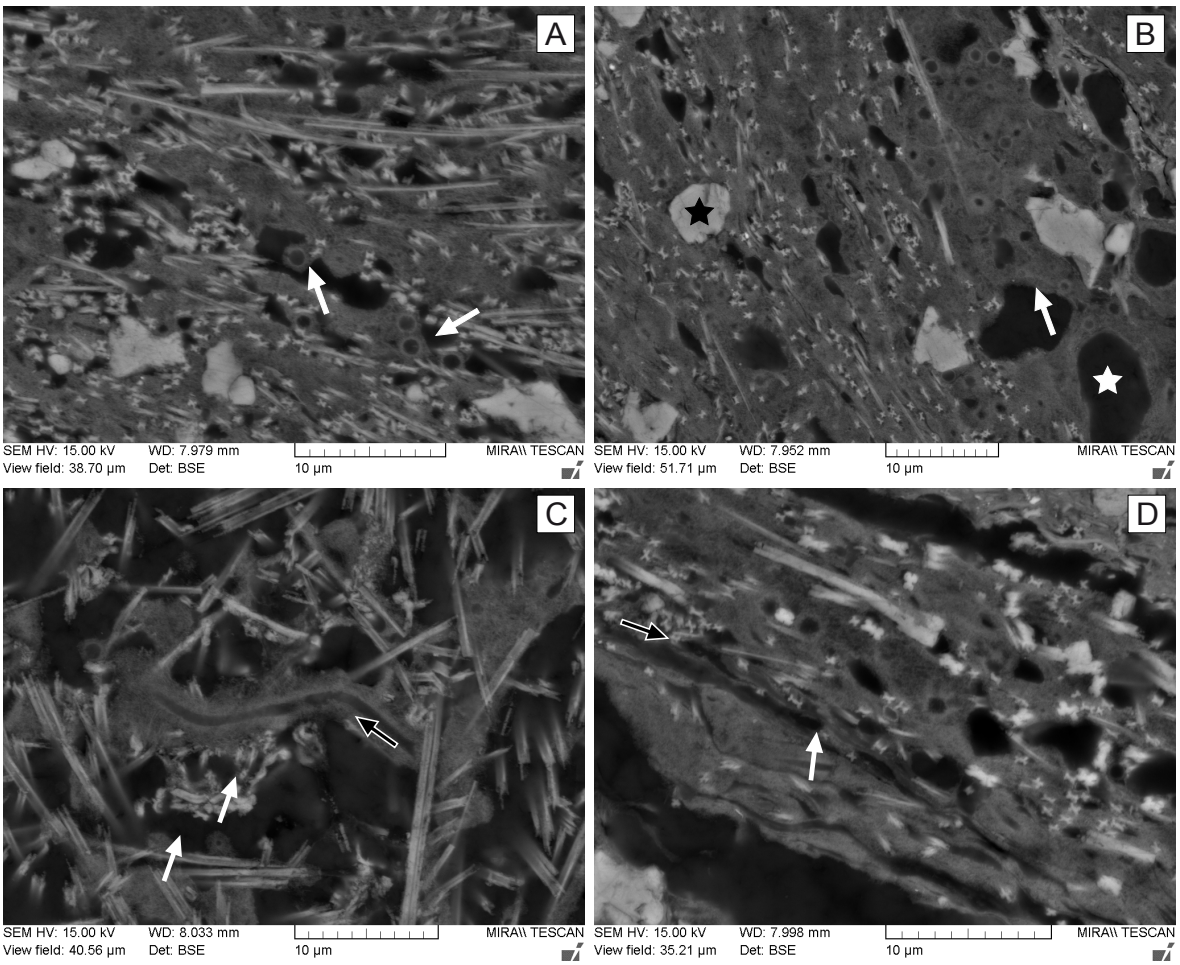

Figure 4.28 - SEM images of a thin section in grain and soil aggregates containing OM, "cotton ball-like" and "coating" macrofacies from the interface between the B and C horizons. **(A)** Overview of the typical organization pattern between nanofibres and NFC. Note the presence of circular structures within nanofibre meshes (arrows). **(B)** Overview of a similar pattern as in A, note the high density of circular structures in the right area of the image (arrow). Note the presence of pores (white star) and trapped mineral grains (black star) within nanofibres and NFC meshes. **(C-D)** Close-up shows filamentous structures (white arrows) and circular structures (black arrow) within nanofibre meshes. Note similarity with the same features in moonmilk crusts (Fig. 4.20). On C, note the cross-sections of NFC displaying different shape as well as dimensions.

(Bindschedler et al. 2010) and 4.2, as well as in Phillips and Self (1987) and Ould Mohamed and Bruand (1994). Random meshes of NFC, as well as NFC bundles, are observed in close association with hyphae associated to roots (Fig. 4.22 & 4.23). Regarding the environment where the sampling has been realized (beech and fir forest, see chapter 3), it can be stated that hyphae are most likely from an ECM fungi. This brings the question of whether NFC genesis might be related to some ecological category of fungi? Blyth and Frisia (2008) have already emphasized the fact that among their studied sites, moonmilk occurred only under rendzinae and fractured limestones. Dubroeucq et al. (1996) have observed NFC and nanofibres in association with pine root trees. Similarly, in this study, the secondary $CaCO_3$ accumulations have been described from forested sites with soil having high OM content in their surficial layer. Moreover, the association of NFC and nanofibres with OM, either living or decaying, suggest a connection between theses calcitic features and OM decaying processes (Fig. 4.16 - 4.18, 4.20, 4.23 & 4.24). Therefore, it can be concluded that a clear relationship with biotic structures exist. However, only speculative conclusions can be drawn regarding the type of fungi, i.e. ECM fungi.

In moonmilk thin sections, and in particular using SEM, a highly organized structuring of these features has been observed (Fig. 4.26). This type of organization might indicate a sort of periodic pattern in their formation, possibly linked to water percolation within the cave environment. Observations of "filament-like" and "tubular" structures in both soil and moonmilk thin sections (Fig. 4.27 - 4.29)

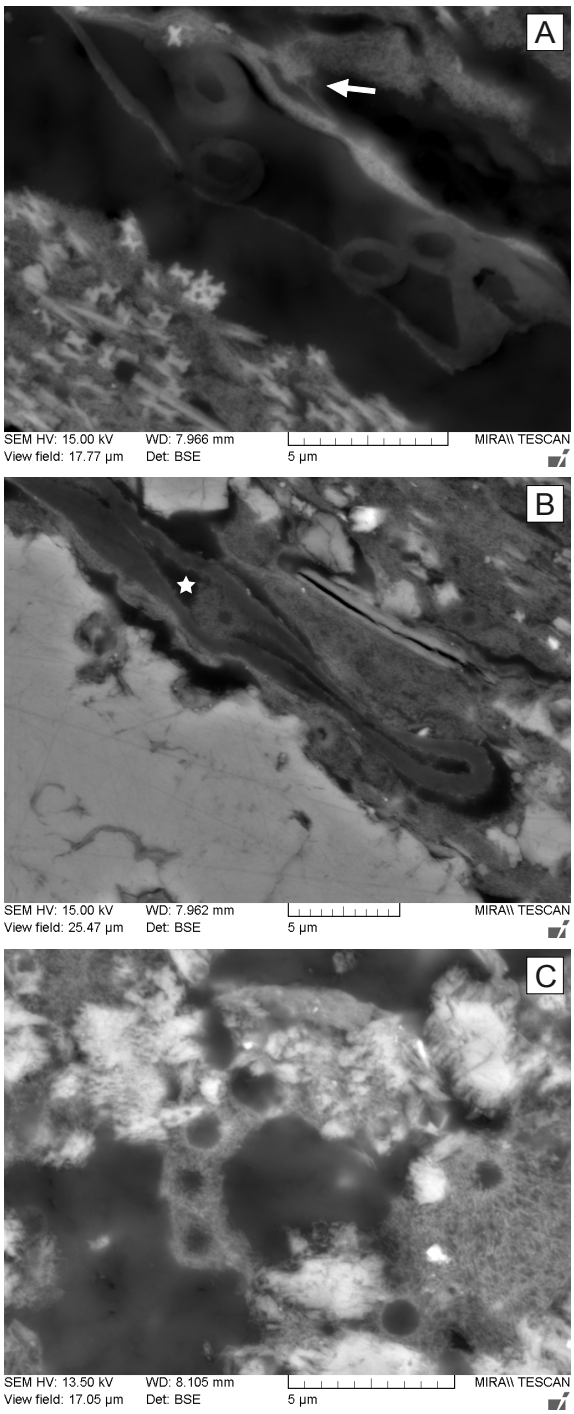

Figure 4.29 - SEM images of a thin section in grain and soil aggregates containing OM, "cotton ball-like" and "coating" macrofacies from the interface between the B and C horizons. **(A)** Cross-section in circular features resembling thick walled hyphae closely associated with nanofibre mesh (arrow). Note the cross-sections of NFC (lower left hand side; NFC embedded in nanofibre mesh) displaying different shape as well as dimensions. **(B)** Longitudinal section in a filamentous feature resembling thick walled hyphae; note the presence of a nanofibre mesh within the structure (star). **(C)** Circular features within nanofibre mesh, arranged in a non-random pattern.

confirm what has already been extensively observed using SEM and TEM, i.e. such structures are ubiquitous in NFC and nanofibres accumulations. Eventually, it is the indication of living forms most likely involved in the genesis of such deposits, as already suggested in § 4.1 and 4.2.

4.3.5 Conclusions

The thin section approach has led to the confirmation of some observations but has also brought new challenging questions. Moreover, it has emphasized the crucial relationship between organic

structures and NFC and nanofibres. However, only a few samples have been treated and the approach should be repeated in order to gather more images. Indeed, being able to investigate a sample using several observational scales is likely to bring further information, as already emphasized by Callot et al. (1985b). Observation by photonic microscopy allows the relationships at the sub-millimetric scale to be treated, while SEM is more devoted to the sub-micrometric scale. However, it must be pointed out that organic samples should be fixed prior to embedding in the epoxy resin in order to be able to perform high-magnification images. Nevertheless, such step is likely to modify structures and relationships between the microfeatures present in the sample.

4.4 Summary of chapter 4

Nanofibres recurrently observed in association with NFC are the result of an incomplete decay of the fungal cell wall. As a result, nanofibres lying on the surface of NFC bundles implies that fungi were once associated to NFC and thus emphasize a fungal origin for NFC.

Striking analogies between structural features of fungal hyphae and morphologies of NFC and nanofibres highlight an intimate relationship between fungi and NFC during their genesis.

Finally, soil thin sections of natural samples demonstrate that fungi and fungal structures are ubiquitous in NFC and nanofibres accumulations. Moreover, it emphasizes the link to the overlying soil and vegetation through the mycorrhizal network.

Chapter 5

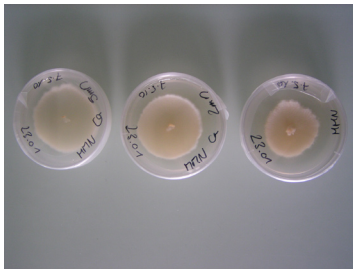

Experimental approaches

Chapter 5 - Experimental approaches to the formation of NFC and nanofibres

The observation approach has brought significant advances in the comprehension of NFC and nanofibres origins. However, observations lead to interpretations, which may always be challenged by other interpretations. Consequently, an experimental approach has been chosen with the aim to confirm the observations and subsequent interpretations. The first part of this chapter aims at demonstrating that fungal hyphae, in particular their cell wall, is a source of organic nanofibres. A sequential enzymatic hydrolysis ("enzymatic dissection/digestion") of the fungal cell wall polymers has been chosen as a mild approach, in order to mimic environmental conditions. The results obtained with this approach are presented in the form of a publication that will be submitted in a near future (§ 5.1). The second part of the chapter is actually based on both, observations and experimentation (§ 5.2). It questions the storage of calcium in the fungal cell wall, as well as inside the hyphae of mycelial strands, as a critical point to explain NFC and nanofibres genesis. Finally, the third part of this chapter concerns the search of organic compounds associated to the different macroscopic facies. These organic compounds may be used as markers of a possible biogenic origin of both NFC and nanofibres (§ 5.3).

5.1 Following the fungal trail: how enzymatic digestion of fungal cell wall may produce soil and cave nanofibres

Submitted to Naturwissenschaften

Bindschedler S[1], Braissant O[2], Cailleau G[1], Millière L[1], Job D[3] and Verrecchia EP[1]

[1] Institute of Geology and Palaeontology, University of Lausanne, Anthropole, CH-1015 Lausanne, Switzerland.
[2] Laboratory of Biomechanics and Biocalorimetry, Biozentrum/Pharmazentrum, University of Basel, Klingelbergstrasse 50-70, CH-4056 Basel, Switzerland.
[3] Laboratory of Microbiology, Institute of Biology, University of Neuchâtel, Emile Argand street 11, CH-2009, Switzerland.

5.1.1 Abstract

Calcitic nanofibres are ubiquitous calcitic habits of secondary calcium carbonate ($CaCO_3$) accumulations observed in calcareous vadose environments. The origin of these nanofeatures remains enigmatic today, its debate centered on three possibilities: i) purely physicochemical processes, ii) mineralization of rod-shaped bacteria and iii) crystal precipitation on organic templates. Nanofibres are often observed in association with needle fibre calcite (NFC), a typical secondary $CaCO_3$ habit of terrestrial environments. Current knowledge attributes a fungal origin to NFC and therefore the possible fungal origin of nanofibres has been investigated in this study. Sequential enzymatic digestion of the fungal cell wall of selected fungal species demonstrates that the fungal cell wall can be a source of nanofibres in the natural environment. The obtained nanofibres show a striking resemblance to their natural counterparts, emphasizing a fungal origin for the calcitic nanofibres observed in association with NFC. In conclusion, the origin of calcitic nanofibres may be attributed to the nucleation of $CaCO_3$ along an organic substrate, which is typically a biologically-influenced mineralization process.

5.1.2 Introduction

Calcitic nanofibres are ubiquitous features of secondary calcium carbonate ($CaCO_3$) deposits observed in various vadose environments (caves – as moonmilk, soils, aqueducts). Nanofibres are always observed in the presence of another typical feature of these secondary $CaCO_3$ deposits, Needle Fibre Calcite (NFC; Fig. 5.1). Moreover, their close physical association, emphasizes an intimate relationship between them (Bindschedler et al. *in press*). NFC is thought to be fungal in origin (Callot et al. 1985b; Phillips and Self 1987; Verrecchia and Verrecchia 1994; Cailleau et al. 2009b), whereas the nanofibres' origin remains unclear. Many authors have reported the presence of nanofibres in various continental environments as "micro-rods" (Phillips and Self 1987; Jones and Khale 1993; Verrecchia and Verrecchia 1994; Loisy et al. 1999), "hyphantic threads" (Klappa 1979), "rod-shaped nanobacteria like" (Benzerara et al. 2003), "needles" (Jones and Ng 1988), and "nanofibres" (Borsato et al. 2000; Richter et al., 2008; Cailleau et al. 2009a&b; Bindschedler et al. 2010). Similarly, many hypotheses for their origin have been proposed: i) physicochemical processes (Jones and Ng 1988; Jones and Khale 1993; Borsato et al. 2000); ii) biomineralization of rod-shaped nano-sized bacteria (Phillips and Self 1987; Verrecchia and Verrecchia 1994; Loisy et al. 1999); and iii) nucleation mediated by an organic template (Benzerara et al. 2003; Olstza et al. 2004). Some authors have put forward the hypothesis of an indirect biogenic origin, which might involve "organic nanofibres coming from a cell wall" (Klappa 1979; Cailleau et al. 2009a; Bindschedler et al. 2010). Indeed, the cell wall of fungi and plants is a potential source of organic nanofibres, as fibrous polymers are part of the cell wall of both types of organisms (Carlile et al. 2001; Paul 2007). Considering the fungal cell wall, many studies investigating its structure revealed that it is roughly composed of two main sheets: an outer one made of amorphous materials and an

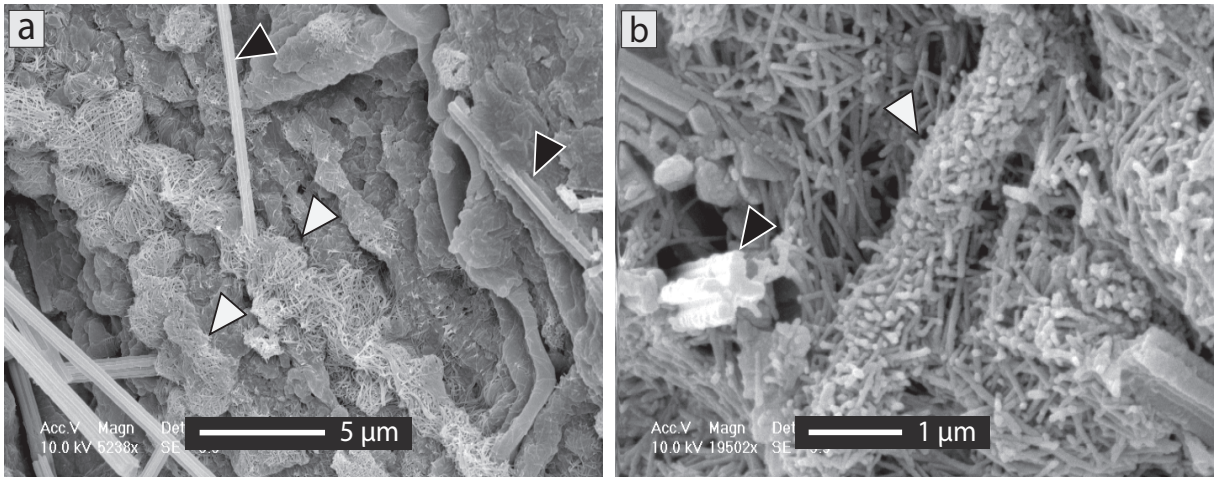

Figure 5.1 - SEM images of natural samples showing organized (i.e. showing preferential orientations and organization) meshes of nanofibres (indicated by white arrows) as well as fungal hyphae and Needle Fibre Calcite (NFC ; black arrows). **(a)** Organized nanofibre meshes displaying a filament-like shape and lying on decaying fungal hyphae from a rhizomorph. Note the presence of associated NFC. Sample of both OM and secondary $CaCO_3$ located at the interface between the organic and mineral soil horizons. **(b)** Organized nanofibre mesh having the shape of a filament and lying on a mesh of randomly-organized nanofibres and associated NFC. Sample from coatings on scree containing decaying fungal rhizomorphs.

inner one, composed of fibrous polymers (Bartnicki-García 1968; Burnett 1979; Farkaš 1979; Ruiz-Herrera 1992; Bowman and Free, 2006). A close-up on the fungal cell wall structure shows different successive layers (Fig. 5.2). Although the exact composition is highly dependant on the fungal taxa, Ruiz-Herrera (1992) provides a general description. The outermost part of the external sheet is often covered with amorphous α-1,3-glucans also called hydrophobins. Adjacent is an amorphous layer made of amorphous mannoproteins as well as β-1,3 and β-1,6-glucans. This layer may also contain melanin, a highly recalcitrant polymer, conferring an enhanced resistance to the fungal cell wall. Finally, the inner part is made of two fibrous polymers, chitin and unbranched β-1,3-glucan, embedded in an amorphous matrix of mannoproteins (Hunsley and Burnett 1970; Ruiz-Herrera 1992; Farkaš 2003). Furthermore, cross-linking of chitin, β-1,3-glucan and glycoproteins in the fibrillar layers results in an enhanced rigidity of the cell wall (Fontaine et al. 1997; Bowman and Free 2006). Chitin is a polymer of N-acetyl-glucosamine and is present in the form of long microfibrils (up to 1 µm), with diameters of 10 to 25 nm (Carlile et al. 2001). It is located in the innermost part of the wall and arranged as an intertwined mesh embedded in an amorphous matrix of mannoproteins (Aronson and Preston 1960; Carlile et al. 2001). β-glucans are polymers of D-glucose. In the fibrous region of the fungal wall, it is present as unbranched β-1,3-glucan. They are usually found in greater amounts than chitin (Carlile et al. 2001; Farkaš 2003). Bindschedler et al. (2010) have demonstrated that organized meshes of nanofibres (i.e. showing preferential orientations) have an organic signature and, therefore might originate from fibrillar components of the fungal cell wall, chitin and/or β-1,3-glucan. Moreover, environments where nanofibres are observed together with NFC are known to be typical fungal environments. Indeed, fungi are common inhabitants of soils and caves either as saprotrophs or as mycorrhizal root symbionts (Paul 2007; Gobat et al. 2003).

The present study aims at demonstrating in the laboratory that fungal hyphae are a potential source of nanofibres. In particular, it seeks at emphasizing that an incomplete decay of the fungal cell wall can reveal nanofibrous material with similar characteristics to their natural counterparts. In order to stay as close as possible to natural conditions, a sequential enzymatic approach has been chosen to mimic the decay of soil organic matter.

5.1.3 Material and methods

5.1.3.1 Cultures of fungal strains

Three strains have been used for enzymatic assays: one ascomycete (*Peziza sp.*) and two basidiomycetes (*Armillaria mellea* and *Boletus edulis*). *Peziza sp.* and *Armillaria mellea* are deposited in the culture collection of the Laboratory of Microbiology at the University of Neuchâtel whereas the *Boletus edulis* strain has been obtained from the Swiss Federal Research Institute WSL, CH-8903 Birmensdorf. *Peziza sp.* and *A. mellea* have been cultivated at room temperature away from any light source on a 1.2% malt-agar medium (malt extract 12 g/L; agar 15 g/L). *B. edulis* has been cultivated at room temperature away from any light source on MMN medium (after Marx and Bryan (1971) : D-glucose 10 g/L ; malt extract 3 g/L; $(NH_4)_2HPO_4$ 250 mg/L; KH_2PO_4 500 mg/L; $MgSO_4.7H_2O$ 150 mg/L; $FeCl_3$ 12 mg/L ; $CaCl_2$ 50 mg/L ; NaCl 25 mg/L ; thiamine 0.1 mg/L ; agar 15 g/L). All strains have been cultivated in Petri dishes of 55 mm diameter with polycarbonate filters of 0.2 µm pores set upon the solid media in order to be able to harvest solely the mycelium.

5.1.3.2 Enzymatic incubations

The enzymatic approach has been adapted from Hunsley and Burnett (1970). A two-week-old mycelium was used for *Peziza sp.* and *A. mellea*, whereas a two-month old mycelium was used for *B. edulis*, as it has a slower growth rate. The whole mycelium (from the centre to the margin, with the exception of the inoculum) was used for the incubations and was treated aseptically throughout the experiment. Buffer solutions and water have been autoclaved, whereas enzymatic solutions have been sterilized by filtration through 0.2 µm nitrocellulose filters. Enzymes have been mixed according to their lytic activities, either glycolytic or proteolytic. The glycolytic mix contained an alpha-glucanase (10 U/mL ; EC 3.2.1.20), a lyticase (150 U/mL ; EC 3.2.1.58) and a laminarinase (7 U/mL ; EC 3.2.1.6). The proteolytic mix contained a protease (50 U/mL ; commercial mixture of at least three proteolytic activities) and a proteinase K (50 U/mL ; EC 3.4.21.64). All enzymes were supplied from Sigma™.

Mycelia were treated without a prior step of washing. They were separated from the polycarbonate filter and transferred to a 2 mL ependorf filled with ultrapure water, and ultrasonicated for 15 minutes. Then, they were washed once in KOH 5%, re-suspended in 1.5 mL fresh KOH 5%, and incubated at 30°C for 5 days. After KOH treatment, mycelia were washed in deionized water once, and then incubated in 1.5 mL glycolytic enzymatic mix in a pH 7 Z-buffer (modified after Braissant et al., 2009) at 37°C for 3 days in agreement with the enzymatic optimal efficiency (according to SigmaTM information). After this step, mycelia were washed again in deionized water once and incubated in 1.5 mL proteolytic enzymatic mix in a pH 8.8 Tris-HCl buffer at 37°C for 3 days (Fig. 5.2). After each step mycelia were washed and then stored at 4°C until fixation for Scanning Electron Microscopy (SEM).

5.1.3.3 Scanning Electron Microscope observations of laboratory samples

All laboratory samples have undergone primary fixation in 2.5% glutaraldehyde in Phosphate Buffer Solution (PBS) and secondary fixation in 1% osmium tetroxide in PBS. Samples were then dehydrated in ethanol series of increasing concentrations with a Tetramethysilane (TMS) step for final air drying (Dey et al. 1989). Samples were finally placed on a SEM stub and covered with a 18 nm gold coating followed by a 5 nm carbon coating. SEM has been performed using a Tescan Mira LMU operated at a distance of 10 mm and a voltage of 10 to 15 keV acceleration. Elemental microanalysis has been performed with an EDAX Energy Dispersive Spectrometer (EDS) coupled to the SEM.

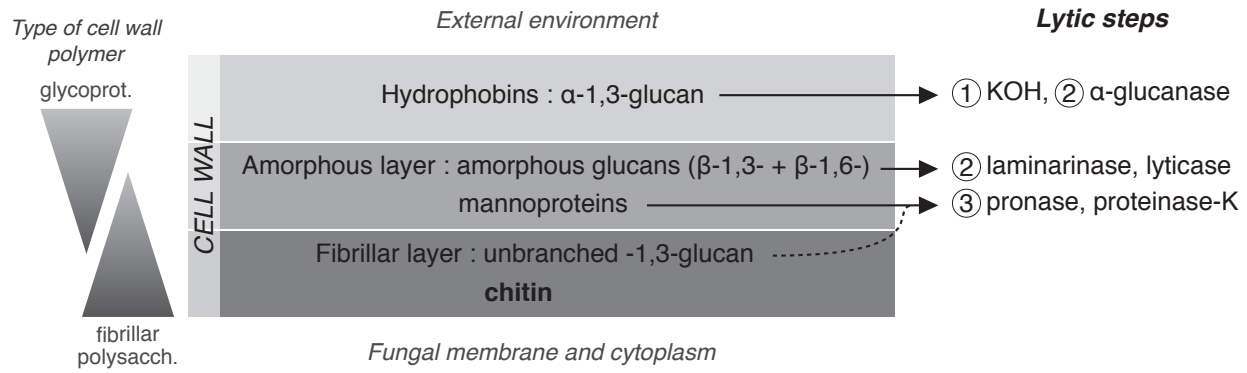

Figure 5.2 - Basic biochemical composition of the fungal cell wall with the applied experimental design. The first layer, made of hydrophobins (amorphous α-1,3-glucan) is digested with KOH 5% (1), followed by β-glucanase (2). The amorphous β-glucans (β-1,3 and β-1,6) of the second amorphous layer are digested by laminarinase and lyticase. Note that it is possible that unbranched fibrillar β-1,3-glucan from the fibrillar underlying layer may be digested as well. The glycoproteins of the third fibrillar layer are digested by pronase and proteinase-K (3). After these treatments, only chitin and probably unbranched β-1,3-glucan remain.

5.1.3.4 Sampling of natural deposits

Secondary CaCO3 accumulations have been sampled in calcic horizons from *calcic Cambisol humic calcaric* (IUSS Working Group WRB 2006) developed on scree slope deposits. The sampling site is a quarry near Villiers (Swiss Jura Mountains, 47°04'N, 6°59'E). Samples were taken both at the quarry front and at the interface between B and C calcic horizons. Samples of pedogenic carbonates exhibit two different macromorphologies: i) cotton ball-like NFC that accumulates in soil pores resulting from cryoclast packing and root voids and ii) white coatings on centimetric to decimetric cryoclasts. Both morphologies are found associated to particulate and amorphous soil organic matter. All samples were collected using tweezers and stored in sterilized 50 mL tubes at 4°C.

5.1.3.5 Scanning Electron Microscope observations of natural samples

Samples from natural deposits have been observed using two different modes of SEM: i) High vacuum SEM (HV-SEM) and iii) Low-temperature SEM (LTSEM). For HV-SEM purposes, natural samples have been fixed with osmium tetroxide vapors after a modified protocol from Pearson et al. (2004) described in Bindschedler et al. (2010), freeze-dried, placed on a SEM stub, and gold-coated (15 nm thick). HV-SEM observations have been performed using a Phillips ESEM-FEG XL30 Field Emission Gun Scanning Electron Microscope (FEG-SEM) as well as a Tescan Mira LMU, both operated at a distance of 10 mm and a voltage of 10 to 15 keV acceleration. LTSEM has been performed using a Gatan cryotransfer system coupled to a Phillips ESEM-FEG XL30. Natural samples were frozen into liquid nitrogen, transferred into a cryo preparation chamber in order to remove water by sublimation and then coated with platinum (10 nm thick). Samples were transferred into the observation chamber of the microscope and all observations were performed at low temperature (-180°C) and high vacuum.

Commercial extracts of chitin and β-1,3-glucan (both supplied by SigmaTM) have been used in order to test osmium tetroxide affinity for fibrillar fungal cell wall polymers (chitin and β-1,3-glucan). They have been treated in the same way as the natural samples following the procedure described above. The presence of osmium has been detected using EDS.

Diameters (widths) of both natural and synthetic nanofibres have been measured directly from SEM images using the measurement tool of Adobe© Photoshop©. Data for natural nanofibres from

randomly organized meshes are from Bindschedler et al. (2010). Data for natural nanofibres from organized meshes and nanofibres produced in the laboratory are average values of 470 and 410 measurements respectively (10 measures of individual nanofibres per SEM image).

5.1.4 Results

Each step of the treatment has led to noticeable differences in hyphal surficial texture, i.e. cell wall surfaces. The cell walls of the three species used in this study, *Armillaria mellea*, *Peziza sp.*, and *Boletus edulis*, have shown similar responses to the treatment (Fig. 5.3). Therefore, the results will be discussed together irregardless of the species. Untreated hyphae exhibit a granular surface (Fig. 5.4 A) and are often embedded in a fibrillar matrix of exopolysaccharidic substances (Fig. 5.4 B). After ultrasonication of hyphae in ultrapure water for 15 minutes, their surface displays a dramatic change with the appearance of a surficial fibro-reticular layer (Fig. 5.4 C). This layer disappears totally after KOH treatment, revealing a smooth surface at this step (Fig. 5.4 D). In few areas however, a close-up of the surface already shows some nanofibres that are totally trapped in an amorphous matrix (Fig. 5.4 E). Then, after the treatment with the glycolytic enzyme mix, the hypha surface shows some areas displaying meshes of nanofibres with a granular appearance, which are still trapped in an amorphous matrix (Fig. 5.4 F). Finally, after incubation in the proteolytic enzymes mix, all three species show a fibrous network composed of organic nanofibres (Figs 5.3, 5.5 & 5.6).

These nanofibres still have a granular appearance (Fig. 5.5 A), and some of them seem to be embedded in a thin film made of an amorphous matrix (Fig. 5.5 B). Nevertheless, their shape, as well as their organization, can be compared with their natural counterparts (Fig. 5.6). Meshes of natural nanofibres organized as tube-like structures (Fig. 5.6 A) are analogous to a transversal view of a hypha after the enzymatic treatment (Fig. 5.6 B). Nest-like structures (Fig. 5.6 C) can be compared to an anastomosis or hyphal branching scar, which after treatment exhibits a mesh of nanofibres organized as a nest (Fig. 5.6 D). Natural nanofibres are often observed structured as meshes showing a filament-like organization (Figs 5.6 E & 5.1). The hyphal structure is often preserved after enzymatic digestion. A hyphal shape composed

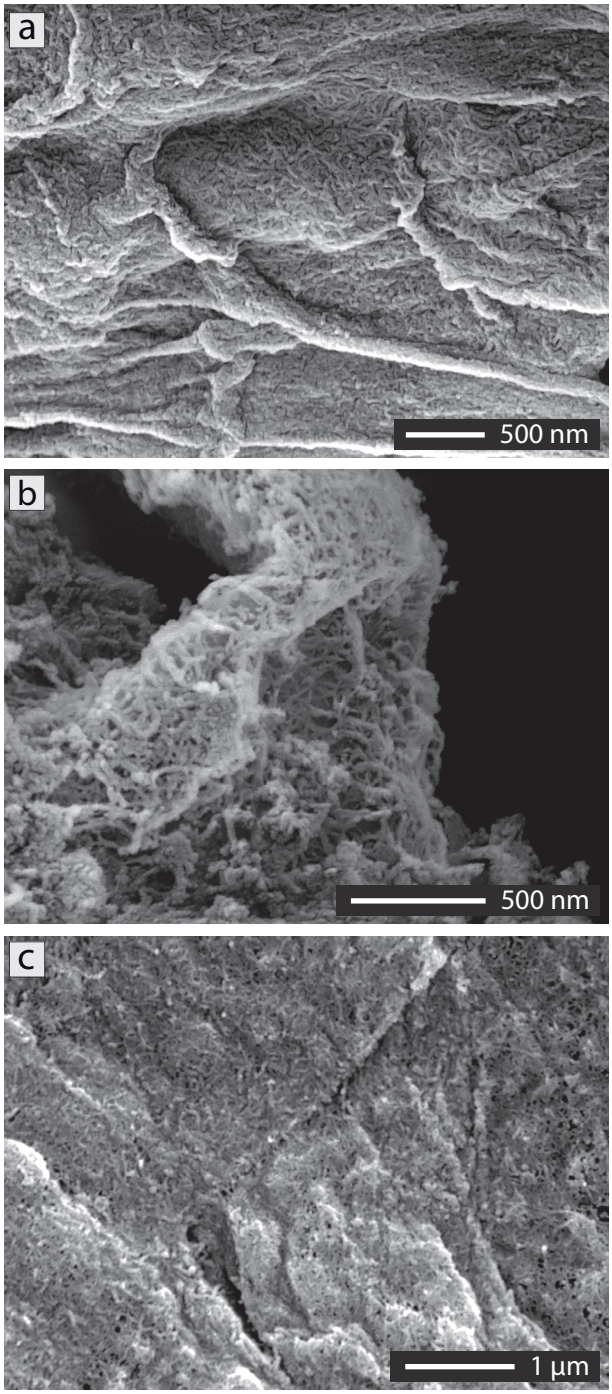

Figure 5.3 - SEM images of mycelia from the three selected species after ultrasonication, KOH and enzymatic treatments showing a similar final result: organic nanofibres organized into meshes preserving a hyphal filamentous structure. **(a)** *Peziza sp.*; **(b)** *Armillaria mellea*; **(c)** *Boletus edulis*.

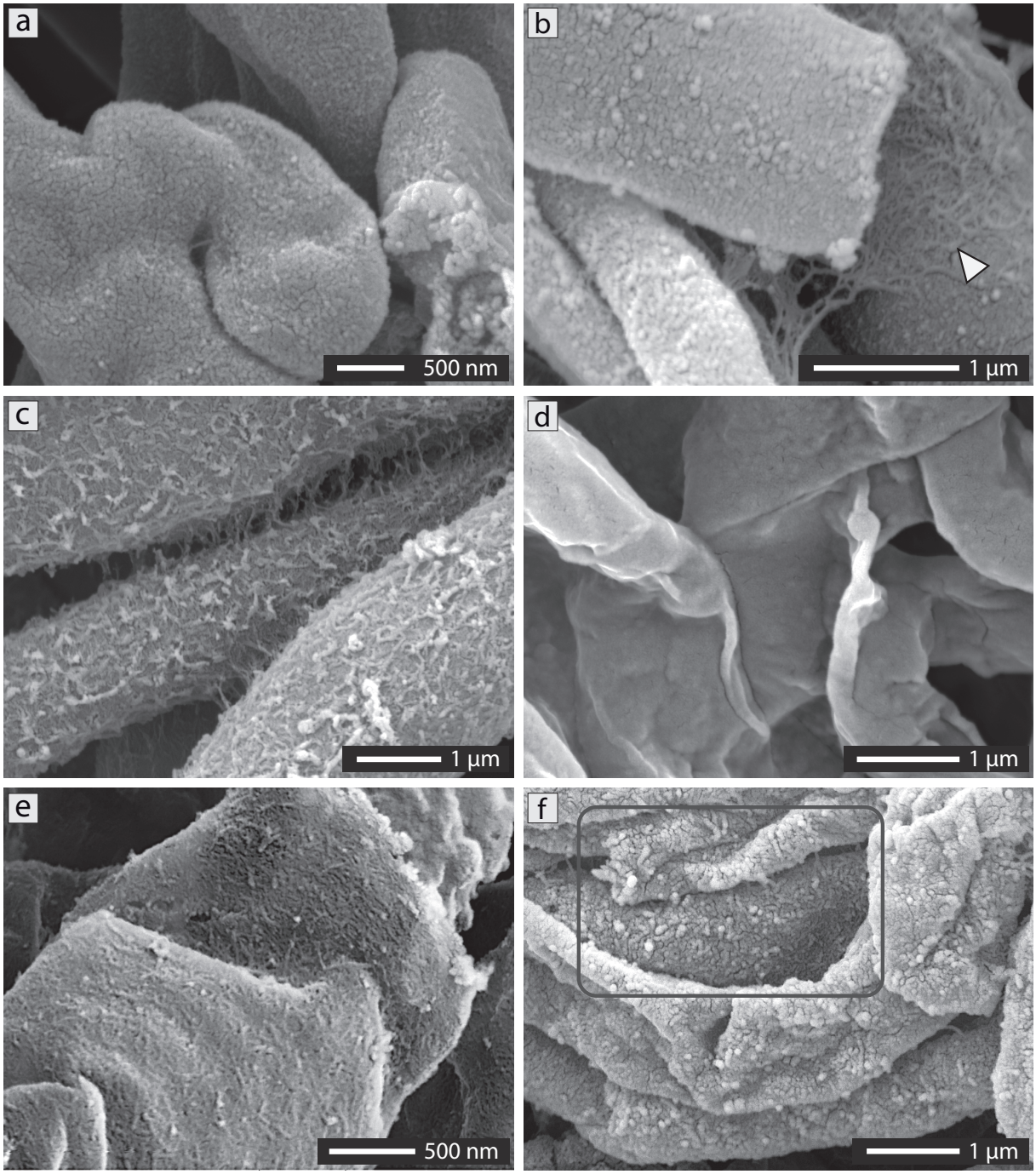

Figure 5.4 - SEM of *Boletus edulis* mycelium after each step of treatment. **(a)** Untreated hyphae showing a granular surface. **(b)** Close-up of a fibrillar mesh of exopolysaccharidic substances observed between hyphae before the treatment (white arrow). **(c)** Hyphae after ultrasonication in ultrapure water, showing a fibro-reticular layer that seems to bind hyphae together. **(d)** Hyphae after incubation in KOH 5% showing a smooth layer. **(e)** Close-up of the hyphal surface after incubation in KOH 5% revealing a mesh of nanofibres completely embedded into an amorphous matrix. **(f)** Hyphae after incubation in the glycolytic mix revealing a fibrillar layer in some areas that seems to be partially embedded in an amorphous matrix (see inside square).

of meshes of organic nanofibres is observed whatever the origin of the sample, be it natural or laboratory produced (Figs 5.3, 5.5 B & 5.6 F). The nanofibres obtained by this method show a mean diameter of 33 nm (+/- 9 nm). Mean nanofibre diameter in natural organized meshes is 56 nm (+/- 9 nm) and mean nanofibre diameter in natural randomly organized meshes is 78 nm (+/- 22 nm; Fig. 5.7). A statistical test (t-test) shows that all three categories are significantly different with a p-value < 0.001. Despite these differences in diameters between nanofibres from natural organized meshes (Figs 5.1 & 5.6 A-C-E) and those produced from fungi in vitro (Figs 5.3, 5.5 & 5.6 B-D-F), the similarity of organization between both features remains convincing.

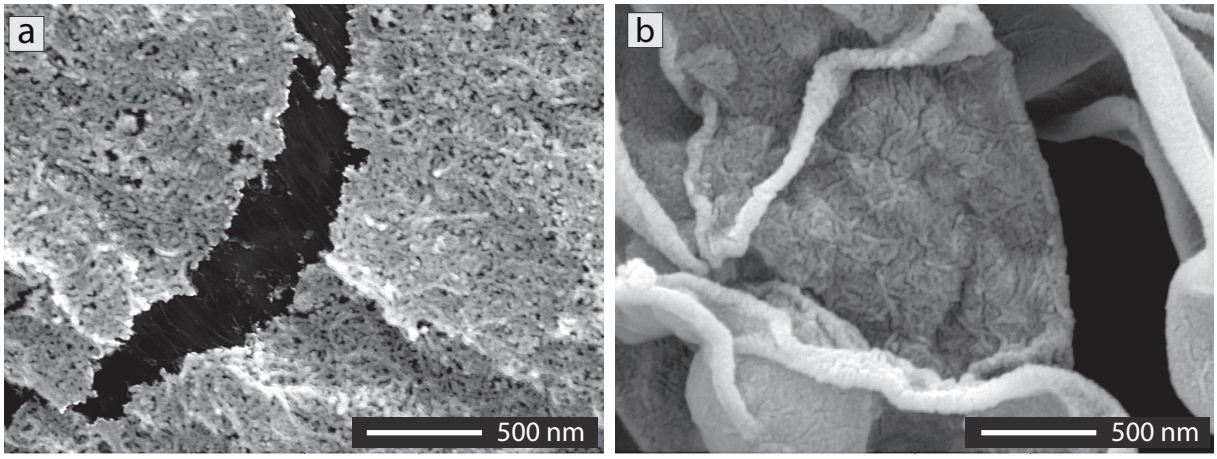

Figure 5.5 - SEM images of mycelia after sequential treatment with ultrasounds, KOH 5%, glycolytic, and proteolytic enzymatic mixes. **(a)** Close-up on cell wall nanofibres of *Boletus edulis* showing a slightly granular texture of nanofibres. Note the weak resistance of these organic nanofibres to the electron beam when observations are performed using a small spot size. **(b)** Meshes of cell wall nanofibres showing a hyphal structure (*Boletus edulis*).

Bindschedler et al. (2010) have demonstrated that organized meshes of nanofibres are stained by osmium revealing their organic nature. Osmium binds more efficiently organic matter rich in double bonds, such as lipids (Dykstra and Reuss 2003). Among fibrous polymers of fungal cell walls, chitin contains one double bond, whereas β-1,3-glucan does not contain any. In order to differentiate if both chitin and β-glucan react in the same way to osmium staining, commercial pure extracts of both compounds have been treated in the same way as natural samples. EDX analyses have shown that commercial chitin binds osmium more efficiently than commercial β-glucan (Fig. 5.8). As natural non-randomly organized meshes of nanofibres show an osmium signature, this suggests that they most probably contain a larger part of chitin compared to β-glucan regarding their osmium signature. In this study, the organic nanofibres produced in the laboratory are most likely composed of a mixture of chitin and β-1,3-glucan nanofibres. Lyticase and laminarinase, used to digest amorphous β-glucans might have digested a part of the fibrous β -1,3-glucan as well. Moreover, cross-linking between fibrillar polymers of the cell wall may lead to the removal of covalently-linked material in an unpredictable way (Farkaš 2003). As a result, the organic nanofibres produced in this study might be composed of a variable combination of chitin and β-1,3-glucan.

5.1.5 Discussion

The structure of the fungal cell wall has been extensively studied using various methods. As a consequence, many procedures exist in order to sequentially digest the successive cell wall “layers”, from harsh chemical treatment to mild enzymatic ones (Aronson and Preston 1960; Ruiz-Herrera 1992; Farkaš 2003). In this study, the enzymatic approach has been chosen as a mild treatment in order to duplicate as closely as possible the natural conditions. In natural environments, the fungal cell wall may be biochemically altered, either by extracellular enzymes of bacteria or other fungi, or by autolysis, the latter being a common trait of fungi (Ko and Lockwood 1970; Santamaria and Reyes 1988; Paul 2007; Sinsabaugh et al. 2008). All the enzymes selected in this study have their optimal activity at pH around 7, or higher, with the exception of laminarinase (an endo-β-glucanase), which has its optimum activity at pH 5 (according to Sigma™ information). Nevertheless, laminarinase showed high activity as its introduction in the enzymatic mix has led to a greater disappearance of the amorphous matrix that embeds nanofibres.

In soils, studies have demonstrated that chitinase and β-glucosidase (an enzyme closely related to β-glucanase) show their optimal activity at acidic pH (Sinsabaugh et al. 2008; Turner 2010). Laboratory

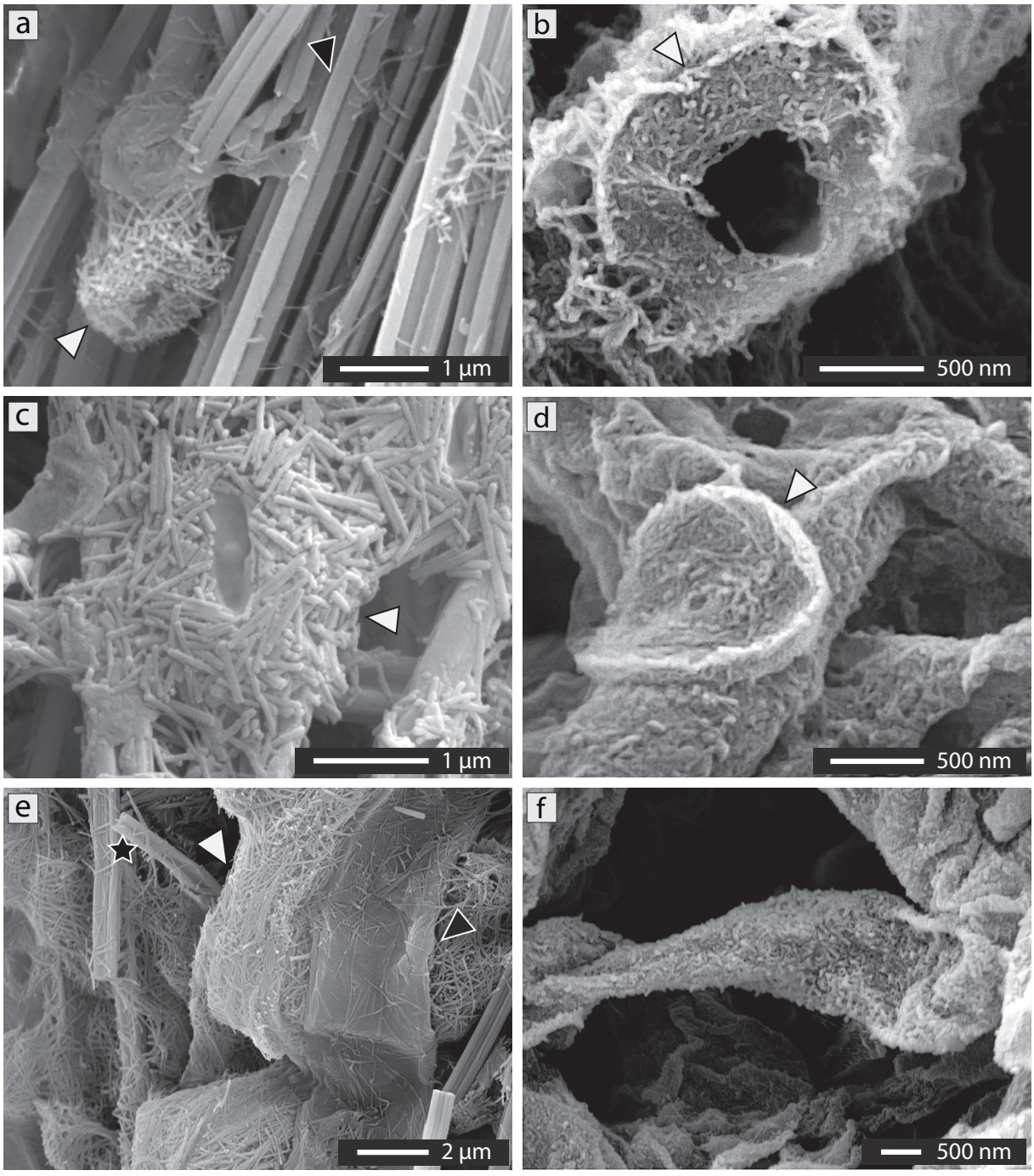

Figure 5.6 - SEM images of both natural and laboratory (post-treated) samples comparing similarities between observed structures. **(a)** Tubular structure made of organized nanofibres (white arrow) associated to NFC (black arrow). Soil sample of both OM and secondary $CaCO_3$ located at the interface between the organic and mineral soil horizons. **(b)** *Armillaria mellea* mycelium after treatment showing a transversal view of a hypha and the relict of the cell wall composed of a mesh of organic nanofibres (white arrow). **(c)** Nest-like structure made of nanofibres (white arrow). Sample of both coatings and cotton ball-like NFC developed on scree clasts. **(d)** *Peziza sp.* mycelium after treatment showing the relict of a septum (either from hyphal anastomosis or branching) composed of a mesh of organic nanofibres (white arrow). **(e)** Organized meshes of nanofibres displaying a filamentous structure (white arrow) observed together with a decaying fungal hypha showing the same filamentous shape (black arrow). Note the presence of associated NFC (black star). Sample containing decaying OM, rhizomorphs, and secondary $CaCO_3$ located at the interface between the organic and mineral soil horizons. **(f)** *Boletus edulis* mycelium after treatment showing meshes of cell wall nanofibres organized into a hyphal filamentous structure.

assays with fungal β-glucanase have shown an optimal activity at pH around 5 (Chesters and Bull 1963c; Rapp 1989). Consequently, it is likely that in calcareous environments, where pH is usually around 7.5-8, pH conditions will decrease or inhibit chitinase and/or β-glucanase activity, allowing the conservation of chitin and/or β-1,3-glucan nanofibres. In addition, chitin, as well as β-1,3-glucan and cellulose, are known as alkali-resistant polysaccharides (Farkaš 2003). The cross-linking between fibrillar polymers of the cell wall is considered as being the reason for this alkali-insolubility (Fontaine et al. 1997). From a purely theoretical point of view, chitin enzymatic hydrolysis is expected to be efficient in the soil environment. But surprisingly, chitin is known to be a recalcitrant polymer of soil organic matter and does not show a high decay rate (Guggenberger et al. 1999; Ehrlich 2010; Fan and Guo 2010). In contrast, D-glucose polymers (such as β-1,3-glucan nanofibres) are expected to be more readily recyclable polymers (Paul 2007; Coleman et al. 2004) and β-1,3-glucan are not known to accumulate in soils. Cross-linking between chitin and β-1,3-glucan in the cell wall could lead to an enhanced preservation of β-1,3-glucan as a result of low chitin decay rate. However, little information exists on the topic and the fate of β-glucans in pedogenic environments remains enigmatic at present.

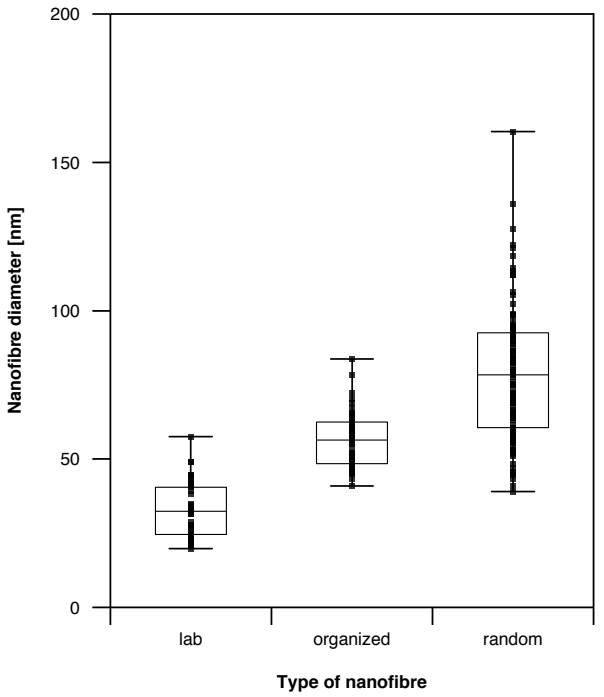

Figure 5.7 - Box plot showing the distribution of diameters with median, standard deviation, maximal and minimal values of laboratory-produced nanofibres (lab; n=410), nanofibres from natural organized nanofibre meshes (organized; n=470) and nanofibres from natural randomly organized meshes (random; n=106 from Bindschedler et al. 2010). Note that all the three categories are significantly different with a *p*-value < 0.001.

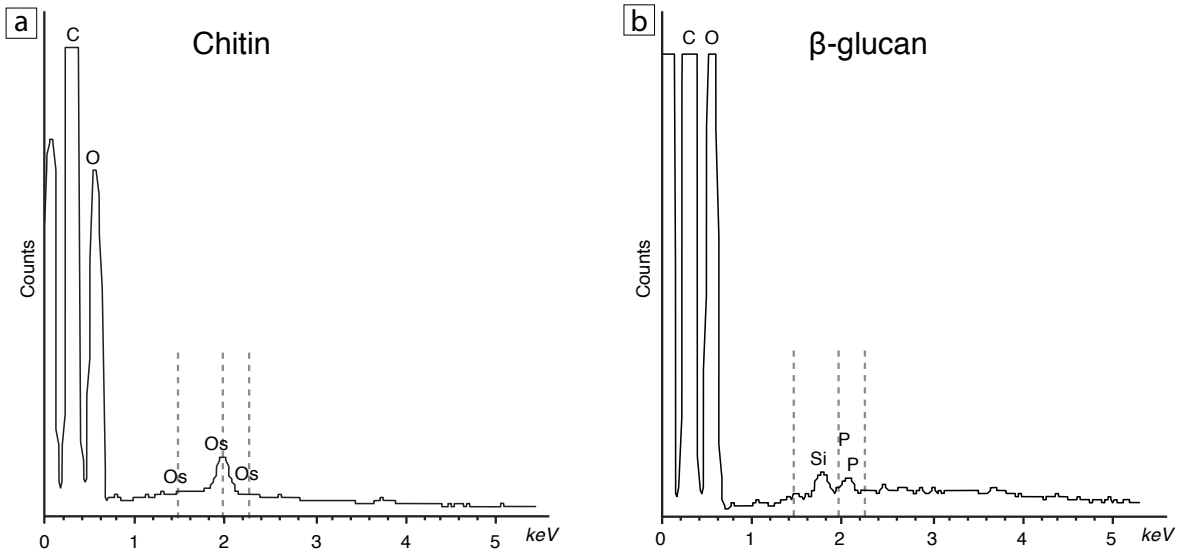

Figure 5.8 - EDS spectra of commercial extracts of chitin **(a)** and β-glucan **(b)**. Dotted lines correspond to osmium peaks (Ma peak at 1.91 keV and two associated peaks). **(a)** Chitin EDS spectrum shows the presence of carbon (C), oxygen (O) and osmium (Os). **(b)** β-glucan EDS spectrum shows the presence of carbon (C), oxygen (O) but no osmium. Note the presence of silicon (Si) and phosphorous (P) due to the preparaation procedure for electron microscopy using tetramethylsilane (TMS) and phosphate buffer solutions (PBS).

Analyses of commercial extracts of chitin and β-glucans have shown that only chitin has the ability to bind osmium (Fig. 5.8). This suggests that natural organized meshes of nanofibres are composed mainly of chitin and of lower amounts of β-1,3-glucan (Bindschedler et al. 2010). When chitin and/or β-1,3-glucan are released after the incomplete decay of the fungal cell wall, they may eventually be preserved due to particular prevailing physicochemical conditions in calcareous environments. Subsequently, chitin (or β-1,3-glucan) nanofibres and/or associated acidic proteins can adsorb calcium on their surfaces when exposed to solutions enriched in calcium, and hence, act as a calcite nucleation enhancer (Wainwright 1963; Furlan et al. 1996; Ehrlich 2010). This process is documented for chitin due to its ubiquity in Arthropods cuticles (Ehrlich 2010). However, β-1,3-glucan could display the same ability, as this process is documented for cellulose (β-1,4-glucan) fibres (Dalas et al. 2000; Cailleau et al. 2009a), which may be considered as structural analogues of β-1,3-glucan.

Nanofibres obtained in this study show similar characteristics to those observed in natural samples, particularly regarding their arrangement as organized meshes showing tubular- and filament-like arrangements (Fig. 5.6). The difference observed in diameter ranges between laboratory and natural nanofibres may be explained by the fact that chitin has the capacity to bind cations. Cations may be directly adsorbed on sites derived from de-acetylation of amino groups or through associated acidic proteins (Wainwright 1963; Furlan et al. 1996; Ehrlich 2010). This adsorption ability might explain why natural nanofibres are smoother (Fig. 5.6) and wider (Fig. 5.8) than those obtained under laboratory conditions. Therefore, on the basis of the arguments made above, natural nanofibres might often be coated either with bounded-Ca^{2+} (ionic bound), Ca^{2+}-bounded macromolecules, or even $CaCO_3$, all three slightly increasing their diameter. Benzerara et al. (2003) have observed thin amorphous layers around nanofibres and have interpreted them as precursor phases of calcite crystallization. Likewise, Cailleau et al. (2009a) suggest a similar process with cellulose nanofibres in experimental procedures. As a result, an increase of organic nanofibre diameter by adsorption of organic or mineral matter is possible.

This study demonstrates that the fungal cell wall may be a source of chitin nanofibres in laboratory conditions. In a natural environment, analogous processes can occur that may further lead to the nucleation of calcite on chitin nanofibres. It must be pointed out that the same conclusion can be drawn for cellulose nanofibres from plant cell walls as suggested by Cailleau et al. (2009a) with synthetic cellulose. Plant cell walls are well known to possess a fibrillar layer made of a dense mesh of fibrous cellulose and hemicellulose (Paul 2007), whereas Fungi possess a cell wall with a layer of fibrous chitin and β-1,3-glucan (Ruiz-Herrera 1992). Interestingly, cellulose and chitin are known as the two most abundant natural polymers on Earth (Furlan et al. 1996; Ehrlich 2010) and both exhibit poor complete degradation in natural environments. In order to complete their full mineralization, the action of a consortium of organisms together with particular physicochemical conditions is often necessary (Paul 2007). Their potential preservation in the environment under certain conditions makes them available to further participate in other soil solution mediated processes, such as acting as template for the nucleation of secondary minerals. Indeed, both cellulose and chitin are known from several studies to be efficient templates for calcite nucleation (Manoli et al. 1997; Dalas et al. 2000; Giraud-Guille et al. 2004; Cromme et al. 2007; Cailleau et al. 2009a; Ehrlich 2010). The fact that organic matter can enhance or govern crystallization is a well-known feature of biomineralization theories (Simkiss and Wilbur 1989; Berman et al. 1993; Dupraz et al. 2009). Finally, other authors have already mentioned the possibility that nanofibres could be the remains of cell walls, either fungal or plant. Klappa (1979) mentions “hyphantic threads” as being the result of “partially decayed organic filaments”. Therefore, the involvement of an organic template in the genesis of calcitic nanofibres seems realistic for all the reasons mentioned above. Finally, this hypothesis has the advantage of explaining in a logical way the existence of tube-like organized

structures in natural samples (Fig. 5.6 A). Moreover, in some cases, cross-linking between chitin and β-1,3-glucan might lead to an enhanced preservation of these structures.

Alternatively, physicochemical processes have been proposed as an origin for calcitic nanofibres (Jones and Ng 1988; Jones and Khale 1993; Borsato et al. 2000). This hypothesis seems unlikely mainly because of the peculiar thread-like habitus of nanofibres. Calcitic nanofibres are believed to be monocrystalline in nature (Cailleau et al. 2009a) with their growth axis parallel to the calcite c-axis (Borsato et al. 2000). Moreover, they are low-Mg calcite in nature (Loisy et al. 1999; Borsato et al. 2000). The habitus of a physicochemically precipitated calcite crystal under no constraint (either by ion poisoning or by the presence of adsorbed organic matter) should have some rhombohedral patterns if following crystallographic rules (Buckley 1951), which is evidently not the case with nanofibres. Moreover, growth constraint by ion poisoning (e.g. Mg^{2+}) is not consistent with their low-Mg calcitic nature. Thus, a physicochemical process alone is not able to explain why such a divergence is observed. In addition, it is inconsistent with the existence of the non-random organized meshes (Fig. 5.6 A-C-E). The presence of an organic template directing the growth of the nanofibre seems more suitable to explain the peculiar habitus of nanofibres. Indeed, organic matter is known to induce great variation from the theoretical crystal habitus (Buckley 1951; Simkiss and Wilbur 1989; Mann 2000). Moreover, it elegantly explains the non-random organization patterns of nanofibres.

Another hypothesis for the origin of nanofibres involves the biomineralization of rod-shaped nano-sized bacteria (Phillips and Self 1987; Verrecchia and Verrecchia 1994; Ould Mohamed and Bruand 1994; Loisy et al. 1999). Nevertheless, this hypothesis seems very unlikely. A controversy exists regarding the putative existence of nanobacteria (Folk 1993; Folk and Lynch 2001). Maniloff (1997) has determined that the lowest diameter for a cell to be viable must be 0.005 μm^3. According to this assumption, Kieft (2000) therefore states that nanobacteria defined by Folk (1993) would have no space for a cytoplasm. Even if the lower size limit for a living cell has still to be defined with precision, it is quite unlikely that they would have a diameter lower than 0.2 µm. This theoretical size limitation arises from solution chemistry. Indeed, solute concentration within cells is often at the level of micromoles (µM) and consequently a very small biovolume would be too tiny to allow the presence of at least one molecule (Kieft, 2000). Therefore, natural nanofibres exhibit dimensions below the reasonable limit for a viable cell. Having an average diameter of 80 nm and an average length of 500 nm, the total bio-volume is 0.0025 μm^3, which is two-fold smaller than the limit of 0.005 μm^3 defined by Maniloff (1997).

The origin of nanofibres has remained enigmatic for so long mainly because of the limits of methodology. Indeed, the lack of routine methods to accurately analyze organo-mineral structures at the submicrometric scale still hinders a clear and unquestionable answer regarding their origin. Nevertheless, regarding the three main theories currently discussed, i.e. physicochemical processes, biomineralization of rod-shaped nano-sized bacteria and nucleation mediated by organic templates, the last one seems to be the most realistic considering our present knowledge of the nature of calcitic nanofibres and results discussed in this study. Indeed, the sequential digestion of the fungal cell wall using enzymes has shown thrilling converging morphologies between laboratory and natural meshes of nanofibres, which are in agreement with biochemical constraints of organic matter breakdown in natural environments.

5.1.6 Conclusions

A fungal origin for calcitic nanofibres, recurrently associated to NFC, has already been put forth by Bindschedler et al. (2010), based on observations of natural samples. This study demonstrates that

the fungal cell wall can be a source of organic nanofibres. They are probably made of chitin and, to a lesser extent, of β-1,3-glucan. The focus has been put purposely on chitin, as little information exists on the dynamics of β -glucans in the environment in comparison to chitin. However, β-1,3-glucan might similarly constitute a significant part of the organic nanofibre pool of pedogenic environments. Furthermore, interesting similarities have been observed between "synthesized" nanofibres and their natural counterparts, indicating that the suggested genetic link between both features clearly exists. Regarding the eventual mineralization of these organic nanofibres in the natural environment, it may be considered as the result of an organomineralization process in the sense defined by Perry et al. (2007) and Dupraz et al. (2009), i.e. all mineral precipitation on an organic matrix that is not genetically controlled. Moreover, it corresponds to a biologically-influenced mineralization process (Dupraz et al. 2009), defined as the passive mineralization of organic matter. Physicochemical parameters of the environment, more than microbial activities, are responsible for creating the conditions leading to $CaCO_3$ nucleation of organic nanofibres. As a result, the process described for the genesis of calcitic nanofibres implies the presence of organic matter for the nucleation of $CaCO_3$, but living organisms are not required. These results emphasize the role of natural polymers as templates for the precipitation of minerals. In this study, the focus has been purposefully put on a fungal origin for nanofibres, essentially those associated to NFC. However, it does not exclude other sources for organic nanofibres. Indeed, other natural polymers display a nanofibrous shape, e.g. cellulose, which may likewise act as a template for $CaCO_3$ nucleation (Cailleau et al. 2009a). As chitin and cellulose are considered to be the two most widespread natural polymers on Earth (Furlan et al. 1996; Ehrlich 2010), this process may have a great, as yet underestimated, influence on both Ca and C biogeochemical cycles.

5.2 Fungal strands and calcium – implication in NFC and nanofibres genesis

5.2.1 Introduction

The implication of fungal strands in NFC genesis has already been suggested by several authors (Callot et al. 1985b; Phillips and Self 1987; Ould Mohamed and Bruand 1994; Verrecchia and Verrechia 1994). Moreover, as already mentioned in this manuscript, natural fungal strands are recurrent features observed in association with the different macroscopic facies of NFC and nanofibres. As emphasized in § 4.1 and 4.2, fungal strands and NFC bundles display similar shapes and organization, suggesting a genetic link between both features. In addition, nanofibres are often observed lying on the surface of NFC bundles. Phillips and Self (1987), as well as Ould Mohamed and Bruand (1994), already noticed this close relationship. They have interpreted that these nanofibres were calcified rod-shaped bacteria, previously involved in the decay of the fungal sheath, leading to the release of NFC from the fungal strands. In this study, an alternative hypothesis is proposed. Nanofibres are the remnants of the decay of a fungal sheath and are composed of resistant cell wall polymers, i.e. chitin nanofibres (see § 4.1; 4.2 & 5.1). Consequently, the presence of nanofibres at the surface of NFC bundles indicates that fungal cell walls were once associated to the NFC bundles, emphasizing the implication of fungal strands in NFC genesis (see Figure 4.8 in § 4.2). Moreover, fungal strands are known as impermeable translocating structures (Schütte 1956; Cairney 1992; Lindhal and Olsson 2004). In highly calcareous environments, it is expected that solutions that are transferred within fungal strands are likely to be calcium-rich and possibly saturated in respect to calcite. It is well known that calcium (Ca^{2+}) is an important element for fungal growth (Jackson and Heath 1993). However it is cytotoxic in high concentrations (Gadd 1993). Fungal strands are expected to react in a different way than single hyphae due to their lower permeability. It may be assumed that fungal strands react to high concentrations of metals such as Ca^{2+}, likely by transporting Ca^{2+} away (Wallander et al. 2002) or by sequestrating Ca^{2+} in preferential locations of the fungal strand (Rizzo et al. 1992; Cole et al. 1998).

Based on these facts, a TEM approach has been chosen as a mean to observe the inner part of fungal strands in order to test the hypothesis of NFC nucleation inside fungal strands. These observations have been performed on fungal strands collected in the field. They have been compared to fungal strands of *Peziza sp.* grown in the laboratory.

In order to evaluate how fungal strands react to high Ca^{2+} concentrations and to supersaturated solutions regarding calcite, a translocation experiment with *Peziza sp.* fungal strands has been set up. *Peziza sp.* has been grown in presence of high concentrations of Ca^{2+} and carbon dioxide (CO_2). The aim of this approach was to cultivate fungal strands in a medium supersaturated regarding calcite and to compare them with fungal strands from natural samples.

5.2.2 Methodology

Fungal strands, either natural or from the laboratory, and mycorrhized roots have been prepared for TEM observations following the procedure described for natural fungal strands in § 4.2. *Peziza sp.* has been chosen as a model organism for this approach mainly because it is an easily cultivable strain that produces a reasonable amount of mycelial strands in controlled conditions (Fig. 5.9) in an acceptable short period of time. *Peziza sp.* has been grown in closed containers in oligotrophic conditions as a way to promote the formation of fungal strands. Wood pieces were provided as carbon source and water was added at the bottom of the containers in order to maintain a reasonable humidity level as well as to provide mineral nutrients in solution. One month before the experiment, 0.1% malt-agar plugs have been provided to a distal part of the fungal strand network (i.e. at strand apex),

as a mean to enhance translocation. In order to reproduce the physicochemical conditions of natural solutions, one container has been Ca^{2+} enriched (up to 60 mg/L of Ca^{2+}) and another one has been similarly Ca^{2+} enriched, as well as CO_2 enriched. One container has been left untreated (control), using tap water as a water source (about 10 mg/L of Ca^{2+}). Ca^{2+} has been added using a Ca^{2+}-rich solution (500 mg/L) resulting from the mixture of different Ca^{2+}-salts ($CaSO_4.2H_2O$ 214.8 mg/L ; $CaCO_3$ 124.8 mg/L; $Ca_3P_2O_8$ 515.9 mg/L & $CaCl_2.2H_2O$ 733.6 mg/L). Ca^{2+} concentration has been adjusted to the values measured in natural samples (§ 4.2). Ca^{2+} has been provided at several time intervals: i) at the beginning of the experiment (Ca1: 60 mg/L Ca^{2+}), ii) after 3 weeks (Ca2: 15 mg/L Ca^{2+}), iii) after 3 months (Ca3: 30 mg/L Ca^{2+}), and iv) after 5 months (Ca4: 30 mg/L Ca^{2+}). CO_2 has been added in a second step, after 3 months of experiment (CO_2). After CO_2 addition the container has been sealed in order to allow CO_2 dissolution in the growth solution. Then, one week later, a small aperture has been created at the top of the container, in order to allow the gradual CO_2 degassing (Fig. 5.10). Fungal strands and growth solution of fungi have been sampled before the experiment and after each treatment. Fungal strands have been fixed following the procedure described for natural fungal strands in § 4.2. Physicochemical characterization of the growth solutions of *Peziza sp.* has been conducted as described in § 3.2 for natural soil solutions.

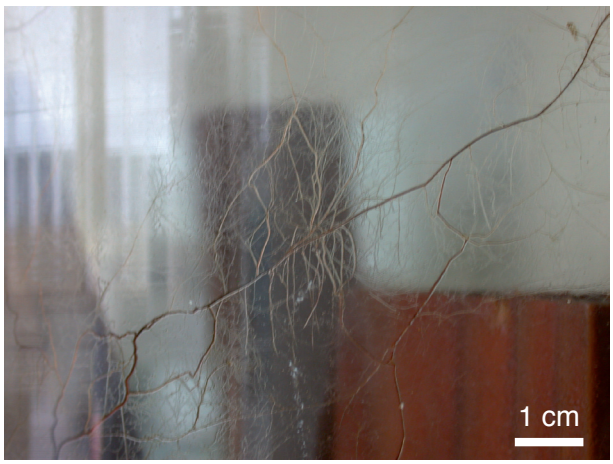

Figure 5.9 – Fungal strands of *Peziza sp.* grown *in vitro*.

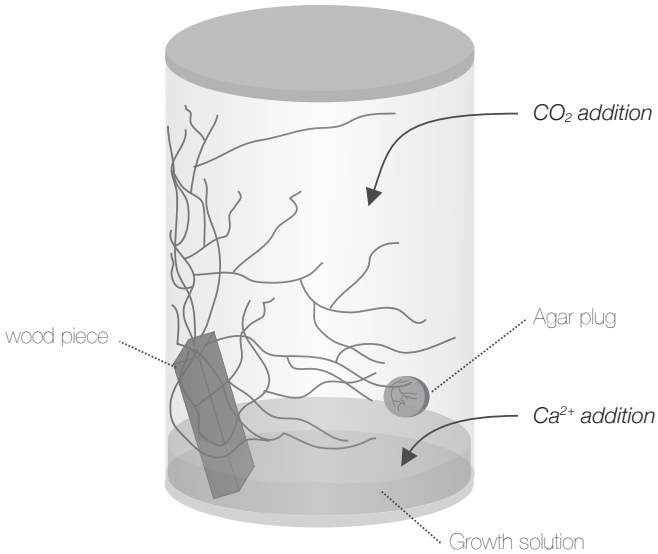

t0	Values before treatment
Ca1	Values after first Ca addition just after t0
Ca2	Values after second Ca addition, three weeks after t0
t3	Values three months after t0
Ca3	Values after third Ca addition just after t3 and three month after t0
CO_2	Values after CO_2 addition one week after Ca3 and three month after t0
t5	Values five months after t0
Ca4	Values after fourth Ca addition just after t5 and five month after t0
Fin	Values at the end of experiment, three days after Ca4 Ca addition and five months after t0
NT	Values for untreated/control container

Figure 5.10 - Experimental design of the translocation experiment. Ca^{2+} is provided by addition of a Ca^{2+}-rich solution to the growth solution. CO_2 is provided by direct addition to the container atmosphere. CO_2 is first allowed to dissolve within the growth solution in a saturated CO_2 atmosphere. One week later, a thin aperture is made at the top of the container in order to allow CO_2 degassing.

5.2.3 Results

5.2.3.1 Observation of natural fungal strands

Observations of fungal strands sections from natural samples have frequently revealed the presence of small inclusions inside hyphae (Fig. 5.11). EDS analyses have shown that they were enriched in Ca^{2+} (Fig. 5.12 a). However, these inclusions do not show any microdiffraction pattern when subjected to microanalysis under the TEM, hence they do not have an organized crystalline nature. EDS analyses performed on cell walls have shown similar Ca^{2+} enrichments within cell walls of hyphae from natural samples (Fig. 5.12 a). To the contrary, untreated laboratory samples have shown neither intrahyphal inclusions nor high concentrations of Ca^{2+} within their cell walls (Fig. 5.12 b).

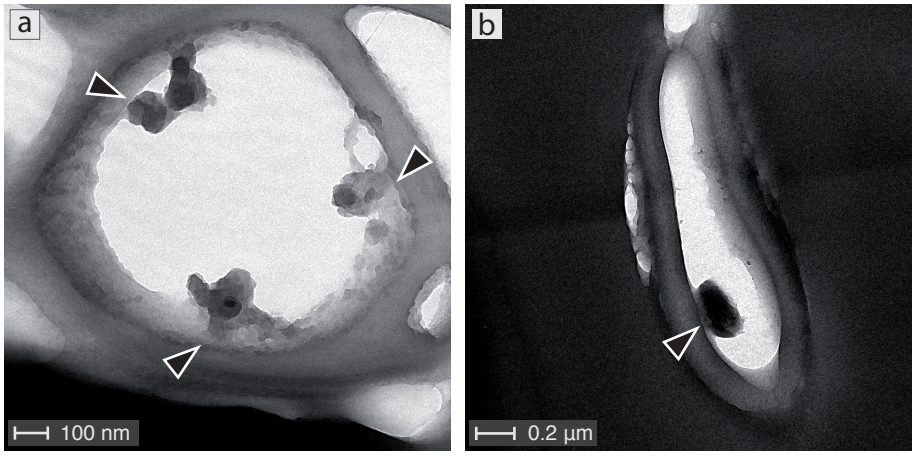

Figure 5.11 - TEM images of fungal strands collected in an inter-grain pore of a C horizon containing "cotton ball-like" macroscopic facies, Villiers (CH01) site. (a-b) inclusions within hyphae are commonly observed.

5.2.3.2 Translocation experiment

After 5 months of treatment, some intrahyphal inclusions have been observed in *Peziza sp.* strands, but no significant differences have been observed between both treatments, i.e. Ca^{2+} and Ca^{2+} + CO_2-treatments. Inclusions have been more often observed after 5 months of treatment, however they are already present after 3 months. The inclusions were very rarely enriched in Ca^{2+}, and chlorine (Cl^-) was regularly detected instead (Fig. 5.13 a). When Ca^{2+} was detected, the EDS peak was small, indicating that Ca^{2+} is present in rather low amount; moreover, Cl^- was also present (Fig. 5.13 b). Cell walls do not show any enrichment, neither in Ca^{2+}, nor in Cl^- (Fig. 5.13 c). Despite the fact that no clear Ca^{2+} enrichment has been noticed in *Peziza sp.* fungal strand, Ca^{2+} added to their growth solution has shown a decreasing pattern following each Ca^{2+} addition (Fig. 5.14 a). Moreover, the decrease of Ca^{2+} concentration seems to happen rather fast. Indeed "Fin" corresponds to Ca^{2+} in solution three days after "Ca4" addition and a decrease between the two points is already noticeable. (Fig. 5.14 a). Alkalinity has slightly decreased in the Ca^{2+}-enriched treatment, whereas it has drastically increased after CO_2 addition in the Ca^{2+} + CO_2-enriched treatment (Fig. 5.14 b). pH has been stable in the Ca^{2+} treatment (Fig. 5.14 c). In the Ca^{2+} + CO_2-treatment, pH was slightly lower at the beginning, drastically decreased after CO_2 addition, but has gradually increased after CO_2 was allowed to degas (Fig. 5.14 c). Calcite saturation index ($SI_{calcite}$) has reached sub-zero levels only twice; thus solutions were undersaturated in respect to calcite all along the experiment. The Ca^{2+} + CO_2-treatment resulted in a sharp decrease of the $SI_{calcite}$ after CO_2 addition. This decrease was then followed by an increase of the $SI_{calcite}$ resulting from the subsequent CO_2 re-equilibration due

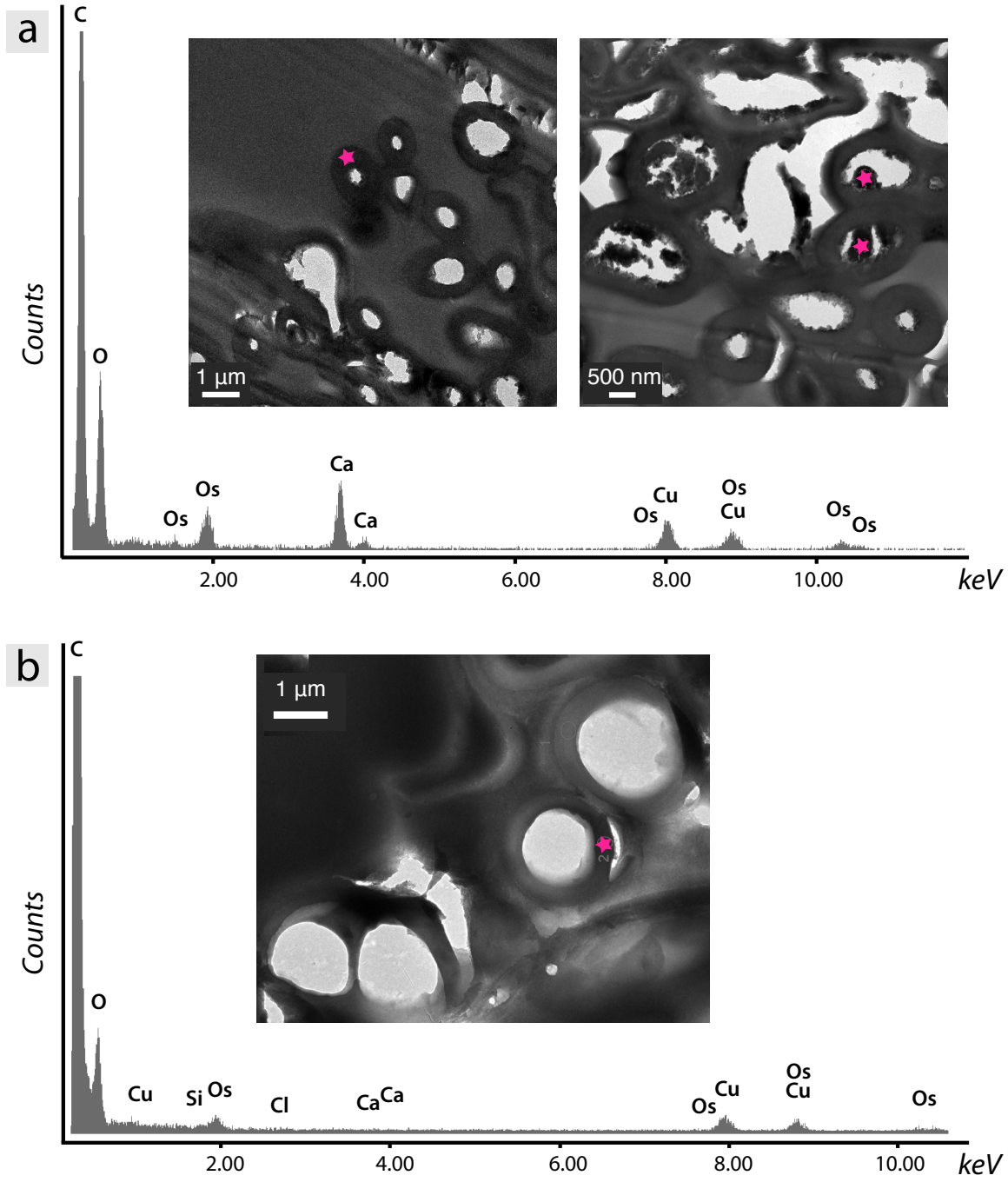

Figure 5.12 - TEM images of fungal strands and associated EDS spectra. Analysed zones are indicated (★). Cu is from the TEM grid. (a) Fungal strands sampled at the interface between the B and C horizons, showing the presence of Ca in both their cell wall (left hand side) and in intrahyphal inclusions (right hand side). Os peak indicates that inclusions also contain OM. (b) Fungal strands from Peziza sp. grown in vitro, do not show any inclusion or Ca accumulation within their cell walls.

to degassing. Moreover, $SI_{calcite}$ has increased after each Ca^{2+} addition and decreased afterwards. Then, in the Ca^{2+} + CO_2-treatment, the $SI_{calcite}$ has gradually increased up to -0.03 at the end of the experiment (Fig. 5.14 d).

5.2.4 Discussion

In natural samples of fungal strands, a much higher concentration of Ca^{2+} is systematically observed in the cell wall of the fungal hyphae, as well as in small inclusions observed in the hyphae (Fig. 5.12). Ca^{2+} accumulation in the cell wall or in intracellular inclusions is not surprising, as it is known that fungi must strictly control their Ca^{2+} content in order to grow properly (Jackson and Heath

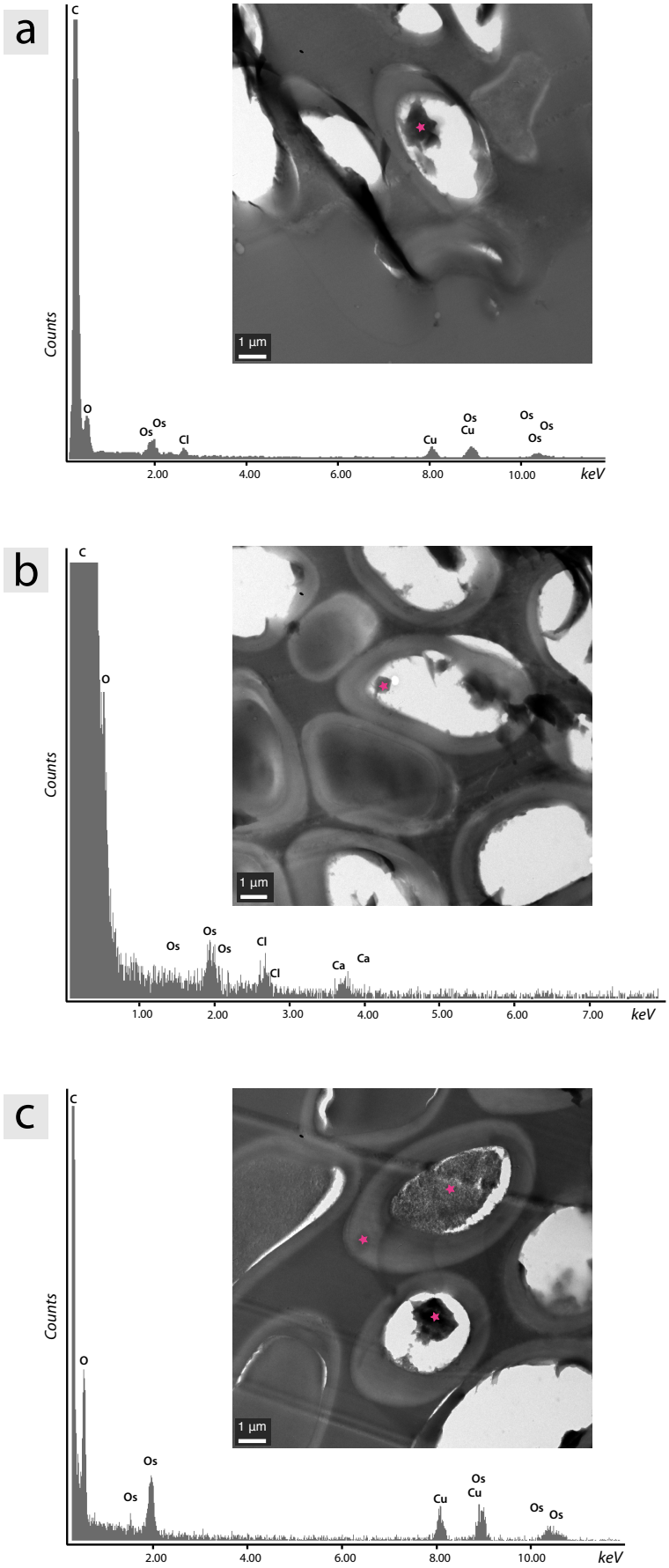

Figure 5.13 - TEM images and associated EDS spectra of *Peziza sp*. fungal strands from the translocation experiment. Analysed zones are indicated (★). Cu is from the TEM grid. **(A)** After 3 months inclusions are already observed, EDS analyses show that Cl, C, O and Os are present. Os indicates that inclusions also contain OM. **(B)** After 5 months, a few inclusions show Ca enrichment and Cl is also present. **(C)** After 5 months, inclusions, inner compartment of hyphae, and cell walls do not show any enrichment as represented by the presence of only O, C and Os peaks.

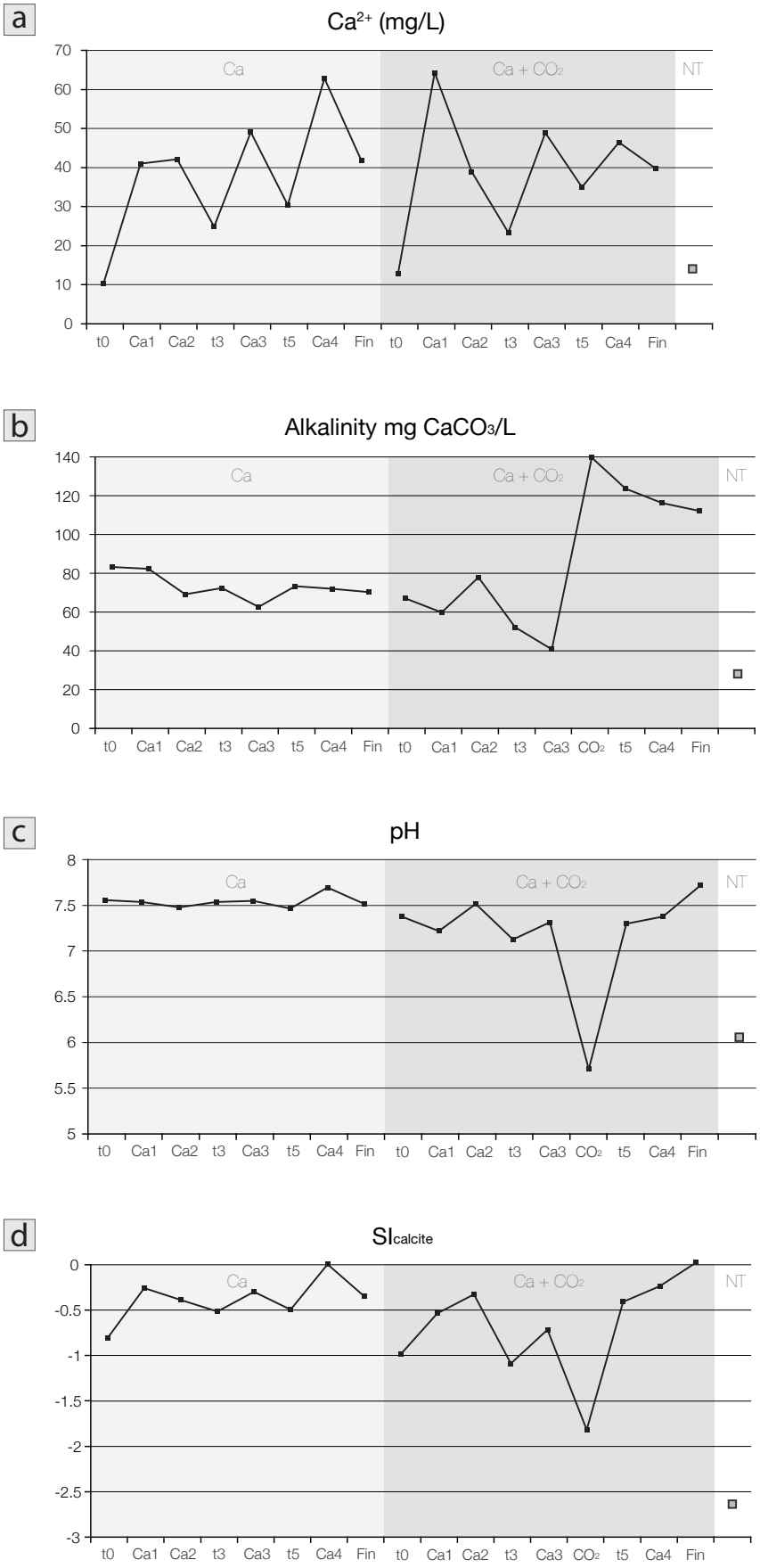

Figure 5.14 - Curves showing the evolution of selected physicochemical parameters in both treatments (Ca and Ca+CO_2) of the translocation experiment. *t0*: before treatment; *Ca1*: after Ca^{2+} addition at t0; *Ca2*: after Ca^{2+} addition 3 weeks after t0; *t3*: growth solution 3 months after t0; *Ca3*: after Ca^{2+} addition 3 months after t0; *t5*: growth solution 5 months after t0; *Ca4*: after Ca^{2+} addition 5 months after t0; *Fin*: end of experiment, 3 days after Ca4 addition. NT represents the values for the control container. **(A)** Ca^{2+} concentration (mg/L). **(B)** Alkalinity (mg $CaCO_3$/L). **(C)** pH. **(D)** Calcite saturation index ($SI_{calcite}$), $SI_{calcite}$ for the CO_2 point has been calculated with Ca^{2+} and Mg^{2+} values at Ca3.

1993). Mean concentration of free Ca^{2+} in the cytoplasm ranges from 100 to 350 nM. Soil solution analyses have shown concentration up to 1.5 mM. This is one order of magnitude higher than intracellular concentration and must therefore represent a source of osmotic stress for fungi in Ca^{2+}-rich environments. The observations of both, inclusions and cell walls enriched with Ca^{2+} are not surprising and have been interpreted as a sequestration of Ca^{2+} in excess. Hence, it demonstrates clearly that the cell wall of fungi is active in detoxifying metals as already suggested by Gadd (1993). The inclusions are more enigmatic and could be either vacuoles or Ca^{2+}-bounded proteic aggregates. However, a question remains: to what and how is this Ca^{2+} bound and/or sequestrated? Eventually, it may be hypothesized that these inclusions might turn into crystalline structures, leading to the formation of NFC.

However, the same pattern was not observed in the translocation experiment. Surprisingly, *Peziza sp.* fungal strands did not show any significant accumulation of Ca^{2+} in both their cell walls and intrahyphal inclusions (Fig. 5.13). Moreover, while inclusions are very common in natural fungal strands, they are far less common in the treated samples. Yet, a few intrahyphal inclusions were observed and sometimes enriched in Cl^- (Fig. 5.13 a-b). As Cl^- has been added in the solution via $CaCl_2$ it might be that Cl^- was preferentially fixed compared to Ca. Cell walls did not show any detectable enrichment (Fig. 5.13 c). This result is even more surprising as the Ca^{2+} that has been added to the growth environment of *Peziza sp.* has displayed decreasing patterns (Fig. 5.14 a). This observation supports the fact that it might have been translocated elsewhere and thus most likely that it has transited into the fungal network. It should also be pointed out that the differences observed in the solutions of both treatments (Ca^{2+} and Ca^{2+}-CO_2) were not reflected in strand microstructures.

These unexpected results might be the consequence of several aspects. First, regarding the fact that fungal strands are slow growing structures, it is possible that the duration of the experiment was not long enough. A longer Ca^{2+}-exposure should be required in order to detect accumulations. Alternatively, the experimental design could be improved. For instance, Ca^{2+} could be provided in a different way. Indeed, Cl^- accumulations (most likely from $CaCl_2$) within intrahypal inclusions suggest that a competition regarding detoxification has occurred. Then again, the fungal strain used for the experiment (*Peziza sp.*) might be a crucial choice and the one selected for this experiment might have reacted differently to Ca^{2+} than fungi from natural samples of this study. For instance, Ca^{2+} might have been transported and deposited as Ca-oxalates in distal parts of the strand (Wallander et al. 2002), rather than accumulated in the cell wall. The fact that the growth solution was undersaturated regarding calcite might also be an explanation for the non-accumulation of Ca^{2+} in a similar pattern as natural fungal strands. Conclusively, as emphasized by Cairney (1992), fungal strands physiology is complex and many other reasons might arise as an explanation for the non-accumulation of Ca^{2+} as expected.

5.2.5 Conclusions

The observation of detectable amount of Ca^{2+} in both intrahyphal inclusions and cells walls of hyphae from natural fungal strand confirms the possible sequestration of Ca^{2+} in fungal structures in Ca-rich environments. It is hypothesized that this process might be a possible prerequisite for further $CaCO_3$ precipitation linked with fungal biomass. However, the translocation experiment did not corroborate with these observations and thus, does not allow to establish a clear link between Ca accumulations observed in natural samples and NFC and/or nanofibres genesis.

5.3 Biomarkers in macroscopic facies

5.3.1 Introduction to the biomarker approach

Biomarkers are organic indicator compounds that can be used as tracers for geological and environmental processes (Simoneit 2005). Therefore, the search for organic molecules in mineral matter might be a way of emphasizing a biotic origin of this particular mineral. An organic molecule may be trapped within the crystal lattice by two main processes. First, the nucleation and/or the crystal growth are controlled by an organic matrix, which is then subsequently trapped in the crystal lattice (Simkiss and Wilbur 1989). Second, OM present in the environment is passively trapped in between crystal planes of polycrystalline phases (Stumm 1992). This latter process has therefore no influence on crystallogenesis *sensu stricto*. However, it may still be used as an environmental or biogeochemical proxy.

Retrieving biomarkers from environmental samples may be approached by two means. The analysis may be performed on a bulk sample, which is then most likely a mixture of several phases. By this method, the presence of a given biomarker may indicate the presence of an organism or a metabolism (depending on the nature of the biomarker), but it does not necessarily indicate an implication of the targeted organism in the crystal genesis (Blyth and Frisia 2008). Alternatively, targeting the inside of the crystal lattice using fine microanalytical tools may be carried out. Yet, this approach implies a critical size for the single crystal in order to be able to focus the analysis (Yoon 2009).

In order to get evidences of a biological origin of NFC and nanofibres, the search for a fungal and/or an organic polymer has been carried out in two of the pedogenic macroscopic facies, the “cotton ball-like” and the “coating” facies, as well as on the “moonmilk” facies. As this approach has been performed on “bulk” samples, NFC and nanofibres could not be discriminated during analysis. However, the needle to nanofibres ratio of the “cotton ball-like” is high, whereas it is the opposite for the “coating” and “moonmilk” facies. The biomarker approach has been accomplished using two techniques. The first approach aimed at searching for two typical fungal markers, ergosterol and chitin. Ergosterol is a typical fungal polymer, present in the phospholipidic membrane of fungi (Weete 1980). As a result, it is often used in ecological studies as a mean to estimate the fungal living biomass (Ekblad et al. 1998; Klamer and Bååth 2004). To note that ergosterol might be present in some algae and protozoa; nevertheless, it is still safe to use it as a fungal biomarker (Newell 1992). Chitin is present in rather high amounts in the fungal cell wall and is used as a marker to estimate total fungal biomass (Ekblad and Näsholm 1996). To the contrary of ergosterol, it allows the measurement of both, metabolizing and non-metabolizing hyphae (Ekblad et al.1998). However, chitin is also present in the exoskeleton of arthropods, and results should be taken cautiously.

The second approach aimed at searching for an organic signal by using broad-spectrum methods, UV fluorescence spectroscopy, and FT-IR fingerprinting. UV fluorescence consists of measuring the quantity of light emitted by a sample after its excitation with light emitted at different wavelengths (UV and visible). Emission is measured for each emitted wavelength. Only compounds able to fluoresce will be detected. Fluorescence ability is provided by the presence of delocalizable electrons, which are able to move to an excitation sate at the next energy level. When the electron moves back down to the lower energy level, energy is released as a photon (Mc Quarrie and Rock 1992). For instance, aromatic compounds, such as humic and fulvic acids, are easily detected with UV fluorescence (van Beynen et al. 2001).

FT-IR is the acronym for Fourier Transformed InfraRed spectroscopy. This method is based on the absorption of an infrared radiation by the sample. Characteristic vibrations of chemical bounds are detected in function of the emission wavelength. It allows the specific determination of which

chemical bonds, and hence chemical functions, are present in the sample.

5.3.2 Methodology

Prior to analysis, all samples were cleaned from noticeable foreign material (particulate OM and mineral grains) with tweezers under the binocular.

5.3.2.1 Ergosterol assays

Ergosterol assays have been performed following a modified protocol of Young (1995) and Larsen et al. (2004). The principle of this method is the extraction of hydrophobic substances from environmental samples, their HPLC separation and subsequent detection by UV spectrophotometry.

Ergosterol measurements have been performed on two sets of samples i) "coating" and "cotton ball-like" macroscopic facies from soils (CH01 site) and cave moonmilk crusts (CH02 site); and ii) on soil samples coming from Spain (SP03 site) and France (FR01, 02, 03 & 05 sites). These samples always consisted of soil elements, i.e. mineral grain, mineral-organic aggregates when present, and secondary calcium carbonate, either present as "alveolar", "coating" or "cotton ball-like" macroscopic facies. An emphasis on "cotton ball-like" macroscopic facies has been done on purpose, as this facies is considered as the initial one (Cailleau et al. 2009b) and is the most likely to contain ergosterol.

Freeze-dried and finely crushed samples have been treated with methanol in alkaline solution at 85°. The resulting suspension has been neutralised and centrifuged. The supernatant has been mixed with pentane in order to extract the hydrophobic part of the sample. Pentane has been further evaporated under a N_2 flux and samples have been re-suspended in methanol prior to analysis. HPLC separation has ben performed in a Nucleosil 100-5 C18 column. Analysis has been carried out following an isochratic program using a 95 :5 methanol acetonitrile mixture. UV detection has been performed at 282 nm.

5.3.2.2 Chitin assays

Chitin assays have been performed following a modified protocol of Ekblad and Näsholm (1996) and Costa et al. (1989). The method of chitin detection consists in the hydrolysis of chitin (Ekblad et al. 1996) and the subsequent detection of glucosamin units with HPLC. HPLC measurements have been performed at the Department of Fundamental Microbiology (University of Lausanne) after Costa et al. (1989) procedure for amino-acids. Tests using standard glucosamine have shown that it was perfectly well detected. Proteins and amino-acids that could interfere with HPLC detection of glucosamin have been removed in a first step with NaOH. Chitin measurements have been performed on "coating" and "cotton ball-like" macroscopic facies from soils (CH01 site) and cave moonmilk crusts (CH02 site). Freeze-dried and finely crushed samples have been treated with 0.2N NaOH for 6h at 20°C and then at 100°C for another 17.5h in fresh 0.2N NaOH. After this treatment, samples have been washed with distilled H_2O four times. pH of the water has been adjusted at 9 in order to prevent calcite dissolution. An acid hydrolysis has been performed on the NaOH washed samples in 6N HCl at 100° for 7h. Glucosamine from hydrolysed samples has been converted with o-Phthalaldehyde (OPA) into a fluorescent product. Separation has been performed in a ODS-hypersil column and OPA-glucosamin derivatives have been detected with a fluorescence detector coupled to the HPLC (excitation 348 nm, emission at 450 nm).

5.3.2.3 UV fluorescence

UV fluorescence spectroscopy has been performed on “coating” and “cotton ball-like” macroscopic facies from soils (CH01 site) and on cave moonmilk crusts (CH02 site). Samples were washed in calcium hypochlorite in order to remove adsorbed OM. Washed samples were suspended in ultrapure water and calcite was dissolved in 6N HCl down to pH 2. This solution was filtered with a 0.45 µm polycarbonate filter and Ca^{2+} was removed by dialysis. Dialysis membranes with molecular weight cut-offs of 3.5 – 5 kDa were used. Fluorescence was measured with a Perkin-Elmer LS-50, equipped with FL-WINLAB software, at the Institute of Chemical Science and Engineering (EPFL, Lausanne, Switzerland). The emission spectra were measured at wavelengths from 280 to 580 nm, for excitation wavelengths between 220 and 470 nm with increments of 5 nm and a scan speed of 1200 nm/min.

5.3.2.4 FT-IR

FT-IR analyses have been performed only on the “cotton ball-like” macroscopic facies from soils (CH01 site), as this facies is assumed to be the initial one (Cailleau et al. 2009b). Infrared spectra were collected on a Perkin-Elmer Spectrum 100 FTIR spectrophotometer equipped with a single reflection diamond ATR unit. The spectra were evaluated with Spectrum 6.3.5 software. The spectra were recorded against air background from 4000 to 650 cm^{-1}, with a resolution of 2 cm^{-1} and 32 accumulations.

5.3.3 Results

5.3.3.1 Ergosterol

No ergosterol could be detected in the purely calcitic samples (“coating” and “cotton ball-like” macroscopic facies and moonmilk crusts; Table 5.1). As a result, quantification have not been performed for soil samples; therefore only the presence or absence of ergosterol in soil samples will be discussed.

In samples from the SP03 site (Arcusa; Table 5.1), soil samples from deep layers or from hardened crusts presented mostly negative samples. The horizon that contained the most roots (Bca horizon between 8 and 28 cm) also presented few positive samples. Interesting results arised in an intermediate layer, which contained the “cotton ball-like” macroscopic facies in discrete spots (K horizon between 28 and 100cm). In soil samples without cotton balls, ergosterol was detected only in one sample (over six samples analyzed); on the other hand, in soil samples containing “cotton ball-like” macroscopic facies, ergosterol was detected in all the samples tested.

In samples from the FR02 site (Bonaguil; Table 5.1), no clear difference was found regarding soil layer depths. However, samples from the lower part of the Cca horizon (between 90 and 110 cm) present more positive results than the deeper soil layers (Kc horizon between 110 and 190 cm and Ccak2 horizon between 190 and 215 cm). Other punctual sites in France were sampled in order to test ergosterol concomitance with “cotton ball-like” macroscopic facies. In site FR01, no difference has been detected between spots with and without cotton-ball like NFC. In site FR03 and FR05, both soil samples present positive results for ergosterol.

5.3.3.2 Chitin

No chitin has been detected in any of the sample investigated by using the extraction and HPLC detection method.

Table 5.1 - Ergosterol detection in natural samples in function of the type of macroscopic facies. Note that CH samples are purely calcitic in nature, whereas FR and SP are a mixture of secondary calcite and soil aggregates.

Sample location	Macroscopic facies	nr of positive samples
Switzerland (CH01 & 02)		
CH01 C horizon	Cotton ball-like	*n.d.*
CH01 C horizon	Coatings	*n.d.*
CH02 cave walls	Moonmilk	*n.d.*
Spain (SP03)		
Upper part of Bca (8-28 cm), presence of roots	Cotton ball-like	4/11
K (28-100 cm) with sporaric NFC	Cotton ball-like	4/4
	Without	1/6
Kc/Km (160-200 cm)	Alveolar	1/6
Cca/Km (260-280 cm)	Alveolar	3/6

Sample location	Macroscopic facies	nr of positive samples
France (FR01, 02, 03 & 05)		
FR01 C horizon with sporadic NFC	Cotton ball-like	1/2
	Without	1/1
FR03 C horizon	Cotton ball-like	1/1
FR05 C horizon	Cotton ball-like	1/1
FR02 lower part of Cca (60-110 cm)	Cotton ball-like to alveolar	3/4
FR02 lower part of Kc (110-190 cm)	Alveolar	2/5
FR02 upper part of Ccak2 (190-215 cm)	Cotton ball-like	3/6

5.3.3.3 UV fluorescence

All samples have shown a signal. “Coating” macroscopic facies and moonmilk samples show similar patterns, represented by two fluorescence centres: one at the excitation-emission pair of 310-350:405-430 nm and another one at 270-280:420-430 nm (Fig. 5.15 a & b). “Cotton ball-like” macroscopic facies samples show only one fluorescence centre at 280-295:400-410 nm (Fig. 5.15 c). However the signal is rather weak in comparison with the two other samples. The fluorescence centre at 310-350:405-430 nm is interpreted as humic-like, probably fulvic acid, the one at 270-280:420-430 nm, as humic and/or protein like, and the one at 280-295:400-410 nm as a fulvic acid source (Baker and Genty 1999).

5.3.3.4 FT-IR

No OM was detected in the “cotton ball-like” macroscopic facies samples and the FT-IR spectrum shows the typical $CaCO_3$ peaks around 1420, 880 and 710 cm^{-1} (Fig. 5.16). When compared to the spectrogram of pure calcite sample *(Carrara marble* used as a standard in stable isotopes analyses), no shift is observed between the peaks of both samples. However, it appears that the peak of the standard calcite is more symmetrical. (Fig. 5.16). This dissimilarity is attributed to differences in the sizes of crystal lattices. A broader peak is generally the result of a larger crystal lattice (Loste et al. 2003). As NFC and nanofibes are submicrometric habits of calcite, this seems to be a reasonable explanation.

5.3.4 Discussion

In purely calcitic samples of NFC macroscopic facies and moonmilk, neither ergosterol, nor chitin have been detected. This could mean that none of them are present in association with NFC and nanofibres and that fungi are absent. However, fungal hyphae have been frequently observed in

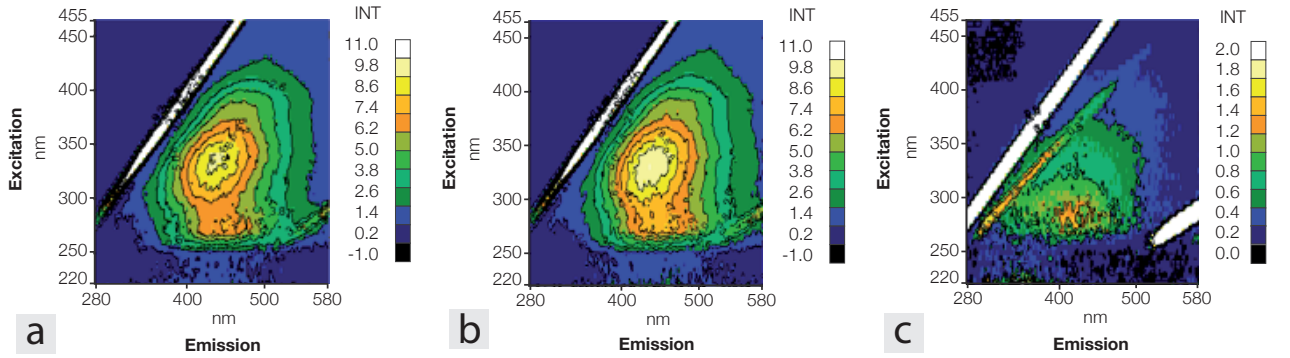

Figure 5.15 - Fluorescence EEM (excitation and emission matrix). **(a)** "coating" macroscopic facies. Peaks at Ex 310-350, Em 405-430 nm and Ex 270-280, Em 420-430 nm. **(b)** moonmilk. Peaks at Ex 310-350, Em 405-430 nm and Ex 270-280, Em 420-430 nm. **(c)** "Cotton ball-like" macroscopic facies. Peak at Ex 280-295, Em 400-410 nm. The intense line at the upper left hand side and the spot at the lower right hand side are artefacts due to water autofluorescence (1st and 2nd orders Rayleigh scattering).

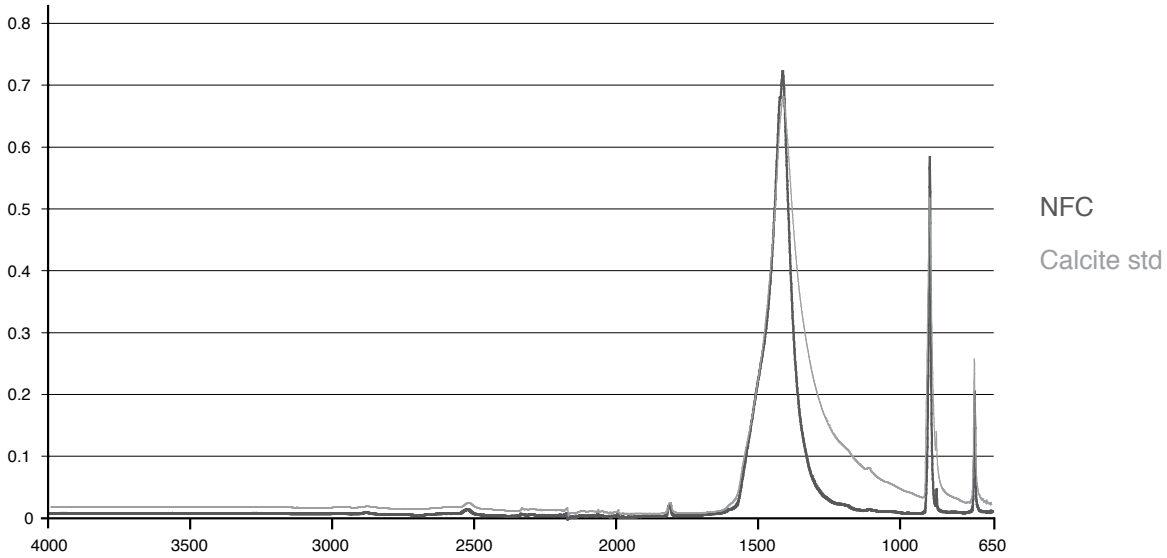

Figure 5.16 - FTIR spectra of NFC *sensu lato* (sample of "cotton ball-like" macroscopic facies) and a calcite standard (*Carrara marble* used as a standard in stable isotopes analyses). Peaks of both samples correspond perfectly and occur at 1420, 880 and 710 cm^{-1}, which correspond to the typical pattern of the C-O bound of $CaCO_3$. Note the symmetrical aspect of the standard calcite spectrum in comparison to NFC spectrum.

natural samples (see chapter 4). Ergosterol is considered as a marker indicating the presence of metabolizing fungi (Klamer and Bååth 2004). Consequently, the absence of ergosterol could indicate that fungal hyphae involved in NFC genesis are non-metabolizing hyphae. In contrary to ergosterol, chitin is considered as a marker for both, metabolizing and non-metabolizing hyphae. So, it might have been expected to detect chitin, which was not the case at the end. The non-detection of these two markers has been interpreted as insufficient quantities of ergosterol and/or chitin in samples to be detected (quantities under the threshold detections). Alternatively, it might be the result of an analytical limitation due to the purely calcitic nature of the samples, e.g. inhibition either by a high pH or a high Ca^{2+} concentration. In soils, the detection of ergosterol in K horizons, associated with "cotton ball-like" facies indicates living fungal biomass in these NFC spots. However, it does not represent a proof of fungal involvement in NFC genesis. In the surface horizon, which contains roots, ergosterol was not detected in all the samples. This is rather surprising, as surface soil layers are believed to contain a large part of the soil fungal biomass (Paul 2007).

UV fluorescence results have been interpreted as soil humic substances associated to the macroscopic facies, and are thus considered as "contaminants" rather than being proof of

involvement in NFC genesis. However, the humic signal observed in moonmilk sample shows that pedogenetic OM is provided to the cave environment by water percolation. This fact is not new, as humic compounds are often detected in association with speleothems (van Beynen et al. 2001). Nevertheless it demonstrates a clear link between the overlying soil and the cave environment. Finally, it should be pointed out that UV fluorescence detects mostly aromatic compounds and thus was considered as being too restrictive for our aim. Consequently, the approach was not further developed. FT-IR spectra did not show the presence of OM. This technique is not very sensitive and likewise to UV fluorescence is not really appropriate to measure traces of organic compounds. Actually, the main aim in using these two methods was to evaluate if OM was present and at which level. The conclusion that can be drawn is that OM is present as demonstrated by UV fluorescence. However it is not possible to state if it is linked to the genesis of NFC and/or nanofibres. Furthermore, FT-IR fingerprinting demonstrates that OM is rather present as traces, as no organic signal could be detected.

5.3.5 Perspectives regarding the search for organic molecules in NFC or nanofibres

The poor results obtained with the "extraction-analysis" approach applied to ergosterol and chitin, together with the specificity and/or poor resolution of broad-spectrum methods, emphasizes the need of using a fine-scale analytical approach. Indeed, the study of organic molecules possibly trapped into the crystal lattice of sub-micrometric objects such as NFC and nanofibres requires tools with a very high spatial and chemical resolution power. Indeed, they exhibit submicron sizes, which are often very near or under the resolution limits of most of the methods available nowadays in the field of *in situ* microscopy and microanalysis. The use of SEM has allowed us to observe different organization and sizes of these features, as well as to discriminate the mineral/organic nature of nanofibres with osmium tetroxide and EDS. TEM can be used to determine the crystalline nature of NFC and nanofibres. Qualitative chemical analysis with EDS will only bring elemental composition, but no indication on the types of chemical bonds. Moreover, the electron interaction volume often exceeds the dimension of NFC and nanofibres. Electron Energy Loss Spectroscopy (EELS) and Electron Spectroscopic Imaging (ESI) coupled to the TEM are very powerful microanalysis tools, as together they presents a high elemental and spatial resolution. This last feature corresponds well with the sizes of the objects to be analyzed, but a major problem exists because of the high heterogeneity of natural samples. As a result, spectrograms obtained with such samples are almost impossible to interpret, as too many peaks are present. This problem was not encountered in lab experiments, as shown in a study by Cailleau et al. (2009a). Therefore, it appears that this method is not adapted to the investigation of natural samples. An accurate investigation of the chemistry of NFC and nanofibres strongly requires a microanalytical tool of very high spatial and spectral resolution, which is also able to focus on one element at a time, such as Scanning Transmission X-ray Microscopy (STXM). For instance, STXM could be used to detect chitin remains in the calcitic nanofibres. Chitin is a polymer of N-acetyl-glucosamin, so as it contains nitrogen, the aim would be to detect nitrogen (or the nitrogen-carbon bound) in the crystal lattice of calcitic nanofibres using STXM. Indeed, STXM appeared to be an appropriate tool for several reasons. First, previous similar studies questioning the biogenecity of some minerals have found relevant information using STXM (Benzerara et al. 2004 & 2006). From a technical point of view, this method has for the moment a spot size of 30 to 15 nm (Benzerara et al. 2004; Yoon 2009), which allows a resolution in the range of the object to be analyzed. Furthermore, to be able to look at the object being analyzed through X-ray images is a very important point in this matter. As NFC and nanofibres usually occur together, it is important to be able focalising the beam on the exact object (i.e. nanofibres) to be analyzed rather than working on a bulk sample. Second, the use of NEXAFS (Near edge X-ray absorption

fine structure) spectrometry allows very high mass resolution, which is appropriate to look at light elements such as C, N, O and Ca. Moreover, analysis with fine X-ray sources give the opportunity to retrieve information regarding the bond types between elements and is therefore a tool of choice when studying OM. Indeed, OM is often composed of the same major elements (C, H, O, N), but the difference lies on the bond types between these elements. Finally, a last very interesting point of this method is that it allows the analysis of hydrated environmental samples (Yoon 2009). By this mean, it is possible to avoid the complex preparation of samples prior to observation, which can potentially bring artefacts to the sample. All these characteristics make STXM a tool of very high analytic resolution, able to retrieve nanometer scale chemical information under *in situ* environmental conditions (Yoon 2009). NanoSIMS (Secondary Ion Mass Spectrometry) could also represent a valuable option, in particular for NFC, as it exhibits also very high lateral and mass resolutions. It has a lateral resolution around 50 nm (Wagner 2009), which is in the ranges of NFC. However, nanoSIMS does not give the possibility to analyze bond types, as does the STXM. This capability is of great importance when studying OM as explained above. However, fine elemental mapping as well as isotopic discrimination may be undertaken (Wagner 2009). This could lead to the recovery of either an isotopic or elemental pattern for NFC, which may help to discuss its origin.

5.3.4 Conclusions

The negative results of the biomarker approach might be the result of two problems. First, if no organic signature is detected, it could mean that no OM is present inside the crystal lattice of NFC and nanofibres. Alternatively, it might be related to the fact that the organic signal cannot be detected. The “extraction-analysis” approach requires OM to be present in a critical amount to be detected. In the first step of extraction, losses may happen and in the second step OM quantity should be above a certain threshold in order for a signal to be detected. For these reasons, the use of microanalytical tools of both high spatial and chemical resolution power seems to be a more appropriate approach in order to get relevant information at sub-micrometric scales (Yoon 2009).

5.4 Summary of chapter 5

The mild enzymatic treatment of fungal mycelium has demonstrated that the fungal cell wall is a source of nanofibrous features. In natural environment the same process is likely to happen as a result of microbial enzymatic lyses. Consequently, nanofibres associated to NFC should often represent the relict of the fungal cell wall. Their mineralization happens probably as a result of an organomineralization process, i.e. fluids, which are supersaturated in respect to calcite, passively mineralize organic nanofibres.

TEM observation of natural fungal strands has shown that numerous intrahyphal inclusions were present in hyphae. Furthermore, these inclusions, as well as the hyphae cell walls, are highly enriched in Ca^{2+}. These observations suggest that this might represent a pre-requisite to $CaCO_3$ nucleation, leading to NFC genesis. However, this hypothesis could not be confirmed by the translocation experiment, as it has not been possible to reproduce the Ca enrichment in the experimental procedure.

The biomarker approach has not lead to definitive results in reason of methodological limitations. It emphasizes the need of analytical tools with both high spatial and chemical resolutions for the study of calcitic phases such as NFC *sensu lato* and moonmilk, which are composed of submicrometic features organized in an heterogeneous pattern.

Chapter 6

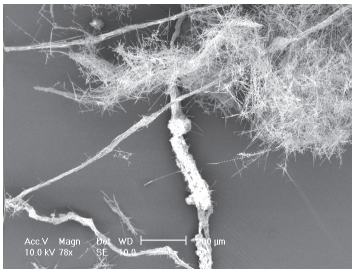

General discussion & Conclusions

Chapter 6 - General discussion, outlooks and conclusions

The primary aim of this Ph.D. project was to understand how fungi are implicated in the formation of NFC. To do this, several approaches were attempted. The observation of natural settings harbouring NFC *sensu lato* accumulations gave initial indications that the formation of NFC could not be easily reproduced on an experimental setup. Therefore, it was essential to start by understanding the environmental factors that could be implicated on the formation of NFC macroscopic accumulations (Chapter 3). This was followed by an attempt to understand the mutual relationship between NFC, nanofibres, and other features from their environment of origin through microscopic techniques (Chapter 4). Finally, an effort was carried out to reproduce the formation of nanofibres and NFC in the laboratory, as well as to evaluate the existence of fungal or organic biomarkers on already formed NFC macroscopic facies (Chapter 5). In this final chapter, some key connecting elements on the processes involved in the genesis of NFC and nanofibres will be discussed into detail.

6.1 The origin of NFC and nanofibres

6.1.1 Importance of nanofibres as a tool for discussing the origin of NFC

In the quest for understanding the formation of NFC, most researchers have neglected their co-occurrence with nanofibres in the natural samples. However, the recurrent association of nanofibres to NFC was too intriguing to be left aside. Even more intriguing was the observation of organized structures made of nanofibres, structures, which could not be the result of random reworking processes (§ 4.1 and 4.2). As a result, in this study the unravelling of nanofibres origin was used as an indirect, yet more informative, tool to understand the origin of NFC.

Many studies that have investigated the origin of either soil secondary carbonate or moonmilk facies (both containing NFC and nanofibres) have rarely emphasized the differences between NFC and nanofibres. Nonetheless, the fact that two features with distinct dimensions are recurrently associated may not be random, and finding the cornerstone between NFC and nanofibres could allow unravelling all or part of their history. In this study, it was assumed that these micro-features do not share a genetic link.

Due to their submicrometric dimensions, the understanding of the relationship between NFC, nanofibres, and fungi, was made using electron microscopy techniques. Scanning electron microscopy (SEM) was the most suited and easiest method, as environmental samples do not require extensive preparation steps. However, a major limitation that arises is that, while the structures are easy to discern, the distinction between organic and mineral features is problematic. Such a differentiation under *in situ* conditions is actually difficult to achieve, mostly due to the high heterogeneous nature of natural samples.

Finding an easy way to differentiate mineral from organic matter (OM) by using osmium tetroxide labelling has led to a step forward in the understanding of nanofibres characteristics. Indeed, it has been demonstrated that non-randomly organized meshes of nanofibres were often organic in origin (Bindschedler et al. 2010). However, osmium labelling does not state if these nanofibres are fungal in origin. Such a confirmation may only be obtained by a laboratory experiment. Both, fungi and plants possess fibrous material with similar characteristics to nanofibres within their cell walls (Carlile et al. 2001; Paul 2007). This study only explored the fungal contribution, based on the fact that it has been previously suggested that NFC is most likely fungal in origin (Cailleau et al. 2009b).

In laboratory assays, the isolation of the fibrillar part of the fungal cell wall has been achieved by

using enzymatic lyses. This clearly demonstrates that in natural environment the same process is likely to occur. Consequently, nanofibres associated to NFC should often represent the relict of fungal cell walls.

6.1.1.1 Origin and preservation of organic nanofibres in natural environments

Accepting the organic origin of nanofibres, two linked questions remain: what are the processes at the basis of organic polymers degradation and how these polymers resist complete decaying? The processes leading to the preservation of fibrous polymers in pedogenic environments are poorly understood. While much is known on the fungal cell wall structure and its susceptibility to several chemicals (Ruiz-Herrera 1992; Farkaš 2003), much less is known about the fate of fungal cell wall polymers in the soil environment.

The complete mineralization of complex polymers such as cellulose, chitin and β-1,3-glucan usually involves either enzymatic complexes or guilds of organisms (Chesters and Bull 1963b; Paul 2007; Yaroslavtsev et al. 2009). Chitin is a significant source of nitrogen in soil (Paul 2007) and its degradation depends mostly upon bacteria (including actinobacteria). A diversity of chitinases is found among several microorganisms with chitinolytic capabilities (Krsek and Wellington 2001; Yaroslavtsev et al. 2009). On the other hand, very little information can be found regarding the enzymatic degradation of β-1,3- and β-1,6-glucans in natural environments (Chesters and Bull 1963a). Due to their similarity with cellulose (β-1,4-glucan), it may be assumed that β-1,3- and β-1,6-glucan are more readily recyclable in comparison to chitin. Cross-linking between chitin and β-1,3-glucan may lead to the preservation of both components, even though they should display different liabilities. As a result, their accumulation in pedogenic environments may occur. Indeed, chitin is known to accumulate in some environments (Guggenberger et al. 1999; Langley and Hungate 2003; Ehrlich 2010; Fan and Guo 2010). Some of the factors that can contribute to preservation of cell wall fibrous polymers are: i) inactivation or inhibition of enzymatic activities due to inappropriate pH or temperature, ii) the presence of chelating ligands leading to the inaccessibility of the substrate (Dalias et al. 2003; Ehrlich 2010; Sinsabaugh et al. 2010) and, iii) cross-linking providing cell wall fibrillar polymers with a reduced susceptibility to decay (Fontaine et al. 1997).

In this study, it was demonstrated that fungal cell wall polymers are likely to be preserved in conditions similar than those prevailing in the soil environment. They may further act as a template for calcite nucleation. While a fungal origin for nanofibres was established in a laboratory assay, it may be assumed that any other fibrous polymer could lead to the same result as emphasized by Cailleau et al. (2009a) with cellulose. As a result, nanofibres associated to NFC testify for fungal presence, but it is possible that not all of them have a fungal origin. In particular, the great accumulation of nanofibres in “coating” macroscopic facies and moonmilk could be the result of the accretion of calcified nanofibres of different origins, which have been carried by water circulation. Indeed, water circulating within pedogenic environments gets enriched in various macromolecules, which may eventually reach deeper soil layers and cave environments. The detection of humic compounds in both soil and moonmilk samples confirms that such per-descensum transfer of OM occur indeed in the studied environments (§ 5.3).

6.1.1.2 A scenario for nanofibres mineralization

While it has been possible to produce in the laboratory nanofibres using fungal hyphae as a starting material, it has not been possible to provoke experimentally their mineralization. This could be due to multiple reasons: i) methodological limitations resulting from the dimensions of such features,

ii) complexity of reproducing natural occurring processes and, iii) the temporal dimension of the processes linked to the kinetics of $CaCO_3$ nucleation. However, based on the observations made with the TEM, it is assumed that Ca^{2+} sequestration in the cell wall could represent a prerequisite for nanofibres calcification (§ 4.2). Ca^{2+} adsorbed or bounded to cell wall polymers, possibly chitin (Furlan 1996; Ehrlich 2010), may enhance further calcite nucleation around these polymers by creating a "precursor" zone. In fact, in nanofibres found on a meteorite fragment, Benzerara et al. (2003) highlighted the presence of a narrow zone of amorphous nature around them. These authors favour as interpretation that this amorphous layer is a precursor phase leading to calcite crystallization. Under the usual temperature and pressure conditions found in surficial formations, amorphous $CaCO_3$ phases should be highly unstable. Their stability is probably enhanced by organic polymers (Addadi et al. 2003), emphasizing the presence of OM as a pre-requisite for calcite nucleation. Moreover, Cailleau et al. (2009a) showed under laboratory conditions that Ca^{2+} adsorbs readily at the surface of cellulose fibres, enhancing the further nucleation along the fibre. Therefore, it seems that the sequestration of Ca^{2+} on the fungal cell wall nanofibres is a condition to their subsequent mineralization. Finally, nanofibres represent the typical result of an organomineralization process, which consists of a passive mineralization of OM. In this process, the physicochemical parameters leading to $CaCO_3$ nucleation are the result of environmental conditions rather than induced by microbial activity (Dupraz et al. 2009).

6.1.1.3 Dynamics of nanofibres in the environment

Obvious syntactic growth of calcite has rarely been observed on nanofibres, whereas the opposite is true regarding NFC. Meshes of nanofibres are mostly observed as smooth nanofibres associated to poorly diagenetized needles. However, meshes of smooth nanofibres are also observed with MB type needles (in particular in cave environments). Yet, such observations are seldom. It might be that nanofibres are preferential sites of nucleation for syntactic growth and as a result are rapidly obliterated. Alternatively, another process restricts nucleation on their surface, leading to their neat preservation.

6.1.2 Controls on NFC formation

The unravelling of NFC origin is delicate. While the conditions necessary for the production of nanofibres are fairly easy to imagine, the ones leading to NFC genesis are more difficult to conceive. The results obtained in this study are mainly interpretations stemming from SEM and TEM observations. The recurrent observation of analogies between fungal and NFC structural and ultrastructural features are strong evidences confirming the fact that NFC is generated inside a mould that constrains the needle growth. Hence, needles are casts of the fungal hypha and as such, display characteristic features of fungal hyphae. These observations have clarified that NFC is intimately linked to fungal hyphae.

These observations also opened a large number of questions related to the processes of translocation, nucleation and the metabolic implications for the fungi. Since NFC would form inside fungal hyphae, as suggested by several authors (Callot et al. 1985b; Phillips and Selp 1987; Verrecchia and Verrecchia 1994; Cailleau et al. 2009b) and supported in this study, the physiological processes involved and leading to NFC genesis need to be clarified. Nanofibres recurrently associated to NFC bundles suggest that mycelial strands and rhizomorphs (due to analogies of dimension and organization; see § 4.2) are likely to be involved in NFC genesis, rather than single hyphae. The difference of permeability between single hyphae and fungal strands might be a crucial point regarding this issue. While single hyphae are permeable structures, fungal strands are known for

their lower permeability conferred by thick-walled hyphae (Watkinson 1979; Cairney 1992). This trait may even be enhanced by melanization due to the hydrophobic nature of these molecules (Rosas et al. 2000; Pareek et al. 2001). Thus, the translocation of fluids that are supersaturated regarding calcite, could eventually lead to nucleation within fungal strands lacking permeability. The observation of Ca^{2+} rich inclusions in hyphae from fungal strands supports this suggestion. Nevertheless, if NFC precipitate only in fungal strands, it is true to say that single hyphae are not at all involved? Also, does nucleation of $CaCO_3$ happen after nucleation due to high supersaturation or is it enhanced by an organic matrix acting as a heterogeneous nucleus? Furthermore, the metabolic implications for fungi remain an open question. Does the nucleation of $CaCO_3$ within fungal hyphae happen passively or do metabolic processes induce it? Does NFC form inside metabolically or non-metabolically active hyphae? Finally, is NFC genesis restricted to some particular species or is it a common fungal feature? If NFC genesis is restricted to fungal strands and rhizomorphs, it might be possible to define taxonomic groups that are more likely to be involved.

Cairney (1992) suggests that bi-directional translocation in rhizomorphs occur in spatially different hyphae. Translocation of carbon towards growing apices (acropetal translocation) most likely occurs in empty vessels hyphae. On the contrary, the translocation of nutrients solutions, down from growing apices to older parts of the mycelial network (basipetal translocation), is thought to be restricted to living hyphae. Thus, the soil solution is likely to be translocated in living hyphae suggesting that the sequence of events leading to NFC formation might be under the control of the fungal metabolism. The physiological processes possibly involved are most probably linked with Ca^{2+} sequestration and DIC equilibrium within cell compartments (Fig. 6.1).

Furthermore, an energetic profit for the fungus may be envisaged, such as the *trans* calcification process proposed by McConnaughey and Whelan (1997). They suggest that this type of calcification generates a proton gradient, which may further be used to activate a Ca^{2+}-ATPase involved in Ca^{2+} ejection from the cytosol. For instance, sequestration of Ca^{2+} within the fungal vacuole (Jackson and Heath 1993) might lead to this situation.

Well-designed physiological experiments are likely to answer most of the open questions. A first attempt was carried out in this study in the form of a translocation experiment that was intended to bring insights into the role of Ca^{2+} sequestration into fungi and its link to NFC genesis. However, reproducing natural conditions in the laboratory can be arduous due to the high level of heterogeneity of natural environments. The right set of factors needs to be defined first in order to obtain experimental conditions, which are equivalent to natural conditions. As long as this is not achieved, it may prevent the understanding of complex processes still for quite some time.

6.1.2.1 Considerations about NFC peculiar morphology and the *c*-axis problem

The morphological elongation of NFC and nanofibres in one direction implies that some crystal faces are inhibited. If NFC and nanofibres were purely physicochemical products, such an inhibition is most likely to occur as a result of foreign ions (mostly Mg^{2+}) or OM adsorbed to some crystal faces, inhibiting the addition of Ca^{2+} and CO_3^{2-} ions. As both, NFC and nanofibres are constantly composed of low Mg-calcite, the Mg^{2+} poisoning hypothesis is rather unlikely. On the other hand, the production of highly reproducible morphologies with such complex features such as NFC, are often the result of an organic polymer control (Mann 2000). Yet, the implication of OM emphasizes the involvement of a biological process.

Several authors have demonstrated that the NFC lengthening axis diverges from the calcite *c*-axis showing constant diverging values (Vergès et al. 1982; Phillips et al. 1987). To the contrary Richter et al. (2008) have shown that this divergence was not constant, ranging from sub-parallel orientations

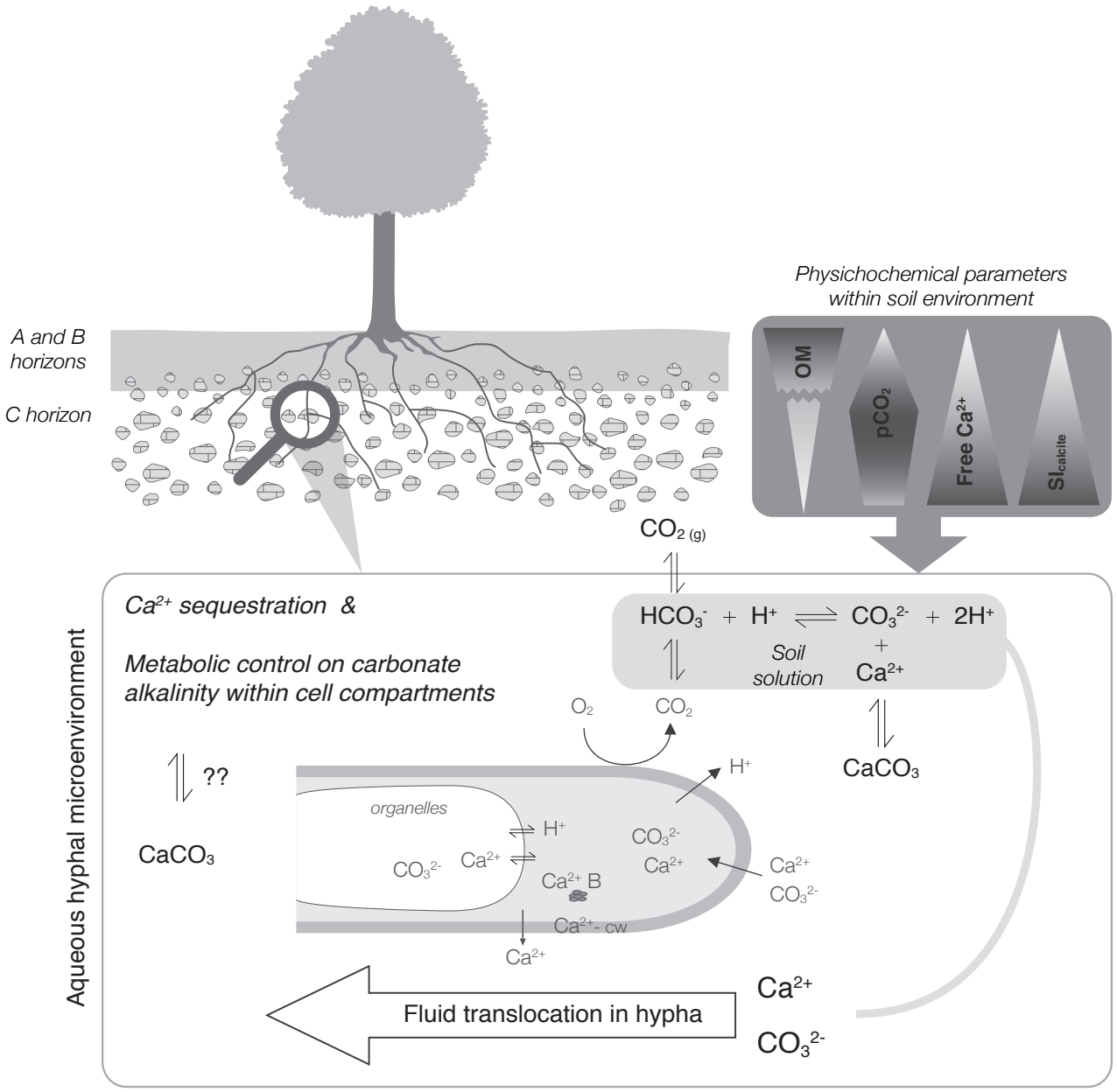

Figure 6.1 - Synthetic sketch of the environmental perspective on NFC formation. Ecosystem-related processes are represented in the upper part of the sketch. They depend mostly on (i) the physical organization of the site (presence of pores), (ii) the presence of pre-existing $CaCO_3$, (iii) OM decaying processes and root related processes, (iv) and the presence of free Ca^{2+}, which will create the physicochemical conditions leading to the possible precipitation of $CaCO_3$, i.e. the increase of the $SI_{calcite}$. Processes occurring at the fungal microenvironment scale are represented in the lower part of the sketch. They are mostly related to (i) the alkalinity levels of the fungal microenvironment, (ii) Ca^{2+} sequestration rate by the fungi and, (iv) metabolic control on intra-hyphal alkalinity levels of translocated solutions. Nevertheless, the sequence of events leading to $CaCO_3$ nucleation within hyphae is still to elucidate.

to almost perpendicular ones. A constant divergence between the elongation axis and the calcite *c*-axis could indicate that nucleation is controlled at all time by the same molecule or function, which is oriented on the substrate in exactly the same direction. The initial unit cell is therefore generated after a particular orientation, which corresponds to the organic molecule acting as a heterogeneous nucleus. This process has been suggested for calcite-dendrites of cold-water tufa, whose elongation axis is perpendicular to the calcite *c*-axis. In this particular case, it is suggested that the negative charges of EPS surfaces repelled CO_3^{2-} and thus force their orientation in $CaCO_3$ planes (Turner and Jones 2005). For NFC a different physical constrain is proposed. An inconstant divergence could indicate that either different molecules or functions with different properties are involved in calcite nucleation or that this molecule is randomly oriented in its environment. For instance, if calcite nucleation happens on the fungal cell membrane or cell wall, whatever the

nucleus initial orientation, it will be confronted to a physical barrier as fungal hyphae are tubular constrained environments. As a result, the calcite crystal is forced to grow according to the fungal hypha geometry/morphology. Such as process may lead to random divergences between the needle elongation axis and the calcite *c*-axis.

As mentioned by Richter et al. (2008), the clear resolution of the origin of NFC needs to be resolved in laboratory experiments, as it was the case with nanofibres. However, regarding the morphological characteristics of NFC and the issues of the "*c*-axis problem", the growth of NFC inside constrained environments such as fungal hyphae is currently the best explanation.

6.1.2.2 Linking NFC to soil OM

Observations methods, i.e. SEM, TEM as well as micromorphology, have demonstrated that a close relationship exists between OM in soil (living or decaying), NFC, and nanofibres. Owing to the present-day knowledge, it seems obvious that the overlying vegetation, associated microflora, and OM recycling processes are essential for creating and maintaining the physicochemical conditions allowing $CaCO_3$ precipitation. Environmental factors such as OM decay, pCO_2, and free Ca^{2+} concentration (Fig. 6.1) control the carbonate alkalinity status and thus the $SI_{calcite}$ of the soil solution. The balance between these factors may be in turn assumed to dictate NFC genesis. Finally, if NFC is formed inside living hyphae, fungi must control the last step leading to $CaCO_3$ precipitation by the control of both free Ca^{2+} and carbonate alkalinity levels within cell compartments.

In addition, within the processes described above, what would be the status of calcified filaments in comparison to NFC? Calcified filaments are often observed in the same deposits than NFC and nanofibres, and at least some of them are interpreted as being of fungal origin (Klappa 1979; Phillips et al. 1987; Verrecchia 1990). It may be assumed that calcified filaments represent extracellular precipitation, whereas NFC corresponds to an intracellular precipitation. Is this difference controlled by the environment or by the fungal metabolism? The answer to this question might lead to the clarification of the processes leading to NFC genesis. Moreover, the importance of both, the total environment and the fungal microenvironment are critical in this issue. Indeed, the understanding of the functioning at both scales, as well as their mutual relationships, is a crucial point that needs to be explored in the future.

6.2 Large-scale perspective of NFC and nanofibres occurrence

6.2.1 Environmental and climatic considerations

Caves and soils behave differently regarding the variation of their physicochemical parameters. Caves are highly buffered systems, and parameters such as temperature and humidity are stable over the year. Humidity is usually around 100% saturation and temperature corresponds to (or is near to) the MAST (Mean Annual Surface Temperature) for the region (Northup and Lavoie 2001). On the contrary, soils are more sensitive to climatic variation, and consequently are less buffered systems with respect to temperature and humidity. Temperature is regulated from the surface; as a result, buffering capacity of soils increases with depth and deep mineral layers are more constant than surface layers. Humidity is a less stable factor in soils, which depends mostly on soil texture, as well as pore dimensions and connectivity (Gobat et al. 2003). As a result, temperature and humidity are not regulated to the same extent in both environments. Yet, similar forms, i.e. NFC and nanofibres are observed in samples from both cases. Hence, the difference in buffering of physicochemical parameters between soils and cave suggests that evaporitic stress may not be the cause of NFC and nanofibres precipitation as suggested by several authors (James 1972; Vergès et

al. 1982; Jones and Ng 1988). Indeed, evaporitic stress similar to the one that may occur in soils is very unlikely to happen in cave environments.

However, there is a difference in the types of facies observed in soils and caves. In caves, nanofibres are more abundant than needles. The typical moonmilk facies corresponds to the "coating" facies. To the contrary, the "cotton-ball-like" facies is common in soils and far less common in cave environments. This difference in the occurrence of the various types of facies might be the result of the non-similar buffering capacities between soils and caves.

The soil accumulations investigated in this study have the particularity to occur in scree slope deposits. At the interface between soil and scree deposit layers, a drastic change of pore dimensions happens, inducing intense water drainage. Moreover, depending on pore connectivity of the scree deposit layer, as well as the presence of a connexion with the external environment, airflow may happen leading to changes in physicochemical (e.g. temperature, humidity) gradients in the soil. All the sites investigated in this study displayed either, a quarry front and/or bare scree/colluviums areas, suggesting that a connexion between the scree deposit layer and the external environment is possible. This fact is probably of importance to understand the physicochemical conditions leading to $CaCO_3$ precipitation. Moreover, $\delta^{13}C$ values measured from the Villiers (CH01) site show that a re-equilibration with atmospheric values happens in the scree deposit atmosphere, demonstrating that pores are connected (Hasinger 2009). Most likely, this causes CO_2 degassing from soil solutions with high pCO_2 percolating within the soil, leading to an increase of the $SI_{calcite}$ (Suarez et al. 1992). In caves, the arrival of percolating water with a high pCO_2 will similarly degas and lead to an increase of total alkalinity and thus to an increase of the $SI_{calcite}$. As a result, it seems that processes related to carbonate equilibria are involved in NFC and nanofibres genesis. However, even though the parent solution is slightly saturated or supersaturated in respect to calcite, it does not imply that NFC and nanofibres originate from physicochemical rather than biological processes.

6.2.2 NFC as a paleoclimatic proxy

In earlier studies, NFC has often been used as a paleoclimatic proxy indicating arid to semiarid climates (see references in Wright 1984 and Strong et al. 1992). However, as mentioned by Wright (1994) and Strong et al. (1992), it is wrong to consider that NFC *sensu lato* forms only under xeric conditions as NFC is observed in many environments that do not correspond to the definition of arid to semiarid climates, such as temperate and intertropical soils or cave environments (Table 2.2). Actually, the preservation of NFC in paleosols (most of the time present as "alveolar" facies) indicates low leaching processes due to a negative hydric balance, which postdates the accumulation (Strong et al. 1992). Moreover, the "alveolar" facies, which is already the result of a negative hydric balance (Fig. 2.10), is also observed in areas where climate is not considered as arid to semiarid (such as the Villiers site). This feature actually demonstrates the importance of pedoclimatic versus general climatic conditions. Pedogenic environments are highly heterogeneous in nature. As a result, pedoclimatic conditions may not necessarily correspond to the regional climatic conditions. Moreover, pedogenic environments contain numerous microenvironments and each one of them is likely to harbour particular microclimatic conditions (Gobat et al. 2003). Therefore, microenvironments displaying a low water activity are likely to lead to "arid-like" conditions in areas with a humid regional climate. This may be the case of scree deposit layers that have a highly draining nature and display airflow within the pore network, leading to dryer pedoclimates in between rain episodes. As a result, accurate paleoclimatic indications are more likely to result from a combination of several microfeatures including NFC and its different macroscopic facies (Wright 1984; Zhou and Chafetz 2009). Finally, while NFC may not be considered as a climatic marker, it still might be considered as

an environmental marker. Its occurrence may be related to pedogenetic processes and thus, to the existence of “soil environments”, as well as to the presence of fungi (Millière et al. 2011).

6.3 Critical aspects and outlooks

6.3.1 Sampling bias

In this study, the initial sampling was performed at the quarry front. From SEM observation of these samples, only a few organic structures were observed. However, when secondary $CaCO_3$ sampling was carried out closer to the soil organic compartment, the presence of fungal hyphae was widespread when samples were observed by SEM. Besides, using thin sections, the ubiquity of fungi was again confirmed also in purely calcitic samples. The experience gained in this study has demonstrated that the most interesting and relevant observations could be made on samples with visually identifiable OM, leading to the observation of close relationships between organic and calcitic features, which may not result from random reworking processes. This demonstrates that an adequate sampling is a prerequisite in the study of NFC and that, in the past, sampling has suffered from a bias. Moreover, it should be pointed out that in previous studies NFC has been investigated mostly by geologist and soil scientists, whom unconsciously neglected the biological aspects of sampling. This fact may have lead to the misidentification of some structures. Likewise, the term *pseudomycelium* defined by Kubiëna (1938) might have lead to the convincing of fungal implication in NFC genesis, even before their association was confirmed.

6.3.2 Methodological limitations

One of the major concerns faced in this study was the technical limitation encountered when working on submicrometric features such as NFC and nanofibres. The main problem arises from the fact that during sampling, it is impossible to differentiate between NFC and nanofibres and hence to know exactly what is going to be analyzed. The different macroscopic facies exhibit different proportion of NFC and nanofibres, and this can represent an indirect mean of differentiation. However, this is very imprecise and might lead to great, yet totally unevaluated, bias.

The range of tools that have been used to investigate NFC and nanofibres, demonstrates these methodological limitations. Most of the studies devoted to pedogenic carbonate and moonmilk have used petrographic descriptions and concepts (soil micromorphology, XRD, SEM and TEM; Kubiëna 1938; Vergès et al. 1982; Wright 1984 & 1986; Phillips and Self 1987; Verrecchia and Verrecchia 1994; Borsato et al. 2000; Cailleau et al. 2009b). Some studies have measured stable isotopes composition (Strong et al. 1992; Bajnóczi and Kovács-Kis 2006 ; Millière et al. 2011). Fewer authors have used in vitro cultivation of environmental microorganisms (Cañaveras et al. 1999; Gillet et al. 2000; Curry et al. 2009), a method known to lead to great underestimation of real *in situ* processes (Nannipieri et al. 2003). Other authors have used DNA-based approaches (Cañaveras et al. (2006) with moonmilk samples) and fingerprinting of organic molecules (Blyth and Frisia (2008) with moonmilk samples). All these studies have been made on bulk samples, i.e. an indeterminate mixture of NFC, nanofibres and associated microorganisms. The fact that most studies have focused on microscopic techniques emphasizes the difficulty of interpreting “bulk “methods. Thus, it often precludes a clear understanding of the respective genesis of NFC and nanofibres. As mentioned by Blyth and Frisia (2008), “bulk” analyses allow only a process or an organism to be detected. However they do not specify the genetic relationships between NFC, nanofibres, and associated microorganisms.

Because NFC and nanofibres are not genetically related, being able to analyze each feature

separately, rather than as a “bulk” sample, is crucial in order to retrieve individual information. The methodological tools to perform such analyses are scarce, however they exist. As already mentioned, using tools with high spatial and/or chemical resolution power could hopefully bring new insights into NFC and nanofibres chemistry. Auger electron spectroscopy (AES) and Electron energy loss spectroscopy (EELS) have fine spatial and chemical resolutions. However, spectrograms obtained with such methods are difficult to interpret due to the presence of numerous overlapping peaks in heterogeneous natural samples. Therefore, both methods are more adapted to material than to environmental sciences. Among the methods with fine spatial (down to the nanometer scale) and chemical resolutions, soft X-ray spectromicroscopy and nanoSIMS, seem the most appropriate tools to advance in the understanding of both NFC and nanofibres chemistry. Soft X-ray spectromicroscopy allow obtaining nanometre-scale chemical information under *in situ* conditions. Moreover, it is possible to deal with wet samples, which is a great advantage in environmental science, as it exempts the fastidious preparation of humid biological samples (Yoon 2009). In addition, information of high spectral resolution can be obtained using NanoSIMS, and in particular isotopic compositions and elemental distribution (Wagner 2009).

In this study, the approach on “bulk” samples did not lead to definitive results and thus emphasizes the need of using more powerful tools to get new insights in NFC and nanofibres (bio)chemical composition.

6.3.3 Dynamics of NFC and nanofibres genesis

No direct information on the dynamics of NFC and nanofibres (i.e. time lapse of formation) has been acquired in this study. Indirect information may serve in the definition of a time-slot in which their genesis is likely to have occurred. A maximal time span for NFC genesis can be inferred at the ecosystem scale, by comparing NFC occurrence to the age of the host formation. However, this time span represents large time intervals (150-200 years after Cailleau et al. (2005) and 10’000 years for scree slope deposits investigated in this study) and do not give any information regarding the actual time span required for the formation of NFC and nanofibres. Nanofibres result from organomineralization processes. Therefore, their formation depends on the rates of OM decay leading to the release of organic nanofibres as well as on kinetics of $CaCO_3$ nucleation. NFC formation most likely depends on fungal physiological processes such as Ca^{2+} sequestration and intracellular carbonate alkalinity regulation. Physiological experimentation with fungi might lead to a better understanding of the physicochemical parameters likely to influence the system and the rate of the processes of NFC genesis. Furthermore, as mentioned earlier, the understanding of the sequence of events leading to NFC formation should be deciphered using an experimental approach. Microcosm experiments are the typical experimental design used to understand processes resulting from the interaction of several processes in natural systems. However, such an approach is highly reductive and requires choosing a combination of factors for the experimental setup, leading sometimes to poor results due to an inappropriate set of initial factors. Nevertheless, microcosms allow interactions between organisms and their environment to be understood in approximate natural conditions.

6.3.4 Ca-oxalates vs. calcite

Fungi are known as producers of large amounts of Ca-oxalate. Indeed, fungal hyphae coated with oxalate crystals (most likely of calcium) have been recurrently observed in our secondary $CaCO_3$ samples containing OM. However, fungal hyphae lacking oxalate crystals were observed in deeper

soil layers. Is there a link between Ca-oxalate production and consumption and calcite precipitation? What is this relationship? This relation has already been discussed by Verrecchia and Dumont (1996), but would need further investigations. From our observations, it seems that bacteria do not mediate this relationship, in contrary to other studies focusing on oxalate deposits in soil (Braissant et al. 2004).

6.3.5 Role of organic residues as nucleating agents

The importance of microbial surfaces and organic polymers as nucleating agents is well known from biomineralization theories (Simkiss and Wilbur 1989). However, the hypothesis regarding the origin of nanofibres opens a new perspective on the fate of some polysaccharides, in particular polymers from the cell wall, in pedogenic environments. Regarding the amount of nanofibres and their nature, it should be kept in mind that chitin and cellulose are the two most common polymers on Earth (Ehrlich 2010). Therefore, the associated organomineralization process proposed in this study is likely to have an influence on C and Ca biogeochemical cycles, which needs to be evaluated.

Humic substances have been detected in both soil and cave secondary calcite using UV fluorescence spectroscopy (§ 5.3). The presence of humic compounds in those samples is likely to be the cause of fluorescence as viewed in thin sections (§ 4.3). Kubiëna (1938) describes the occurrence of organic colloids at the surface of the pores in which NFC is observed. As humic colloids are known to adsorb calcium, growth of NFC and nanofibres under their influence should be addressed in future studies.

6.4 Conclusions

It has been possible to demonstrate that calcitic nanofibres, recurrently associated to NFC, are fungal in origin. Thereby, this result emphasizes the potential fungal origin of NFC. Nanofibres are the relict of the fungal sheath in which NFC have been formed. The great variety of shapes and mutual organization between each feature, as well as their mutual relationships, is the result of the dynamic balance between physicochemical (i.e. early diagenesis) and physical (i.e. reworking) processes occurring in pedogenic and epikarstic environments (Fig. 6.2).

Nanofibres origin and ultrastructural features of NFC confirm that the fungal origin hypothesis is realistic. Furthermore, the observation that Ca^{2+} can be sequestrated into fungal cell walls, as well as in inclusions, suggest that this step represents a pre-requisite to $CaCO_3$ nucleation. Although NFC origin may not be 100% confirmed unless it is reproduced under experimental conditions, the results presented here show strong converging evidence supporting the fact that NFC cannot be the result of a purely physicochemical process. As a result, processes happening at the fungal hypha scale (fungi microenvironment, as well as inner hyphal space; Fig. 6.1) need to be clarified in order to understand the sequence of events leading to NFC genesis.

Moreover, environmental parameters of the ecosystems where NFC and nanofibres occur appear to be crucial to their genesis. A necessary link with soil OM seems to arise (Fig. 6.1). This fact opens a wide range of questions, such as in which way is this link necessary? And through which processes? Blyth and Frisia (2008) have mentioned the fact that caves exhibiting moonmik are largely occurring under rendzinae lying over fractured limestone. Furthermore, in this study, the investigated sites are all forested sites displaying soils with high OM content in superficial soil layers. Does this fact demonstrate an essential link with overlying soil and vegetation? This observation emphasizes the importance of an ecosystemic approach. The understanding of a process occurring in a natural environment may be the result of a multitude of factors; hence the evaluation of processes at

several scales is indeed essential.

Finally, this study emphasizes the importance of fungi as important actors in mineral nutrient cycles. As both NFC and nanofibres are ubiquitous features in terrestrial environments, it highlights once again the importance of both OM and microorganisms (especially fungi in this case) as essential actors of biogeochemical cycles. Nanofibres origin opens challenging questions regarding the decay rate, as well as the fate of certain polysaccharides, in particular cell wall residues, in pedogenic environments. Moreover, it questions the implication of such a process in the coupled Ca and C cycles.

Figure 6.2 - Synthetic sketch summarizing NFC and nanofibres genesis including their mutual relationships. The left hand side of the sketch summarizes the fungal origin of NFC. Simple needles (MA type) are formed within hyphae of fungal strands and (?) of single hyphae. The partial decay of the fungal cell wall leads to the release of the MA type needles which may further undergo syntactic growth of calcite leading to MAB and MB type needles. The right hand side of the sketch summarized the fungal origin of nanofibres. The fungal cell wall undergoes an incomplete decay, leading to the release of meshes of organic nanofibres in the environment. Organic nanofibres serve as template for the nucleation of $CaCO_3$. These meshes may be organized or randomly reworked. The lower part of the sketch synthesizes the different types of mutual relationships between NFC and nanofibres that are observed in natural environments and that results from the balance between physical and chemical processes.

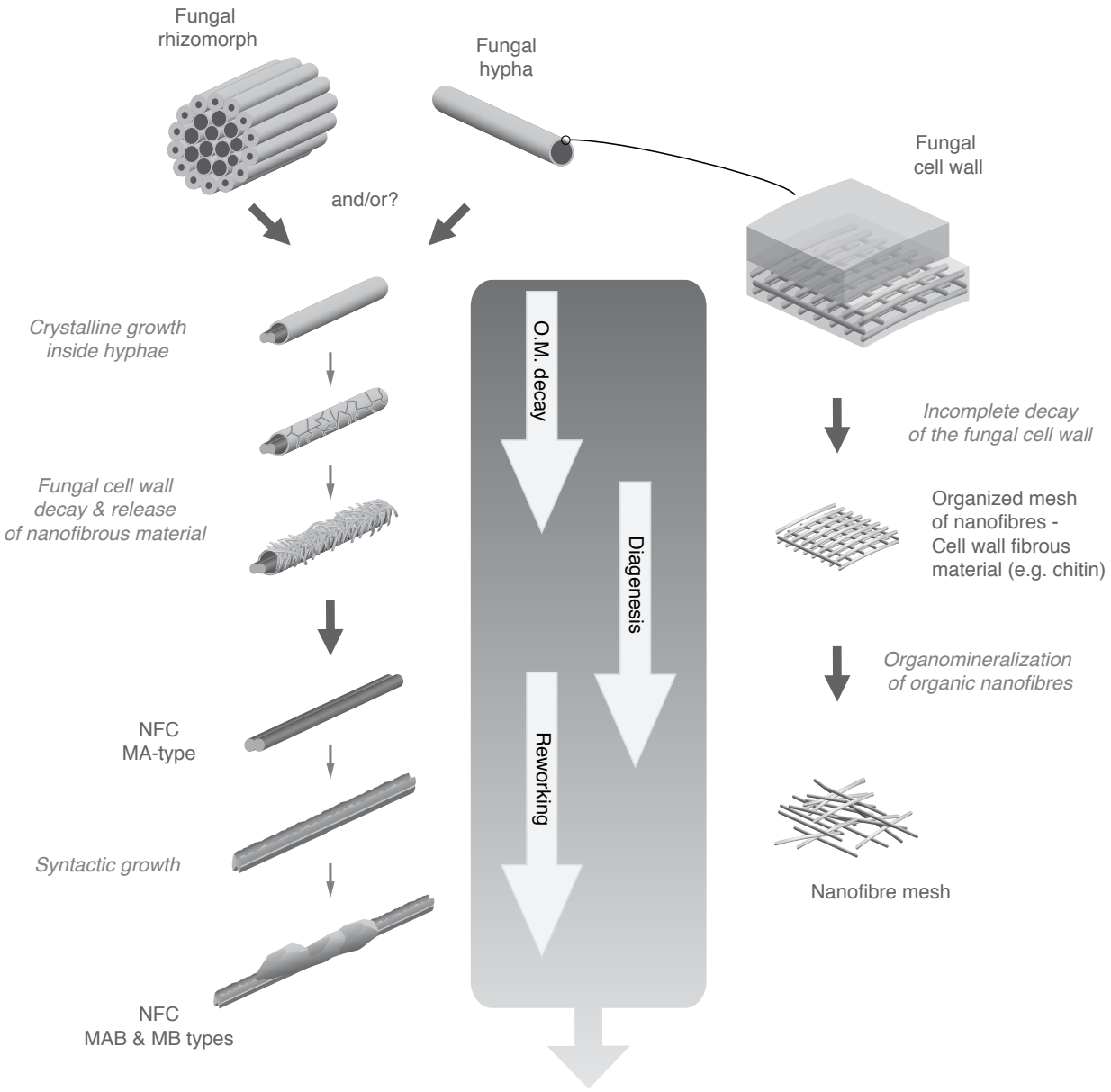
Fungal rhizomorph
Fungal hypha
Fungal cell wall
and/or?
Crystalline growth inside hyphae
Fungal cell wall decay & release of nanofibrous material
NFC MA-type
Syntactic growth
NFC MAB & MB types
O.M. decay
Diagenesis
Reworking
Incomplete decay of the fungal cell wall
Organized mesh of nanofibres - Cell wall fibrous material (e.g. chitin)
Organomineralization of organic nanofibres
Nanofibre mesh

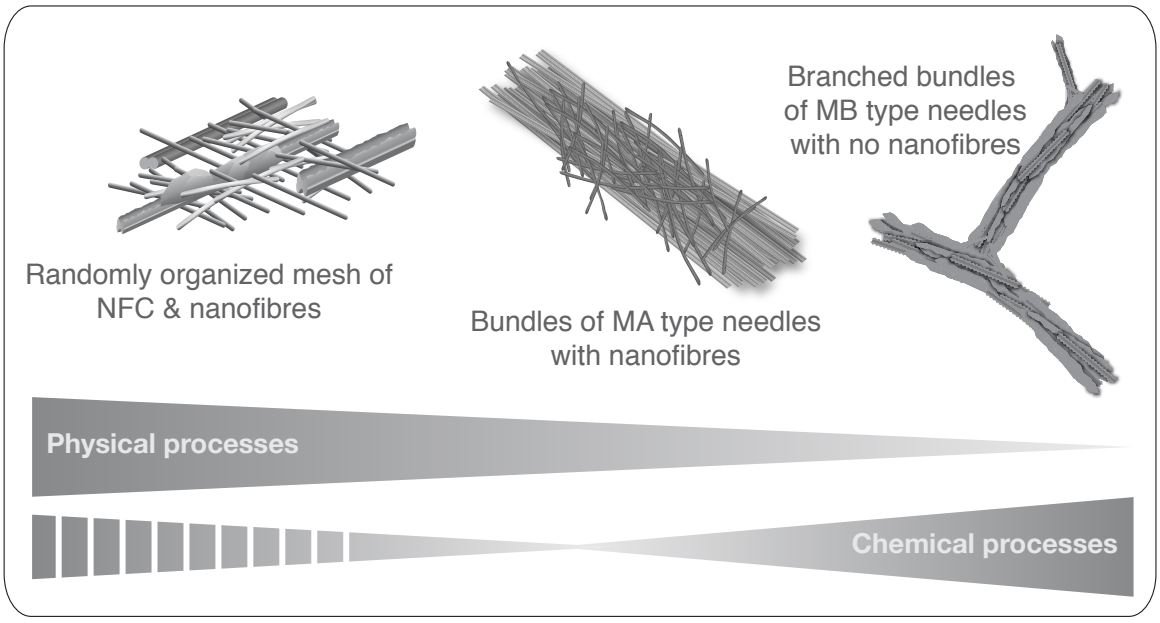
Randomly organized mesh of NFC & nanofibres
Bundles of MA type needles with nanofibres
Branched bundles of MB type needles with no nanofibres
Physical processes
Chemical processes

References

References

Addadi L, Raz S, and Weiner S. 2003. Taking advantage of disorder: amorphous calcium carbonate and its roles in biomineralization. Advanced Materials 12: 959-970.

Adolphe JP. 1972. Obtainment of carbonated incrustations by experimental gel. Comptes rendus hebdomadaires des séances de l'Académie des Sciences Série D 274: 1139-1142.

Ahmad A, Rautaray D, and Sastry M. 2004. Biogenic calcium carbonate: Calcite crystals of variable morphology by the reaction of aqueous Ca^{2+} ions with fungi. Advanced Functional Materials 14: 1075-1080.

Alonso-Zarza AM and Jones B. 2007. Root calcrete formation on quaternary karstic surfaces of Grand Cayman. Geological Acta 5: 77-88.

Amrhein C and Suarez DL. 1987. Calcite supersaturation in soils as a result of organic matter mineralization. Soil Science Society of America Journal 51: 932-937.

Andersen CB. 2002. Understanding carbonate equilibria by measuring alkalinity in experimental and natural systems. Journal of Geoscience Education 50: 389-404.

Arnand RR, Phang C, Wildman JE, and Lintern MJ. 1997. Genesis of some calcretes in the southern Yilgarn Craton, Western Australia: Implications for mineral exploration. Australian Journal of Earth Sciences 44: 87-102.

Aronson JM and Preston RD. 1960. An electron microscopic and x-ray analysis of the walls of selected lower phycomycetes. Proceedings of the Royal Society of London. Series B, Biological Sciences 152: 346-352.

Association française pour l'étude des sols. 2008. Référentiel pédologique. Editions Quae, Versailles. 405 p.

Badger MR and Price GD. 1994. The role of carbonic anhydrase in photosynthesis. Annual Review of Plant Physiology and Plant Molecular Biology 45: 369-392.

Bae HC, Cota-Robles EH, and Casida LE Jr. 1972. Microflora of soils as viewed by transmission electron microscopy. Applied Microbiology 23: 637-648.

Baize D and Jabiol B. 1995. Guide pour la description des sols. INRA, techniques et pratiques. 388 p.

Bajnóczi B and Kovács-Kis V. 2006. Origin of pedogenic needle-fiber calcite revealed by micromorphology and stable isotope composition—a case study of a Quaternary paleosol from Hungary. Chemie der Erde 66: 203-212.

Baker A and Genty D. 1999. Fluorescence wavelength and intensity variations of cave waters. Journal of Hydrology 217: 19-34.

Bartnicki-García S. 1968. Cell wall chemistry, morphogenesis and taxonomy of fungi. Annual Reviews of Microbiology 22: 87-108.

Barton HA, Spear JR, and Pace NR. 2001. Microbial life in the underworld: Biogenicity in secondary mineral formations. Geomicrobiology Journal 18: 359-368.

Barton HA and Northup DE. 2007. Geomicrobiology in cave environments : past, current and future perspectives. Journal of Cave and Karst Studies 69: 163-178.

Beckett A, Heath IB, and McLaughlin DJ. 1974. An atlas of fungal ultrastructure, Longman Group Limited, London. 221p.

Becze-Deák J, Langohr R, and Verrecchia EP. 1997. Small scale secondary $CaCO_3$ accumulations in selected sections of the European loess belt. Morphological forms and potential for paleoenvironmental reconstructions. Geoderma 76:221-252.

Benzerara K, Menguy N, Guyot F, Dominici C, and Gillet P. 2003. Nanobacteria-like calcite single crystals at the surface of the Tataouine meteorite. Proceedings of the National Academy of Sciences of the United States of America 100: 7438-7442.

Benzerara K, Yoon TH, Tyliszczak T, Constantz B, Spormann AM, and Brown GE. 2004. Scanning transmission x-ray microscopy study of microbial calcification. Geobiology 2: 249-259.

Benzerara K, Menguy N, Lopez-Garcia P, Yoon TH, Kazmierczak J, Tyliszczak T, Guyot F, and Brown GE. 2006. Nanoscale detection of organic signatures in carbonate microbialites. Proceedings of the National Academy of Sciences of the United States of America 103: 9440-9445.

Berman A, Hanson J, Leiserowitz L, Koetzle TF, Weiner S, and Addadi L. 1993. Biological control of crystal texture: A widespread strategy for adapting crystal properties to function. Science 259: 776-779.

Bindschedler S, Millière L, Cailleau G, Job D, and Verrecchia EP. 2010. Calcitic nanofibres in soils and caves: A putative fungal contribution to carbonatogenesis. In: Pedley HM and Rogerson M, editors. Tufas and Speleothems – Unravelling the Microbial and physical controls. Geological Society Special Publications 336, London. P 225-238.

Blyth AJ and Frisia S. 2008. Molecular evidence for bacterial mediation of calcite formation in cold high-altitude caves. Geomicrobiology Journal 25: 101-111.

Boquet E, Bordonat A, and Ramos Cormenzana A. 1973. Production of calcite crystals by soil bacteria is a general phenomenon. Nature 246: 527–528.

Borsato A, Frisia S, Jones B, and Van der Borg K. 2000. Calcite moonmilk: crystal morphology and environment of formation in caves in the Italian Alps. Journal of Sedimentary Research 70: 1179-1190.

Boswell GP Jacobs H, Ritz K, Gadd GM, and Davidson FA. 2007. The development of fungal networks in complex environments. Bulletin of mathematical biology 69: 605-634.

Bouma TJ, Nielsen KL, Van Hal J, and Koutstaal B. 2001. Root system topology and diameter distribution of species from habitats differing in inundation frequency. Functional Ecology 15: 360-369.

Bowman SM and Free SJ. 2006. The structure and synthesis of the fungal cell wall. Bioessays 28: 799-808.

Braissant O, Cailleau G, Dupraz C, and Verrecchia EP. 2003. Bacterially induced mineralization of calcium carbonate in terrestrial environments: the role of exopolysaccharides and amino acids. Journal of Sedimentary Research 73: 485-490.

Braissant O, Cailleau G, Aragno M, and Verrecchia EP. 2004. Biologically induced mineralization in the tree *Milicia excelsa* (Moraceae) : its causes and consequences to the environnement. Geobiology 2: 59-66.

Braissant O, Decho AW, Przekop KM, Gallagher KL, Glunk C, Dupraz C, and Visscher PT. 2009. Characteristics and turnover of exopolymeric substances in a hypersaline microbial mat. FEMS Microbiology Ecology 67: 293-307.

Braithwaite CJR. 1980. The petrology of oolitic phosphorites from Esprit (Aldabra), western Indian ocean. Royal Society (London), Philosophal Transactions B288: 511-543.

Bricker OP. 1971. Carbonate cements. The Johns Hopkins Press, Baltimore and London. 376 p.

Bruand A. 1980. Analyses de la superposition de profils en vallée sèche de Champagne Crayeuse. Mémoire de D.E.A de Pédologie, Université Paris 7. 50 p.

Buchalo A, Mykhaylova O, Lomberg M and Wasser S. 2009. Microstructures of vegetative mycelium of macromycetes in pure cultures. Alterpress, Kiev. 224 p.

Buckley HE. 1951. Crystal growth. Wiley & Sons, New York and Chapman & Hall, London. 571 p.

Burazerovic S, Gradinaru J, Pierron J, and Ward R. 2007. Hierarchical self-assembly of one-dimensional streptavidin bundles as a collagen mimetic for the biomineralization of calcite. Angewandte Chemie 46: 1-5.

Burford EP, Kierans M, and Gadd GM. 2003. Geomycology: Fungi in mineral substrata. Mycologist 17: 98-107.

Burford EP, Hillier S, and Gadd GM. 2006. Biomineralization of fungal hyphae with calcite ($CaCO_3$) and calcium oxalate mono- and dihydrate in carboniferous limestone microcosms. Geomicrobiology Journal 23: 599–611.

Burnett JH. 1979. Aspects of the structure and growth of hyphal walls. In: Burnett JH and Trinci APJ, editors. Fungal walls and hyphal growth. British Mycological Society Symposium, Cambridge University Press. P 1–25.

Cacchio P, Contento R, Ercole C, Cappuccio G, Martinez MP, and Lepidi A. 2004. Involvement

of microorganisms in the formation of carbonate speleothems in the Cervo Cave (L'Aquila-Italy). Geomicrobiology Journal 21: 497-509.

Cailleau G. 2005. Carbon cycle and carbonate biomineralization in terrestrial environments : Diagenesis of oxalate-carbonate phases. PhD thesis, Neuchâtel University, Switzerland. 175 p.

Cailleau G, Braissant O, Dupraz C, Aragno M, and Verrecchia EP. 2005. Biologically induced accumulations of $CaCO_3$ in orthox soils of Biga, Ivory Coast. Catena 59: 1-17.

Cailleau G, Dadras M, Abolhassani-Dadras S, Braissant O, and Verrecchia EP. 2009a. Evidence for an organic origin of pedogenic calcitic nanofibres. Journal of Crystal Growth 311: 2490–2495.

Cailleau G, Verrecchia EP, Braissant O, and Emmanuel L. 2009b. The biogenic origin of needle fibre calcite. Sedimentology 56: 1858-1875.

Cailleux A. 1965. Quaternary secondary chemical deposition in France. In: Wright HE and Frey DG, editors. 8th International Quaternary Conference, Denver, Colorado. Geological Society of America, Special Paper 84: 125-139.

Cairney JWG. 1991a. Rhizomorphs: organ of exploration or exploitation? Mycologist 5: 5-10

Cairney JWG. 1991b. Structural and ontogenic study of ectomycorrhizal rhizomorphs. Methods in Microbiology 23: 331-340.

Cairney JWG. 1992. Translocation of solutes in ectomycorrhizal and saprotrophic rhizomorphs. Mycological Research 96: 135-141.

Callot G, Mousain D, and Plassard C. 1985a. Concentrations de carbonate de calcium sur les parois des hyphes mycéliens. Agronomie 5: 143-150.

Callot G, Guyon A, and Mousain D. 1985b. Inter-relations entre aiguilles de calcite et hyphes mycéliens. Agronomie 5: 209-216.

Calvet F and Julia R. 1983. Pisoids in the caliche profiles of Tarragona NE Spain. In: Peryt TM, editor. Coated grains. Springer-Verlag, Berlin. P 456-473.

Canadell J, Jackson RB, Ehleringer JR, Mooney HA, Sala OE, and Schulze ED. 1996. Maximum rooting depth of vegetation types at the global scale. Oecologia 108: 583-595.

Cañaveras JC, Hoyos M, Sanchez-Moral S, Sanz-Rubio E, Bedoya J, Soler V, Groth I, Schuman P, Laiz L, Gonzalez I, and Saiz-Jimenez C. 1999. Microbial communities associated with hydromagnesite and needle-fiber aragonite deposits in a karstic cave (Altamira, Northern Spain). Geomicrobiology Journal 16: 9-25.

Cañaveras JC, Sanchez-Moral S, Sloer S, and Saiz-Jimenez C. 2001. Microorganisms and microbially induced fabrics in cave walls. Geomicrobiology Journal 18: 223-240.

Cañaveras JC, Cuevza S, Sanchez-Moral S, Lario J, Laiz L, Gonzalez JM, and Saiz-Jimenez C. 2006. On the origin of fiber calcite crystals in moonmilk deposits. Naturwissenschaften 93: 27-32.

Carlile MJ, Watkinson SC, and Gooday GW. 2001. The Fungi, 2nd edition. Elsevier Academic Press, London. 588 p.

Carregaro FB, Spanamberg A, Sanches EMC, Argenta JS, Pereira DIB, Zanette R, Santurio JM, de Barcellos DESN, and Ferreiro L. 2010. Fungal microbiota isolated from healthy pig skin. Acta Scientiae Veterinariae 38: 147-153.

Casida LE Jr. 1977. Small cells in pure cultures of *Agromyces ramosus* and in natural soil. Canadian Journal of Microbiology 23: 214-216.

Castanier S, Le Métayer-Levrel G, and Perthuisot JP. 2000. Bacterial roles in the precipitation of carbonates minerals. In: Riding RE and Awramik SM, editors. Microbial sediments. Springer, Berlin. P 32-39.

Chesters CGC and Bull AT. 1963b. The enzymatic degradation of Laminarin. 1. The distribution of laminarinase among micro-organisms. Biochemical Journal 86: 28-31.

Chesters CGC and Bull AT. 1963b. The enzymatic degradation of Laminarin. 2. The multicomponent nature of fungal laminarinase. Biochemical Journal 86: 31-38.

Chesters CGC and Bull AT. 1963c. The enzymatic degradation of Laminarin. 3. Some effects of temperature, pH and various chemical reagents on fungal laminarinase. Biochemical Journal 86: 38-46.

Chirienco M. 2004. The crystalline phase of the carbonate moonmilk: a terminology approach. Acta Carsologica 33: 257-264.

Cojan I and Renard M. 1999. Sédimentologie. Dunod, Paris. 418 p.

Cole L, Orlovich DA, and Ashford AE. 1998. Structure, function, and motility of vacuoles in filamentous fungi. Fungal Genetics and Biology 24: 86-100.

Coleman DC, Crossley DA Jr, and Hendrix PF. 2004. Fundamentals of soil ecology. Elsevier Academic Press, Amsterdam. 386 p.

Costa M, Pecci I, Pensa B, Fontana M, and Cavallini D. 1989. High-performance liquid chromatography of cystathionine, lanthionine and aminoethylcysteine using o-phthaldialdehyde precolumn derivatization. Journal of Chromatography 490: 404–410.

Cromack K Jr, Sollins P, Todd RL, Fogel R, Todd AW, Fender WM, Crossley ME, and Crossley DA Jr. 1977. The role of oxalic acid and bicarbonate in calcium cycling by fungi and bacteria : some possible implications for soil animals. Soil Organisms as Components of Ecosystems. Ecology Bulletin, Stockholm 25: 246-252.

Cromme P, Zollfrank C, Muller L, Muller FA, and Greil P. 2007. Biomimetic mineralisation of apatites on Ca^{2+} activated cellulose templates. Materials Science & Engineering C-Biomimetic and Supramolecular Systems 27: 1-7.

Cunningham KI, Northup DE, Pollastro RM, Wright WG, and LaRock EJ. 1995. Bacteria, fungi and biokarst in Lechuguilla Cave, Carlsbad Caverns National Park, New Mexico. Environmental Geology 25: 2-8.

Curry MD, Boston PJ, Spilde MN, Baichtal JF, and Campbell AR. 2009. Cottonballs, a unique subaqeous moonmilk, and abundant subaerial moonmilk in Cataract Cave, Tongass National Forest, Alaska. International Journal of Speleology 38: 111-128.

Dalas E, Klepetsanis PG, and Koutsoukos PG. 2000. Calcium carbonate deposition on cellulose. Journal of colloid and interface science 224: 56-62.

Dalias P, Kokkoris GD, and Troumbis AY. 2003. Functional shift hypothesis and the relationship between temperature and soil carbon accumulation. Biology and Fertility of Soils 37: 90-95.

de Boer W, Folman LB, Summerball RC, and Boddy L. 2005. Living in a fungal world: impact of fungi on soil bacterial niche development. FEMS Microbiology Reviews 29: 795-811.

Défarge C. 2011. Organomineralization. In: Reitner J and Volker T, editors. Encyclopedia of Geobiology. Springer, Heidelberg. P 697-701.

Dey S, Basu Baul TS, Roy B, and Dey D. 1989. A new rapid method of air-drying for scanning electron microscopy using tetramethylsilane. Journal of microscopy 156: 259-261.

Dix NJ and Webster J. 1995. Fungal ecology. Chapman & Hall, London. 549 p.

Dubroeucq D, Geissert D, and Roger P. 1996. Pine root-induced petrocalcic horizons in volcanic ash soils of the Mexican altiplano. Memorias del III Simposio Internacional sobre Suelos volcanicos endurecidos. Quito, diciembre 1996. P 98-106.

Ducloux J, Butel P, and Dupuis T. 1984. Microséquence minéralogique des carbonates de calcium dans une accumulation carbonatée sous galets calcaires dans l'Ouest de la France. Pédologie 34: 161-177.

Dupraz C, Visscher PT, Baumgartner LK, and Reid RP. 2004. Microbe-mineral interactions: early carbonate precipitation in a hypersaline lake (Eleuthera Island, Bahamas). Sedimentology 51: 745-765.

Dupraz C, Reid RP, Braissant O, Decho AW, Norman RS, and Visscher PT. 2009. Processes of carbonate precipitation in modern microbial mats. Earth-Science Reviews 96: 141-162.

Durand R. 1980. L'évolution d'une rendzine encroûtée sur la craie de Champagne. Association Française d'Etude des Sols, Bulletin, Science du Sol 3: 201-216.

Dykstra MJ and Reuss LE. 2003. Biological Electron Microscopy, 2nd edition. Kluwer Academic / Plenum Publisher, New York. 534 p.

Ehlers J and Gibbard PL. 2004. Quaternary glaciations - extent and chronology. Part I: Europe. Developments in Quaternary science 2. Rose J, editor. Elsevier, Amsterdam. 475 p.

Ehrlich H. 2002. Geomicrobiology. Marcel Dekker Inc, New York. 768 p.

Ehrlich H. 2010. Chitin and collagen as universal and alternative templates in biomineralization. International Geology review 52: 661-699.

Ekblad A and Näsholm T. 1996. Determination of chitin in fungi and mycorrhizal roots by an improved HPLC analysis of glucosamine. Plant and Soil 178: 29-35.

Ekblad A, Wallander H, and Näsholm T. 1998. Chitin and ergosterol combined to measure total and living fungal biomass in ectomycorrhizas. New Phytologist 138: 143-149.

Fan PP and Guo DL. 2010. Slow decomposition of lower order roots: a key mechanism of root carbon and nutrient retention in the soil. Oecologia 163: 509-515.

Farkaš V. 1979. Biosynthesis of cell-walls of fungi. Microbiological Reviews 43: 117-144.

Farkaš V. 2003. Structure and biosynthesis of fungal cell walls: Methodological approaches. Folia Microbiologica 48: 469-478.

Finlay RD and Söderström B. 1992. Mycorrhiza and carbon flow to the soil. In: Allen M, editor. Mycorrhizal functioning: an integrative plant-fungal process. Chapman and Hall, London, UK. P 134-160.

Folk RL. 1993. SEM imaging of bacteria and nannobacteria in carbonate sediments and rocks. Journal of Sedimentary Petrology 63: 990-999.

Folk RL and Lynch FL. 2001. Organic matter, putative nannobacteria and the formation of ooids and hardgrounds. Sedimentology 48: 215-229.

Fomina M, Hillier S, Charnock JM, Melville K, Alexander IJ, and Gadd GM. 2005a. Role of oxalic acid overexcretion in transformation of toxic metal minerals by *Beauveria caledonica*. Applied and Environmental Microbiology 71: 371-381.

Fomina MA, Alexander IJ, Colpaert JV, and Gadd GM. 2005b. Solubilization of toxic metal minerals and metal tolerance of mycorrhizal fungi. Soil Biology & Biochemistry 37: 851-866.

Fomina M, Podgorsky VS, Olishevska SV, Kadoshnikov VM, Pisanska IR, Hillier S, and Gadd GM. 2007. Fungal deterioration of barrier concrete used in nuclear waste disposal. Geomicrobiology Journal 24: 643-653.

Fomina M, Burford EP, Hillier S, Kierans M, and Gadd GM. 2010. Rock-building fungi. Geomicrobiology Journal 27: 624-629.

Fontaine T, Mouyna I, Hartland RP, Paris S, and Latgé JP. 1997. From the surface to the inner layer of the fungal cell wall. Biochemical Society Transactions 25: 194-199.

Furlan L, de Fávere VT, and Laranjeira MCM. 1996. Adsorption of calcium ions by graft copolymer of acrylic acid on biopolymer. Polymer 37: 843-846.

Gadd GM. 1993. Interactions of fungi with toxic metals. New Phytologist 124: 25-60.

Gadd GM. 1999. Fungal production of citric and oxalic acid: Importance in metal speciation, physiology and biogeochemical processes. Advances in Microbial Physiology 41: 47–92.

Gadd GM. 2006. Fungi in biogeochemical cycles. Cambridge University Press. 469 p.

Gadd GM. 2007. Geomycology: biogeochemical transformations of rocks, minerals, metals and radionuclides by fungi, bioweathering and bioremediation. Mycological Research 111: 3-49.

Giesler R, Lundstrom US, and Grip H. 1996. Comparison of soil solution chemistry assessment using zero-tension lysimeters or centrifugation. European Journal of Soil Science 47: 395-405.

Gillet P, Barrat JA, Heulin T, Achouak W, Lesourd M, Guyot F, and Benzerara K. 2000. Bacteria in the Tatahouine meteorite: nanometric-scale life in rocks. Earth and Planetary Science Letters 175 : 161-167.

Giraud-Guille MM, Belamie E, and Mosser G. 2004. Organic and mineral networks in carapaces, bones and biomimetic materials. Comptes Rendus Palevol 3 : 503-513.

Gobat J-M, Aragno M, and Matthey W. 2003. Le sol vivant, 2ème édition. Presses polytechniques et universitaires romandes, Lausanne. 568 p.

Gradziński M, Szulc J, and Smyk B. 1997. Microbial agents of moonmilk calcification. Proceedings of the 12th International Congress of Speleology 1: 275-278.

Guggenberger G, Frey SD, Six J, Paustian K, and Eliott ET. 1999. Bacterial and fungal cell-wall residues in conventional and no-tillage agroecosystems. Soil Science Society of America Journal 63: 1188-1198.

Harrison RS. 1977. Caliche profiles: indicator of nearsurface subaerial diagenesis, Barbados West Indies. Bulletin of Canadian Petroleum Geology 25: 123-173.

Hasinger O. 2009. Etude du cycle du carbone dans un sol carbonaté sous une végétation de type C3: Du CO_2 atmosphérique aux carbonates pédogéniques. Travail de Master, Biogéosciences, Université de Neuchâtel et Université de Lausanne. 84 p.

Hill CA and Forti P. 1997. Cave minerals of the world, 2nd edition. National Speleological Society, Huntsville, AL. 463 p.

Hishi T. 2007. Heterogeneity of individual roots within the fine root architecture: causal links between physiological and ecosystem functions. Journal of Forest Research 12: 126-133.

Hoffland E, Kuyper TW, Wallander H, Plassard C, Gorbushina AA, Haselwandter K, Holmstrom S, Landeweert R, Lundstrom US, Rosling A, Sen R, Smits MM, van Hees PAW, and Breemen N. 2004. The role of fungi in weathering. Frontiers in Ecology and the Environment 2: 258-264.

Homeijer SJ ,Olszta MJ ,Barrett RA, and Gower LB. 2008. Growth of nanofibrous barium carbonate on calcium carbonate seeds. Journal of Crystal Growth 310: 2938-2945.

Houghton RA. 2003. The contemporary carbon cycle. In: Holland HD and Turekian KK, editors. Treatise on geochemistry, volume 8, Biogeochemistry. Elsevier, Amsterdam. P 473-513.

Hunsley D and Burnett JH 1970. Ultrastructural architecture of walls of some hyphal fungi. Journal of General Microbiology 62: 203-218.

IUSS Working Group WRB. 2006. World references base for resources 2006. 2nd edition. World Soil Ressources Reports No. 103, FAO Rome. 132 p.

Iwanoff LL. 1906. Ein Wasserhaltiges Calcium Carbonat Aussen Umbegung von Nowo-Alexandria (guv. Lublin). Annalen der Geologie und Mineralogie der Russland 8: 23-25.

Jackson SL and Heath IB. 1993. Roles of calcium ions in hyphal tip growth. Microbiological Reviews 57: 367-382.

Jackson RB, Moore LA, Hoffmann WA, Pockman WT, and Linder CR. 1999. Ecosystem rooting depth determined with caves and DNA. Proceedings of the National Academy of Sciences of the United States of America 96: 11387-11392.

James NP. 1972. Holocene and Pleistocene calcareous crust (caliche) profiles: criteria for subaerial exposure. Journal of Sedimentary Research 42: 817-836.

Jasinska EJ, Knott B, and McComb AJ. 1996. Root mats in ground water: A fauna-rich cave habitat. Journal of the North American Benthological Society 15 : 508-519.

Jeong GY and Chun YS. 2006. Nanofiber calcite in Asian dust and its atmospheric roles. Geophysical Research Letters 33 (24): L24802, doi: 10.1029/2006GL028280.

Jones B. 2001. Microbial activity in caves - a geological perspective. Geomicrobiology Journal 18: 345–357.

Jones B. 2010. Microbes in caves: agents of calcite corrosion and precipitation. In: Pedley HM and Rogerson M, editors. Tufas and Speleothems – Unravelling the Microbial and physical controls. Geological Society Special Publications 336, London. P 7-30.

Jones B and Khale CF. 1993. Morphology, relationship, and origin of fiber and dentrite calcite crystals. Journal of Sedimentary Research 63: 1018-1031.

Jones B and Ng K-C. 1988. The structure and diagenesis of rhizoliths from Cayman Brac, British West Indies. Journal of Sedimentary Petrology 58: 457-467.

Jones D. 1970. Ultrastructure and composition of cell walls of *Sclerotinia sclerotiorum*. Transactions of the British Mycological Society, 54, 351-360.

Jones PCT and Mollison JE. 1948. A technique for the quantitative estimation of soil microorganisms. Journal of General Microbiology 2: 54-69.

Jongmans AG, van Breemen N, Lundström U, van Hess PAW, Finlay RD, Srinivasan M, Unestam T, Giesler R, Melkerund P-A, and Olsson M. 1997. Rock-eating fungi. Science 389: 682-683.

Jurado V, Porca E, Cuezva S, Fernandez-Cortes A, Sanchez-Moral S, and Saiz-Jimenez C. 2010. Fungal outbreak in a show cave. Science of the Total Environment 408: 3632-3638.

Khormali F, Abtahi A, and Stoops G. 2006. Micromorphology of calcitic features in highly calcareous soils of Fars Province, Southern Iran. Geoderma 132: 31-46.

Kieft TL. 2000. Size matters: Dwarf cells in soil and subsurface terrestrial environments. In: Colwell RR and Grimes DJ, editors. Nonculturable microorganisms in the environment. ASM Press, Washington DC. P 19–47.

Kirk PM, Cannon PF, Minter DW, and Stalpers JA Ashton H. 2008. Ainsworth & Bisby's dictionary of the fungi, 10th edition. CABI Europe-UK, Wallingford CT. 771 p.

Klamer M and Bååth E. 2004. Estimation of conversion factors for fungal biomass determination in compost using ergosterol and PLFA 18:2w6,9. Soil Biology & Biochemistry 36: 57–65.

Klappa CF. 1979. Calcified filaments in Quaternary calcretes: Organo-mineral interactions in the subaerial vadose environment. Journal of Sedimentary Petrology 49: 955-968.

Klappa CF. 1980. Rhizoliths in terrestrial carbonates: classification, recognition, genesis and significance. Sedimentology 27: 613-629.

Klein DA and Paschke MW. 2004. Filamentous fungi: the inderterminate lifestyle and microbial ecology. Microbial Ecology 47: 224-235.

Ko WH and Lockwood JL. 1970. Mechanism of lysis of fungal mycelia in soil. Phytopathology 60: 148-154.

Kolo K, Keppens E, Préat A, and Claeys P. 2007. Experimental observations on fungal diagenesis of carbonate substrates. Journal of Geophysical Research 112: 1-20.

Kubiëna WL. 1938. Micropedology. Collegiate Press, Ames, Iowa. 235 p.

Krsek M and Wellington MH. 2001. Assessment of chitin decomposer diversity within an upland grassland. Antonie van Leeuwenhoek 79: 261-267.

Lacroix A. 1901. Minéralogie de la France et de ses anciens Territoires d'Outre-Mer, volume 3. Librairie A. Blanchard, Paris. 816 p.

Lal R and Kimble JM. 2000. Pedogenic carbonates and the global carbon cycle. In: Lal R, Kimble JM, Eswaran H, and Stewart BA, editors. Global climate change and pedogenic carbonates. Lewis Publishers, Boca Raton. P 1-14.

Lal R, Kimble JM, Eswaran H, and Stewart BA. 2000. Global climate change and pedogenic carbonates. Lewis Publishers, Boca Raton. 305 p.

Langley JA and Hungate BA. 2003. Mycorrhizal controls on belowground litter quality. Ecology 84: 2302-2312.

Larsen T, Axelsen J, and Ravn HW. 2004. Simplified and rapid method for extraction of ergosterol from natural samples and detection with quantitative and semi-quantitative methods using thin-layer chromatography. Journal of Chromatography A 1026: 301-304.

Latgé J-P. 2003. Activity Reports, Institut Pasteur, Paris. World Wide Web Address: http://www.pasteur.fr/recherche/RAR/RAR2003/print/Aspergil-en.html.

Leake JR, Duran AL, Hardy KE, Johnson I, Beerling DJ, Banwart SA, and Smits MM. 2008. Biological weathering in soil: the role of symbiotic root-associated fungi biosensing minerals and directing photosynthate-energy into grain-scale mineral weathering. Mineralogical Magazine 72: 85-89.

Lebron I and Suarez DL. 1998. Kinetics and mechanisms of precipitation of calcite as affected by pCO_2 and organic ligands at 25°C. Geochimica et Cosmochimica Acta 62: 405-416.

Lindhal BD and Olsson S. 2004. Fungal translocation – creating and responding to environmental heterogeneity. Mycologist 18: 79-88.

Loisy C, Verrecchia EP, and Dufour P. 1999. Microbial origin for pedogenic micrite associated with a carbonate palaeosol (Champagne, France). Sedimentary Geology 126: 193-204.

Longman MW. 1980. Carbonate diagenetic textures from nearsurface diagenetic environements. American Association of Petroleum Geologists bulletin 64: 461-487.

Lowenstam HA and Weiner S. 1989. On biomineralization. Oxford University Press, New York. 324 p.

Loste E, Wilson RM, Seshadri R, and Meldrum FC. 2003. The role of magnesium in stabilising amorphous calcium carbonate and controlling calcite morphologies. Journal of Crystal Growth 254: 206-218.

Magnuson JK and Lasure LL. 2004. Organic acid production by filamentous fungi. In: Lange J and L, editors. Advances in fungal biotechnology for industry, agriculture and medicine. Kluwer Academic/Plenum Publisher, New York. P 307-340.

Maniloff J. 1997. Nannobacteria: Size limits and evidence. Science 276: 1776-1776.

Mann S. 2000. The chemistry of form. Angewandte Chemie. 39 : 3392-3406.

Mann S. 2001. Biomineralization, principles and concepts in bioinorganic materials and chemistry. Oxford University Press, Oxford. 198 p.

Manoli F, Koutsopoulos S, and Dalas E. 1997. Crystallization of calcite on chitin. Journal of Crystal Growth 182: 116-124.
Marx DH and Bryan WC. 1971. Influence of ectimycorrhizae on survival and growth of aseptic seedlings of loblolly pine at high temperature. Forest Science 17: 37-41.

Masaphy S, Zabari L, Pastrana J, and Dultz S. 2009. Role of fungal mycelium in the formation of carbonate concretions in growing media - An investigation by SEM and synchrotron-based x-ray tomographic microscopy. Geomicrobiology Journal 26: 442-450.

Mayewski PA, Rohling EE, Stager JC, Karlén W, Maasch KA, Meeker LD, Meyerson EA, Gasse F, van Kreveld S, Holmgren K, Lee-Thorp J, Rosqvist G, Rack F, Staubwasser M, Schneider RR, and Steig EJ. 2004. Holocene climate variability. Quaternary Research 62: 23-255.

Mc Quarrie DA and Rock PA. 1992. General chemistry, 3rd edition. De Boeck, Bruxelles. 1083 p.

Millière L, Hasinger O, Bindschedler S, Cailleau G, Spangenberg JE, and Verrecchia EP. 2011. Stable carbon and oxygen isotope signatures of pedogenic needle fibre calcite. Geoderma 161: 74-87.

Moore GW. 1952. Speleothem - a new cave term. National Speleological Society News, 10: 2.

Morse JW and Mackenzie FT. 1990. Geochemistry of sedimentary carbonates. Elsevier, Amsterdam. 707 p.

Mügge O. 1914. Über die Lublinit genannte, augeblich neue Modification des kohlensauren Kalkes. Zentralblatt für Mineralogie, Geologie und Paläontologie 1914: 673–675.

Nannipieri P, Ascher J, Ceccherini MT, Landi L, Pietramellara G, and Renella G. 2003. Microbial diversity and soil functions. European Journal of Soil Science 54: 655-670.

Newell SY. 1992. Estimating fungal biomass and productivity in decomposing leaf litter. In: Carrol GC and Wicklow DT, editors. The fungal community: Its organization and role in the ecosystem, 2nd edition. Marcel Dekker, New York. P 521– 561.

Newman BD, Norman DI, Gundimeda M, and Levy S. 1996. Understanding the genesis of nonmarine calcite deposits through quadrupole mass spectrometric analysis of fluid inclusion gases. Chemical Geology 132: 205-213.

Newman BD, Campbell AR, Norman DI, and Ringelberg DB. 1997. A model for microbially induced precipitation of vadose-zone calcites in fractures at Los Alamos, New Mexico, USA. Geochimica and Cosmochimica Acta 61: 1783-1792.

Northup DE and Lavoie KH. 2001. Geomicrobiology of caves: A Review. Geomicrobiology Journal 18: 199-222.

Olstza MJ, Gajjeraman S, Kaufman M, and Gower LB. 2004. Nanofibrous calcite synthesized via a solution-precursor-solid mechanism. Chemistry of Materials 16: 2355-2362.

Ould Mohamed S and Bruand A. 1994. Morphology and origin of secondary calcite in soils from Beauce, France. In: Ringrose-Voase AJ and Humphreys GS, editors. Soil micromorphology : Studies in management and genesis, Proceedings of the IX International Working Meeting on Soil Micromorphology, Townsville, Australia, July 1992. Developments in Soil Science 22. Elsevier, Amsterdam. P 27-36.

Pareek M, Cole L, and Ashford AE. 2001. Variations in structure of aerial and submerged rhizomorphs of *Armillaria luteobubalina* indicate that they may be organs of absorption. Mycological Research 11: 1377-1387.

Paul EA. 2007. Soil Microbiology, ecology and biochemistry, 3rd edition. Academic Press, San Diego. 340 p.

Paul EA and Clark FE. 1996. Soil Microbiology and Biochemistry, 2nd edition. Academic Press, San Diego. 340p.

Pearson VK, Kearsley AT, and Sephton MA. 2004. The in-situ detection of organic material in extraterrestrial samples. Microscopy and Analysis 18: 5-8.

Perry RS, Mcloughlin N, Lynne BY, Sephton MA, Oliver JD, Perry CC, Campbell K, Engel MH, Farmer JD, Brasier MD, and Staley JT. 2007. Defining biominerals and organominerals: direct and indirect indicators of life. Sedimentary Geology 201: 157–179.

Pessoni RAB, Freshour G, Figueiredo-Ribeiro RL, Hahn MG, and Brage MR. 2005. Cell-wall structure and composition of *Penicillium janczewskii* as affected by inulin. Mycologia 97: 304-311.

Phillips SE and Self PG. 1987. Morphology, crystallography and origin of needle-fibre calcite in Quaternary pedogenic calcretes of South Australia. Australian Journal of Soil Research 25: 429-444.

Phillips SE, Milnes AR, and Foster RC. 1987. Calcified filaments: an example of biological influences in the formation of calcrete in South Australia. Australian Journal of Soil Research 25: 405-428.

Pitt D and Ugalde UO. 1984. Calcium in fungi. Plant Cell and Environment 7: 467-475.

Pouget M and Rambaud D. 1980. Quelques types de cristallisation de calcite dans les sols à croûte calcaire (steppes algériennes). Apport de la microscopie électronique. In: Cristallisation-Déformation-Dissolution des carbonates, Univeristé de Bordeaux III, Institut de Géodynamique. P 371-380.

Pregitzer KS, De Forest JL, Burton AJ, Allen MF, Ruess RW, and Hendrick RL. 2002. Fine root architecture of nine North American trees. Ecological Monographs 72: 293-309.

Prescott LM, Harley JP, and Klein DA. 2003. Microbiologie, 2ème édition française. De Boeck Université, Bruxelles. 1164p.

Prosser JI and Trinci APJ. 1979. A model for hyphal growth and branching. Journal of General Microbiology 111: 153-164.

Rapp P. 1989. 1,3-β-Glucanase, 1,6-β-Glucanase and β-Glucosidase activities of *Sclerotium glucanicum*: Synthesis and properties. Journal of General Microbiology 135: 2847-2858.

Richter DK and Niggemann S. 1995. Calcitnadeln in der Hüttenbläserschachthöhle bei Iserlohn (Nordrhein-Westfalen). Speleog. Jb. 1994: 25–32.

Richter DK, Immenhauser A, and Neuser RD. 2008. Electron backscatter diffraction documents randomly orientated c-axes in moonmilk calcite fibres: Evidence for biologically induced precipitation. Sedimentology 55: 487-497.

Rizzo DM, Blanchette RA, and Palmer MA. 1992. Biosorption of metal ions by *Armillaria* rhizomorphs. Canadian Journal of Botany 70: 1515–1520.

Rosas ÁL, Nosanchuk JD, Gómez BL, Edens WA, Henson JM, and Casadevall A. 2000. Isolation and serological analyses of fungal melanins. Journal of Immunological Methods 244: 69-80.

Ruiz-Herrera J. 1992. Fungal cell wall: structure, synthesis and assembly. CRC Press, Boca Raton, Florida. 256 p.

Ruiz-Herrera J, Leon CG, Carabez-Trejo A, and Reyes-Salinas E. 1996. Structure and chemical composition of the cell walls from the haploid yeast and mycelial forms of *Ustilago maydis*. Fungal Genetics and Biology 20: 133-142.

Sands D. 1993. Introduction to crystallography. Dover Publications, New York. 165 p.

Santamaria F and Reyes F. 1988. Proteases produced during autolysis of filamentous fungi. Transactions of the British Mycological Society 91: 217-220.

Sarbu SM, Kane TC, and Kinkle BK. 1996. A chemoautotrophically based cave ecosystem. Science 272: 1953–1955.

Schilling JS and Jellison J. 2005. Oxalate regulation by two brown rot fungi decaying oxalate-amended and non-amended wood. Holzforschung 59: 681-688.

Schlesinger WH, Palmer Winkler J, and Megonigal JP. 2000. Soils and the global carbon cycle. In: Wigley TML and Schimel DS, editors. The carbon cycle. Cambridge University Press, Cambridge. P 91-114.

Schultze-Lam S, Fortin D, Davis BS, and Beveridge TJ. 1996. Mineralization of bacterial surfaces. Chemical Geology 132: 171-181.

Schütte KH. 1956. Translocation in the fungi. New Phytologist 55: 164-182.

Shankar N and Achyuthan H. 2007. Genesis of calcic and petrocalcic horizons from Coimbatore, Tamil Nadu : Micromorphology and geochemical studies. Quaternary International 175: 140-154.

Shen YH, Xie AJ, Yang YM, Huang FZ, Chen L, and Huang JT. 2007. Growth of calcium bilirubinate crystal controlled by functional polymer. Reactive and Functional Polymers 67: 241-246.

Simkiss K. 1986. The process of biomineralization in lower plants and animals-an overview. In: Landbeater BSC and Riding R, editors. Biomineralization in lower plants and animals, Systematics Association Special Volume 30. Clarendon, Oxford. P 19-37.

Simkiss K and Wilbur KM. 1989. Biomineralization, cell biology and mineral deposition. Academic Press Inc, San Diego, 337 p.

Simoneit BRT. 2005. A review of current applications of mass spectrometry for biomarker/molecular tracer elucidations. Mass Spectrometry Reviews 24: 719-765.

Sinsabaugh RL, Lauber CL, Weintraub MN, Ahmed B, Allison SD, Crenshaw C, Contosta AR, Cusack D, Frey S, Gallo ME, Gartner TB, Hobbie SE, Holland K, Keeler BL, Powers JS, Stursova M, Takacs-Vesbach C, Waldrop MP, Wallenstein MD, Zak DR, and Zeglin LH. 2008. Stoichiometry of soil enzyme activity at global scale. Ecology Letters 11: 1252-1264.

Skinner HCW. 2005. Biominerals. Mineralogical Magazine 69: 621-641.

Smith SE and Read DJ. 1997. Mycorrhizal symbiosis, 2nd edition. Academic Press, Amsterdam. 605 p.

Steinen P. 1974. Phreatic and vadose diagenetic modification of Pleistocene limestone: petrographic observations from the subsurface of Barbados, West Indies. American Association of Petroleum Geologists bulletin 58: 1008-1024.

Sterflinger K. 2000. Fungi as geologic agents. Geomicrobiology Journal 17:97-124.

Stoops GJ. 1976. On the nature of “lublinite” from Hollanta (Turkey). American Mineralogist 61: 172.

Stoops G. 2003. Guidelines for the analysis and description of soil and regolith thin sections. Soil Science Society of America Inc, Madison, Wisconsin, USA. 184 p.

Strong GE, Giles JRA, and Wright VP. 1992. A Holocene calcrete from North Yorkshire, England: Implications for interpreting palaeoclimates using calcretes. Sedimentology 39: 333-347.

Stumm W and Morgan JJ. 1996. Aquatic chemistry: Chemical equilibria and rates in natural waters, 3rd edition. John Wiley & Sons Inc, New York. 1022 p.

Stumm W. 1992. Chemistry of the solid-water interface: Processes at the mineral-water and particle-water interface in natural systems. John Wiley & Sons Inc, New York. 428 p.

Suarez DL, Wood JD, and Ibrahim I. 1992. Reevaluation of calcite supersaturation in soils. Soil Science Society of America Journal 56: 1776-1784.

Supko PR. 1971. “Whisker” crystal cement in a Bahamian rock. In: Bricker OP, editor. Carbonate Cements. John Hopkins University, Studies in Geology 19: 143-146.

Thompson W. 1984. Distribution, development and fuctionning of mycelial cord systems of decomposer basidiomycetes of the deciduous woodland floor. In: Jennings DH and Rayner ADM, editors. The ecology and physiology of the fungal mycelium. British Mycological Society Symposium. Cambridge University Press, Cambridge. P 185-214.

Timonen S and Marschner P. 2006. Mycorrhizosphere concept. In: Mukerji KG, Manoharachary C and Singh J, editors. Microbial Activity in the Rhizosphere (Soil Biology, Volume 7). Springer-Verlag, Berlin-Heidelberg. P 155-172.

Trichet J and Défarge C. 1995. Non-biologically supported organomineralization. Bulletin de l’Institut Océanographique (Monaco), Numéro Spécial 14, 203–236.

Trinci APJ. 1979. The duplication cycle and branching in fungi. In: Burnett JH and Trinci APJ, editors. Fungal walls and hyphal growth. British Mycological Society Symposium. Cambridge University Press, Cambridge. P 93-113.

Trinci APJ. 1984. Regulation of hyphal branching and hyphal orientation. In: Jennings DH and Rayner ADM, editors. The ecology and physiology of the fungal mycelium. British Mycological Society Symposium. Cambridge University Press, Cambridge. P 23-52.

Turner BL. 2010. Variation in pH optima of hydrolytic enzyme activities in tropical Rainforest soils. Applied and Environmental Microbiology 76: 6485-6493.

Turner BR and Makhlouf I. 2005. Quaternary sandstones, northeast Jordan: Age, depositional environments and climatic implications. Palaeogeography Palaeoclimatology Palaeoecology 229: 230-250.

Turner EC and Jones B. 2005. Microscopic calcite dendrites in cold-water tufa: implications for nucleation of micrite and cement. Sedimentology 52: 1043-1066.

van Beynen P, Bourbonniere R, Ford D, and Schwarcz H. 2001. Causes of colour and fluorescence in speleothems. Chemical Geology 175: 319-341.

van Schöll L, Kuyper TW, Smits MM, Landeweert R, Hoffland E, and van Breemen N. 2008. Rock-eating mycorrhizas: their role in plant nutrition and biogeochemical cycles. Plant and Soil 303: 35-47.

Vergès V, Madon M, Bruand A, and Bocquier G. 1982. Morphologie et crystallogenèse de monocristaux supergènes de calcite en aiguilles. Bulletin of Mineralogy 105: 351-356.

Verrecchia EP. 1990. Litho-diagenetic implications of the calcium oxalate-carbonate biogeochemical cycle in semiarid calcretes, Nazareth, Israel. Geomicrobiology Journal 8: 87-99.

Verrecchia EP. 2000. Fungi and sediments. In: Riding RE and Awramik SM, editors. Microbial Sediments. Springer-Verlag, Berlin-Heidelberg. P 69–75.

Verrecchia EP, Dumont J-L, and Rolko KE. 1990. Do fungi building limestones exist in semi-arid regions? Naturwissenschaften 77: 584-586.

Verrecchia EP, Dumont J-L, and Verrecchia KE. 1993. Role of calcium-oxalate biomineralization by fungi in the formation of calcretes – a case-study from Nazareth, Israel. Journal of Sedimentary Petrology 63: 1000-1006.

Verrecchia EP and Verrecchia KE. 1994. Needle fiber calcite: a critical review and a proposed classification. Journal of Sedimentary Research 64: 650-664.

Verrecchia EP and Dumont J-L. 1996. A biogeochemical model for chalk alteration by fungi in semiarid environments. Biogeochemistry 35: 447-470.

Visscher PT and Stolz JF. 2005. Microbial mats as bioreactors: populations, processes and products. Palaeogeography, Palaeoclimatology, Palaeoecology 219: 87–100.

Wagner M. 2009. Single-cell ecophysiology of microbes as revealed by Raman microspectroscopy or Secondary Ion Mass Spectrometry Imaging. Annual Review of Microbiology 63: 411-429.

Wainwright SA. 1963. Skeletal organization in coral, *Pocillopora damicornis*. Quarterly Journal of Microscopical Science 104(2): 169-183.

Wallander H, Johansson L, and Pallon J. 2002. PIXE analysis to estimate the elemental composition of ectomycorrhizal rhizomorphs grown in contact with different minerals in forest soil. FEMS Microbiology Ecology 39: 147-156.

Watkinson SC. 1979. Growth of rhizomorphs, mycelial strands, coremia and sclerotia. In: Burnett JH and Trinci APJ, editors. Fungal walls and hyphal growth. British Mycological Society Symposium. Cambridge University Press, Cambridge. P 93-113.

Watkinson SC. 1984. Morphogenesis of the *Serpula lacrimans* colony in relation to its function in nature. In: Jennings DH and Rayner ADM, editors. The ecology and physiology of the fungal mycelium. British Mycological Society Symposium. Cambridge University Press, Cambridge. P 165-184.

Webster J. 1980. Introduction to Fungi, 2nd edition. Cambridge University Press, 669 p.

Weete JD. 1980. Lipid biochemistry of fungi and other organisms. Plenum Press, New York. 388 p.

Weiner S and Dove PM. 2003. Overview of biomineralization processes and the problem of the vital effect. In: Dove PM, De yoreo JJ and Weiner S, editors. Biomineralization. Mineralogical Society of America, Washington DC. P 1-29.

Went FW. 1969. Fungi associated with stalactite growth. Science 166: 385-386.

Whitney KD. 1989. Systems of biomineralization in the fungi. In: Crick RE, editor. Origin, evolution and modern aspects of biomineralization in plants and animals. Plenum Press, New York. P 433-441.

Wollast R. 1971. Kinetic aspects of the nucleation and growth of calcite from aqueous solutions. In: Bricker OP, editor. Carbonate cements. The Johns Hopkins Press, Baltimore and London. P 264-273.

Wright VP. 1984. The significance of needle fiber calcite in a lower Carboniferous palaeosol. Geological Journal 19: 23-32.

Wright VP. 1986. The role of fungal biomineralization in the formation of early Carboniferous soil fabrics. Sedimentology 33(6): 831-838.

Wright VP. 1990. A micromorphological classification of fossil and recent petrocalcic microstructures. Developments in Soil Science 19: 401-407.

Yaroslavtsev AM, Manucharova NA, Stepanov AL, Zvyagintsev, and Sudnitsyn II. 2009. Microbial destruction of chitin in soils under different moisture conditions. Eurasian Soil Science 42: 797-806.

Yoon TH. 2009. Applications of soft x-ray spectromicroscopy in material and environmental sciences. Applied Spectroscopy Reviews 44: 91-122.

Young JC. 1995. Microwave-assisted extraction of the fungal metabolite ergosterol and total fatty-acids. Journal of Agricultural and Food Chemistry 43 : 2904-2910.

Yu S-H. 2006. Bio-inspired crystal growth by synthetic templates. In: Naka K, editor. Biomineralization II, Mineralization using synthetic polymers and templates. Topics in current chemistry, vol. 271. Springer-Verlag, Berlin. P 79-118.

Zhou J and Chafetz HS. 2009. Biogenic caliches in Texas: The role of organisms and effect of climate. Sedimentary Geology 222: 207-225.

Zhu J-H, Song J-M, Yu S-H, Zhang W-Q, and Shi J-X. 2009. Mineralization for micropatterned growth of carbonates nanofibers. CrystEngComm 11: 539-541.

Annexes

Table summarizing the references mentioning NFC and/or nanofibres, the environment of the description, the used methodology, as well as the terminology, dimensions, and proposed origins for each features.

			NFC			Nanofibres		
Reference	Environment	Methodology	Terminology	Dimensions Width/Lenght in µm	Origin	Terminology	Dimensions Width in nm Lenght in µm	Origin
Kubiena 1938	East european soils (cambisol & chernozems)	Micromorphology	Pseudomycelium, needle shaped crystals	Brunisols: W 1-1.4 & L max 50. Chernozems : W 0.7-0.8 & L 350	Evaporation of supersaturated solutions, propable influence of organic colloids	Not mentionned	--	--
Supko 1971	Bedded Bahamian calcarenite, in phreatic zone	Micromorphology, SEM	"Whisker" like crystals, probably of aragonite	W 2-4 & L 50-60	Formation in the phreatic zone after supersatuation	Not mentionned	--	--
Klappa 1979	Calcretes from the western Mediterranean (Spain)	Petrographic description (SEM and optical microscopy)	Needle calcite / hyphantic calcite needle	Not specified	Not specified	Needle / hyphantic threads	W 100 & L 1-2	Described at the surface of filaments, assumed to be resistent components of their cell wall. May serve as template for mineralization
Vergès et al. 1982	Soils (Champagne & Mediterranean Midi)	SEM & TEM	Calcite en aiguilles	W 1-5	Rapid growth from highly supersaturated solutions	Calcite en bâtonnets	W 100	Rapid growth from highly supersaturated solutions
Wright 1984	Calcrete crust from the lower Carboniferous	Literature review, petrographic description	Needle-fibre calcite	W 1.5-3 & L up to 70	Indirect precipitation by fungi on decaying rootlets	Not mentionned	--	--
Callot et al. 1985b	Rendzinas on scree slopes	Binocular observations, SEM	Aiguilles de calcite	W 0.1-1 & L up to 0.5 cm	Fungal origin, related to dry conditions	Not mentionned, probably confused with NFC	--	--
Wright 1986	Paleosols in lower carboniferous limestones	Literature review, petrographic description	Needle-fibre calcite	W few microns & L several hundreds	Fungal origin	Not mentionned	--	--
Phillips & Self 1987	Calcrete of South Australia	SEM, TEM, XRD	Needle-Fibre calcite	Smooth needles W 0.5-2 & L 2-120. Serrated edged needles W 0.75-2 to 1.5-6 & L 7-30 to 4-90	Genesis in mycelial strands	Micro-rods	W 100 or less & L 1	Calcified rodshaped bacteria involved in fungal sheath lysis
Jones & Ng 1988	Rhizoliths in limestones of the Pleistocene Ironshore Formation	SEM	Needles and calcite rhomb chains	Rhomb chains W 4 & L 100	Physicochemical origin although indirect influence of OM may not be rejected	Grain-coating calcite needle mats and constituent of type II filaments	W 100 & L 6	Precipitation from pore-filling fluids, type II filaments are calcified filaments
Strong et al. 1992	Strongly indurated calcrete horizon in glacial gravels from North Yorkshire	C & O isotopes, SEM	Needle-fibre calcite	W 1-2 & L 50-100	Origin related to the presence of mucigel (roots, fungi, bacteria)	Not mentionned	--	--
Jones & Khale 1993	Alterated limestones	SEM and review of the literature	Fiber calcite crystals	W 05-1 & L 300	Precipiation from supersaturated fluids	Not mentionned	--	--
Bruand 1994 Ould Mohamed &	Cambisol developped on cryoturbated Miocene lacustrine limestones	Micromorphology, SEM	Needle calcite & serrated-edged needle	Needle W 1-3 & L 10-60 serrated-edged needles W 4-6 & L 10-25	Simple needle form in mycelial strands, rough needles are simple needles covered with bacteria & serrated edged needle result from dissolution/reprecipitation of simple neeldes	Micro-rods	W 100-500 & L 1-3	Calcified bacteria that grew from organic matter of hyphae. Mention filaments whose "walls are made of micro-rods"
Verrecchia & Verrecchia 1994	Carbonate soils and calcretes	Micromorphology, SEM and literature review	Needle-fiber calcite	L from 4 to 10^4 their W	Genesis in mycelian bundles	Micro-rods (M-type NFC)	W <500 & L <2	Physicochemical nuclei or calcified bacteria
Dubroeucq et al. 1996	Volcanic ash soils associated to pine trees	SEM, micromorphology	Needle fiber calcite	W 0.5-1	Growth from gel-like material rich in Ca, Si & Al covering actinomycetes filaments 0.1 µm in diameter	Identified as actinomycetes filaments	W 100	Microbial filaments organized in mats, genetic link with NFC
Newman et al. 1996	Pedogenic calcite from New-Mexico	Quadrupole MS, SEM	Calcite which consists of apparent fungal fibers	Not specified	Originate in reducing conditions, probably linked with methanotrophic activity	Gel-like material associated with apparent bacterial forms.	Not sepcified	Not specified
Arnand et al. 1997	Calcretes developped on greenstone, Western Australia	SEM, XRD, cartography	Needles (commonly branched) & serrated-edged needles	Needles: W 0.5-2 & L 20-160. Serrated-edged needles: W 5-25	Fungal origin (Phillips et al. 1987)	Single micro-rod with round termination	L up to 20	Calcified rodshaped bacteria (Phillips and Self 1987)
Becze-Deak et al. 1997	Quaternary loess paleosoil sites	Micromorphology, SEM	Needle-fiber calcite	MA type: W 0.5-1 & L 15-20. MB type: W 2 & L similar to MA types	Fungal origin (after Verrecchia & Verrecchia 94)	Not mentionned	--	--
Gradzinski et al. 1997	Moonmilk from a karstic cave, Poland	SEM, *in vitro* culture	Needle fibre calcite	Not specified	Calcite nucleation on calcified filamentous bacteria	Interpreted as a filamentous bacterial mat	Not sepcified	Autolytical mineralization of filamentous bacterial mats, genetic link with NFC
Canaveras et al. 1999	Karstic (partly dolomitized) cave with calcite/aragonite moonmilk	SEM, XRD, *in vitro* culture	Needle-fiber aragonite	Smooth single needles: W 0.5-1 & L 50 Polycrystals: W 2-20 & L 10-100	Physicochemical precipitation, acicular habit controlled by adsorbed ions (Mg^{2+}, Na^{+}, SO_4^{2-}), clays or OM	Mentionned as filamentous microbial films embedding NFC	W 100-200 & L 5	Identified as organic features
Loisy et al. 1999	Indurated horizons from a rendzina overlying periglacial chalk formation	SEM, TEM, micromorphology, XRD	Needle-fiber calcite (MA & MB types)	MA type: W 0.5-2 & L <100. MB type: W 2-20 & L 30-1000	Fungal origin (after Callot et al. 85; Verrecchia & Dumont 96)	M-type NFC or micro-rods. Two types mentionned: smooth and single rods & smooth flexible threadlike rods	1st cat: W 150 & L 2-3. 2nd cat: W 80 & L 2-6	Centripetal calcification around an organic nucleus, likely rod-shaped bacteria
Borsato et al. 2000	Moonmilk in Italian caves	SEM, TEM, XRD, radioC dating	Microfibers	W 0.5-2 & L >10	Physicochemical origin, originate from nanofibres	Nanofibres	W 50-150 & L >10	Physicochemical origin, crystal growth by VLS mechanism. Observed as constituent of filaments, identified as calcified filaments
Gillet et al. 2000	Tataouine meteorite, south Tunisia	SEM, TEM and *in vitro* culture	Not observed	--	--	Rod-shaped forms (RSF)	W 70-808 & L 0.1-0.6	Remnants or real rod-shaped bacteria
Canaveras et al. 2001	Karstic (partly dolomitized) cave with calcite/aragonite moonmilk	SEM and physicochemical analyses	Needle-fiber calcite	W 1-2 & L >5	Bioinduced by actinomycetes activity	Actinomycetes hyphal networks, embedding NFC	W <200 & L <2	Identified as organic features
Benzerara et al. 2003	Tataouine meteorite, South Tunisia	SEM, TEM	Not observed	--	--	Rod-shaped nanobacteria like	W averag. 70-80, min. 30 & L averag. 300-500 (200-800)	Well crystallized calcite single crystals with a thin outer amorphous layer. No evidence of calcified nanobacteria, probable involvment of an organic compound
Cailleau et al. 2005	Tropical soils containing bio-induced calcite	SEM, XRD	Needle fiber calcite (MA and MAB types)	MA type: W 0.4 & L 150-200	Fungal origin (after Verrecchia & Verrecchia 94)	M type microrods	W 100 & L 2-3	Calcified rod-shaped bacteria (after Loisy et al. 1999)
Bajnoczi & Kovacs-Kis 2006	Paleosol in quaternary travertines in Hungary	SEM, TEM, micromorphology, isotopes	Needle-fiber calcite	W 1 for smooth needles and 1-4 for serrated-edged needles & L averag. 40-100, up to 200	Biogenic origin, supports the fungal origin	Microrods or M-type NFC	W 50-200 & L 0.5-2	Physicochemical nuclei or calcified bacteria
Canaveras et al. 2006	Moonmilk in caves	SEM, bulk XRD and DNA-based approach	Monocrystalline rods & polycrystals (rhomb chains), similar to needle-fiber crystals described by Verrecchia and Verrecchia 1994	Monocrystals: W 0.2-2 & L 100-300	Heterogeneous nucleation on biological substrata, fibrous structures synthesized through a solution–precursor (organic)–solid mechanism	Filaments, bacterial hyphae	W 100-500 & L 5-200	Fibrous structures synthesized through a solution–precursor (organic)–solid mechanism
Alonso-Zarza & Jones 2007	Root calcrete formation on quaternary karstic surfaces, Bahamas	Micromorphology, SEM	Needle-fiber calcite	Not specified	Not specified	Micro-rods but confusion with NFC as also mentioned as needles	W 80 & L 0.3, found around microborings,as aggregates or on surface of calcified filaments. Larger fibers mentionned, W 100 & L 2, located in pores and at outermost part of microboring walls.	Biogenic origin, possibly related to bacteria or fungi, but physicochemical origin also possible
Blyth & Frisia 2008	Cold high-altitude caves, North Italy	GC lipidic biomarkers	Needle-fibre crystals	L/W ratio of >6/1	Nucleation promoted by bacteria. Fibrous morphology controlled by physical lateral growth by bacteria.	Nanofibres	W 50-150 & L 1->10	Precipitation by inorganic processes, elongated shape as a result of polymers in solution
Richter et al. 2008	Moonmilk in caves in Devonian massive limestones	SEM, EBSD, isotopes	Needle-shaped crystals	W 0.5-2(5) & L up to 200	Biologically induced origin may explain the non-statistical orientation of the *c*-axes.	Nanofibres as constituents of 1) "polycrystalline threads characterized by a central channel" and 2) "irregularly shaped polycrystalline mats which bind or cover NFC and threads"	W 50-100 & L <10	Not specified
Cailleau et al. 2009a	Pedogenic and karstic environments	Laboratory synthesis, TEM, EELS, ESI	Needle fiber calcite	W approx. 2	Specified in Cailleau et al. 2009b	Nanofibres	W 19-30 & L up to 1.6	Pseudomorphosis of organic polymers (e.g. cellulose) by supersaturated pore-filling fluids
Cailleau et al. 2009b	Calcareous soils from 11 sites in various climates	SEM (review on morphologies), isotopes	Needle fibre calcite	L from 4 to 10^4 their W	Crystal growth inside fungal hyphae	Mentioned in Cailleau et al. 2009a	--	--
Curry et al. 2009	Karstic caves, Alaska	*In vitro* cultures & quantification, SEM, Inorg&OrgC, XRD, Isotopes	Needle-fiber calcite	Monocrystals: W 1-3 & L 30-267 and polycrystals W 6-24 & L 45-126	Biologically influenced organomineral	Nano-fibers, mostly associated to NFC monocrystals	W <1	Biologically influenced organomineral
Zhou and Chafetz 2009	Biogenic caliche in Texas along a climatic gradient (moist subhumid to aridic)	Micromorphology, SEM	Needle fiber calcite	W 0.5-2 & L averag. 10-50, up to 100	Support a biologically influenced process	Micro-rods	Not specified	Related to microbial activity

Physicochemical parameters of soil solutions from Villiers (CH01) and moonmilk solution from *Vers-chez-le-Brandt* (CH02) cave. All the samples analyzed are shown with the differences in retrieved values depending on cations (Ca^{2+} and Mg^{2+}) measurement technique. Sampling method is specified for each sample; T: tray method; L: lysimeters method; C: centrifugation method. The instrument used for measuring Ca^{2+} and Mg^{2+} concentrations is indicated; ICP LS: ICP-MS measurements performed at Lausanne University; ICP NE: ICP-MS measurements performed at Neuchâtel University; IC: Chromatography measurements performed at Lausanne University. The two rightmost columns indicate the ratio between measurements obtained with ICP LS and ICP NE (ICP LS/ICP NE) for both Ca^{2+} and Mg^{2+} for the same samples analyzed with both instruments. The same calculation is given for Ca^{2+} and Mg^{2+} measured with IC and ICP LS from moonmilk samples.

	Alcalinity [mg $CaCO_3$ /L]	pH	Ca^{2+} [mg/L]	Mg^{2+} [mg/L]	$SI_{calcite}$	Sampling method	Ca/Mg method	Ratio ICP LS / ICP NE Ca	Mg
soil surface - organic layer A	81.32	7.67	36.56	0.57	-0.37	T	***ICP LS***		
"	"	"	32.40	0.52	-0.41	"	***ICP NE***	1.13	1.10
soil surface - organic layer A	73.01	7.69	36.10	0.56	-0.40	T	***ICP LS***		
"	"	"	32.40	0.54	-0.44	"	***ICP NE***	1.11	1.04
soil surface - organic layer A	177.14	7.98	*n.a.*	*n.a.*	*n.a.*	L			
mid soil - mineral layer B	122.75	8.19	*n.a.*	*n.a.*	*n.a.*	L			
interface organic-mineral layer B-C_{ca}	146.38	6.98	52.73	0.78	-0.67	T	***ICP LS***		
"	"	"	42.13	0.71	-0.76	"	***ICP NE***	1.25	1.10
interface organic-mineral layer B-C_{ca}	125.44	8.01	35.88	0.53	0.14	T	***ICP LS***		
"	"	"	33.53	0.53	0.11	"	***ICP NE***	1.07	1.00
in scree clasts pores C_{ca}	156.42	8.32	56.11	0.97	0.70	L	ICP NE		
in scree clasts pores C_{ca}	162.81	8.00	60.22	1.29	0.43	C	ICP NE		
in scree clasts pores C_{ca}	*n.a.*	*n.a.*	32.45	2.45	*n.a.*	C	ICP LS		
in scree clasts pores C_{ca}	*n.a.*	*n.a.*	15.91	*n.d.*	*n.a.*	C	IC		
in scree clasts pores C_{ca}	179.52	8.20	9.44	0.13	-0.09	C	IC		
moonmilk	82.78	7.71	41.20	3.16	-0.28	C	***ICP LS***	*Ratio IC / ICP LS*	
moonmilk	85.97	7.86	114.42	52.94	0.23	C	***IC***	2.78	16.72

Original publications

Papers

Bindschedler S, Millière L, Cailleau G, Job D, and Verrecchia EP. 2010. Calcitic nanofibers in soils and caves: a putative fungal contribution to carbonatogenesis. Tufas and Speleothems: Unravelling the Microbial and Physical Controls. Geological Society, London, Special Publications 336, 225-238.

Millière L, Hasinger O, Bindschedler S, Cailleau G, Spangenberg JE, Verrecchia EP. 2011. Stable carbon and oxygen isotopic signatures of pedogenic needle fibre calcite. Geoderma 161:74-87.

Braissant O, Bindschedler S, Daniels AU, Verrecchia EP, Cailleau G. *Accepted*. Microbiological activities in moonmilk monitored using isothermal microcalorimetry (Cave of «Vers Chez le Brandt», Neuchâtel, Switzerland). Journal of Cave and Karst Studies.

Posters

Bindschedler S, Millière L, Cailleau C, Job D and Verrecchia EP. Analogy between secondary calcium carbonate crystals and fungal structures: clues for a biogenic origin of Needle Fibre Calcite. International Mycological Congress 9, 1-6 August 2010, Edinburgh.

Bindschedler S, Millière L, Cailleau G, Job D and Verrecchia E. Fungal implication in secondary calcium carbonate accumulation in soils and caves. 3rd Swiss Microbial Ecology Meeting, January 28-30 2009, Einsiedeln, Switzerland.

Bindschedler S, Millière L, Cailleau G, Job D and Verrecchia E. The complex and diverse fungal processes involved in soil carbonatogenesis. 2007 Annual Scientific Meeting of the British Mycological Society, 9-12 September 2007, University of Manchester, UK AND SwissSed, 16th meeting of swiss sedimentologists, 22 February 2008, University of Fribourg, Switzerland.